Mapping the Functional Expression Profile of K_v7 Channels in Somatosensory Neurons of Different Sensory Modalities

Frederick Paul Jones

Submitted in accordance with the requirements for the degree of Doctor of Philosophy

University of Leeds

School of Biomedical Sciences

Eli Lilly & Co

September 2021

The candidate confirms that the work submitted is his own and that appropriate credit has been given where reference has been made to the work of others.

Acknowledgements

Foremost, I wish to express my gratitude to Professor Nikita Gamper for the opportunity to read for a PhD and providing support and guidance throughout. It is with your continued support and belief that I have been able to produce this work and I am fortunate to call you a great friend as well as an exceptional supervisor. Similarly, I would extend my gratitude to Dr Emanuel Sher, my industrial supervisor from Eli Lilly & Co who has provided me with all the tools to succeed and gave me, along with Dr Keith G Philips, a most pleasant experience of the pharmaceutical side of science.

I thank the past and present members of the Gamper lab and Eli Lilly & Co who have all contributed to my development as a research scientist and as a person. I would particularly like to thank Alexandra Hogea and Rosmaliza Ramli for being my first mentors. To Shihab Shah and Stephen Milne for taking the time to provide feedback on this thesis, for being great mentors and my best friends for the duration of my PhD and to Pierce Mullen for sharing wisdom far beyond his years. Thank-you to Alice Gregorie for, above all else, being my whirlwind of a best friend and to Greta Telešova, Yuan-Ming Tsai and Varinder Lall for being great colleagues and friends.

Thank-you to Eli Lilly & Co for sponsorship and welcoming me into the company, especially to Charlotte Dunbar for giving me a place to live and becoming a great friend. To Charles Arlott (the rodent whisperer) for training in behavioural and injection techniques as well as unparalleled guidance in animal handling, also to Louisa Appel and Chris Holton for training in behavioural techniques. A special thank-you to Mike Conway for training in intrathecal injections and Baolin Li for generation of *Kcnq2* knockout mice. Also, to Rudolph Zwaart and Claire Pouchon for help with in vitro work. Finally, to Grace Ford, my friend and hero.

To my parents, I will forever be grateful for your love, support and understanding and to my partner Minttu for always standing by my side. Matt, Steve and Sarah you're the best siblings I could have asked for.

The truth is, to acknowledge everyone that deserves it would be longer than this thesis, but in thanks, I promise to pay forward the kindness and wisdom I have received through the rest of my career and life.

Abstract

Pain is a regular and unavoidable experience that dramatically impacts people's quality of life. Current treatments are often inadequate, expensive or invasive, thus, despite advances, the clinical need is still left unmet and new therapeutic targets are needed. K_v7 ('M') potassium channels may represent such a target as these impose strong control over neuronal excitability. Functional M channels are present in peripheral somatosensory neurons but there is currently no consensus as to what the functionally dominant subunit is. Here we combine measures of gene and protein expression with functional patch clamp analysis and behavioural testing to extensively study K_v7 in the peripheral sensory system. We demonstrated that all but $K_v7.1$ are expressed in rat sensory neurons and that $K_v7.2$, $K_v7.3$ and $K_v7.5$ are abundantly expressed. $K_v7.2$ showed a bias to small-diameter neurons and $K_v7.5$ toward larger neurons with significant overlap between the various subunits in rats and mice. Effects of $K_v7.2$/$K_v7.3$ selective potentiator, ICA-27243, and *Kcnq2* knockdown suggest $K_v7.2$ is the predominant subunit controlling M current in TRPV1 positive nociceptors. ICA-27243 also significantly attenuated acute and inflammatory pain with comparable efficacy to retigabine. *Kcnq2* knockdown significantly reduced the M current and rheobase in TRPV1 positive neurons and significantly increased the excitability of these neurons. This translated to a reduction in thermal and mechanical pain thresholds and an increased pain response to acute painful stimuli when *Kcnq2* was knocked down *in vivo*. There were changes in some parameters associated with neuronal excitability and pain behaviour with *Kcnq5* knockdown. These findings identified $K_v7.2$ as the functionally dominant K_v7 subunit in nociceptors and for response to painful stimuli.

Contents

Publications

Papers

Jones F, Gamper N, Gao H Kv7 Channels and Excitability Disorders In: Pharmacology of Potassium Channels (Gamper N, Wang K, Eds), *Springer-Nature* 2021 DOI: 10.1007/164_2021_457

Hogea, A., Shah, S., **Jones, F**., Carver, C.M., Hao, H., Liang, C., Huang, D., Du, X. and Gamper, N. (2021), Junctophilin-4 facilitates inflammatory signalling at plasma membrane-endoplasmic reticulum junctions in sensory neurons. J Physiol, 599: 2103-2123.

Tsai YM, **Jones F**, Mullen P, Porter KE, Steele D, Peers C, Gamper N Vascular Kv7 channels control intracellular Ca2+ dynamics in smooth muscle. *Cell Calcium*, 2020. 92: p. 102283. DOI: 10.1016/j.ceca.2020.102283

Han H., Ramli R., Wang C., Liu C., Shah S., Mullen P., Lall V., **Jones F**., Shao J., Zhang H., Jaffe D.B., Gamper N., Du X (2021) Spinal ganglia control nociceptive input to the central nervous system. *Advanced Science* (Under Consideration)

Posters and Presentations

Jones F., Milne S.W., Gamper N., (2021) Kv7.2 is the functionally dominant Kv7 subunit in peripheral nociceptors. *Society for Neuroscience Annual Meeting, Chicago.*

Jones F., Milne S.W., Gamper N., (2021) Mapping the Functional Expression of Kv7 Subunits in Peripheral Sensory Neurons. *Leeds Post-Graduate Symposium Annual Meeting, Leeds.*

Jones F., Milne S.W., Gamper N., (2019) Mapping the functional expression profile of Kv7 channels in somatosensory neurons of different sensory modalities. *International Kv7 Channel Symposium, Naples.*

Jones F., Gamper N., (2018) Mapping the functional expression profile of Kv7 channels in somatosensory neurons of different sensory modalities *Society for Neuroscience Annual Meeting, San Diego.*

List of Figures

List of Tables

Abbreviations

AHP after-hyperpolarisation,

AP action potential,

BBB Blood-brain barrier,

BHB β-hydroxybutyric acid,

CaMKI Calmodulin-dependent kinase 1

CaMKII Calmodulin-dependent kinase 2

CER Conditional emotional response,

CFA Complete Freund's Adjuvant,

CHO Chinese Hamster ovary,

Cl^- Chloride,

CNS Central nervous system,

COX Cyclooxygenase,

Ct Cycle threshold,

DAG Diaglycerol,

DNFA2 Non-syndromic autosomal dominant deafness,

DRG Dorsal root ganglion,

DRN Dorsal raphe nucleus,

GABA Gamma-aminobutyric acid,

GABOB γ-amino-β-hydroxybutyric acid,

GPCR G protein coupled receptor,

H_2O_2 Hydrogen peroxide,

HEC hydroxyethylcellulose,

HEK293 Human embryonic Kidney line 293,

Hprt1 hypoxanthine phosphoribosyltransferase 1

IB4 Isolectin B4,

ICV Intracerebroventricular,

IHC Inner hair cells,

I_M M current,

IP3 Inositol triphospate,

IVA Isovaleric acid,

JLN Jervell and Lang-Nielsen syndrome,

LQTS long-QT syndrome,

LSC lumbar spinal cord,

miRNA microRNA,

MTX Mallotoxin,

NAPQI N-acetyl-p-benzoquinone imine,

NF200 Neurofilament 200 kD,

NGF Nerve growth factor,

NSAID Non-steroidal anti-inflammatory,

NTC non-targeting control,

OHC Outer hair cells,

PAG Periaqueductal gray,

PCP Phencyclidine,

Pirt Phosphoinositide-interacting protein,

PTZ Pentylenetetrazole,

qPCR Quantitative Polymerase Chain Reaction,

REST l repressor element-1 silencing transcription factor,

RISC RNA induced silencing complex,

RMP Resting membrane potential,

RNAi RNA interference,

RW Romano-Ward syndrome,

SAID Steroidal anti-inflammatory,

shRNA short hairpin RNA,

siRNA small interfering RNA,

SQTS Short QT syndrome,

SsTx Ssm Spooky toxin,

STORM Stochastic optical reconstruction microscopy,

TEA Tetraethylammonium,

TG Trigeminal ganglia,

TRPA1 Transient receptor potential ankyrin 1 channel,

TRPM8 Transient receptor potential methanol 8 channel,

TRPV1 Transient receptor potential vallinoid 1 channel,

VPL Ventral posterolateral nucleus,

VSMC Vascular smooth muscle cells,

VTA Ventral tegmental area,

Chapter 1: Introduction

1.1 Voltage-Dependent Ion Channels

In order to be electrically excitable, cells, such as neurons, cardiomyocytes, skeletal and smooth muscle myocytes, must express a wide range of pore forming ion channels that allow the flux of ions across the plasma membrane in response to changes in membrane voltage (Hodgkin and Huxley, 1952, Michaelis 1925). The common feature of all ion channels is a pore region made up of two membrane spanning regions joined by a loop in the extracellular region. The pore domain is formed by multiple copies of these two transmembrane regions either as part of the same protein or as independent subunits that combine to form a pore (Zheng and Trudeau, 2015). The addition of ion selective pores into the membrane of a cell or organelle allows the flow of ions in an aqueous solution to across the water insoluble membrane (Hille, 1978). The flow of ions allows cells to maintain a homeostatic electrical potential in relation to the external environment, despite utilising cellular processes that can change the potential of the cell. As well as allowing the cell to sense and respond to changes in the external environment or utilise the flow to secrete other substances from the cells (Hille *et al.*, 1999, Hille 2001). Therefore, ion channels range from constitutively open pores that allow the normal flow of ions in and out of the cell, to ion channels that detect chemicals in the external or internal environment or the change in shape or size of the cell and open or close accordingly and even to open or close in response to changes in the electrical charge of the cell (Goldman 1965). These ion channels that detect the change in charge across the membrane are said to be voltage-dependent, i.e., their activity is determined by the balance of charge between the inside and outside of the cell.

Voltage-dependent ion channels have the same pore region as mentioned above, with the addition of a voltage sensing domain consisting of four transmembrane (TM) regions joined by alternating intracellular and extracellular linkers (Zheng and Trudeau, 2015). In the case of voltage-dependent potassium channels (K_V) that selectively conduct potassium ions (K^+), the channel is made up of four subunits that combine as a tetramer, each subunit consisting of a voltage sensing domain (S1-S4) and a pore domain (S5-S6) (Kamb *et al.*, 1987, Papazian *et al.*, 1987, Long *et al.*, 2007) **(Figure 1.1A)**.

Comparing the overall impression of K_v channels to other voltage-dependent channels that conduct the cations calcium (Ca^{2+}) and sodium (Na^+), known as voltage-dependent calcium (Ca_v) and sodium (Na_v) channels, there are a number of similarities and differences. Ca_v and Na_v channels consist of 24 transmembrane regions, which are separated into four repeating domains of 6 TM regions (Noda *et al.*, 1986, Tanabe *et al.*, 1987). Essentially, this is the same tetrameric formation seen in K_v channels, but rather than four separate subunits containing 6 TM regions, Ca_v and Na_v channels comprise of a single large protein where the four subunits are linked together as part of the structure, usually with the addition of an auxiliary subunit.

Interestingly, it seems that Na_v channels evolved from Ca_v channels; intracellular and extracellular Ca^{2+} is used a second messenger in prokaryotes whereas there is no evidence for Na^+ channels in prokaryotes or early eukaryotes such as algae and plant species, despite the presence of Ca_v and numerous types of K^+ channel (Durell and Guy, 2001, Hille 2001). It is likely that as excitable cells developed in animals (but not other organisms), there was an evolutionary advantage to an influx of Na^+ over Ca^{2+}, perhaps because Na^+ does not act as a second messenger and poses faster conduction, thus could serve a specialised function.

A more detailed look into how K_v channels are specialised to conduct K^+ over other ions and how changes in voltage open or close the channels follows.

1.1.1 Voltage-dependent Potassium Channels

There are 12 subfamilies of K_v channels (K_v1-12) and within the family there are 40 genes encoding for K_v channel subunits in humans. The subunits vary drastically in function and in their interactions with other subunits of the same family. As a consequence, subunits can form K_v channels as homo-tetramers or hetero-tetramers, potentially consisting of up to 4 different subunits in one channel, with the ratio of these various formations within a cell having drastic effects on the function of the channel in that cell. There are also splice variants of many K_v subunits and variable post-translational modifications to the proteins. In addition to this, there are a number of beta-subunits that can interact with various subunits across all the K_v channels; for example, these could be KCNE subunits or intracellular proteins such as KChiPs (Crump and Abbott, 2014, Takimoto and Ren, 2002, Bähring, 2018).

Each K_v subunit consists of 6 transmembrane domains, the first four domains (S1-4) make up the voltage sensing region, consisting of the S4 voltage sensing domain and S1-S3, which act as accessory domains that provide support to the S4 domain. Within this region there are three linkers joining the transmembrane regions, two of which are extracellular (S1-S2 linker and S3-S4 linker) and one is intracellular (S2-S3 linker). These linkers can be subject to modification to change the voltage sensing properties or gating of the channel. The S5 and S6 transmembrane domains make up the pore region that allows the passage of ions across the membrane. The voltage sensing domain and pore domain are joined at the intracellular side by the S4-S5 linker, and the pore-forming subunits joined at the extracellular side by the S5-S6 linker or P loop **(Figure 1.1A)**. The pore region and voltage sensing domains are discussed in more detail in the following sections.

Overall, it is important to note that there is a great deal of diversity in K_v channels, and this allows these channels to be functional across equally diverse cell types, serving a spectrum of physiological roles. Many K_v channels have a primary role in repolarisation of the membrane during an action potential in neurons and cardiac myocytes. In neurons the vast array of K^+ channels expressed allows for significant fine tuning of the neuronal output based on its function; K_v channels can control whether a neuron is burst firing, silent, rapidly or slowly adapting (Gan and Kaczmarek, 1998). In addition, K_v channels in various forms play a significant role in setting resting membrane potential, repolarisation (Gan and Kaczmarek, 1998), the amplitude and duration of after-hyperpolarisation (Davies *et al.*, 2006). Similarly, in cardiac myocytes K_v channels control repolarisation and the refractory period and are sufficient to change heart rate when required (Sanguinetti and Jurkiewicz, 1990). K_v channels are also involved in very different processes such as limiting insulin secretion from beta-pancreatic cells (MacDonald *et al.*, 2001, Jacobson and Philipson, 2007, MacDonald and Wheeler, 2003).

Potassium Selectivity

Small ions such as K^+ and Na^+ are present in the intracellular and extracellular aqueous environment, bound to water molecules and yet must pass through the hydrophobic membrane of cells through ion channels. Despite the presence of both ions and Na^+ ions having a smaller anatomic radius than K^+, potassium channels are able to select for K^+ over Na^+ at a ratio of 1000 to 1, whilst conducting K^+ near to the

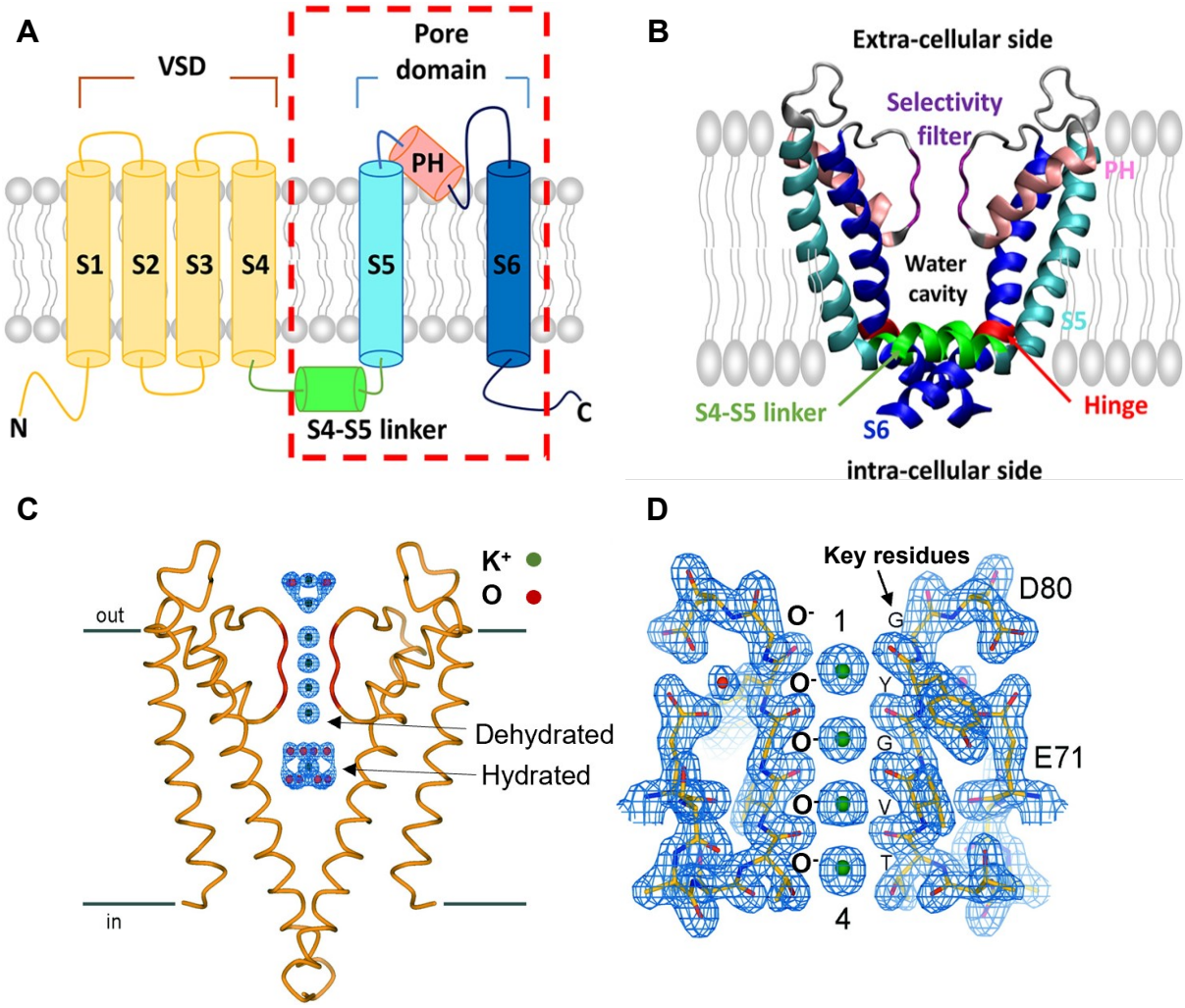

Figure 1.1 Voltage-dependent potassium (K_v) channel structure. **(A)** General structure of a voltage-dependent potassium channel (Lee *et al.*, 2020). **(B)** Overview of potassium channel pores from the current research (Lee *et al.*, 2020). **(C-D)** X-ray crystal structure and density of the potassium selectivity filter and key residues (GYGV) (D) (Zhou and MacKinnon, 2003).

diffusion limit. The diffusion limit is the maximum flow rate of an ion through a pore, if there is little resistance to ion flux then the flow becomes limited by the rate at which the ions can arrive at the pore in an aqueous solution and is result of the electrochemical gradient of that ion (Läuger, 1976). Thus, a sophisticated mechanism is required to achieve this level of selectivity with little impact on conductance.

The linker that connects the S5 and S6 pore is an extracellular loop that enters the pore of the channel forming a D shape inside the pore **(Figure 1.1B-C)**. The short loop is an uncoiled strand of amino acid residues with the sequence TXGXG common to all potassium channels and is known as the P loop **(Figure 1.1D)** (Heginbotham *et al.*, 1994, Doyle *et al.*, 1998). Most potassium channels have a TVGYG sequence, with notable exceptions including ERG channels and Kir6 with a GFG sequence, though tyrosine and phenylalanine only differ by the presence of one hydroxyl group so the functional difference is seemingly minimal (Kim and Nimigean, 2016). X-ray crystallography of the structure of bacterial KcsA K^+ channels, solved by Zhou and MacKinnon revealed that this sequence results in a run of carbonyl groups, with a negatively charged oxygens (O^-) facing the interior of the pore and a forming the narrowest point of the pore **(Figure 1.1D)** (Zhou and MacKinnon, 2003). The solved structure included K^+ ions trapped in the structure in their hydrated state at the entry to the channel and in the aqueous cavity after the P loop but four K^+ ions were trapped in between the P loops in a dehydrated state, evenly spaced **(Figure 1.1C)**. The four TVGYG containing P loops of each of the four subunits create four binding sites for dehydrated K^+ with eight oxygen atoms surrounding each site **(Figure 1.1D)** (Zhou and MacKinnon, 2003). This is significant as it suggests that the P loop selectivity filter works by electrostatic attraction of the positively charged K^+ ion with the negatively charged oxygens in the filter. The oxygens of the amino acids replace the oxygens from the water molecules allowing the dehydrated K^+ to pass through the selectivity filter, whilst being too small for a hydrated Na^+ molecule to pass and too far apart for dehydrated Na^+ (Israelachvili, 2011). On average 2 ions occupy the selectivity filter, either at positions 1 and 3 or 2 and 4, with the entry of the next ion repelling the previous ion into the next position (Zhou and MacKinnon, 2003). This means that the entry of a third K^+ ion represents a transient, unstable state in the filter requiring an ion to be expelled.

Solving the structure of the selectivity filter provides some understanding of why K^+ channels are selective against Na^+. Historically, there were two opposing theories on why this is the case long before the structure was known. Bezanilla and Armstrong proposed that oxygens in the K^+ pore are a fixed distance apart and a dehydrated K^+ is the correct size to contact all four oxygens at once, whereas dehydrated Na^+ is too small to contact all four and could only contact two, therefore could not pass through the filter (Bezanilla and Armstrong 1972). This theory relies on the assumption that the helices attached to the P loop never move, change shape or rotate, something that is rarely true of biological structures.

George Eisenman presented the opposing theory that the structures are not rigid and instead the interaction is dictated by the strength of electrochemical field. He calculated that when an ion would enter the pore, there would either be a strong or weak electrochemical field. A strong field would pull the carbonyl oxygens towards the ion, as they suggest is the case with potassium but when Na^+ enters the field is weak and cannot attract the oxygens (Eisenman, 1962). Eisenman's theory does not account for ion selectivity or the conservation of structure, which Armstrong's theory does, but Armstrong does not take field forces into account.

Bertil Hille combined the two theories, hypothesising that "the narrowest part of the K channel is a circle of oxygen atoms about 3 Å in diameter with a low electrostatic field strength" (Hille 1973). Indeed, the structure presented by MacKinnon shows that the position and structure of the channels holds the carbonyl oxygens in a position ideal for K^+ but too large for Na^+ to contact all oxygen atoms, supporting Armstrong's theory. However, the electron density also suggests a low electrostatic potential in the selectivity filter, preventing Na^+ and O^- being pulled closer to interact and the carbonyl position is not fixed and rigid, supporting Eisenman's theory. In fact, the selectivity filter resembles more of a spring. The positioning of carbonyl oxygens is optimised for K^+ and the low electrostatic potential and structural constraints prevent the filter being pulled in for Na^+ interactions, but the filter can expand to allow larger single valency ions such as rubidium (Rb^+) and caesium (Cs^+) to pass at a significant energetic cost (Doyle *et al.*, 1998, Zhou and MacKinnon, 2003).

Voltage-Dependence

As with the selectivity filter, the structure and critical amino acids of the voltage sensor are conserved throughout voltage-dependent potassium channels. The true voltage sensor is the S4 domain as it contains the positive residues necessary to respond to changes in voltage. The S1-S3 domains act as accessory domains, aiding the S4 voltage sensing domain to function through the positioning of these domains and the positioning of residues that interact with the S4 domain, contributing to how the S4 moves upon depolarisation. Thus, the S4 is discussed in detail as the true voltage sensing domain, with the understanding that S1-S3 and the linkers are important for the voltage dependency of the channel despite not directly sensing changes in voltage as the S4 domain does. The most prominent theory for how K^+ channels detect voltage is that the S4 domain moves towards the extracellular matrix and rotates, pulling the S4-S5 linker to open the channel. This theory was explored along with the key structural components by solving the structure of the potassium channel voltage sensor in a complex with a lipid membrane-like environment via X-ray crystallography (Long *et al.*, 2007). The authors created a chimera channel from $K_v1.2$ but replacing the voltage sensing 'paddle' (S3-S4) with that of $K_v2.1$, the chimera was functionally the same as $K_v1.2$ suggesting that the voltage sensing mechanism is conserved between K_v channels. The crystal structure shows the S4 overall is tilted away from S1 and S2 on the extracellular side, creating an aqueous cleft in the membrane **(Figure 1.2A)**. There are two negatively charged clusters, one externally, in the aqueous cleft, formed from two glutamates. The second negative cluster consists of two glutamates and an aspartate that are not exposed to the internal aqueous solution and are around 10 Å inside the membrane from the internal surface **(Figure 1.2A)**. There are 7 crucial positive residues present in the S4 domain (arginine (R) 0-6 and lysine (K) 5). K5 and R6 form hydrogen bonds with the internal negative cluster and R3 and R4 form hydrogen bonds with the external cluster **(Figure 1.2A)**. These interactions mean that when the cell membrane depolarises, the positively charged residues are repelled, moving towards the external solution, this movement brings R3/R4 and K5/R6 into contact with those negative clusters, stabilising the S4 and pulling on the S4-S5 linker to open the channel (Long *et al.*, 2007).

Direct evidence for movement of the S4 domain utilised the substituted cysteine accessibility method (SCAM). SCAM involves mutating a specific residue of interest

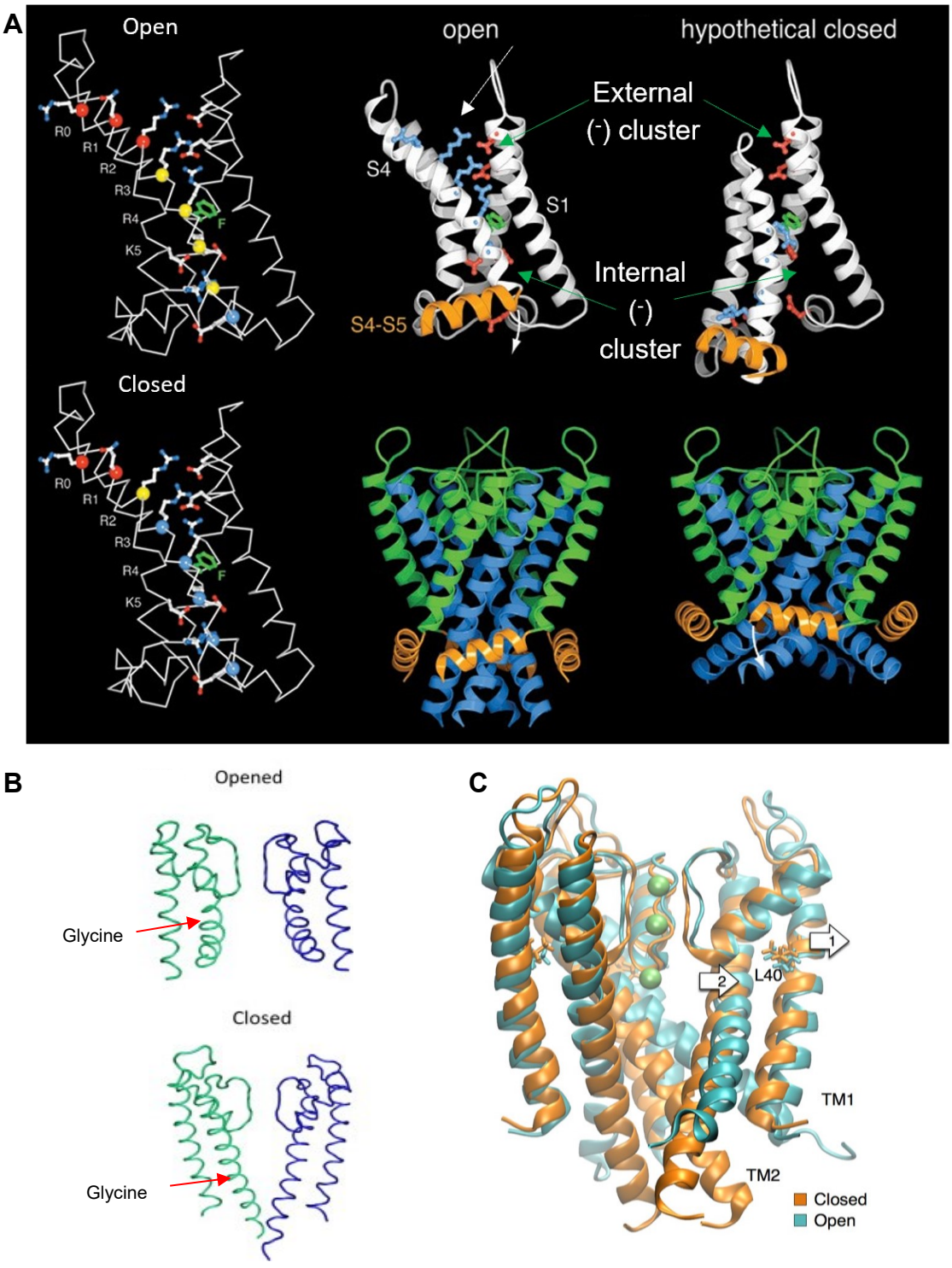

Figure 1.2 Voltage-dependent potassium (K_v) channel gating. **(A)** structure of the voltage sensor in the open and closed state showing the key residues and binding pockets. Red spheres- accessible to methanethiosulfonate (MTS) from extracellular space, yellow spheres- Inaccessible to MTS, blue spheres- accessible to MTS from the intracellular space (Long *et al.*, 2007). **(B-C)** Structural differences between the pore domain of open and closed potassium channels. **(B)** shows the change in shape of S6 and the location of the glycine hinge. **(C)** compares the structure of the whole transmembrane region of the channel in the open (cyan) and closed state (orange). (Heer *et al.*, 2017).

to cysteine and treating with methanethiosulfonate (MTS) (Larsson *et al.*, 1996). MTS forms sulphide bonds with cysteines but cannot access residues not exposed to aqueous solution. MTS had minimal effect on the wild-type *Shaker* K^+ channels but did abolish the current of some cysteine mutants only when the channel is open or closed (Larsson *et al.*, 1996). In the open conformation R0, R1 and R2 are accessible to MTS in the external solution and R3, R4, K5 and R6 are inaccessible from external or internal solution **(Figure 1.2A)**. In the closed state, R0 and R1 were still accessible to MTS, but R2 became inaccessible from either side and R3, R4, K5 and R6 were then accessible to MTS on the intracellular side **(Figure 1.2A)** (Larsson *et al.*, 1996, Long *et al.*, 2007). Supporting the idea that the S4 domain extends out into the extracellular space in the open conformation and in the closed conformation, becomes exposed to the internal solution (Larsson *et al.*, 1996, Long *et al.*, 2007). This makes sense as the positive residues will be attracted to the negative internal potential at rest and be repelled into the membrane upon depolarisation, opening the channel. One hypothesis suggested that the movement of S4 opens the channel through pulling the S4-S5 linker by tilting it down and closes by pushing onto the N terminal end to close it **(Figure 1.2A)** (Long *et al.*, 2007). Another proposal is that gating is due to a critical, conserved glycine in the S6 helix, glycine being small neutral amino acid so can adopt various angles so can be flexible, thus acts as a hinge in the S6 helix, widening the distance between S6 domains of each subunit **(Figure 1.2B)** (Jiang *et al.*, 2002, Ding *et al.*, 2005). A further look into the structure suggests that it may be a combination of the two, both helices are differently orientated in the open conformation and the S6 glycine is close to the S4-S5 linker, so movement of S4-S5 linker may result in S6 moving out at the hinge **(Figure 1.1.1C)** (Lee *et al.*, 2020).

1.2 Voltage-Dependent Potassium Channel Subfamily 7 (K_v7)

Of the members of the K_v channel family, the K_v7 channels are characterised by the negative threshold at which the channels conduct K^+ at, coupled with the kinetics of the channel; slow activation and deactivation kinetics and a distinct non-inactivating current, with the exception of $K_v7.1$ (Delmas and Brown, 2005, Schroeder *et al.*, 2000a, Du *et al.*, 2018, Gamper and Shapiro, 2015). Generally, the threshold for channel activation is around -60 mV but depending on the tetrameric organisation and intracellular factors, the threshold can be as negative as -80 mV (Perez-Flores *et al.*,

2020). K_v7 channels are also controlled by a diverse array of intracellular mechanisms including calmodulin binding, interactions with protein kinase A (PKA) and phosphatidylinositol 4,5-bisphosphate (PIP2). These properties allow modulation of K_v7 channels in response to a variety of internal and external stimuli, making them ideally suited for controlling cellular excitability in electrically active cells. The following section will look at the properties of K_v7 channels in more detail.

For clarity, from here on, *KCNQX* (human variant) or *KcnqX* (animal/rodent variant) when italicised refers to the gene or mRNA and K_v7.X or KCNQX when not italicised refer to the protein.

1.2.1 Discovery of the K_v7 Subfamily

Through the 1980s and 1990s, three slowly activating K^+ currents were discovered in three very different tissues. The first, a muscarine-inhibited outward current active at negative voltages in sympathetic neurons, was discovered by David Brown and colleagues. The muscarine sensitivity was attributed to the activation of the G protein coupled acetylcholine receptor (mAChR), thus Brown and colleagues coined the name 'M current' (I_M) for this phenomenon (Brown and Adams, 1980, Constanti and Brown, 1981, Adams *et al.*, 1982). Subsequently, the inhibitory effect of mAChRs on so called M channels (now a subset of K_v7) was identified as a principal mechanism of acetylcholine mediated increases in neuronal excitability (Brown *et al.*, 1997).

A few years later, PKA activated K^+ current was discovered in the heart with even slower activation and deactivation kinetics than David Brown's M current. This current, termed I_{Ks}, is responsible for the initial slow repolarisation of the cardiac action potential and is potentiated by adrenaline through PKA activation and modulation (Walsh and Kass, 1988). Nearly 10 years later, long-QT syndrome (LQTS) was associated with mutations in a 'novel' cardiac K^+ channel named K_vLQT1 (Wang *et al.*, 1996, Shalaby *et al.*, 1997, Yang *et al.*, 1997). This gene turned out to be responsible for I_{Ks}, hence why loss-of-function mutations result in LQTS.

The third, a slow activating K^+ current, was identified in the basolateral membrane of epithelial cells (Lohrmann *et al.*, 1995, Warth *et al.*, 1996). This current was determined to be conducted by a constitutively active channels with small-conductance, which were sensitive to chromanol 293B, a compound previously known to block I_{Ks} but at the time that epithelial K^+ current was not thought to be closely

related to I_{Ks} or I_M because the current is constitutively active (Lohrmann *et al.*, 1995, Warth *et al.*, 1996).

In order to identify the genetic basis for M current, genetic positional cloning was utilised and identified two genes related to K_vLQT1 in humans that when mutated, were responsible for an infant epilepsy known as Benign Familial Neonatal Convulsions (BFNC) (Biervert *et al.*, 1998, Singh *et al.*, 1998). BFNC is an autosomal dominant epilepsy with loci mapped to 20q13.3 and 8q24 in humans (Charlier *et al.*, 1998, Yang *et al.*, 1998). When expressed in Xenopus oocytes, these genes conferred selective K^+-selective currents with slow activation and deactivation kinetics and an activation at particularly negative voltages (-50 to -80 mV) that increased and plateaued at positive voltages (Biervert *et al.*, 1998). These properties emulated those of I_M, and indeed expression of these genes in mammalian cell lines showed the same kinetics, mAChR inhibition and pharmacology of the neuronal I_M discovered by Brown and colleagues (Wang *et al.*, 1998, Selyanko *et al.*, 2000, Shapiro *et al.*, 2000). These two genes responsible for I_M and epilepsy, were named *KCNQ2* and *KCNQ3* with K_vLQT1 being renamed *KCNQ1*. I_{Ks} was found to be made up of K_v7.1 (KCNQ1) complexing with β-subunit KCNE1 (Kaczmarek and Blumenthal, 1997). Similarly, the expected unrelated epithelial current arises from the complex of K_v7.1 with β-subunit KCNE3 (Bleich and Warth, 2000, Schroeder *et al.*, 2000b).

Around the same time, a similar K^+ current to those mentioned above and a gene associated with autosomal dominant deafness were identified in the hair cells of the ear, the auditory nuclei in the brain and later, the sensory spiral ganglia in the cochlea (Kubisch *et al.*, 1999, Kharkovets *et al.*, 2000, Lv *et al.*, 2010). This deafness related gene is known as *KCNQ4* and encodes the so-called K_v7.4 subunit. The final gene in the KCNQ family is *KCNQ5*, which encodes for another neuronal subunit K_v7.5 (Schroeder *et al.*, 2000a, Lerche *et al.*, 2000a). Both K_v7.4 and K_v7.5 were also found to be particularly highly expressed in smooth muscle and important in controlling contractility (Ohya *et al.*, 2003, Brueggemann *et al.*, 2007, Mackie *et al.*, 2008).

K_v7 channels are created by the homomeric or heteromeric association of varying combinations of the K_v7 subunits as well as β-subunits and are modulated by a variety of secondary messengers. These properties make these channels interesting to study due to the wide variety in assembly, modulation and expression.

1.2.2 K_v7 Channel Biophysical Properties

The role of K_v7 channels in controlling cellular excitability pertains to the distinct biophysics of the subfamily however, the modulation, subunit composition and presence of auxillary proteins can drastically change the biophysics of the channels.

As a general rule, $K_v7.2$- $K_v7.5$ channels conduct slowly activating voltage-dependent K^+ currents, with negative activation thresholds around -60 mV and no inactivation $K_v7.1$ channels are the most divergent from the other K_v7 channels; these homomers do inactivate to some extent (Tristani-Firouzi and Sanguinetti, 1998) and $K_v7.1$/KCNE3 channel complexes have been shown to be constituitively active (Schroeder *et al.*, 2000b). K_v7 channels activate at around -60 mV and reach maximal open probability at 0 to 20 mV when expressed in cell lines. Yet, due to the extensive intracellular modulation of these channels, the activation threshold can fall between -80 and -50 mV in various cell types depending on the cellular conditions thus making them very useful for influencing membrane excitability **(Figure 1.3A)**.

Slow activation and deactivation kinetics mean that macroscopic current can be recorded for 400-600 ms **(Figure 1.3B)**. The majority of subunit compositions have activation time constants of 100-200 ms with the exception of $K_v7.1$/KCNE1 complexes that activate over 500 ms. Similarly, deactivation time constants range from 100-200 ms for current produced by the majority of K_v7 channels. Unsurprisingly, $K_v7.1$ and $K_v7.1$/KCNE1 complexes have slower activation and deactivation times; with $K_v7.1$ activating at 210 ms at 0 mV and deactivating over 400 ms at -60 mV; the complex taking 200 ms to deactivate at -60 mV (Gamper *et al.*, 2003a). In terms of subunit arrangements, homomeric current tends to deactivate slower compared to heteromeric channels with the $K_v7.2/3$ heteromers the fastest (Gamper *et al.*, 2003b). $K_v7.2/7.3$ heteromers activate over 170 ms at 0 mV and deactivate over 75-100 ms at -60 mV (Gamper *et al.*, 2003a). Whereas homomers take longer, $K_v7.2$ activates over 210 ms at 0 mV and deactivates around 155 ms at -60 mV. $K_v7.3$ activates over 150 ms at 0 mV and deactivates over 100 ms at -60 mV (Gamper *et al.*, 2003a). Similarly, $K_v7.4$ and $K_v7.5$ activate over 180 ms and 160 ms at 0 mV and deactivate over 100 ms and 125 ms at -60 mV respectively (Gamper *et al.*, 2003a).

The slow kinetics reveal a lot about the role of K_v7 channels in excitable cells, with activation times suggesting that the channels are unlikely to play a role in action potential repolarisation. The slow increase in K^+ outward current and slow deactivation

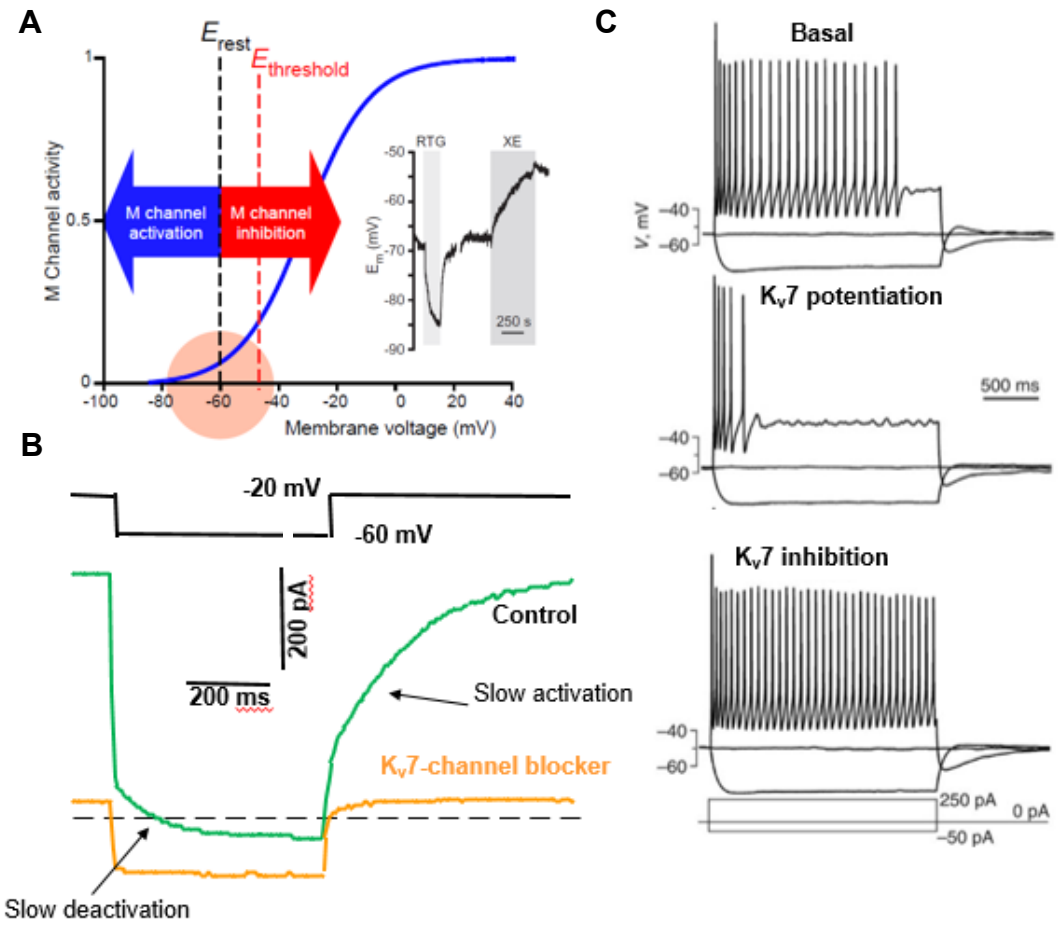

***Figure 1.3 Biophysical properties of K_v7 channels*. (A)** Link between K_v7 channel activation and resting membrane potential in peripheral neurons. Inset changes in membrane potential upon application of retigabine (RTG) or XE-991 (XE) (Du *et al.*, 2018). **(B)** Activation and deactivation kinetics of K_v7 current (I_M). **(C)** Impact of potentiating and inhibiting K_v7 channels on neuronal excitability, assessed through action potential frequency (Gamper *et al.*, 2006).

of the channels effectively increase the threshold for subsequent action potentials (Gamper *et al.*, 2006, Du *et al.*, 2014), a potentially accumilative effect upon each subsequent action potential in a train **(Figure 1.3A-C)**. Increasing the threshold with each action potential leads to burst accomodation, which is the reduced likelihood of a subsequent action potential occuring after the firing of the previous. Therefore, an increased threshold can have the effect of reducing the number of action potentials in a burst or reducing the frequency of action potentials in a burst, thereby reducing output **(Figure 1.3C)**.

The negative activation threshold of K_v7 channels allows a portion of the channels to be open at the resting membrane potential and a larger portion of channels will open the membrane potential rises. The V½ or voltage for half maximal microscopic current is generally between -20 and -40 mV for $K_v7.2$-$K_v7.5$, however for $K_v7.1$ and $K_v7.1$/KCNE1 the V1/2 is 15 mV and 0-8 mV, respectively (Jones *et al.*, 2021). A higher conductance of K_v7 channels would have the effect of hyperpolarising the membrane potential (Du *et al.*, 2014), which aids in keeping certain types of cells silent or stop them activating spontaneously. This is particularly important in neurons such as nociceptors which are involved in transducing painful (noxious) stimuli, so spontaneous activity would be detrimental.

K_v7 channels have relatively small single channel conductance (γ) though there is significant variation berween the subunits. $K_v7.1$ γ has been shown to be less than 2 pico-siemens (pS) in 5 mM K^+ (Werry *et al.*, 2013) but increases to up to 6 pS when combined with KCNE1 in 10 mM K^+ (Pusch, 1998). This is also the case for $K_v7.4$ and $K_v7.5$ (~2 pS) in 5 mM K^+ (Li *et al.*, 2004a), whereas it is larger for $K_v7.2$ (~6 pS) and $K_v7.3$ (~9 pS) in 5 mM K^+ (Li *et al.*, 2004a) and approximately 9 pS for $K_v7.2/3$ heteromers in 2.5 mM K^+ (Selyanko *et al.*, 2001). Conductances were measured in bath concentrations of 25 mM (Selyanko *et al.*, 2001) or 40 mM (Li *et al.*, 2004a) K^+ to set resting membrane potential of the cells to -30 mV. This translates to the whole-cell K_v7 current in expression systems with $K_v7.2/3$ heteromers have 4-10 times the current than the channel homomers (Zhang *et al.*, 2003).

In order to open, K_v7 channels require PIP2 to be bound to the channel, therefore PIP2 affinity and channel conductance are inextricably linked. $K_v7.3$ subunits have the highest affinity for PIP2 and the highest maximal opening probability at saturating

voltages ($P_{o,max}$ of ~1), whereas $K_v7.2$, $K_v7.4$ and $K_v7.5$ have a $P_{o,max}$ of 0.2 or below; accordingly, these subunits have much lower affinity for PIP2 (Li *et al.*, 2004a, Zhang *et al.*, 2003). $K_v7.2/3$ heteromers have a Po around 0.3-0.4 and a PIP2 affinity between those of $K_v7.2$ and $K_v7.3$ (Zhang *et al.*, 2003, Li *et al.*, 2005). Though it is important to note that macroscopic current amplitude and open probability of the channel do not necessarily have linear relationsips, thus $K_v7.3$ homomers have highest open probability but generate perhaps the lowest whole-cell current amplitudes, as compared to other subunits (Wang *et al.*, 1998, Zhang *et al.*, 2003). Its higher affinity for PIP2 but low current output could be another reason for $K_v7.3$ forming complexes with other subunits.

1.2.3 Modulation of K_v7 Channels

PIP2 and calmodulin are critical co-factors for K_v7 channel activity (their role in normal channel function is discussed in 1.2.5) and cells regulate these two co-factors in a number of ways, with different types of cells employing varying methods to do so. In addition, different stimuli can also regulate these co-factors. Here we will explore the modulation of K_v7 channels through control of these critical co-factors and by other regulatory proteins that interact with the K_v7 subunits.

Cardiac cells increase contractility and heart rate in response to noradrenaline. $K_v7.1$ is activated through beta-adrenergic stimulation to increase I_{Ks}, hence maintaining rhythmic beating as heart rate increases. Noradrenaline intiates Gs coupled β-adrenergic receptor activation which induces adenylyl cyclase activity, converting adenosine triphosphate (ATP) to cyclic AMP (cAMP). cAMP activates protein kinase A (PKA) by removing its regulatory domain from the catalytic domain, allowing PKA to phosphorylate serine 27 of $K_v7.1$ with the aid of a scaffolding protein, Yotiao (AKAP9), to facilitate phosphorylation **(Figure 1.4A)** (Potet *et al.*, 2001, Marx *et al.*, 2002). As well as aiding in posphorylation of other proteins, there is also evidence that phosphylation of Yotiao that is directly bound to $K_v7.1$ is an important part of β-adrenergic stimulation (Chen *et al.*, 2005). $K_v7.4$ and $K_v7.5$ in vascular smooth muscle are also activated by adrenergic stimulation, however, when exogenously expressed, only $K_v7.5$ homomers and $K_v7.4/5$ heteromers were enhanced by β-adrenergic stimulation, not $K_v7.4$ homomers (Mani *et al.*, 2016). This suggests that in smooth muscle, $K_v7.5$ is required for cAMP mediated regulation of M current. $K_v7.2/7.3$

channels are also potentiated by PKA (Schroeder *et al.*, 1998), though the exact mechanism of this effect is still under investigation.

Aside from Gs coupled PKA-induced modulation, K_v7 channels are also modulated by $G_{q/11}$ coupled receptors, seemingly in a number of different ways. The initial K_v7 channel current discovered by David Brown was named the M current due to its sensitivity to muscarine, the muscarinic acetylcholine receptor (mAChR) agonist. It was confirmed in sympathetic neurons and expression systems that muscarine induced inhibition of I_M was not due to direct channel blocker but in fact due to activation of the G_q pathway (Selyanko *et al.*, 1992, Selyanko *et al.*, 2000). This was achieved using the cell-attached method of patch clamp and applying muscarine. K_v7 channels in the patch were sealed off from the direct effects of muscarine and yet were inhibited all the same, suggesting an indirect second messenger to be the trigger (Selyanko *et al.*, 1992, Selyanko *et al.*, 2000). There are numerous paths in the resulting cascade that could lead to K_v7 channel inhibition. As mentioned PIP2 is a crucial co-factor required for K_v7 activation, and $G_{q/11}$ activation results in the hydrolysis of PIP2 into inositol triphospate (IP3) and diaglycerol (DAG) via phospholipase C (PLC) activation. Hydrolysis of PIP2 reduces the amount of intact PIP2 available to interact with K_v7 channels, therefore preventing channel opening **(Figure 1.4B)** (Zhang *et al.*, 2003, Suh and Hille, 2002). This PIP2 hydrolysis seems to be the driving factor behind mAChR mediated K_v7 channel inhibition **(Figure 1.4B)** (Zhang *et al.*, 2003, Suh *et al.*, 2004, Horowitz *et al.*, 2005).

However, PIP2 hydrolysis does not seem to be the main factor in K_v7 inhibition by other $G_{q/11}$PCRs. The bradykinin activated receptor B_2R is one such example. In sympathetic and sensory neurons, bradykinin inhibits M current through the $G_{q/11}$ pathway without significant changes to global membrane PIP2 levels (Cruzblanca *et al.*, 1998, Liu *et al.*, 2010). Rather, PLC hydrolyses PIP2 into DAG and IP3, IP3 binds to IP3 receptors present in the ER, releasing Ca^{2+} from ER stores. This Ca^{2+} release inhibits K_v7 channels through calcifying calmodulin (Cruzblanca *et al.*, 1998, Liu *et al.*, 2010) **(Figure 1.4B)**. The other side of the pathway induces DAG to activate protein kinase C (PKC). PKC phosphorylation (aided by AKAPs) has the effect of priming the channel to increase its sensitivity to mAChRs by reducing PIP2 affinity **(Figure 1.4B)** (Hoshi *et al.*, 2003, Zhang *et al.*, 2011b). Experimentally M_1, M_2 and M_3 mAChRs, B_2 bradykinin receptor, protease-activated receptor (PAR_2), purigenic P_2YR and

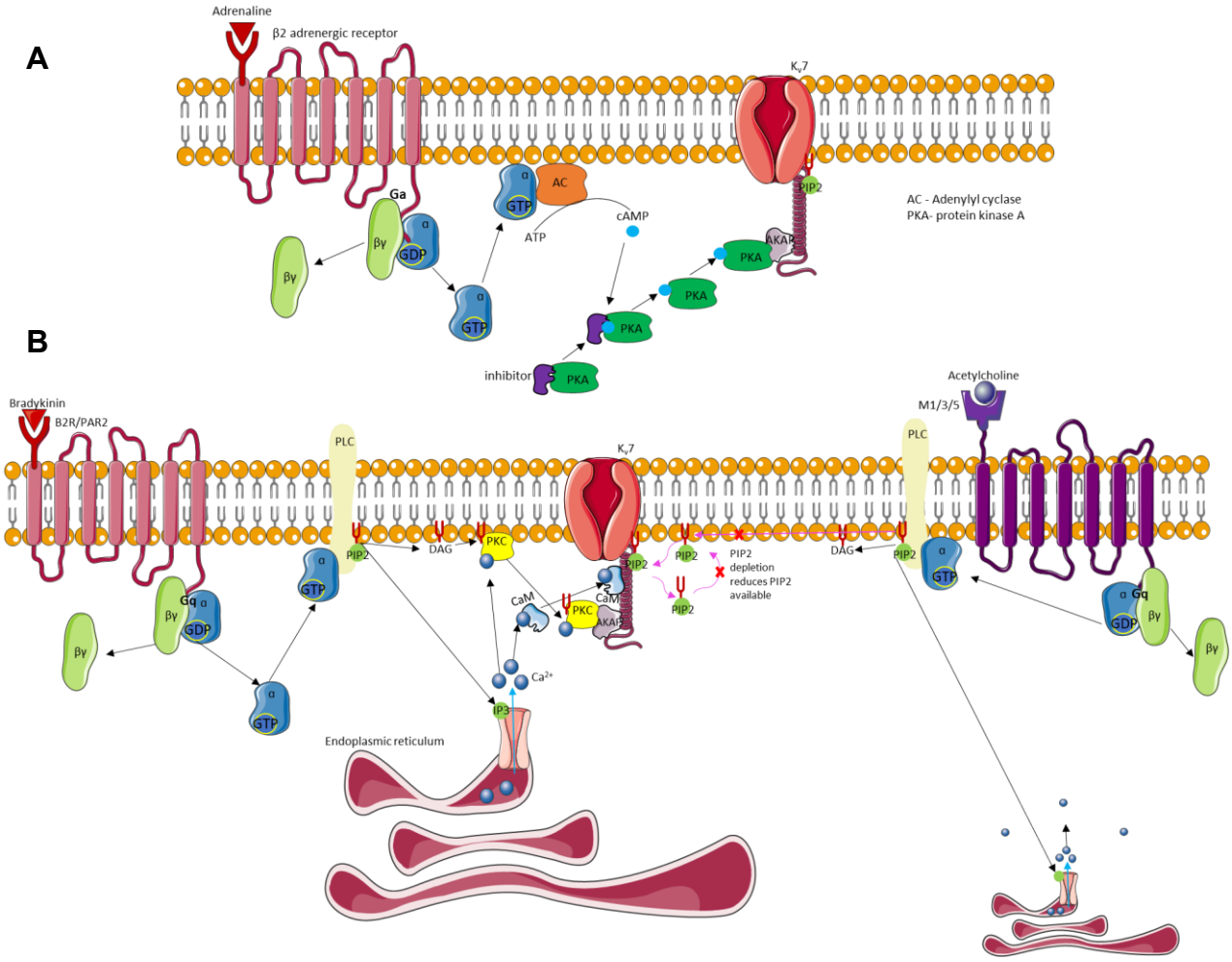

Figure 1.4 K_v7 channel modulation. **(A)** G_s protein coupled receptor – protein kinase A mediated phosphorylation of K_v7 channels. **(B)** Differential $G_{q/11}$PCR inhibition of K_v7 channels. Bradykinin: G_q mediated PIP2 hydrolysis to IP3 and DAG. Resultant increase in calcium (Ca^{2+}) via IP3 receptors close to the GPCR and K_v7 channel, binding to calmodulin and inhibiting K_v7. DAG activation of PKC and subsequent phosphorylation of K_v7 channels (increases sensitivity to inhibition). Muscarine: PIP2 hydrolysis to IP3 and DAG, depleting PIP2 from the membrane, resulting in K_v7 inhibition.

angiotensin II (AT_1) have all been identified as supressors of K_v7 currents. The contribution of each of the potential pathways differ depending on cell type and the receptor activated. In sympathetic neurons, B_2Rs and P_2Y receptors evoke IP3 mediated Ca^{2+} rises whereas M_1 and AT_1 do not. All of these receptors have been shown to elicit strong PIP2 hydrolysis in certain cell types, yet in sensory neurons, B_2Rs and PAR_2 receptors evoke IP3 mediated Ca^{2+} increases without global PIP2 depletion. The divergence in mechanism is suggested to be whether the GPCR is present in a microdomain with IP3Rs and K_v7 channels, allowing the local Ca^{2+} release from the ER via IP3R1 to reach a concentration that will reliably inhibit K_v7 channels **(Figure 1.4B)**. B_2R have been shown to be present in these microdomains in sympathetic neurons (Delmas and Brown, 2002) and sensory neurons (Jin *et al.*, 2013, Hogea *et al.*, 2021). This local increase in Ca^{2+} is particularly important because the local concentration of Ca^{2+} can reach as high as 50 μM near to the channel, but rapidly reduces to ~100 nM as Ca^{2+} diffuses away from the release site (Rizzuto and Pozzan, 2006). This is relevant because modest increases in Ca^{2+} concentration have been reported to enhance K_v7 current in sympathetic neurons but concentrations over 200 nM begin to inhibit K_v7 current (Marrion *et al.*, 1991, Yu *et al.*, 1994, Marrion, 1996, Selyanko and Brown, 1996). Thus, Ca^{2+} increase in close proximity to K_v7 channels would be more likely to have an inhibitory effect.

Another kinase that inhibits K_v7 channels is Src kinase (tyrosine kinase), though Src is part of a pathway involved in cell proliferation, inhibition of both $K_v7.3$ and $K_v7.5$ was due to direct phosphorylation of two tyrosines, demonstrated by drastically reduced phosphorylation and inhbition after mutation of tyrosine-67 and 349 in $K_v7.3$ (Li *et al.*, 2004b). In $K_v7.2/7.3$ heteromers the effect of Src on $K_v7.3$ is enough to inhibit the heteromers (Li *et al.*, 2004b). Similarly, protons (H^+) also inhibit the maximal current of $K_v7.2/7.3$ heteromers and cause a depolarising shift in voltage-dependence during acidosis largely through inhibition of $K_v7.3$, as the inhibitory effect of H^+ was far greater on $K_v7.3$ homomers than $K_v7.2$ (Prole *et al.*, 2003).

Contrastingly, oxidative modification from oxidisers such as hydrogen peroxide (H_2O_2) or ascorbic acid (Vitamin C) potentiate the currents of $K_v7.2$-7.5 but not $K_v7.1$. This is due to the oxidation of a pocket of three cysteines in the S2-S3 linker of $K_v7.2$-7.5 channels however, $K_v7.1$ only has one cysteine residue in the same area (Gamper *et al.*, 2006). Zinc pyithione has long been used as a pharmacological tool for potentiating

K_v7 currents with little understanding of the molecular mechanism underlying its action. Recently it was discovered that zinc is the main contributor to the effect and that increases in intracellular zinc leads to K_v7 channel potentiation. The effect is possibly zinc stabilising K_v7 channels in a similar conformation to when PIP2 is bound, perhaps mimicking the effect of PIP2 binding, hence reducing channel dependence on PIP2 (Gao *et al.*, 2017).

1.2.4 K_v7 Auxillary Proteins

As well as forming an array of homomers and heteromers, K_v7 channel subunits also bind to an array of auxillary subunits that change various channel properties.

KCNEs are a group of five single transmembrane proteins beta subunits (KCNE1-5) that bind to K_v7 channels in a subunit dependent manner, changing channel properties. The interaction of KCNE subunits with $K_v7.1$ is the most studied, with $K_v7.1$ interacting with all five KCNE subunits. $K_v7.4$ binds to KCNE1-4 and $K_v7.5$ selectively interacts with KCNE1 and KCNE3 (Roura-Ferrer *et al.*, 2009, Jones *et al.*, 2021). KCNE1 is the component that converts $K_v7.1$ homomeric currents into currents resembling the I_{Ks} seen in cardiac cells. Consistent with that, mutations in KCNE1 give rise to long QT syndrome, the same as mutations in $K_v7.1$ do. The effect of KCNE1 binding to $K_v7.1$ is a dramatic slowing of the activation by around 1,000-fold, a positive shift in voltage dependence and an increase in single-channel conductance. This is also accompanied by removal of the mild inactivation of $K_v7.1$ homomers and stabilizing the open state (Tristani-Firouzi and Sanguinetti, 1998). KCNE1 binding also changes the channels sensitivity to pharmacological compounds by reducing sensitivity to XE-991 (Wang *et al.*, 2000) and increasing sensitivity to chromanol 293B, a blocker of I_{Ks} (Busch *et al.*, 1997). These changes have led to the suggestion that KCNE1 subunits (and likely the others due to the close conservation between subunits) may interact with the pore forming S5-S6 region of $K_v7.1$. The cryo-EM structure of $K_v7.1$ and KCNE3 solved by Sun and MacKinnon showed binding of four KCNE3 proteins, one for each of the $K_v7.1$ subunits. KCNE3 interacted between S1, S4, S5 and S6, in a manner suggesting this region wraps around KCNE3 (Sun and MacKinnon, 2020). Similarly, a number of models of KCNE1 binding suggest KCNE1 binds by 'piercing' the channel pore (Kang *et al.*, 2008, Tian *et al.*, 2007). However, there must be some important differences in binding as $K_v7.1$ co-assembly with KCNE3 and KCNE2 result in constituitively open channels, whereas KCNE1 does not

(Schroeder *et al.*, 2000b). Even KCNE2 and KCNE3 have opposing effects, with KCNE3 potentiating $K_v7.1$ current (Schroeder *et al.*, 2000b) and KCNE2 inhibiting it (Bendahhou *et al.*, 2005) when $K_v7.1$ currents were recorded whilst co-expressed with either β-subunit. Furthermore, KCNE2 also accelerates activation and deactivation kinetics in $K_v7.2$ and $K_v7.2/3$ heteromers (Tinel *et al.*, 2000b). KCNE3 has been shown to supress $K_v7.4$ currents whereas KCNE4 seems to potentiate $K_v7.4$ current (Abbott, 2016). $K_v7.5$ activation is slowed by KCNE1, whereas KCNE3 inhibits macroscopic currents (Roura-Ferrer *et al.*, 2009). Also, both KCNE4 and KCNE5 suppress $K_v7.1$ current when expressed together in cell-lines (Roura-Ferrer *et al.*, 2009). The mechanisms and physiological relevence of the KCNQ-KCNE interactions are not fully understood for all K_v7 subunits but KCNE subunits clearly influence the behaviour of $K_v7.1$ in various tissues, controlling $K_v7.1$ properties by KCNE subunit expression.

Aside from KCNE beta subunits, K_v7 channels also interact with syntaxin 1A and Ankyrin G in neurons. Both of these proteins target peptides to specific neuronal sites. Syntaxin 1A is a pre-synaptic targeting protein allowing K_v7 channels to accumilate at pre-synaptic areas, likely providing an inhibitory effect on repetative signalling to post-synaptic terminals (Regev *et al.*, 2009). Ankyrin G localised K_v7 channels and Na_v channels to the axon initial segment and nodes of Ranvier in myelinated neurons (Pan *et al.*, 2006, Cooper, 2011) where K_v7 channels likely play an inhibitory role on repeated action potential propogation or helping set resting membrane potential. K_v7 channels may also interact with TRPV1 and L-type calcium channels, perhaps in a similar complex to with bradykinin (B2R) receptors. Research into this area is in its infancy but superresolution microscopy (STORM) showed that clusters of $K_v7.2$ with TRPV1 or L-type calcium channels in nodose neurons and that this clustering was dependent upon AKAP150, as clustering was lost in AKAP150 knockout mice (Zhang *et al.*, 2016a). The functional implication of these clusters in sensory neurons, is not yet known, but it could be postulated that activation of TRPV1 in response to noxious heat, allows the influx of calcium, that increases local calcium concentration to a level that inhibits K_v7 channel to increase depolarisation caused by the stimulus.

1.2.5 Latest Insights into Channel Structure

K_v7 channels have the same overall structure as other K_v channels. They are tetrameric channels formed of 4 subunits that consist of 6 transmembrane domains, with S1-S4 making up the voltage sensing domain and S5-S6 which incorporate the

pore domain. The pore domain contains the typical GYG potassium selectivity filter, detailed in section 1.1.1 and each domain is linked by alternating intracellular and extracellular loops **(Figure 1.5A-B)**. A particular feature of K_v7 channel structure is the large carboxy-terminus (C-terminus) shared by all K_v7 subunits, which makes up around half of each subunit. The C-terminus comprises four alpha helices, A-D, which are heavily involved in the binding of regulatory proteins and multimerization of homomeric and heteromeric channels with the same or other K_v7 subunits **(Figure 1.5A-B)**. Helices A and B are the major binding sites for regulatory molecules, with all subunits requiring PIP2 for activation and calmodulin for proper assembly and activity **(Figure 1.5C&D/Figure 1.6 E&F)**. Calmodulin acts as a modulator by altering the calcium sensitivity of the channel (Kosenko and Hoshi, 2013, Gamper *et al.*, 2003b, Gamper *et al.*, 2005) as well as being essential for assembly and trafficking, in a calcium-dependent manner (Ghosh *et al.*, 2006, Shamgar *et al.*, 2006, Etxeberria *et al.*, 2008).

Helices C and D are responsible multimerization as they allow for interaction between the various subunits. This is important, as K_v7 heteromization is not random between subunits, but very specific. $K_v7.1$ does not heteromerise with other K_v7 subunits (Schwake *et al.*, 2003), $K_v7.2$ subunits only interact with $K_v7.3$ (Wang *et al.*, 1998), whereas $K_v7.3$ co-assembles with $K_v7.2$, $K_v7.4$ (Bal *et al.*, 2008) and $K_v7.5$ (Wickenden *et al.*, 2001). $K_v7.4$ and $K_v7.5$ also co-assemble (Brueggemann *et al.*, 2014c, Chadha *et al.*, 2014). All of the K_v7 subunits form functional homomeric channels, though $K_v7.3$ produces very small currents in its homomeric configuration. Replacing *KCNQ1* C and D helices with *KCNQ3*, allowed the $K_v7.1/3$ chimera to combine with $K_v7.2$, increasing surface expression and current amplitude (Schwake *et al.*, 2003), suggesting that the increased current amplitude seen with $K_v7.2/3$ heteromers is at least partly due to increased surface expression. This hypothesis is supported by the substitution of the D helix of *KCNQ2* with that of *KCNQ1*, this increased surface expression and current of $K_v7.2$ as homomers (Schwake *et al.*, 2003). This is significant because $K_v7.1$ does not heteromerize with the other subunits suggesting that perhaps that helix D in this channel is sufficient to promote full surface expression , but $K_v7.2$ requires $K_v7.3$ to maximise expression.

This specific pattern of co-assembly suggests some key differences in the C-terminus of K_v7 subunits, which are likely found in the C or D helices. Minor Jr. and colleagues

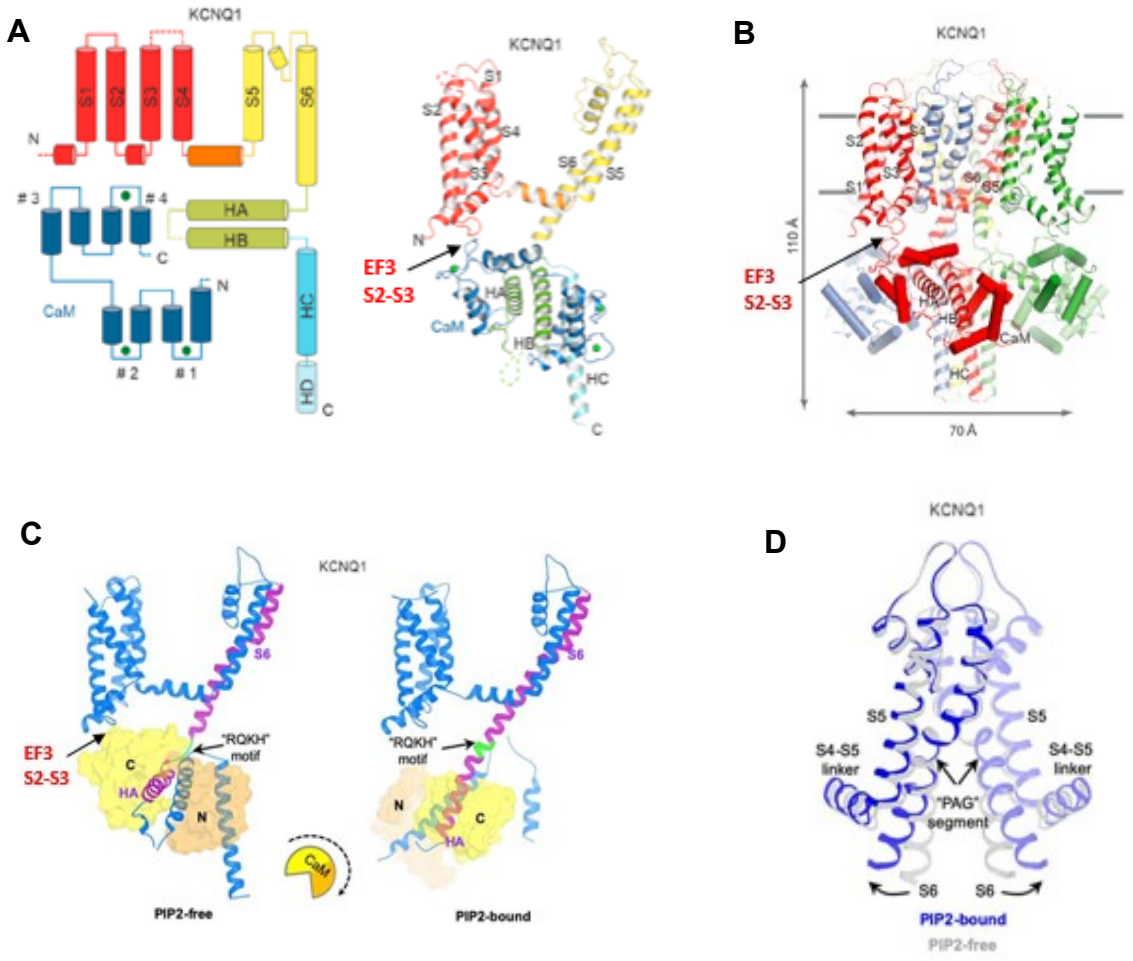

Figure 1.5 K_v7.1 channel structure and binding of critical co-factors. **(A)** Overall channel map and corresponding 3D structure (Sun and MacKinnon, 2017). **(B)** K_v7.1 channel structure with calmodulin bound (red opaque cylinders) (Sun and MacKinnon, 2017). **(C-D)** K_v7.1 channel structure and changes when PIP2 and calmodulin are bound compared to calmodulin alone (Sun and MacKinnon, 2020).

succeeded in solving the crystal structure of the C-terminus of K_v7.4. This data showed the C-terminus to be a double coiled coil structure with some key charged residues present in the D helix. The group mapped the interactions between charged residues in the monomers of K_v7.1-5, showing where the oligmerisation of homomeric channels occurs. K_v7.1, 2, 4 and 5 all have 4-6 electrostatic contacts in the D helix of monomers, creating a stable oligomer. K_v7.3 however, has only 3 electostatic contacts as well as a phenylalanine at position 619 instead of the two closely related amino acids leucine (present in K_v7.1 and K_v7.2) and valine (present in K_v7.4 and K_v7.5). These changes are significant as phenylalanine has a large aromatic residue that valine and leucine do not possess; futhermore the presence of negatively charged amino acids (aspartate 631 and and glutamate 633) in the place of positive residues that are found in other K_v7 channels mean that phenylalanine expands the size of the hydrophobic core thus allowing the negatively charged residues to interupt any electrostatic interactions that may occur (Howard *et al.*, 2007). The result is an unstable formation of K_v7.3 homomers and is likely the explanation for poor currents reported for such channel organisation/orientation (Wang *et al.*, 1998, Zhang *et al.*, 2003). Indeed, mutation of the phenylalanine to leucine resulted in improved tetramisation of K_v7.3 homomers, as did the double electrostatic mutation (D631S/G633E) alone (Howard *et al.*, 2007). As K_v7.3 is able to form heteromers with other K_v7 channels, it is likely that the phenylalanine and D631/G633 residues have no bearing on heteromisation because the large side chain of phenylalanine has less impact if there is only two and the D631/G633 form complementary electroatatic interactions with K_v7.2, but are not with other K_v7.3 subunits (Nakajo and Kubo, 2008). Also, in K_v7.3 homomers, 4 large phenyalanine side chains (one from each monomer) keep the subunits further apart, preventing the formation of a stable homotetrameric structure (Howard *et al.*, 2007).

However, a single alanine to threonine (A315T) in the P loop of K_v7.3 increased current density of homomeric channels 10-fold without effecting surface expression, arguing against a lack of expression resulting in the lack of macroscopic current, but does not argue against unstable homo-tetramer formation (Zaika *et al.*, 2008). There is further evidence to the contrary of surface expression being the reason for low K_v7.3 currents; replacing the C-terminus of K_v7.2 with K_v7.3 did not increase current amplitude despite increasing surface expression when co-expressed with K_v7.3 (Etxeberria *et al.*, 2004). Moreover, mutating the phenylalanine or D631/G633 of *KCNQ3* did not increase

current amplitude, which suggests that the lack of current flowing through $K_v7.3$ homomers is not only due to poor tetramer formation or preventing surface expression but involves some other mechanism (Howard *et al.*, 2007).

As mentioned previously, calmodulin has been shown to be essential for the expression of K_v7 channels but the exact role in this process is currently unclear. Membrane expression relies on a number of complex processes after the translation of the protein such as assembly of the channel through dimerization and tetramerization, release of the subunits in various formations (monomer, dimer, tetramer) from the endoplasmic reticulum (ER), trafficking to and insertion into the membrane. Interupting any one of these processes would reduce surface expression and calmodulin may be important in some or all of these processes. Abolishing calmodulin binding at the A and B helices in $K_v7.2$ resulted in a failure to produce a K^+ current when expressed with $K_v7.3$, despite retaining membrane expression and the ability of $K_v7.2$ or $K_v7.3$ to pull-down the other subunit in co-immunopreciptiation, suggesting no effect on trafficking or assembly (Wen and Levitan, 2002). Calmodulin binding is drastically reduced in the BFNC associated R353G and I340E mutations, which results in the mutant KCNQ2 being retained in the ER. Furthermore, overexpressing the mutant also increased the ER retention of co-expressed wild-type channels. Expression of a dominant-negative calmodulin (no calcium binding ability) caused ER retention of wild-type KCNQ2 as was the case with the non-calmodulin binding mutant KCNQ2, but the retention was far less than with the mutant (Etxeberria *et al.*, 2008). This would suggest that calmodulin binding is required for the channel to exit the ER, but its ability to bind calcium is not essential to this process. Yet mutant $K_v7.2$ membrane expression was not effected when expressed with $K_v7.3$, this discrepency perhaps suggests that the co-assembly of $K_v7.2$ and $K_v7.3$ (Wen and Levitan, 2002) was able to overcome the ER retention of $K_v7.2$ seen when expressed alone (Etxeberria *et al.*, 2008). Helix A leucine (L339R) mutation interupts channel trafficking to the membrane, as current was drastically reduced in the mutant and membrane expression (monitored by the incorporated HA tag immunoreactivity) was reduced. This channel was also tagged with CFP and the CFP co-localised with pDsRed2-ER, used as an ER marker. pDsRed2-ER is a fluorescent vector that includes the ER targeting sequence of calreticulin and KDEL, an ER retention sequence (Alaimo *et al.*, 2009). In co-immunoprecipitation experiments the mutant

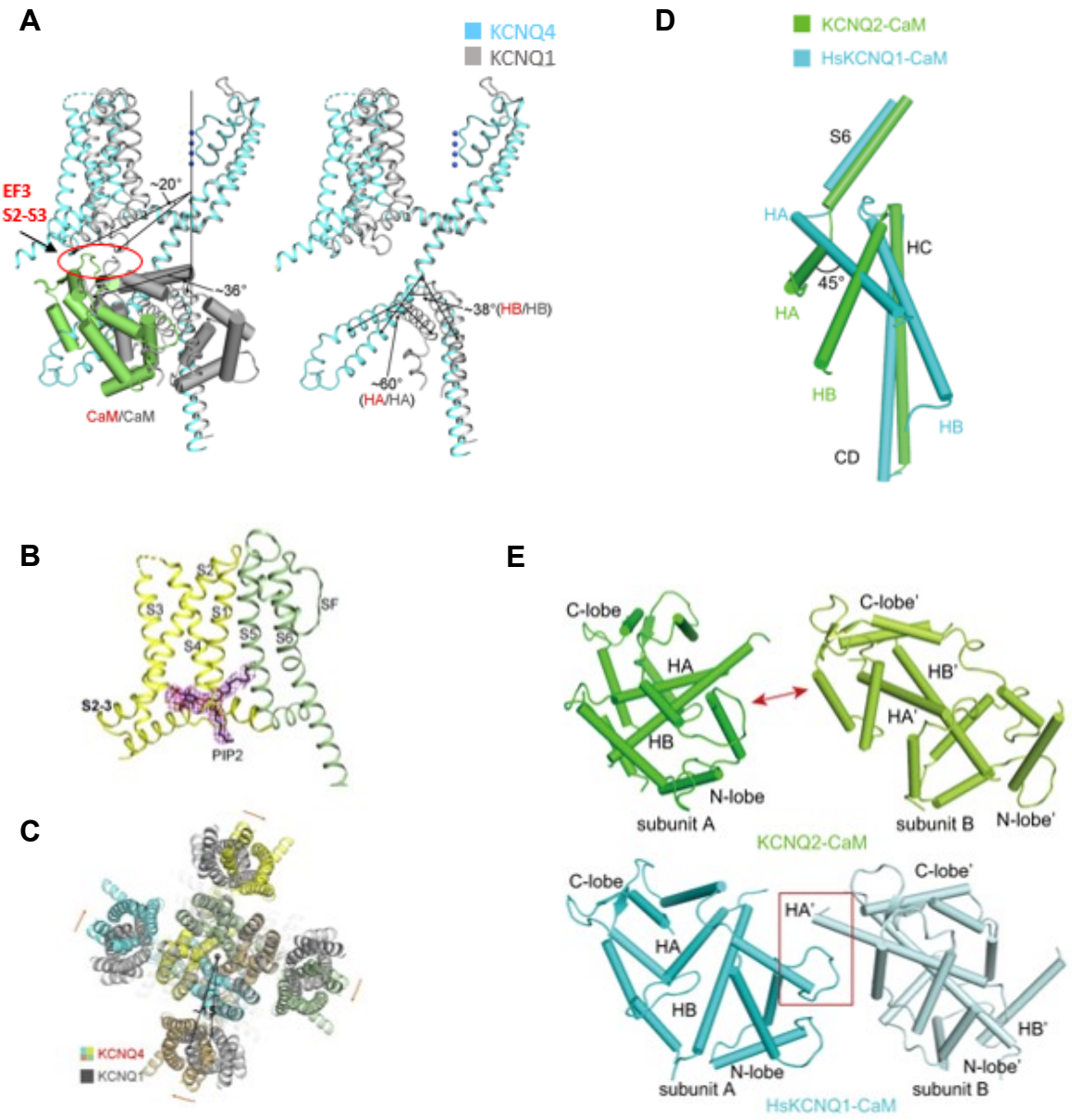

Figure 1.6 $K_v7.2$ and $K_v7.4$ channel structure and binding of critical co-factors. **(A)** Structures of $K_v7.4$ (blue) and $K_v7.1$ (grey), with calmodulin bound. **(B-C)** Binding site for PIP2 between the voltage-sensing domain and pore domain of $K_v7.4$ and the increase in pore radius (C) (Li *et al.*, 2021a). **(D-E)** Calmodulin binding comparison between $K_v7.2$ and $K_v7.1$ (Li *et al.*, 2021b).

$K_v7.2$ failed to pull-down calmodulin suggesting the mutant disrupts calmodulin binding to the channel, resulting in ER retention (Alaimo *et al.*, 2009).

Insights into the role of channel co-factors such as calmodulin are complicated and the apparent differences between K_v7 subunits make understanding of the binding and function of co-factors more difficult. However, recent solving of the cryo-EM structures of $K_v7.1$ (Sun and MacKinnon, 2017), $K_v7.2$ (Li *et al.*, 2021b) and $K_v7.4$ (Li *et al.*, 2021a) allow for comparisons between the structures and binding sites to be made.

The calmodulin binding site is one such example. Sun and KacKinnon initially resolved the cryo-EM structure of $K_v7.1$ with calcium-bound calmodulin interacting with helix A and helix B of the C terminus **(Figure 1.5A-C)** (Sun and MacKinnon, 2017). Later, the structure was solved with PIP2 also bound, which revealed a 180^o rotation of calmodulin and the helices, causing S6 to move to a more open state (Sun and MacKinnon, 2020) **(Figure 1.5C-D)**. This perhaps explaining why calmodulin has opposing effects on different K_v7 subunits, i.e. $K_v7.1$ is activated by calmodulin. In contrast, calmodulin mediates Ca^{2+} inhibition of $K_v7.2$-5, but interestingly, recent solving of $K_v7.2$ and $K_v7.4$ structures confirm that calmodulin is indeed bound to the A and B helices despite differing activity on these channels as compared to $K_v7.1$ **(Figure 1.6A-E)** (Li *et al.*, 2021b, Li *et al.*, 2021a).

However, when calmodulin bound $K_v7.4$ was overlayed with calmodulin bound $K_v7.1$, there was a shift of around 36^o between the two binding sites, which may represent a potentially important difference in the structures **(Figure 1.6A-C)**. Additionally, comparing the interactions between calmodulins and $K_v7.1$ vs. $K_v7.2$ homomeric channels, shows some distance between each calmodulin bound to each of the four $K_v7.1$ subuints, whereas each calmodulin bound to each of the four $K_v7.2$ subunits are in much closer proximity to one another and could be interacting **(Figure 1.6D-E)**. Similarly, the 36^o shift in $K_v7.4$ also brings the calmodulins close together, similar to what was found with $K_v7.2$. This difference may indicate why there is a difference in modulation between $K_v7.1$ and $K_v7.2$-5, as interaction between the four calmodulin proteins may make PIP2 binding more difficult, leading to inhibition, whereas the distance between calmodulin when bound to $K_v7.1$ subunits may facilitate PIP2 binding, thus potentiating the current. The structures also revealed that the third EF hand (EF3), one of the four Ca^{2+} binding domains of calmodulin, is in close proximity

to the S2-S3 linker and recently, this S2-S3 linker-calmodulin EF3 hand interaction has indeed been confirmed, demonstrating a calmodulin binding site on K_V7 channels distinct from the C-terminus **(Figure 1.5A-E)** (Kang *et al.*, 2020).

1.2.6 KCNQ Transcriptional Regulation

Understanding the transcriptional changes, particularly ones encoding proteins controlling excitability, can provide answers regarding the development of both constructive and pathological changes in protein expression that occur during processes such as synaptic plasticity. Identifying the proteins that regulate particular genes can also open up potential therapeutic avenues and help build the puzzle of complex pathological conditions. KCNQs are regulated positively by Sp1 and NFAT and negatively by REST (repressor element 1-silencing transcription factor) (Mucha *et al.*, 2010, Zhang and Shapiro, 2012, Iannotti *et al.*, 2013). REST is generally expressed at very low levels in neurons, this is because it is a transcrption factor that supresses the expression of some neuronal genes in non-neuronal cells, KCNQ genes contain the REST binding motif between exons 1 and 2, suggesting they are surpressed by REST (Mucha *et al.*, 2010). In chronic pain conditions, REST expression increases dramatically in sensory neurons of the DRG (dorsal root ganglia) (Uchida *et al.*, 2010, Rose *et al.*, 2011), which coincides with decrease in *Kcnq2* expression and increased excitability in sensory neurons and with the development of chronic hyperalgesia. Moreover, artificially increasing REST expression is sufficient to induce a chronic pain like phenotype (Zhang *et al.*, 2019). Genetic peripheral sensory neuron knockout of REST abolished the chronic pain associated with inflammatory pain and neuropathic pain (Zhang *et al.*, 2018, Zhang *et al.*, 2019, Zheng *et al.*, 2013). The same REST increase results in a strong downregulation of *Kcnq2* (Rose *et al.*, 2011) and *Kcnq3* (Zheng *et al.*, 2013) and knockout of REST prevented *Kcnq2* downregulation, as well as other genes (Zhang *et al.*, 2019).

NFAT mediated upregulation of *Kcnq2* and *Kcnq3* is dependent upon activity, as activity in hippocampal and sympathetic neurons increases, *Kcnq2* and *Kcnq3* expression is upregulated to protect against overexcitability (Zhang and Shapiro, 2012). Ca^{2+} accumulation in the cell activates calcineurin, a Ca^{2+} dependent phosphatase. Calcineurin dephosphorylates NFAT, allowing NFAT to translocate into the nucleus (Beals *et al.*, 1997) to interact with the NFAT binding motif on *Kcnq2* and *Kcnq3*, increasing expression and I_M (Zhang and Shapiro, 2012).

There is still much more to learn about the interaction between K_v7 channels and transcription factors, but is a promising avenue of research yielding interesting results.

1.3 K_v7 Pharmacology

1.3.1 Non-Selective K_v7 Current Enhancers and Blockers

K_v7 Blockers

TEA (tetraethylammonium) is often used to block K_v channel pores through binding to aromatic residues lining the extracellular portion of the pore (Heginbotham and MacKinnon, 1992). It has been used to analyse the effect of blocking potassium channels on the action potentials of various species from the giant squid to the neurons of aplasia and in mammals (Armstrong 1971, Armstrong and Hille 1972, King and Szurszewski, 1988). However, K_v channel sensitivity to TEA differs and the K_v7 subfamily are no exception. TEA inhibits $K_v7.1$ with an IC_{50} of 5 mM, $K_v7.2$ is the most sensitive to TEA inhibition with an IC_{50} of 0.3 mM, $K_v7.3$ is comparatively insensitive with an IC_{50} of over 30 mM, $K_v7.4$ intermediate with an IC_{50} of 3 mM and $K_v7.5$ by far the least sensitive, with an IC_{50} of 70 mM (Hadley *et al.*, 2000, Schroeder *et al.*, 2000a). $K_v7.2/7.3$ heteromers have an IC_{50} of 3.2-3.8 mM, a sensitivity between that of $K_v7.2$ and $K_v7.3$ homomers (Prole and Marrion, 2004, Hadley *et al.*, 2000). $K_v7.5/7.3$ heteromers are less sensitive to TEA than either homomer, with an IC_{50} of 200 mM (Table 1.1) (Schroeder *et al.*, 2000a). Thus, TEA can be used to differentiate between subunits somewhat, at least $K_v7.2$ or $K_v7.2/7.3$ compared to $K_v7.3$, $K_v7.5$ or $K_v7.5/7.3$.

Chromanol 293B was initially identified as a blocker of I_{Ks} and antiarrhythmic compound before the molecular correlates of the current were fully known (Bosch *et al.*, 1998). It was first suggested to selectively inhibit minK (Busch *et al.*, 1996, Bosch *et al.*, 1998), the name given to KCNE1 when it was still thought to be an ion channel (Takumi *et al.*, 1988). Later work would discover that minK was in fact heterologously expressed KCNE1 (minK at the time) combining with $K_v7.1$ endogenously expressed in Xenopus oocytes, resulting in the formation of $K_v7.1$-KCNE1 complexes (Sanguinetti *et al.*, 1996, Mercer *et al.*, 1997) and therefore chromanol 293B was inhibiting this complex, largely due to its binding to $K_v7.1$, not KCNE1 (Table 1.1) (Lerche *et al.*, 2007) (Lerche *et al.*, 2000b). The binding site for chromanol 293B in $K_v7.1$ has been localised to the inner pore region in the lower portion of the selectivity filter, single point mutations identified isoleucine 337 and phenylalanine 340 at the bottom of the selectivity filter to be critical for chromanol 293Bs channel blocking ability

(Lerche *et al.*, 2007). KCNE1 increases the sensitivity of $K_v7.1$ to chromanol 293B as compared to $K_v7.1$ homomers alone but a binding site for chromanol 293B on KCNE1 was not found, suggesting that KCNE1 facilitates chromanol 293B independently of direct binding (Lerche *et al.*, 2000b).

Selective K_v7 subunit blockers for $K_v7.2$-7.5 are not currently available so the non-selective K_v7 pore blockers, XE-991 and linopirdine are used to reduce K_v7 current. XE-991 is quite non-selective between $K_v7.1$-$K_v7.4$, with IC_{50}s in the range of 1-5 μM (Søgaard *et al.*, 2001b, Wang *et al.*, 2000). $K_v7.5$ is far less sensitive to XE-991 with an IC_{50} of 50-60 μM, co-assembly with $K_v7.3$ rescues sensitivity somewhat (Table 1.1) (Schroeder *et al.*, 2000a, Tsai *et al.*, 2020). Holding cells at -70 mV where K_v7 channel activation is very low, the outward current was unaffected by XE-991, but depolarising to -40 mV or 0 mV, in the presence of XE-991 resulted in the decay of outward current over 20 seconds, in contrast, the current was maintained in the absence of XE-991. Linopirdine had a similar effect but with a more pronounced decrease in the initial amplitude upon depolarisation (Greene *et al.*, 2017). This suggests that these compounds bind and block the channel in its open state not closed, this is consistent with XE-991 becoming trapped in the pore blocking it. Although XE-991 has not been directly shown in its binding site, Li and colleagues recently solved the structure of $K_v7.4$ with linopirdine bound deep in the pore, blocking it up **(Figure 1.7C)** (Li *et al.*, 2021a).

Table 1.1: K_v7 Channel Blockers

Compound	K_v7 channel selectivity	Binding site	Mode of action	Non-selective effects
Blockers				
TEA	$K_v7.2$> $K_v7.4$> $K_v7.2/7.3$>$K_v7.1$> $K_v7.3$> $K_v7.5$> $K_v7.3/5$	Extracellular pore lining aromatic residues	Pore blocker	Most voltage-dependent potassium channels
Chromanol 293B	$K_v7.1$/KCNE1> $K_v7.1$	Inner pore region	Pore blocker	
Linopirdine XE-991	$K_v7.1$≈$K_v7.4$> $K_v7.5$	Deep inner pore region	Pore blocker	Not reported
Ssm Spooky toxin (SsTx) from centipede venom	Non-selective $K_v7.1$-5	Aspartate residues lining the outer pore region	Pore blocker	Not reported

K_v7 Current Enhancers

Triaminopyridines

The prototypic K_v7 potentiators, retigabine and flupirtine are triaminopyridine class compounds that non-selectively bind to the pore region of $K_v7.2$-$K_v7.5$ but not $K_v7.1$. Both compounds are almost identical, only differing by the presence of a nitrogen in the phenyl aromatic ring of flupirtine and both significantly potentiate K_v7 current through a negative shift in voltage-dependence and augmenting macroscopic conductance. The hyperpolarising shift in voltage-dependence elicited by retigabine was most striking in $K_v7.3$ channels, followed by $K_v7.2/7.3$, $K_v7.2$ and $K_v7.4$ (Tatulian *et al.*, 2001a). *Kcnq5* had only recently been cloned at the time so was not directly compared but later studies show responses of $K_v7.5/7.3$ heteromers to be similar to that of $K_v7.2/7.3$ heteromers and $K_v7.5$ homomer responses to be akin to $K_v7.4$ homomers (Wickenden *et al.*, 2001, Schenzer *et al.*, 2005a). Mutating tryptophan, a large aromatic amino acid at position 265 in the cytosolic pore-region of *KCNQ3* to a leucine, a smaller aliphatic but still hydrophobic amino acid, abolished retigabine sensitivity. Mutating the corresponding tryptophan in *KCNQ2* (W236), *KCNQ4* (W242) and *KCNQ5* (W235) also abolished retigabine sensitivity in the homomeric channels (Schenzer *et al.*, 2005a). Thus, it seems this tryptophan is crucial for retigabine binding affinity in K_v7 channels. Supporting this notion, replacing the leucine in $K_v7.1$ that corresponds to the tryptophan in the other subunits, with a tryptophan (L266W) converted $K_v7.1$ homomers from retigabine insensitive to retigabine sensitive (Schenzer *et al.*, 2005a).

Employing a strategy whereby *KCNQ3* chimeras with the inner pore of *KCNQ1*, thus retigabine insensitive, was used to determine other residues important for retigabine sensitivity. This was achieved by identifying the amino acids that were not conserved between $K_v7.3$ and $K_v7,1$ in this area and mutating those amino acids in the chimeras back to the amino acid present in $K_v7.3$ in various combinations (Lange *et al.*, 2009). In this way, in addition to tryptophan 265, a number of leucine's in close proximity to each other on S5 and Leucine 338 of the S6 domain of the adjacent subunit were identified that form a hydrophobic pocket with the crucial tryptophan at the top of the pocket that holds retigabine (Lange *et al.*, 2009). The cryo-EM structure of $K_v7.2$ also suggests four residues that are critical for the ability of retigabine to stabilize the channel in the open conformation **(Figure 1.7A)** (Li *et al.*, 2021b). Rather than just

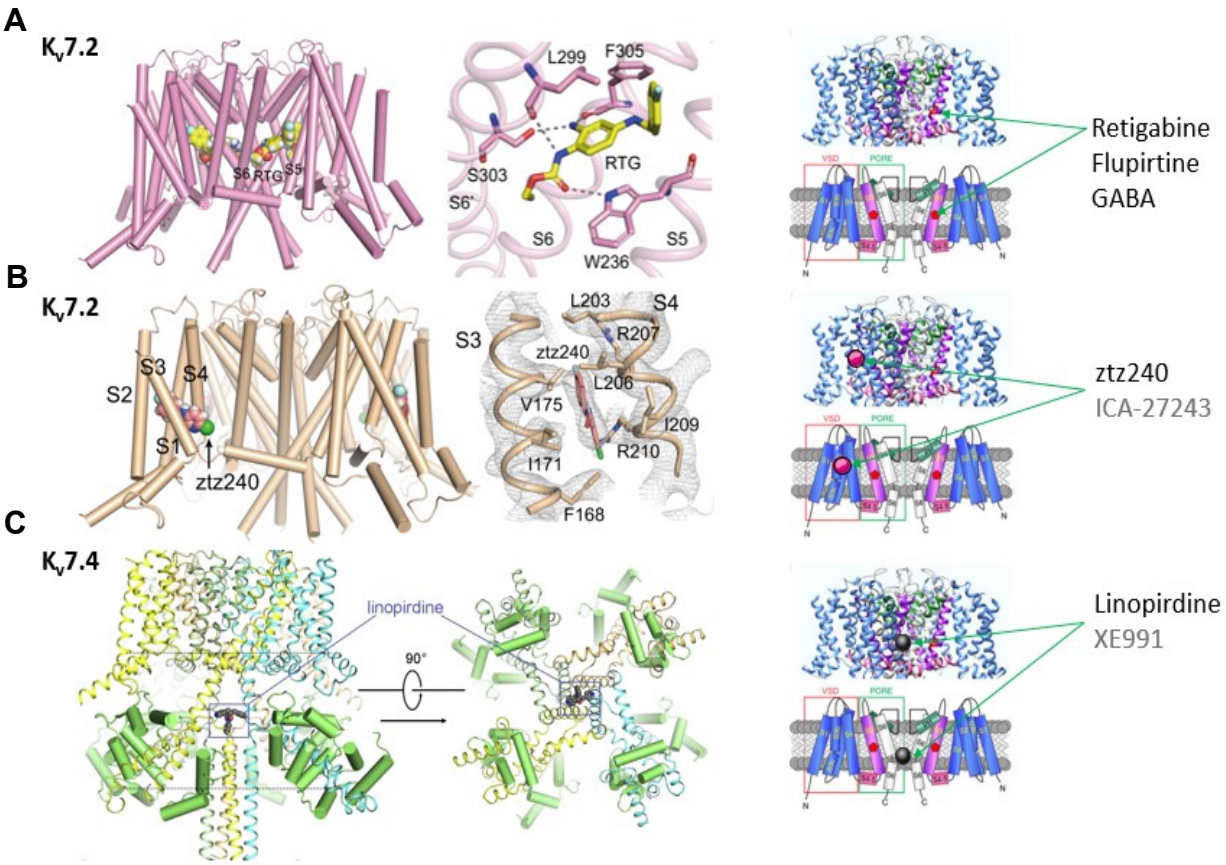

Figure 1.7 Binding sites for K_v7 channel potentiators and blockers. **(A)** Cryo-EM structure of a $K_v7.2$ channel with retigabine bound to a pore region binding pocket (Li *et al.*, 2021b). **(B)** Cryo-EM structure of a $K_v7.2$ channel with ztz240 bound to a binding pocket in the voltage sensing domain (Li *et al.*, 2021b). **(C)** Cryo-EM structure of a $K_v7.4$ channel with Linopirdine blocking the pore (Li *et al.*, 2021a). Grey text indicates compounds that may share the same binding site due to being analogues but have not previously been shown to bind at the same site (ICA-27243 and XE-991). Right panels adapted from (Manville *et al.*, 2018).

tryptophan, there are nine residues directly interacting with retigabine, four of which are not conserved in $K_v7.1$, including the tryptophan. The cryo-EM structure of $K_v7.2$ with retigabine bound suggests that retigabine simply stabilises the open state by just pushing the S5 and S6 from the neighbouring subunit apart by nearly 2 Angstroms (Å), the tryptophan aromatic side chain is also moved out by 2 Å when retigabine is in that space **(Figure 1.7A)** (Li *et al.*, 2021b).

In single-channel recordings of $K_v7.2/7.3$ heteromeric channels expressed in Chinese hamster ovary (CHO) cells, retigabine increased open probability by around 4-fold without increasing single-cell conductance through the channel (Tatulian and Brown, 2003). Thus, retigabine increases macroscopic current through stabilising the channel in the open conformation, increasing the length of time the channel remains open.

The specificity of flupirtine and retigabine has been called into question, particularly with evidence suggesting both compounds increase GABAa receptor response to GABA application (van Rijn and Willems-van Bree, 2003, Klinger *et al.*, 2012). Though this observation often requires 10-fold higher concentrations of flupirtine or retigabine than the 1-3 μM free drug concentration in the plasma after administration of therapeutic doses (Gunthorpe *et al.*, 2012) suggesting its effect on GABAa channels to be minimal during treatment. Evidence for direct binding of retigabine to GABAa channels is limited so the binding site is unclear and potential candidate sites have not been alluded to. However, retigabine and GABA share a site of negative electrostatic potential near to a carbonyl atom, this shared feature allows GABA to bind to the tryptophan of K_v7 channels (discussed in 1.3.3) (Manville *et al.*, 2018). By the same logic, it is possible that retigabine can bind to the GABA binding site on GABAa channels, but this is yet to be demonstrated.

Clinically, flupirtine was approved and used as a non-opioid, centrally active post-operative analgesic from 1984 and retigabine initially approved for epilepsy (Stafstrom 2011). Progressively, their uses have been more and more limited, with both compounds now discontinued in the US (Clark *et al.*, 2015, Harish *et al.*, 2012). Though several countries such as India still use flupirtine for post-operative pain and is making a resurgence as a potential treatment for fibromyalgia (Lawson K *et al.*, 2021). The limited use of these drugs is largely due to the poor risk/benefit ratio, particularly bladder retention, sedation and motor impairment, with bladder retention

and blue skin discoloration being the main clinical complaints with retigabine and liver damage with flupirtine (Clark *et al.*, 2015, Harish *et al.*, 2012). These side effects have the same mechanism, as oxidation of both produces electrophilic quinone metabolites. It has been suggested that the quinone metabolite from flupirtine interacts with liver enzymes whereas the retigabine metabolite can dimerize to hydrophenazine, oxidising melanin-like structures, resulting in blue colouration (Bock *et al.*, 2019). By introducing a sulphide bridge this reduced the likelihood of oxidation of the aromatic ring, instead oxidising the compound to a non-electrophilic metabolite (Bock *et al.*, 2019). Producing analogous compounds with adjustments like this may lead to a resurgence in clinical viability of triaminopyridines.

Despite the low clinical viability, flupirtine and retigabine are frequently used as powerful research tools, with retigabine being extensively used in pain models of inflammatory pain, including carrageenan, bradykinin and complete Freund's adjuvant in both systemic and local applications (Passmore *et al.*, 2003, Liu *et al.*, 2010, Hayashi *et al.*, 2014). Retigabine is also effective in alleviating visceral pain induced by intracolonic injection of capsaicin, joint pain and bone cancer pain and trigeminal neuropathy (Hirano *et al.*, 2007, Xu *et al.*, 2010, Zheng *et al.*, 2013, Du *et al.*, 2018). In addition, many of the studies examining expression of K_v7 channels or assessing the role of K_v7 channels in pathological conditions, use application of retigabine or flupirtine to identify K^+ currents sensitive to these compounds and observe changes in the pathological state as a result of these K_v7 potentiators.

Acrylamides

Acrylamides are another class of K_v7 modulating compounds developed by Bristol-Myers Squibb, generally referred to as BMS- or an 'S' compound. The first, S-1 produced a hyperpolarising shift in voltage-dependence of $K_v7.2$, $K_v7.2/7.3$, $K_v7.4$ and $K_v7.5$ and increased whole-cell current amplitude in all subunits, though overall efficacy of S-1 was higher in $K_v7.4$ and $K_v7.5$ (Bentzen *et al.*, 2006). In contrast, $K_v7.1$ was strongly inhibited by S-1, this inhibition was largely removed by $K_v7.1$ co-assembly with KCNE1. The same tryptophan that is required for triaminopyridine action is also critical for the action of S-1 on $K_v7.2$-5 (Bentzen *et al.*, 2006). Although, the recent structure of $K_v7.2$ bound to retigabine suggests the tryptophan side chain is important for opening a space for retigabine to fit, so is likely similar for S- compounds (Li *et al.*, 2021b). Acrylamides are also effective as analgesics in persistent, difficult to treat pain

models. The effect of acrylamide on persistent, non-neuropathic pain was assessed with a formalin injection into rat hindpaw and compared against the analgesic gabapentin. Acrylamide was effective at reducing nocifensive behaviour in the acute pain phase (Phase 1) and in the persistent pain phase (Phase 2) of the formalin injection. Phase 2 is induced by tissue damage and neuromodulator release, gabapentin was only effective during this phase (Wu *et al.*, 2013). Similarly, acrylamide was effective in reducing pain sensitivity in streptozotocin-induced diabetic neuropathy and neuropathy caused by ligation of L5 and L6 spinal nerves. Interestingly, the analgesic effect of acrylamide occurred sooner than gabapentin but decayed also sooner (Wu *et al.*, 2013). An overview of these compounds is provided in Table 1.2.

1.3.2 Selective K_v7 Current Enhancers

Benzamides

Benzamides are a class of K_v7 potentiators selective for $K_v7.2/7.3$ heteromers and $K_v7.2$ homomers over all other K_v7 subunits (Table 1.2). The compound ICA-27243 (ztz233) potentiates $K_v7.2/7.3$ and $K_v7.2$ channels with comparable efficacy to retigabine at somewhat higher concentrations, but only moderately potentiates $K_v7.4$ currents at 10-fold higher concentrations and is ineffective on $K_v7.5/7.3$ heteromers or $K_v7.3$ homomers (Wickenden *et al.*, 2008, Padilla *et al.*, 2009). As ICA-27243 binds on the intracellular side of the channel under the S3-S4 regions, it is suggested that ICA-27243 binds in this area when the channel is open and the S4 region has moved towards the extracellular space, stabilising the open state, therefore is best described as a K_v7 potentiator, as change in voltage causes the initial activation of the channels (Wickenden *et al.*, 2008, Padilla *et al.*, 2009, Li *et al.*, 2021b). ICA-27243 also did not potentiate GABA currents like some have suggested with retigabine (Wickenden *et al.*, 2008). A similar compound to ICA-27243, ztz240 has a similar structure and binding site but different specificity. Ztz240 is reported as potentiating $K_v7.2$ homomers, $K_v7.2/7.3$ heteromers, $K_v7.4$ and $K_v7.5$ over $K_v7.1$ and $K_v7.3$ homomers, demonstrated by increased current (highest in $K_v7.5$, similar in $K_v7.4$ and $K_v7.2/7.3$ and lowest with $K_v7.2$) and a polarising shift in voltage-dependence not seen in $K_v7.1$ and $K_v7.3$ (Gao *et al.*, 2010). Both compounds were shown to bind in the voltage-sensing domain of K_v7 channels (Padilla *et al.*, 2009, Gao *et al.*, 2010). Based on their very similar structure (ztz240 has one less fluorine than ICA-27243) they may bind to similar places in the voltage sensor, though difference in specificity for individual

subunits may suggest otherwise. Some clarity has been provided in the solving of K_v7.2 structure with ztz240 bound **(Figure 1.7B)**. The high density between the S3 and S4 regions suggests this is the main binding site for ztz240 in the charge transfer centre. There also seems to be direct hydrophobic interactions with arginine 207 and arginine 210 on S4, which are positively charged residues involved in the movement of S4 **(Figure 1.7B)** (Li *et al.*, 2021b). The resultant conformational change is a 2-5 Å shift towards S5. When the S4 is in the up position, opening the channel, ztz240 fits between S3 and S4, holding the S4 in the up position, stabilising the open state, this also provides support for these compounds as potentiators **(Figure 1.7B)** (Li *et al.*, 2021b).

ICA-27243 protected against electroshock and pentylenetetrazole (PTZ) induced seizures in mice and rats by increasing the latency until seizure onset after injection, with motor impairment only becoming a factor above four times the efficacious seizure dose. Negative effects on cognition were minimal since rats and mice were still able to learn and remember where the platform was in the Morris water maze (Roeloffs *et al.*, 2008). The compound has also been studied to some extent as an analgesic and is comparably effective to retigabine when administered orally against an inflammatory injection of complete Freund's adjuvant (CFA) but with less motor impairment at analgesic concentrations. Interestingly, injection of XE-991 centrally alleviated motor impairment and sedation but was not very effective at blocking the analgesic effect of ICA-27243 or retigabine, suggesting this aspect was dependent on peripheral K_v7 channels (Du *et al.*, 2018).

After ICA-27243 resulted in liver toxicity during prolonged treatment, ICA-069673 was synthesised as an analogue to recreate the selective effect of ICA-27243 without the toxicity. The two compounds differ only in the presence of a nitrogen in one aromatic ring of ICA-069673 replacing a carbon in ICA-27243 but ICA-069673 is a less potent potentiator of K_v7.2/7.3 than ICA-27243. Despite this, the EC50 of ICA-069673 is still around 1 μM and 10-fold more selective for K_v7.2/7.3 over K_v7.5/7.3 and was not effective at potentiating K_v7.1 current (Amato *et al.*, 2011). Therefore was deemed a K_v7.2/7.3 selective potentiator (Amato *et al.*, 2011) as has been used as such since. However, the initial work did not assess K_v7.2, K_v7.3, K_v7.4 and K_v7.5 homomers, this is significant because ICA-27243 does have some effect on K_v7.4 but at 10-fold higher concentrations (Table 1.2). When later analysed by Brueggemann and colleagues,

$K_v7.4$ was potentiated by 1 μM ICA-069673, $K_v7.5$ was not affected and $K_v7.4/7.5$ heteromers responded but at higher concentrations than $K_v7.4$ homomers (Brueggemann *et al.*, 2014a). This is important because tissues that may express $K_v7.4$ but not necessarily $K_v7.2/7.3$ would still respond to ICA-069673 and may result in less accurate identification of the subunits responsible. Indeed, $K_v7.2/7.3$ channels have been suggested to be involved in the contractility of detrusor smooth muscle, based on the relaxing response of the smooth muscle cells to ICA-069673 (Provence *et al.*, 2015b). However, it is more widely known that $K_v7.4$ and $K_v7.5$ are involved in controlling contractility in smooth muscle cells and are highly expressed in detrusor smooth muscle (Seefeld *et al.*, 2018, Bientinesi *et al.*, 2017, Tykocki *et al.*, 2019). Therefore, it is possible that the effects of ICA-069673 were due to potentiation of $K_v7.4$ rather than $K_v7.2/7.3$, or as well as.

$K_v7.4$ and $K_v7.5$ Selective Compounds

Selective openers/potentiators for $K_v7.4$ and $K_v7.5$ are far more limited than for $K_v7.2/7.3$, however, some target candidates have been identified that are discussed here. Fasudil is a Rho kinase inhibitor that prevents the phosphorylation of Rho GTPases that breakdown GTP. Clinically, Rho kinase inhibitors are used to treat hypertension, glaucoma and urothelial cancer (Moshirfar *et al.*, 2018, Abe *et al.*, 2014). More recently, Zhang and colleagues discovered that Fasudil increased current in $K_v7.4$ and $K_v7.4/7.5$ heteromers similar to retigabine but was ineffective against $K_v7.2$ or $K_v7.2/7.3$ heteromers, even at 100-fold higher concentrations than the EC_{50} on $K_v7.4$ channels (Table 1.2) (Zhang *et al.*, 2016b). The EC_{50} of fasudil on $K_v7.4$ and $K_v7.4/7.5$ were similar, suggesting no selectivity between the homomer and heteromer. The IVs only saw a minor polarising shift in voltage-dependence but whole-cell conductance was strongly potentiated suggesting that fasudil does not affect voltage-dependence but does increase open probability. Individual point mutations of the amino acids that differ between $K_v7.2$, $K_v7.3$ and $K_v7.4$, $K_v7.5$ in the pore region of the channels reduced the current produced by fasudil application in five of the mutations, of which valine-248, leucine 306 and isoleucine 308 mutations, abolished the effect of fasudil (Zhang *et al.*, 2016b). This is taken to mean that this area is important for the efficacy of fasudil and may indicate the binding site, though this is not confirmed by these experiments as the mutations may impact efficacy but not affinity of the compound.

Table 1.2: K_v7 Channel Potentiators

Compound	K_v7 channel selectivity	Binding site	Mode of action	Non-selective effects
Potentiators				
Triaminopyridines				
Retigabine	Non-selective for $K_v7.2$-$K_v7.5$ $K_v7.1$ insensitive	Tryptophan 236	Potentiator Stabilises the pore in the open state by binding in the pore	GABA at 10-fold higher concentrations than plasma concentration
Flupirtine	Non-selective for $K_v7.2$-$K_v7.5$ $K_v7.1$ insensitive	Tryptophan 236	Potentiator Stabilises the pore in the open state by binding in the pore	GABA at 10-fold higher concentrations than plasma concentration
Acrylamides (BMS/S compounds)	$K_v7.4 \approx K_v7.5 >$ $K_v7.2 \approx K_v7.3$ Inhibited $K_v7.1$ current	Tryptophan 236	Potentiator Stabilises the pore in the open state by binding in the pore	Not reported
Benzamides				
ICA-27243 (ztz233)	$K_v7.2/7.3 > K_v7.2 > K_v7.4$ (10-fold higher) $K_v7.1$, $K_v7.3$, $K_v7.5$ insensitive	Intracellular S3-S4 region	Potentiator Stabilises channel in the open state via voltage sensor	Not active against GABA receptors
ICA-069673	$K_v7.2/7.3 \geq K_v7.4 >$ $K_v7.3/7.5$ $K_v7.1$ inhibited	Intracellular S3-S4 region	Potentiator Stabilises channel in the open state via voltage sensor	Effect on GABA receptors not reported
Ztz240	$K_v7.5 > K_v7.4 \approx K_v7.2/7.3 >$ $K_v7.2$ $K_v7.1$ and $K_v7.3$ insensitive	Intracellular S3-S4 region	Potentiator Stabilises channel in the open state via voltage sensor	Not active against GABA receptors
Fasudil	$K_v7.4 \approx K_v7.4/7.5$ $K_v7.5$ not tested $K_v7.2$, $K_v7.3$ insensitive	Possibly pore region. V248, L306 and I308 critical for effect but not a confirmed binding site	Potentiator Mechanism not yet known	Rho kinase (inhibits)
10g	$K_v7.4 > K_v7.5$ $K_v7.1$, $K_v7.2$, $K_v7.3$ $K_v7.2/7.3$ insensitive	Not reported	Not reported Retigabine derivative so possibly similar	Not reported
Go-Slo-SR	Non-selective for $K_v7.2$-$K_v7.5$	Not reported But interacts with the S4-S5 linker on BK channels	Not reported	BK channels (potentiates)

Unfortunately, the relative contribution of $K_v7.5$ to the efficacy of fasudil in the heteromer remains unknown, as $K_v7.5$ homomeric channels were not assessed against the effect of fasudil. Thus, no claims can be made about the effect of fasudil on $K_v7.5$ or $K_v7.5/7.3$ channels. Fasudil has since been used to study the effect of $K_v7.4$ in dopaminergic-related disorders in the brain such as depression (see section 1.5.4) and the vasorelaxant effect of fasudil seen clinically is mediated at least in part by activation of $K_v7.4/7.5$ channels, with application of XE-991 attenuating the vasorelaxant effect of fasudil (Zhang *et al.*, 2016b). Similarly, the compound 10g, a retigabine analogue also displays remarkable specificity for $K_v7.4$ and $K_v7.5$ homomers over $K_v7.2$ and $K_v7.3$ or $K_v7.2/7.3$ channels, providing a K_v7 enhancer with utility in studying $K_v7.4$ and $K_v7.5$ (Wang *et al.*, 2019). However, their utility in endogenous systems has not been assessed. Interestingly, the compound GoSlo-SR exerts a multi-channel effect, it is a potent BK channel activator that also potentiates $K_v7.4$ and $K_v7.5$ currents when the subunits are expressed in HEK293 cells (Table 1.2) (Webb *et al.*, 2015, Zavaritskaya *et al.*, 2020). In endogenous arterial smooth muscle cells, GoSlo-SR produces strong vasorelaxant through the combination of BK and K_v7 activation (Zavaritskaya *et al.*, 2020).

It is evident that selective compounds are beginning to emerge and aid in separating the contribution of different K_v7 subunits to the K_v7 current in various cell types and are promising avenues for more targeted therapies.

1.3.3 Other modulators of K_v7 Channels

Many of the anti-inflammatory NSAIDs are inhibitors of cyclooxygenases COX-1 and COX-2, discussed in section 1.7. These include fenamates such as diclofenac and meclofenamic acid and other NSAIDs, paracetamol and celecoxib. Diclofenac is a selective potentiator for $K_v7.2/7.3$ channels, with an EC_{50} of 2.6 μM, in contrast, the EC_{50} of $K_v7.4$ is 100 μM and $K_v7.5$ is inhibited by diclofenac (IC_{50} of 20 μM) (Peretz *et al.*, 2005, Brueggemann *et al.*, 2011). The effect of diclofenac on $K_v7.4/7.5$ channels therefore equates to nothing, with a small inhibitory effect at concentrations exceeding 100 μM (Brueggemann *et al.*, 2011). Increase in whole-cell $K_v7.2/7.3$ current was accompanied by a hyperpolarising shift in voltage-dependence, similar to NH6 and NH29, two compounds designed from the same core structure as diclofenac but without the ability to inhibit COX1 or COX-2 (Peretz *et al.*, 2007, Peretz *et al.*, 2010). The plasma concentration of orally administered diclofenac peaks around 5 μM which

is within the range of $K_v7.2/7.3$ potentiation but suggests the effect on $K_v7.4$ and $K_v7.5$ is less relevant under therapeutic conditions. Celecoxib is used clinically as a more selective COX-2 inhibitor to reduce the gastrointestinal side effects of non-selective compounds. Contrastingly to fenamates, celecoxib potentiates K_v7 subunits non-selectively with the exception of a lack of effect on $K_v7.3$ and inhibition of $K_v7.1$ channel (Du *et al.*, 2011). In relation to $K_v7.2$, $K_v7.4$ and $K_v7.5/7.3$, celecoxib has a comparable EC_{50} between 2-4 μM (Du *et al.*, 2011), this is significant, as the plasma concentration of celecoxib has been measured at an average of 1.6 μM, suggesting the effect on K_v7 channels may contribute to the therapeutic effect of diclofenac but to a lesser extent than with diclofenac. Interestingly, the initial identification of celecoxib as a K_v7 enhancer was on $K_v7.5$ in smooth muscle (Brueggemann *et al.*, 2009). This initial study by Brueggemann and colleagues, conducted on smooth muscle cells, concluded that diclofenac was not effective against K_v7 channels, this is consistent with the reports above in that diclofenac is selective for $K_v7.2/7.3$ channels, but not for $K_v7.5$. $K_v7.2$ and $K_v7.3$ are not well expressed in smooth muscle and the 20 μM concentration of diclofenac used in that study would not have been sufficient to potentiate the $K_v7.4$ subunits in the smooth muscle. Yet, later, the same group showed a 50% inhibition of $K_v7.5$ channels with the same concentration of diclofenac (Brueggemann *et al.*, 2009, Brueggemann *et al.*, 2011). This apparent discrepancy may be due to smooth muscle cells expressing mostly $K_v7.4/7.5$ heteromers, which were not affected by 20 μM diclofenac, only inhibited with over 100 μM (Brueggemann *et al.*, 2011).

Paracetamol is also a COX-1 and COX-2 inhibitor and one of the most widely used pain killers for mild to moderate pain. It is heavily metabolised, with around 15% being metabolised through the cytochrome P450 pathway, this fraction is the cause of hepatotoxicity in paracetamol overdose through the metabolite N-acetyl-p-benzoquinone imine (NAPQI) (McGill and Jaeschke, 2013). NAPQI, but not unmetabolized paracetamol, potentiated XE-991 sensitive (presumed K_v7) current in DRG neurons and in the dorsal horn of the spinal cord and abolished the inhibitory effect of bradykinin (Ray *et al.*, 2019). Recombinantly expressed $K_v7.2/7.3$ channels were also potentiated by NAPQI, supporting the idea that the K^+ current potentiation in DRG and dorsal horn neurons is due to $K_v7.2/7.3$ channel activation (Table 1.3) (Ray *et al.*, 2019). Paracetamol has a plasma concentration of over 66 μM, as 15% of this is metabolised to NAPQI, the plasma concentration of NAPQI is around 10 μM.

Therefore, as NAPQI was effective at potentiating $K_v7.2/7.3$ current at 1-10 μM, it is likely that some of the therapeutic effect of paracetamol can be attributed to $K_v7.2/7.3$ potentiation. Preliminary evidence suggests that the site of action of NAPQI is a triple cysteine pocket in the intracellular S2-S3 linker loop (Salzer *et al.*, 2020). The effect is likely mediated by oxidation of the cysteines resulting in channel activation. The reasoning for this is that $K_v7.1$ lacks the triple cysteine sequence and was not responsive to NAPQI (Salzer *et al.*, 2020) and hydrogen peroxide (H_2O_2) and ascorbic acid (vitamin C) have long been known to activate K_v7 channels (but not $K_v7.1$) by oxidative modification of the triple-cysteines in the S2-S3 linker (Gamper *et al.*, 2006, Linley *et al.*, 2012, Gao *et al.*, 2017). H_2O_2 also reduced action potential firing in sympathetic neurons, though, H_2O_2 and other reactive oxygen species are released from the mitochondria during cell death and neurodegeneration (Gamper *et al.*, 2006) so is not a viable therapeutic target, but other compounds with the same mechanism of action such as NAPQI, clearly are.

The critical tryptophan required for retigabine sensitivity of K_v7 channels is highly conserved but has no obvious physiological role, Manville and colleagues hypothesised that the tryptophan could be a chemosensor for endogenous ligands, thus reviewed the chemical structure of retigabine versus endogenous ligands (Manville *et al.*, 2018). This screen showed that GABA shared a similar region with a negative electrostatic potential near a carbonyl oxygen, a feature not shared by glutamate. Application of GABA to K_v7 expressing oocytes strongly potentiated $K_v7.3$ and $K_v7.5$, even down to 100 nM GABA in the case of $K_v7.5$. $K_v7.2$ showed some response to higher concentrations of GABA and $K_v7.4$ and $K_v7.1$ did not respond (Table 1.3). The lack of effect on $K_v7.1$ is not surprising as it lacks the critical tryptophan, but there is clearly specificity for potentiation of $K_v7.3$ and $K_v7.5$ despite the affinity of GABA for $K_v7.2$-5 (Manville *et al.*, 2018). $K_v7.2/7.3$ heteromers were also potentiated by GABA, an effect drastically reduced by mutating the tryptophan but not effected by using a GABAB GPCR agonist, suggesting that the potentiation is due to direct binding of GABA to K_v7 channels via the tryptophan, not GPCR modulation **(Figure 1.7A)** (Manville *et al.*, 2018). Despite the discovery that GABA potentiates K_v7 channels via binding to the same site as tryptophan, it is unclear how GABA can reach this site, which is inside the pore of the channel. Retigabine is a small molecule that can cross the membrane to bypass the selectivity filter, GABA is not membrane

permeable, so the question remains as to how GABA accesses the binding site. One likely possibility, at least in DRG neurons, is the presence of GAT GABA transporters in the membrane that transport GABA into the neuron (Du *et al.*, 2017). Allowing GABA to enter the channel pore via the intracellular space as retigabine can.

GABA metabolites, β-hydroxybutyric acid (BHB) and γ-amino-β-hydroxybutyric acid (GABOB) also potentiated K_v7.3 current, albeit at a far lower efficacy (Manville *et al.*, 2018). Interestingly, using the same screening approach for the active components of the *Mallotus oppositifolius* shrub, a herb used as a herbal remedy for seizures, identified a number of chemicals that could bind and activate K_v7 channels (Manville and Abbott, 2018). Both, mallotoxin (MTX) and isovaleric acid (IVA) potentiated K_v7.2/7.3 channels somewhat but not strongly, in silico docking of these chemicals suggested that both would interact in the same hydrophobic pocket as retigabine, where tryptophan is important, but neither chemical alone fit the docking site as retigabine or GABA did. However, docking MTX and IVA together had similar interactions to retigabine and GABA, application of MTX and IVA potentiated K_v7 channels significantly more than either chemical applied alone (Manville and Abbott, 2018). This suggests that chemicals can act on ion channels synergistically and that there are naturally occurring modulators of K_v7 channels.

In the same vein, it was recently discovered that centipede venom blocks K_v7 channels to kill prey. The venom is effective at killing animals more than 10 times the size of the centipede in 30 seconds by simultaneous disruption of the nervous, muscular, respiratory and cardiovascular system… sounds like a K_v7 expression pattern. Ssm Spooky toxin (SsTx) was identified as a key toxin in causing such rapid lethality, it also inhibited K_v7.1, 2, 4 and 5 current when the channels were expressed in HEK293 cells in a dose-dependent and remarkably non-selective manner (Table 1.1) (Luo *et al.*, 2018). Mutating a group of positively charged residues on SsTx significantly attenuated its inhibitory effect on K_v7.4, similarly, mutating two negatively charged aspartate residues near the outer-pore region of K_v7.4 also abolished inhibition by SsTx in the absence of any effect on voltage-dependence of the channel (Luo *et al.*, 2018).

Systemic injection of SsTx alone resulted in vasospasm and hypertension and myocardial ischemia in the cardiovascular system in mice and reduced breathing rate

and bronchial ring contraction in the respiratory system in rats, whereas centipede venom without SsTx only caused mild cardiovascular disruption in mice and *Macaca* monkeys (Luo *et al.*, 2018). The group conducting the study state that SsTx does not cross the blood brain barrier, no direct evidence for this is presented and was not clearly available in related literature, but assuming this is the case, SsTx is likely not involved in the central effects of systemic delivery of SsTx in centipede venom. However, a centipede can penetrate the skull of small animals and indeed administering SsTx locally to the hippocampus of mice resulted in instantaneous seizure activity and mortality (Luo *et al.*, 2018).

Retigabine administration was effective in reversing the vascular, respiratory and seizure effects of SsTx. It also prevented the inverted T wave in the cardiac action potential that results in myocardial ischemia, meaning that this effect is not due to $K_v7.1$ (Luo *et al.*, 2018). Importantly, retigabine was also effective in reversing the cardiovascular and respiratory effects of the unaltered venom, not just SsTX. The effectiveness of retigabine suggests it may be a potential emergency antidote for people bitten by centipedes, which is a cause of concern in places such as Hawai'i and can be fatal (Guerrero, 2007).

Table 1.3: Atypical K_v7 Channel Potentiators

Compound	K_v7 channel selectivity	Binding site	Mode of action	Non-selective effects
Compounds previously identified as potentiators of other proteins				
Diclofenac	$K_v7.2/7.3$ selective 100-fold less sensitive for $K_v7.4$ Inhibits $K_v7.5$	Not reported	Potentiator	COX-1 and COX-2
Celecoxib	Non-selective between $K_v7.2$, $K_v7.4$ and $K_v7.5$ $K_v7.3$ insensitive $K_v7.1$ inhibited	Not reported	Potentiator	COX-2
Paracetamol metabolite N-acetyl-p-benzoquinone imine (NAPQI)	Only $K_v7.2/7.3$ reported	S2-S3 linker	Potentiator	COX-1 and COX-2
GABA	$K_v7.2/7.3$> $K_v7.3 \approx K_v7.5 > K_v7.2$ $K_v7.1$ and $K_v7.4$ insensitive	Tryptophan 236	Potentiator	GABAa channels, GABAb receptors

1.4 Expression of K_v7 Channel Subunits in Mammalian Tissues

K_v7 channels are widely expressed in tissues throughout the body and nervous system with distinct subunit expression patterns between tissue types **(Figure 1.8)**. Whole tissue analysis of humans by Uhlen and colleagues (Uhlén *et al.*, 2015) revealed that $K_v7.1$ is highly expressed 1in muscle cells (including myocytes, skeletal and smooth muscle) and epithelial cells (Uhlén *et al.*, 2015) but not in the brain, spinal cord or peripheral nervous system. $K_v7.2$ and $K_v7.3$ are predominantly expressed in neuronal tissues, whereas $K_v7.4$ and $K_v7.5$ are expressed highly in muscle cells and in specific areas of the brain, such as $K_v7.4$ in the auditory system and $K_v7.5$ in the cortex and brainstem (Uhlén *et al.*, 2015).

1.4.1 Central Nervous System

K_v7 channel expression in the central nervous system has been of particular interest since the discovery that mutations in *KCNQ2* and *KCNQ3* can result in epilepsy and mutations in *KCNQ4* result in deafness.

$K_v7.1$ is not widely or highly expressed in the human brain, however one study has demonstrated expression of $K_v7.1$ in cerebellar purkinje cells (Uhlén *et al.*, 2015). It is important to note that this is the only study to detect $K_v7.1$ in significant numbers and is based on mice with mutated $K_v7.1$ that could be causing changes in expression. In addition, sudden death following an idiopathic epileptic seizure has been linked to mutations in $K_v7.1$ as mice carrying mutations that cause LQTS may also develop epilepsy (Goldman *et al.*, 2009). This epilepsy was accompanied by $K_v7.1$ expression in epileptogenic regions of the brain and changes in EEG (Goldman *et al.*, 2009).

In the brain $K_v7.2$ and $K_v7.3$ have strongly overlapping expression patterns and $K_v7.2$/ $K_v7.3$ heteromeric channels are believed to underly ‘classical’ neuronal M current. Both subunits are highly expressed in the cortex, hippocampus, amygdala, caudate nucleus, cerebellum and olfactory region, with some lower level expression in the brain stem and midbrain **(Figure 1.8A)** (Biervert *et al.*, 1998, Schroeder *et al.*, 1998, Uhlén *et al.*, 2015). Interestingly, both $K_v7.2$ and $K_v7.3$ are expressed in the somata and dendrites of pyramidal and polymorphic neurons in the hippocampus but only $K_v7.2$ is expressed in the mossy and granule cells (Cooper *et al.*, 2000, Cooper *et al.*, 2001). This expression is localised to the axons and termini of the excitatory neurons, supporting the idea that $K_v7.2$ plays a role in synaptic regulation (Cooper *et al.*, 2000,

Cooper *et al.*, 2001). $K_v7.2$ is expressed in dopaminergic and GABAergic neurons of the substantia nigra, and cholinergic neurons of the striatum and globus pallidus (Cooper *et al.*, 2001). $K_v7.2$ is also widely expressed through the hippocampal formation **(Figure 1.8A)** (Klinger *et al.*, 2011), consistant with XE-991s ability to enhance learning and memory, detailed in 1.6.2. *Kcnq2* is also relatively highly expressed in the nucleus ambiguus, an area in the brainstem where the efferent fibres of the vagus nerve reside (Rouillard *et al.*, 2016), although there have been no reports of the functional impact of this expression directly, epilepsy patients with KCNQ2 mutations may also present with bradycardia (low heart-rate) and retigabine hyperpolarises isolated vagal nerves (Weckhuysen *et al.*, 2013, Passmore *et al.*, 2012).

$K_v7.4$ is specifically expressed throughout the auditory system; $K_v7.4$ can be found in the auditory nuclei in the brain stem and the presynaptic calyx terminals (Kharkovets *et al.*, 2000). In addition, $K_v7.4$ is expressed in the mesolimbic dopamine system, specifically in dopaminergic neurons in the ventral tegmental area, which is significant as the downregulation of $K_v7.4$ here is associated with depression in mice (Li *et al.*, 2017, Su *et al.*, 2019). $K_v7.5$ is also expressed in the calyx of Held as well as the hippocampus and descending vestibular and auditory nuclei **(Figure 1.8A)** (Tzingounis *et al.*, 2010, Caminos *et al.*, 2007).

$K_v7.2$ is also strongly expressed in the second order sensory neurons in the dorsal horn of the spinal cord and some possible expression in the cell bodies of the ventral horn motor neurons, also located in the spinal cord **(Figure 1.8B)** (Dedek *et al.*, 2001, Devaux *et al.*, 2004). A recent study has also shown expression of $K_v7.2$ in the central pattern generator interneurons and $K_v7.2$ and $K_v7.3$ in the motoneurons of the ventral horn of the spinal cord (Verneuil *et al.*, 2020). This was accompanied by an increase in locomotion after intrathecal injection of ICA-069673, a selective $K_v7.2/7.3$ potentiator (Amato *et al.*, 2011) or retigabine and a decrease after XE-991 injection, suggesting that $K_v7.2$ plays an important role in the control of speed of locomotion, although, no effect was seen on gait or interlimb co-ordination (Verneuil *et al.*, 2020). This conclusion is taken with the caveats that the antibodies were not tested for reactivity against $K_v7.4$ or $K_v7.5$ and ICA-069673 has only been shown as selective for $K_v7.2/7.3$ over $K_v7.5/7.3$, the compounds effect on $K_v7.4$ was not tested (Amato *et al.*, 2011) and a later report demonstrated that $K_v7.4$ and $K_v7.4/7.5$ channels were

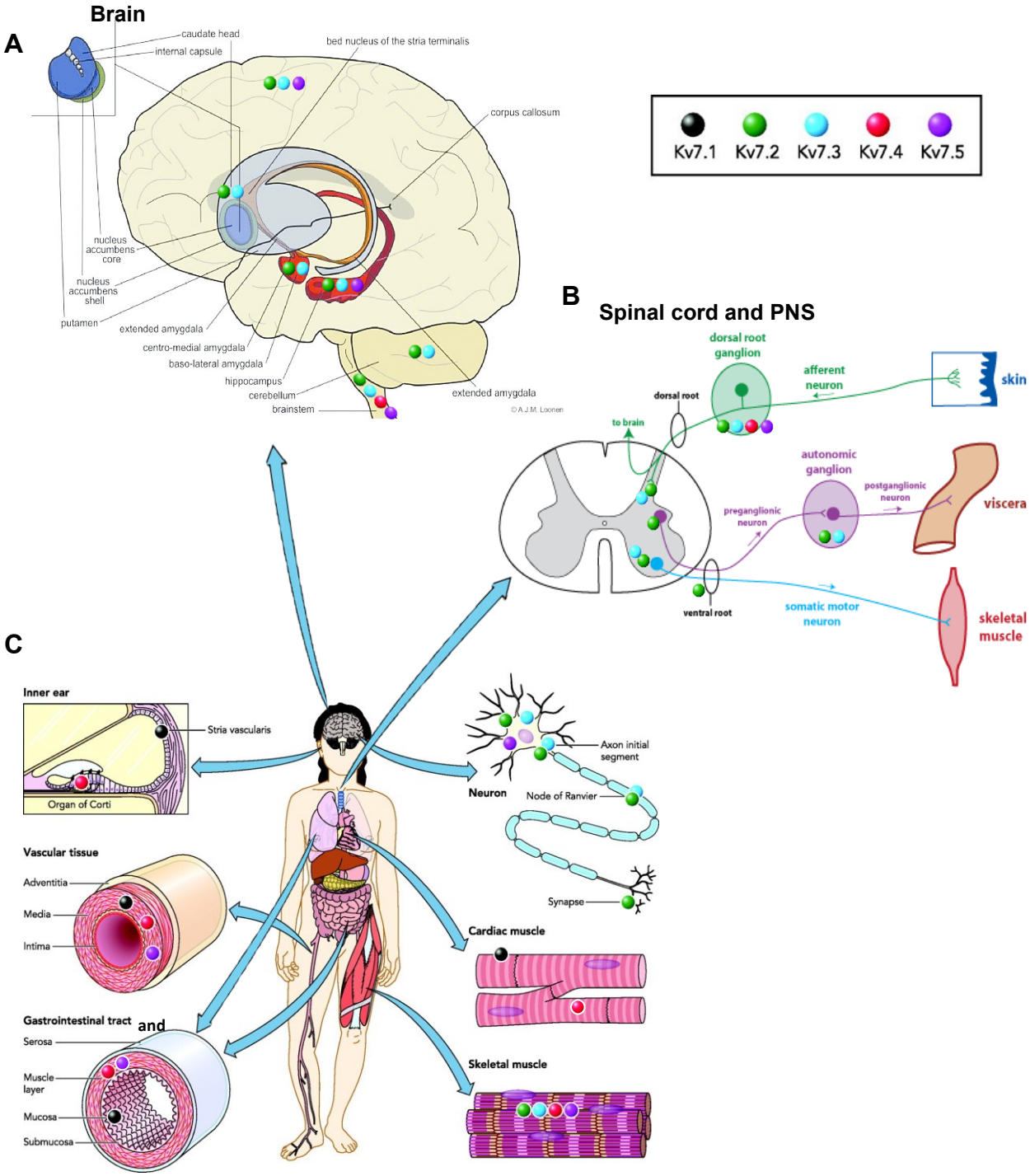

Figure 1.8 Expression of K_v7 channels in mammals. Key areas of K_v7 expression in the **(A)** brain, **(B)** spinal cord and peripheral nervous system (PNS), including the sensory, motor and autonomic fibres and **(C)** peripheral organs and tissues. **Key:** $K_v7.1$- Black, $K_v7.2$- Green, $K_v7.3$- Blue, $K_v7.4$- Red, $K_v7.5$- Purple. Base graphics adapted and updated from (1) (Loonen *et al.*, 2016), (2) (Soldovieri *et al.*, 2011a).

potentiated at similar concentrations to K_v7.2/7.3 (Brueggemann *et al.*, 2014a). Also, XE-991 is described in the study as selective for K_v7.2/7.3, in fact XE-991 is quite non-selective between K_v7.1-7.4 (Søgaard *et al.*, 2001b, Wang *et al.*, 2000) but less selective for K_v7.5 (Schroeder *et al.*, 2000a, Tsai *et al.*, 2020). Thus, leaving open the possibility that other subunits contribute to the observed effects. However, a dominant role for K_v7.2 in the ventromedial interneurons was demonstrated through recording increased excitability of these neurons when isolated from transgenic mice expressing a mutant *Kcnq2* that results in half the M current of wild-type channels (Verneuil *et al.*, 2020). In turn providing further evidence for K_v7.2 being the subunit responsible for M current in these interneurons. The intrathecal injections of K_v7 modulators is curious, as the compounds could also impact on peripheral sensory neurons in the DRG, where M current is partially responsible for the excitability of proprioceptors, touch, temperature and nociceptors (discussed below). The K_v7 channels in the sensory neurons of the dorsal horn would also be affected if the compounds enter the spinal cord. Therefore, is it possible that changes in proprioception or tactility (such as changes in the perception of pressure) could change locomotion? In addition, it demonstrates the complexity of intrathecal injection, the spinal cord, DRG, dorsal and ventral roots are possibly accessible through the space and some self-delivering RNA based compounds seem to affect the DRG more than the spinal cord (Tan *et al.*, 2009, Hogea *et al.*, 2021). Thus, the chemical structure of the injected substance, perhaps the delivery vehicle, the volume and amount of substance may impact what tissues are affected by the injection. Location of the needle when injected may also be an important factor.

1.4.2 Peripheral Nervous System

The original M current was identified in bullfrog sympathetic neurons by Brown and Adams (Brown and Adams, 1980) and since then, M current has been identified in mammalian sympathetic and sensory neurons **(Figure 1.8B)**. In sympathetic neurons, phasic (burst fire) neurons have large M current amplitudes, with tonic (continuous train of action potentials) neurons having much lower current amplitudes, which is consistent with K_v7 channels controlling firing of action potential trains (Wang and McKinnon, 1995, Jia *et al.*, 2008).

As patients with epilepsy due to KCNQ2 mutations may also present with bradycardia, this has been suggested to be due to increased excitability of the parasympathetic

vagal nerve innervating the heart and lungs (Weckhuysen *et al.*, 2013). Indeed, retigabine was able to produce hyperpolarisation in isolated vagal nerves, an effect strongly reduced in the presence of the K_v7 blocker, linopirdine (Passmore *et al.*, 2012). Although, the K_v7 subunit expression in the vagal nerve has not been reported, these studies suggest that K_v7 channels are expressed.

Sensory neurons in the somatosensory ganglia DRG and trigeminal ganglia (TG) and the nodose ganglia, which consist of both somatic and visceral sensory neurons express K_v7 channels. In the DRG, $K_v7.2$-$K_v7.5$ have been identified with $K_v7.4$ seemingly expressed in a particular subpopulation of Aβ neurons (**Figure 1.8**) (Kharkovets *et al.*, 2000, Heidenreich *et al.*, 2012), whereas the expression of $K_v7.2$, 7.3 and 7.5 in different types of neurons is more abundant but less clear, though there is a consensus that $K_v7.2$ is strongly expressed, with some expression of $K_v7.3$ and 7.5 (Passmore *et al.*, 2003, Rose *et al.*, 2011, Rivera-Arconada and Lopez-Garcia, 2006, Zheng *et al.*, 2019). Currently, there is evidence for $K_v7.2$ being expressed mostly in small neurons (Rose *et al.*, 2011), evidence that $K_v7.5$ is mostly in small neurons and $K_v7.2$ in larger neurons more so than small (King and Scherer, 2012) and evidence that both are expressed (Passmore *et al.*, 2003). However, *Kcnq5* and *Kcnq3* mRNA has been shown to be expressed at far lower levels in small-diameter neuron populations than *Kcnq2*. This discrepancy is discussed further in later sections and providing further clarity to which subunit is expressed is the first aim of this thesis.

What is clear, is that K_v7 channels are important for nociceptive signalling in peripheral sensory neurons. K_v7 channels have been identified and been shown to have a functional impact in the cell body, axons and nerve terminals of peripheral sensory neurons (Rivera-Arconada and Lopez-Garcia, 2006).

Extracellular recordings from the dorsal roots were performed with retigabine and XE-991 application directly to the root, retigabine increased the current required to elicit dorsal root potentials but XE-991 was less effective but did reverse the effect of retigabine. In addition, retigabine application hyperpolarised the primary afferents, as is consistent with potentiation of M current in the dorsal root (Rivera-Arconada and Lopez-Garcia, 2006).

The cell bodies of sensory neurons in the DRG are regularly used to research K_v7 channels so not all these studies are considered here. Application of retigabine

hyperpolarises and XE-991 depolarises the membrane of sensory neurons through activating or blocking M current (Du *et al.*, 2014). This is somewhat in contrast to the dorsal root, where XE-991 is less effective (Rivera-Arconada and Lopez-Garcia, 2006). Retigabine is also sufficient to reduce action potential firing and K_v7 blockers increase firing in sensory neuron cell bodies (Passmore *et al.*, 2003, Du *et al.*, 2014). A number of endogenous and exogenous modulators are also effective at regulating M current and neuronal excitability in the cell body, this includes inflammatory mediators such as bradykinin and proteases (Linley *et al.*, 2008, Liu *et al.*, 2010, Linley *et al.*, 2012).

$K_v7.2$ and $K_v7.5$ are expressed in the fibres of the spinal nerves under physiological and pathological conditions when using immuno-fluorescence to detect the proteins (Rose *et al.*, 2011, King and Scherer, 2012, Roza *et al.*, 2011, Passmore *et al.*, 2012). Retigabine was also effective at reducing firing frequency in the nerve and XE-991 increased firing frequency in an isolated skin-nerve preparation, suggesting there are functional K_v7 channels in the peripheral nerve also (Passmore *et al.*, 2012).

Additionally, local injection of K_v7 blockers increased pain response to sensitizers and are sufficient to cause pain alone, whereas K_v7 potentiators have a strong analgesic effect, suggesting that the terminals or very distal fibre also express K_v7 channels (Linley *et al.*, 2008, Liu *et al.*, 2010, Linley *et al.*, 2012). The functional impact of sensory neuron expression is discussed in detail in section 1.8.

The predominant K_v7 subunits expressed in the cochlear are $K_v7.1$ and $K_v7.4$, mutations to either of which lead to forms of deafness (see section 1.6.1). $K_v7.1$ is expressed in the vestibular dark cells of the stria vascularis **(Figure 1.9)**, whereas $K_v7.4$ is expressed in the outer and inner hair cells as well as the sensory neurons of the spiral cochlear ganglia **(Figure 1.9)**.

1.4.3 Musculature Expression

$K_v7.1$/KCNE1 channels are responsible for the I_{Ks} current that repolarises cardiac action potentials and is thus expressed in the myocytes responsible for the contraction of the atria and ventricles of the heart (Yang *et al.*, 1997). $K_v7.4$ has also been identified in the mitochondria of around 40% of cardiomyocytes **(Figure 1.8C)** (Testai *et al.*, 2015). $K_v7.1$, $K_v7.4$ and $K_v7.5$ are all expressed in the smooth muscle of the vasculature **(Figure 1.8C)** (Ng *et al.*, 2011, Hedegaard *et al.*, 2014, Fosmo and

Skraastad, 2017). The role of $K_v7.1$ is not fully understood, but $K_v7.4$ and $K_v7.5$ are important for controlling the contractility of smooth muscle through cellular excitability (Ng *et al.*, 2011, Jepps *et al.*, 2011, Stott *et al.*, 2015). Indeed, reducing K_v7 activity in these cells results in hypertension and reduces the vasodilatory effect of adenosine and hypoxia (Hedegaard *et al.*, 2014).

Non-vascular smooth muscle also express K_v7 channels; this includes airway smooth muscle (Brueggemann *et al.*, 2012), gastrointestinal smooth muscle (*Kcnq4* and K*cnq5*) (Jepps *et al.*, 2009), gastric antral smooth muscle of the stomach (*Kcnq1* and *Kcnq3*) (Ohya *et al.*, 2002) and myometrial smooth muscle (*Kcnq1* and *Kcnq5*) **(Figure 1.6C)** (McCallum *et al.*, 2009). Bladder smooth muscle has also been suggested to express K_v7 subunits, but there is no consensus on the subunits that are expressed, with mostly *Kcnq4* (Svalø *et al.*, 2012, Anderson *et al.*, 2013) and some expression of *Kcnq3* and *Kcnq2* being proposed (Anderson *et al.*, 2013) with others suggesting both $K_v7.2/3$ heteromers and $K_v7.4/5$ heteromers based on pharmacological experiments (Provence *et al.*, 2015a, Provence *et al.*, 2018) however, M current was not assessed. Other groups, that have assessed K^+ current have not detected any K_v7 currents in bladder smooth muscle and instead suggested the pharmacological effect is due to afferent inhibition (Thorneloe and Nelson, 2003, Tykocki *et al.*, 2019). Skeletal muscle expresses all K_v7 subunits to an extent, with the lowest expression being $K_v7.2$ and the others expressed at higher levels (Iannotti *et al.*, 2010).

1.4.4 Epithelial Expression

$K_v7.1$ is expressed in the basolateral membranes of the epithelial cells of the colon, small intestine, stomach and kidney **(Figure 1.8C)** (Dedek and Waldegger, 2001, Demolombe *et al.*, 2001, Horikawa *et al.*, 2005, Vallon *et al.*, 2001) along with KCNE2 (Tinel *et al.*, 2000a) and KCNE3 (Schroeder *et al.*, 2000b), making the channel voltage independent and constitutively active to keep a negative membrane potential, for the co-secretion of chloride.

1.5 K_v7 Channels and CNS Excitability Disorders

1.5.1 Epilepsy

Loss-of-function mutations to *KCNQ2* and *KCNQ3* lead to autosomal dominant human BFNC, characterised by tonic-clonic seizures during early infancy that resolve after 15-20 weeks of life; severe cases can be accompanied by encephalopathy and

patients are more susceptible to seizures across their lifetime. The majority of mutations discovered have been found in *KCNQ2*, however at least 15 mutations have been identified in *KCNQ3* (Biervert *et al.*, 1998, Singh *et al.*, 1998, Singh *et al.*, 2003, Miceli *et al.*, 2013). Recently, four mutations in *KCNQ5* have been identified in patients that present with different symptoms. Two mutations resulted in patients with intellectual dysfunction but not seizures. The third consisted of severe intellectual dysfunction and absent seizures from 2 years of age. The fourth mutation led to severe intellectual dysfunction, seizures from 5 months old and recurrent tonic seizures (Lehman *et al.*, 2017) with these symptoms being closer to *KCNQ2* mediated BFNC than the first two but still distinct, particularly in time of onset. Moreover, the fourth mutation is a gain of function mutation in *KCNQ5* (Lehman *et al.*, 2017). Mutations in *KCNQ2* or *KCNQ3* result in a reduction of K_v7 current to differing levels; the extent to which current is lost seems to be linked to the extent of recurrent seizures (Watanabe *et al.*, 2000). Indeed, it has been demonstrated that reduction of M current in CA1 and CA3 hippocampal neurons increases action potential firing (Miceli *et al.*, 2013, Yue and Yaari, 2004).

Studying the effects of *Kcnq2* knockout in epilepsy in early life is difficult as homozygous knockout mice die due to pulmonary atelectasis (collapsed lung). Heterozygotes do not develop spontaneous seizures, but the animals are hyper-effected by pentylenetetrazole-induced seizures (Watanabe *et al.*, 2000) with reduced thresholds to electrically induced seizures (Singh *et al.*, 2008). It may be that M current was reduced enough to lower the threshold for induced seizures but not reduced enough to result in spontaneous seizures. However, it must be noted that animals with knock-in mutations found to cause BFNC do experience spontaneous tonic-clonic seizures in early life as humans seen to do (Singh *et al.*, 2008).

Conversely, knocking-in a mutant *Kcnq2* with a serine-559 to alanine mutation prevented PKC-mediated phosphorylation of the channel, resulting in mice with higher resistance to seizures. The knock-in had no detriment to basal M current but was less responsive to inhibition by muscarinic acetylcholine receptors. Knock-in mice were resistant to pilocarpine and kainite-induced seizures and subsequent epileptogenesis, cell death or mortality (Greene *et al.*, 2018). After sacrifice of the animals, c-Fos expression was analysed as a measure of hyper-excitability and Fluoro Jade C staining to detect damaged, apoptotic neurons, levels of both in the mutant were

significantly lower than in the wild-type animals treated with pilocarpine and were comparable to untreated wild-type animals (Greene *et al.*, 2018). Therefore, reducing K_v7.2 channel sensitivity to muscarinic inhibition resulted in an anti-convulsant effect, reduced neuronal hyper-excitability and protection against cell death. This suggests that in K_v7.2 channels without this type of mutation (reduced sensitivity to neurotransmitter inhibition) neurotransmitter release during seizure activity may exacerbate seizures through suppression of M current. It also brings forth the possibility that recurring seizures in BFNC could be due to periods of further suppression of M current by neurotransmitters, in addition to the already reduced basal current as a result of *KCNQ2* loss-of-function mutations. In addition, as the majority of M current in the brain is thought to be carried by K_v7.2/7.3 heteromers, the data also suggests that K_v7.2 is responsible for M current suppression via mAChRs.

The following summarises the theories for why patients with BFNC have seizures that cease in early life but become more susceptible to seizures thereafter. One proposal is that the reduced basal M current results in seizures in early life and not in later life, is due to the neonatal brain relying more on the inhibitory effect of K_v7 channels due to GABAergic neurons exerting an excitatory effect during development. GABAergic neurons then take on an inhibitory role after this stage, compensating for the lower basal M current (Okada *et al.*, 2003). The increased susceptibility to seizures later in life may then be due to the combination of reduced M current as a result of the mutation and triggering of increased neurotransmitter release, this inhibiting M current further resulting in hyperexcitability and triggering a seizure (Greene *et al.*, 2018). Another possible mechanism for the cessation of seizures in later life is that K_v7.2 is expressed earlier developmentally than K_v7.3. K_v7.2 is expressed three days after birth, whereas K_v7.3 expression is low at this time and increases in later weeks (Tinel *et al.*, 1998, Zhang and Shapiro, 2012) and therefore there is no initial formation of K_v7.2/7.3 heteromers, which produce a larger whole-cell current amplitude than K_v7.2 homomers.

A knock-in dominant-negative *Kcnq5* was developed that did not result in any epileptic seizure phenotype or any clear impact on intelligence or brain morphology however more research is required before the contribution of K_v7.5 channels in epilepsy can be made (Tzingounis *et al.*, 2010).

1.5.2 Learning and Memory

K_v7 subunits are expressed throughout the brain regions involved in memory formation, particularly the hippocampus, suggesting K_v7 channels are important for this process. Initially, linopirdine, a K_v7 channel blocker, was recognised for its cognitive and memory enhancing effect after being developed as an Alzheimer's treatment (Fontana *et al.*, 1994), which led to the development of XE-991 as an improved compound (Zaczek *et al.*, 1998). Indeed, in aged monkeys, inhibiting K_v7 channels restored firing frequency of delay neurons in the prefrontal cortex to those seen in younger animals (Wang *et al.*, 2011). These delay neurons begin to persistently fire upon receiving information entering the working memory and continue to fire during the 'delay period' before recall of the information (Goldman-Rakic, 1995). For example, in a situation one is given a passcode and needing to recall it a short time later, it is due to the continuous firing of the delay neurons that a person is able to retain that information. Thus, inhibiting K_v7 channels to allow those neurons to fire action potentials can help retain information in that way (Wang *et al.*, 2011). Similarly, activation of M1AChRs, β-adrenergic receptors (βAR) or D5 dopamine receptors (D5R) in the basolateral amygdala promote fear memory consolidation through, in part, inhibition of K_v7 channels. Retigabine reversed the memory consolidation that occurred when activating any of the receptors, however, retigabine or XE-991 administered alone had no effect on fear conditioning itself, only reversing (retigabine) or enhancing (XE-991) the effect of M1AChR, βAR or D5R agonists (Young and Thomas, 2014). Recently, Kosenko and colleagues demonstrated that reducing the sensitivity of $K_v7.2$ to MAChR mediated inhibition via $K_v7.2$ (S559A) knock-in mice, significantly impairs long-term object recognition memory, with no effect to short-term memory retention or learning (Kosenko *et al.*, 2020). Similarly, knock-in mice were unable to recognise scents they were previously exposed to in a social odour test; mice are introduced to a bead with the odour of another mouse to familiarise themselves with, then a second odour bead is introduced where intact memory retention would have the mouse pay closer attention to the new scent over the now familiar one. XE-991 administration was able to recover the memory deficits observed and the level of c-Fos, which is increased as neuronal activity is increased induced by training was reduced in $K_v7.2$ (S559A) mice (Kosenko *et al.*, 2020). In contrast to the previous study, fear memory was unaffected by the reduction in $K_v7.2$ sensitivity to

MAChRs, despite Young and Thomas showing fear memory to rely on MAChR mediated inhibition of K_v7 channels (Kosenko *et al.*, 2020, Young and Thomas, 2014).

Conversely, stress-induced downregulation of *Kcnq2* and *Kcnq3* expression in rat hippocampal neurons impaired long term potentiation in the hippocampus, resulting in defective retrieval of special memories (Li *et al.*, 2014). Loss-of-function mutations in *Kcnq2* and K*cnq5* can also result in intellectual deficits that include memory in epilepsy patients (Lehman *et al.*, 2017). Suppression of M current in mice by expressing a dominant-negative *Kcnq2* in the brain resulted in spontaneous seizures, spatial memory deficits and behavioural hyperactivity. Expressing the mutant from birth resulted in spontaneous seizures (as in BFNC) and aberrant hippocampus morphology. Whereas expression of dominant-negative *Kcnq2* after the early developmental period revealed significant deficits in hippocampus-dependent spatial memory and CA1 pyramidal neuron hyperexcitability (Peters *et al.*, 2005). In drosophila, the loss-of-function of single d*Kcnq* (a single *Kcnq* gene present in this species) caused deficits in short and long-term memory. There was a reduction in K_v7 channel expression in wild-type drosophila as the flies aged and memory became impaired but impressively, memory deficits were somewhat rescued by overexpression of d*Kcnq* implying an important role for K_v7 channels in memory formation (Cavaliere *et al.*, 2013).

Evidence for the importance of K_v7 channels in memory is compelling, yet there is no clear answer as to whether M current activity has a positive or negative effect on memory. Likely, the different locations, types of memory and types of neurons and networks studied are the reasons for discrepancies.

An important but understudied area of research is the impact of K_v7 on the autism spectrum disorder. Heterozygous *Kcnq2* knock-out mice displayed repetitive grooming behaviour and compulsive-like behaviour particularly in males, as well as reduced sociability (Kim *et al.*, 2020). Concurrently, in humans, a patient exhibiting autism behaviours was found to carry a frameshift mutation in *KCNQ3*, truncating the C-terminus (Li *et al.*, 2020). Further analysis of the truncated $K_v7.3$ subunit revealed that it was able to assemble with $K_v7.2$ but was unable to stabilise the heteromer as a functionally expressed channel (Li *et al.*, 2020), suggesting that $K_v7.2/7.3$ heteromer expression is important in protecting from the development of autism. It is possible

$K_v7.2$ homomers are unable to compensate due to the lower current amplitude, however, when expressed with $K_v7.2$, the truncated $K_v7.3$ did exert some dominant negative effect on $K_v7.2$ (Li *et al.*, 2020). Prior to this, a mutation effecting $K_v7.3/7.5$ heteromer formation but not $K_v7.2/7.3$ heteromer formation was discovered in patients displaying autistic symptoms (Gilling *et al.*, 2013).

1.5.3 Addiction

The ventral tegmental area (VTA) is part of the mesolimbic pathway that processes reward, pleasure seeking behaviour and mood, and is the key pathway that is altered during addiction and withdrawal symptoms. M current has been recorded from dopaminergic VTA neurons with ethanol inhibiting the current and increasing spontaneous firing frequency in these neurons (Koyama *et al.*, 2007). Later, ethanol was shown to inhibit $K_v7.2/7.3$ heteromers via PIP2 depletion (Kim *et al.*, 2019). Furthermore, ethanol also reduces trafficking of $K_v7.2$ channels in neurons of the nucleus accumbens, which is also part of the mesolimbic pathway and directly innervated by the VTA (McGuier *et al.*, 2016). Direct evidence of K_v7 channel impact on alcohol addiction comes in the form of retigabine reducing ethanol consumption in rats and XE-991 increasing it, either when administered directly to the nucleus accumbens or systemically (Knapp *et al.*, 2014, McGuier *et al.*, 2016). The mechanism by which M channel activation may reduce alcohol addiction is by reducing firing frequency of dopaminergic neurons, thus reducing dopamine receptor activation, which would become desensitised due to dopamine release in normal conditions where K_v7 activation does not occur (dopaminergic neurons would continue to fire and release dopamine).

Furthermore, addiction to stimulants such as cocaine, phencyclidine (PCP) and methamphetamine is caused by excessive dopamine release, resulting in the desensitisation of D2 dopamine receptors. D2R receptor activation increases M current through $G_{i/o}$ protein mediated PKA inhibition, though the exact mechanism by which PKA inhibition activates K_v7 channels is not yet understood (Ljungstrom *et al.*, 2003); this would explain why desensitisation of D2R results in hyperexcitability. Retigabine was able to reduce c-Fos expression and excessive movement induced by cocaine, PCP or methamphetamine (Hansen *et al.*, 2007); direct injection to the prefrontal cortex also reduced drug-seeking behaviour in rats (Parrilla-Carrero *et al.*, 2018), which is better model of addiction than acute application of stimulant.

1.5.4 Depression

In addition to its role in addiction, the VTA is very important for modulation of mood and is impacted by mood disorders such as depression. In a social defeat model of depression by prolonged, repeated exposure of the mouse to a more aggressive mouse, *Kcnq3* expression was increased in mice that did not develop symptoms of depression (Krishnan *et al.*, 2007). Indeed, viral overexpression of *Kcnq3* in the VTA reduced dopaminergic hyperexcitability and depression-like behaviour, as did systemic or VTA injection of retigabine (Friedman *et al.*, 2016). More recently, $K_v7.4$ has been identified as crucial for controlling excitability of dopaminergic VTA neurons and activation of $K_v7.4$ selectively with a $K_v7.4$-selective potentiator, Fasudil or with non-selective retigabine reduced depression-like behaviour (Li *et al.*, 2017). In *Kcnq4* knockout mice, retigabine remains effective but Fasudil does not, but interestingly, *Kcnq4* knockout mice did not show increased depression-like behaviour compared to wild-type mice (Li *et al.*, 2017). Thus, removing $K_v7.4$ does not seem to result in or worsen depression. However, after induction of depression-like behaviour, the D2R-$K_v7.4$ pathway was interrupted in the VTA-nucleus accumbens pathway where dopamine failed to reduce the firing rate (Su *et al.*, 2019). The mechanism by which dopamine loses its action during depression is not fully understood, but is a consistent observation (Lo Iacono *et al.*, 2018). The mechanism could be similar to that in addiction with desensitisation downregulation, inhibition of the D2R receptor or another reason all being plausible for this effect.

1.5.5 Anxiety

K_v7 channels have also been implicated in anxiety. Human pre-operative patients treated with flupirtine for post-operative pain, scored lower on measurements of preoperative anxiety compared to placebo-treated patients (Yadav *et al.*, 2017). Retigabine also improves performance on unconditioned tests of anxiety, including marble burying (rats compulsively bury marbles when stressed) and zero maze (a circular track with covered and open areas, less anxious/more comfortable animals will explore the open areas more often) (Korsgaard *et al.*, 2005) but did not affect conditional emotional response (CER) (Munro *et al.*, 2007). However, CER is sometimes described as fear inducing rather than anxiety and doses of retigabine were not maximal (Munro *et al.*, 2007). Retigabine also alleviated post-seizure (kainite-

induced) anxiety when tested in open-field or the elevated plus maze (Slomko *et al.*, 2014).

The dorsal raphe nucleus (DRN) receives input from multiple forebrain regions involved in anxiety and stress behaviour, thus has been suggested as an important region in anxiety regulation (Lowry *et al.*, 2008). DRN neurons are serotonergic and abundantly express $K_v7.4$, which can modulate excitability of DRN neurons (Zhao *et al.*, 2017). Importantly, 5-HT_{1A} serotonin receptors are expressed on DRN serotonergic neurons and when activated inhibit firing frequency; one of the mechanisms of 5-HT_{1A} mediated auto-inhibition is $K_v7.4$ activation, via PLC inhibition (Zhao *et al.*, 2017). Thus, one can reason that the anti-anxiolytic effect of K_v7 channel potentiators is indeed $K_v7.4$ mediated and probably not due to any other off target effects. Even though the DRN is only one area of the anxiety pathway, administration of a $K_v7.4$ potentiator directly to the DRN may provide more direct evidence for this.

A link between anxiety, serotonin and K_v7 channels has recently been identified in the lateral habenula on alcohol withdrawal-induced anxiety. After alcohol withdrawal, neurons of the medial region of the lateral habenula had a higher basal firing rate than in control rats, which was accompanied by a reduction in *Kcnq2* and *Kcnq3* expression. As expected, hyperexcitability and anxiety behaviours were reversed by application of retigabine (Kang *et al.*, 2017). Later, the same group identified that 5-HT_{2C} serotonin receptor activation increased excitability in lateral habenula neurons and blocking these receptors increased expression of *Kcnq2* and *Kcnq3* compared to untreated rats experiencing alcohol withdrawal (Fu *et al.*, 2020). Interestingly, the medial region neurons of the lateral habenula predominantly innervate the DRN (Proulx *et al.*, 2014), likely providing the link between alcohol withdrawal and anxiety.

1.6 K_v7 Channels and Peripheral Excitability Disorders

1.6.1 Deafness

As stated previously, $K_v7.1$ and $K_v7.4$ are expressed in the cochlear of the ear, the sensory organ that transmits hearing. Both subunits have been implicated in different forms of deafness; patients with Jervell and Lang-Nielsen syndrome (JLN), a form of arrythmia (discussed in 1.6.2) were found to present with bilateral deafness as well as arrythmia. This was accompanied by mutation of $K_v7.1$ located in the stria vascularis of the inner ear (Neyroud *et al.*, 1997). $K_v7.1$ and KCNE1 are both expressed in the

vestibular dark cells of the stria vascularis **(Figure 1.7)** (Nicolas *et al.*, 2001) and KCNE1 knockout mice exhibit degeneration in the epithelial cells of the stria vascularis, which collapses the lymph space resulting in the same effect as with JLN mutations in *KCNQ1* (Nicolas *et al.*, 2001). Therefore, co-assembly of the K_v7.1/KCNE1 complex could be the cause of JLN associated syndromic deafness (deafness presenting with symptoms elsewhere in the body such as arrythmia), generally due to reduction in endolymph secretion or collapse of the endolymph space. This leads to deafness because the endolymph moves in waves in response to sound, activating the receptors on hair cells **(Figure 1.9)**.

Non-syndromic autosomal dominant deafness (DNFA2) is characterised by high-frequency hearing loss in the absence of other non-hearing related symptoms (non-syndromic), hearing loss often becomes complete over time. K_v7.4 was initially localised to the outer hair cells (OHC) **(Figure 1.9)** and DNFA2 has been attributed to *KCNQ4* mutations affecting sensory signalling (Kubisch *et al.*, 1999, Kharkovets *et al.*, 2000). *KCNQ4* mutations have been shown to degenerate OHC cells, possibly due to lack of function, leading to progressive deafness (Kubisch *et al.*, 1999, Nouvian *et al.*, 2003). This is supported by the degeneration of OHCs seen with prolonged pharmacological inhibition of K_v7 channels in OHCs with linopirdine (Nouvian *et al.*, 2003).

However, OHCs are not directly innervated by sensory neurons; instead, they merely amplify auditory signals, thus one may assume that a loss of OHC function would not result in complete hearing loss. Inner hair cells (IHC) directly relay sensory information to the sensory nervous system through innervation by spiral ganglia afferents with both IHCs and the spiral ganglia neurons expressing *KCNQ4* **(Figure 1.9)**. Indeed, K_v7-like currents have been recorded in spiral ganglia sensory neurons (Beisel *et al.*, 2000, Lv *et al.*, 2010). In addition, loss of K_v7.4 in the spiral ganglia results in degeneration of the sensory neurons and progressive hearing loss (Lv *et al.*, 2010, Carignano *et al.*, 2019). Also, IHCs and OHCs receive the same sensory input and IHCs synapse onto the spiral sensory neurons, so would continue to transmit auditory stimuli in the absence of OHCs, Loss of OHCs has previously shown to lead to loss of high frequency hearing alone (Ryan and Dallos, 1975). This suggests that DNFA2 is not due to *KCNQ4* mutations in the OHC alone. Although, in *Kcnq4* knockout mice, the sensory systems and IHC were left largely intact but the OHCs significantly

degenerated (Kharkovets *et al.*, 2006). Further work is required to discern the relative contribution of these various cell types (and $K_v7.4$ expressed therein) in DNFA2, though the importance of $K_v7.4$ is clear.

Most DNFA2-related *KCNQ4* mutations lead to a loss of function typically associated with the pore region of the channel where there is an impairment in ion conduction. Many are associated with the GYG selectivity filter or stabilise the channel in the closed state (Kubisch *et al.*, 1999, Coucke *et al.*, 1999, Xia *et al.*, 2020, Talebizadeh *et al.*, 1999, Van Hauwe *et al.*, 2000, Van Camp *et al.*, 2002). One pore region mutation exerts a dominant-negative effect on wild-type subunits by trapping the channel in the ER and reducing membrane expression (Mencía *et al.*, 2008). Other trafficking mutations have also been identified (Gao *et al.*, 2013, Xia *et al.*, 2020), as well as others in the voltage sensor and cytoplasmic region (Su *et al.*, 2007, Mehregan *et al.*, 2019).

The effect of *KCNQ4* loss-of-function seemingly causes deafness through eventual degeneration of the affected cells. This may either be due to K^+ overload in the cell leading to chronic depolarisation directly or due to the chronic influx of Ca^{2+} resulting from the depolarisation (Xu *et al.*, 2007, Holt *et al.*, 2007). Inner and outer hair cells extrude K^+ through $K_v7.4$ channels to keep the concentration in the cells low at rest, allowing the influx of K^+ to occur upon deflection of cilia when vibratory stimulation occurs. In fact, pharmacological K_v7 inhibitors, XE-991 and Linopirdine block K^+ conductance ($G_{K,n}$) in OHCs as do *KCNQ4* mutations (Marcotti and Kros, 1999, Oliver *et al.*, 2003, Kharkovets *et al.*, 2006). However, $G_{K,n}$ exists at more negative membrane potentials than heterologously-expressed $K_v7.4$ channels are activated at, although recent evidence suggests that $K_v7.4$ clusters in OHCs and clustering of $K_v7.4$ shifts voltage dependence to more negative voltages that fall in the range of $G_{K,n}$

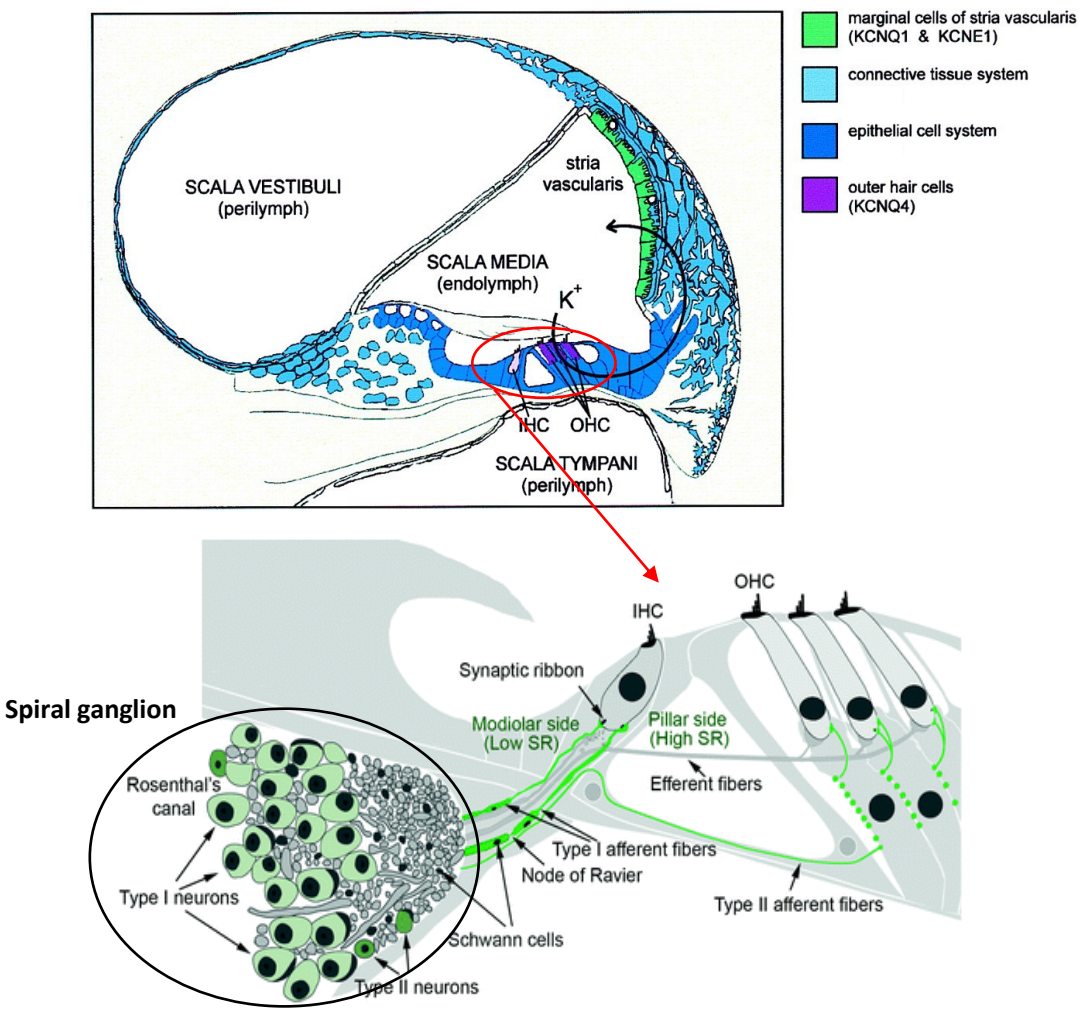

Figure 1.9 Structure of the cochlear in the inner ear and the innervating sensory spiral ganglion. Diagrams adapted from (Holt and Corey, 1999) and (Lang, 2016).

(Perez-Flores *et al.*, 2020). Selective $K_v7.4$ potentiators were able to rescue the current in non-pore-effecting mutations in $K_v7.4$ but not the more prevalent pore-forming mutations (Leitner *et al.*, 2012). Promisingly though, when pore mutants were expressed with wild-type $K_v7.4$ subunits, potentiators can reverse the dominant-negative effect of both pore and non-pore mutant $K_v7.4$ channels (Xia *et al.*, 2020).

1.6.2 Cardiac Arrhythmias

Cardiac arrhythmia refers to a change in contraction of the heart, causing it to beat irregularly (Antzelevitch and Burashnikov, 2011). Long QT syndrome (LQTS) is one such arrhythmia characterised by prolonged ventricular repolarization, resulting in episodic ventricular tachyarrhythmia **(Figure 1.9)**. The clinical manifestation is a prolonged depolarisation phase that leads to ventricular fibrillation and sudden death in otherwise healthy people (Vohra, 2007). Mutations to *KCNQ1* or *KCNE1* can result in LQTS due to the disruption of the $K_v7.1$/KCNE1 channel complex (Schulze-Bahr *et al.*, 1997).

Focussing on *KCNQ1*, there are over 500 arrhythmia-associated mutations with the majority being loss-of-function and localised to the transmembrane region of the channel **(Figure 1.11)** (Moss *et al.*, 2007). Although there have also been many C-terminal mutations identified and only two N-terminal mutations resulting in LQTS **(Figure 1.11)** (Moss *et al.*, 2007). The two most common LQTS conditions are the autosomal dominant, Romano-Ward syndrome (RW), characterised by the mutant channel imposing a dominant-negative effect on the unmutated protein and the autosomal recessive, JLN (see above), where there is no dominant-negative effect of the mutant. Mutations generally affect ion selectivity, voltage dependence, trafficking or multimerization of the complex whereby $K_v7.1$ activity is affected. The lack of a dominant-negative effect seen in JLN-associated mutants on wild-type was thought to be due to the inability of the mutant subunits to heteromerise, meaning wild-type subunits could still assemble into functional channels therefore still producing some activity. This is supported by the number of JLN-associated mutations that result in C-terminus truncations and missense mutations (Schmitt *et al.*, 2000, Loussouarn *et al.*, 2006) in the C-terminus, particularly the A-domain, which are essential areas for tetramerization (Schwake *et al.*, 2003, Maljevic *et al.*, 2003, Howard *et al.*, 2007). Conversely, there are also mutations that do not impair subunit assembly but still lead to JLN (Xu and Minor Jr., 2009) by reducing membrane expression of the channels

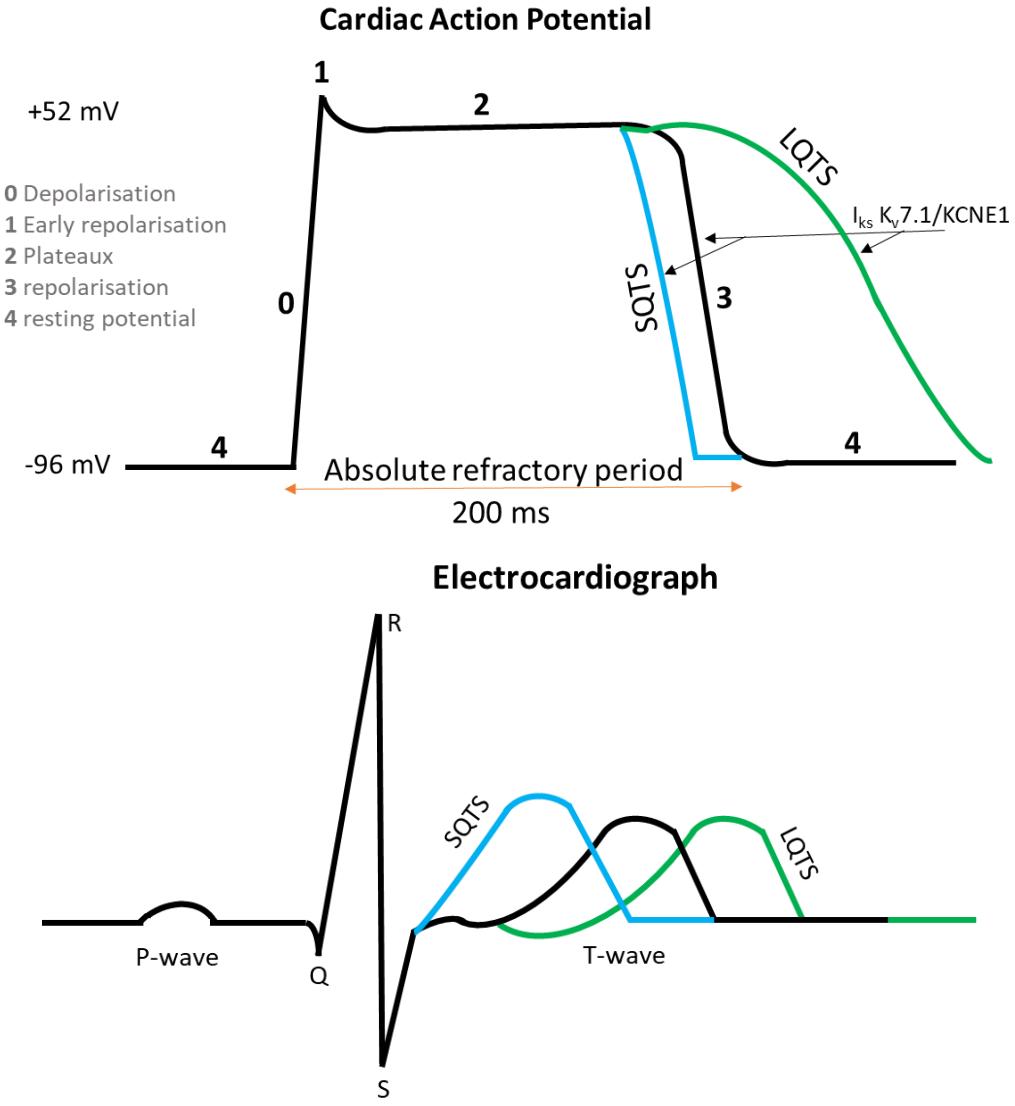

Figure 1.10 Changes to cardiac action potential and electrocardiograph during cardiac arrythmia. Short QT syndrome (SQTS) resulting from KCNQ1 gain-of-function (Blue), Long QT syndrome (LQTS) resulting from KCNQ1 or KCNE1 loss-of-function mutation (Green).

through impaired trafficking or insertion into the membrane (Marx *et al.*, 2002). Mutations to *KCNQ1* in RW syndrome often reduce plasma membrane expression of $K_V7.1$, either through ER retention or impaired Rab-mediated recycling (Dahimène *et al.*, 2006, Peroz *et al.*, 2009, Seebohm *et al.*, 2007, Seebohm *et al.*, 2008). Despite some mutations thought to cause ER retention, heterologous expression of these channels did produce current that was reduced only at positive voltages (Hammami Bomholtz *et al.*, 2020).

Mutations in the C-terminal A-domain of $K_V7.1$ have been analysed using structural X-ray crystallography, revealing disruption of channel binding to AKAP9/yotiao (see above section 1.2.9). This leads to disruption in PKA binding, hence preventing channel activation upon β-adrenergic stimulation (Howard *et al.*, 2007). This would mean cardiac repolarisation is unable to adapt to the increased heart rate; this is seen clinically in patients with PKA-insensitive *KCNQ1* mutations where arrhythmias only develop during exercise or heart stress tests (Bartos *et al.*, 2014). Adaptation to increased heart rate is seemingly also impaired by mutations in the S4 voltage sensing domain through a shift in voltage dependence to more positive potentials (Moreno *et al.*, 2017). As described earlier, PIP2 is required for channel activation and calmodulin potentiates $K_V7.1$ current, thus mutations in the binding sites for PIP2 and calmodulin result in reduced $K_V7.1$ current. Preventing PIP2 binding reduced channel opening whereas loss of calmodulin binding resulted in impaired gating and correct assembly of $K_V7.1$ subunits, resulting in severe loss of function (Ghosh *et al.*, 2006, Shamgar *et al.*, 2006). The most severe mutations in *KCNQ1*, described as mutations with high risk of sudden death, are associated with the selectivity filter, preventing selective permeation of K^+ due to disruption of the carbonyl oxygen atoms making up the filter (Burgess *et al.*, 2012). This demonstrates the importance of $K_V7.1$ channels in the heart.

Aside from LQTS, there are two other cardiac arrhythmias associated with *KCNQ1* mutations: familial atrial fibrillation and short QT syndrome (SQTS) **(Figure 1.8)**. The prolonged cardiac action potential is crucial in allowing ventricular filling during the refractory period between contractions. Patients with SQTS or atrial fibrillation exhibit gain-of-function mutations in *KCNQ1* that result in a constitutively active channel. This can occur through a shift in voltage dependence, changes to activation and deactivation or reduced $K_V7.1$-KCNE1 co-assembly

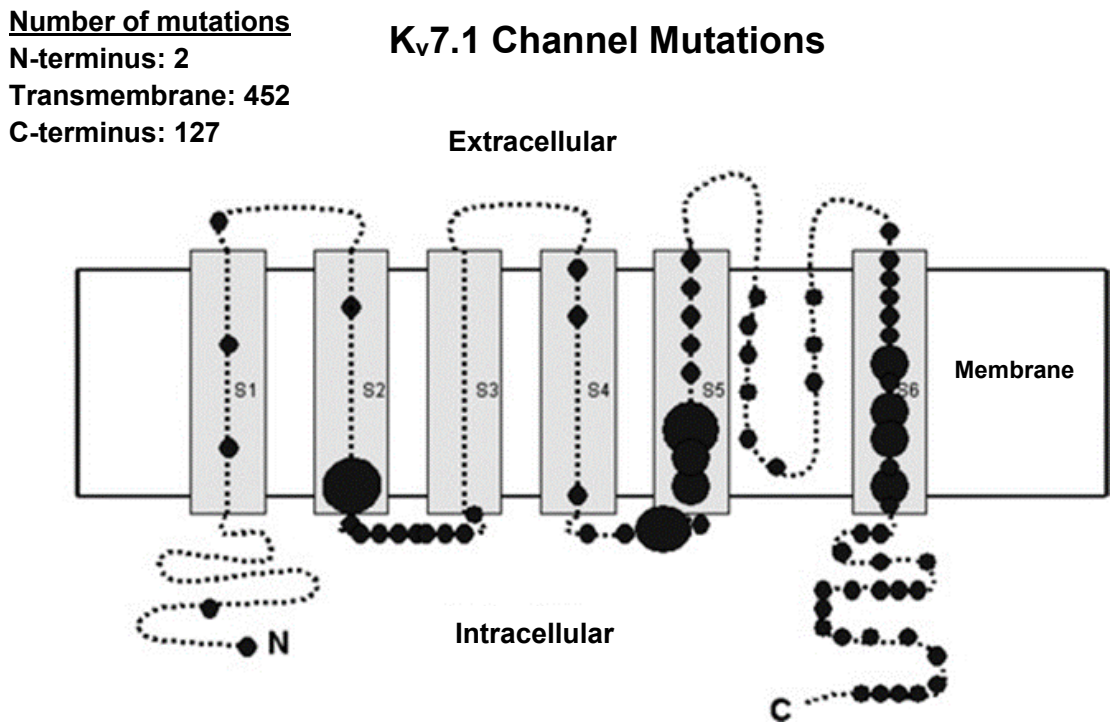

Figure 1.11 K_v7.1 mutations in patients with long QT syndrome (LQTS) across the channel. LQTS causing mutations range across the length of the channel. So far 2 mutations have been identified in the N-terminal region, 452 in the transmembrane region and 127 in the C-terminus. Of particular note, are the clusters of mutations in the intracellular loops and the lack of mutations in the extracellular loops of the transmembrane region. Taken from (Moss *et al.*, 2007).

(Seebohm *et al.*, 2001, Bellocq *et al.*, 2004, Chen *et al.*, 2003, Restier *et al.*, 2008, Moreno *et al.*, 2015).

The drug Rottlerin and its analogues was shown to potentiate K_v7.1/KCNE1 channel current by increasing the deactivation time of the channel, thereby prolonging the flow of current (Lübke *et al.*, 2020). Thus, these compounds may offer a potential treatment for LQTS, though this has not been tested for this condition and may be dependent on the mutation and type of LQTS.

1.6.3 Other Cardiovascular Disorders

K_v7 channels, specifically K_v7.1, K_v7.4 and K_v7.5 are expressed in vascular smooth muscle cells (VSMCs) and aid adaptation of the blood vessels to vasodilate (K_v7 activation) and vasoconstrict (K_v7 inhibition). Thus, K_v7 inhibition can lead to hypertension, a significant risk factor for other potentially fatal diseases such as stroke and cardiovascular diseases (Stott *et al.*, 2014, Fosmo and Skraastad, 2017). K_v7.4/7.5 and K_v7.5 channels are inhibited in vascular smooth muscle by release of Ca^{2+} from the ER via G_qPCR activation by vasopressin or Ca^{2+} influx through L-type Ca_v channels (Holmes *et al.*, 2003, Mani *et al.*, 2013, Tsai *et al.*, 2020). In contrast, K_v7 current was potentiated by PKA during β-adrenergic stimulation in renal vasculature, resulting in vasodilation (Chadha *et al.*, 2012). Adrenergic stimulation, resulting in vasodilation has also been demonstrated in the mesenteric artery (Mani *et al.*, 2016) and other tissues, but it is important to note that adrenergic stimulation often results in vasoconstriction due to its action on alpha-1 receptors also expressed in the vasculature. Therefore, the effect of adrenergic stimulation on contractility is contrasting, depending on the area of vasculature being targeted. The importance of K_v7 in the vasodilatory process is supported by the loss of hypoxia-induced vasodilation when K_v7 channels are inhibited by XE-991 (Hedegaard *et al.*, 2014). K_v7.4 expression is also significantly reduced in rodent models of hypertension (Jepps *et al.*, 2011); one mechanism for downregulation has been identified with angiotensin II inhibiting the interaction between K_v7.4 and HSP90, a heatshock protein, resulting in E3 ubiquitin ligase-mediated protein degradation (Barrese *et al.*, 2018). This suggests K_v7.4 downregulation is a key component of hypertension induction. Although vasopressin-mediated inhibition of K_v7 current is PKC dependent, K_v7.4 is largely insensitive to PKC-dependent phosphorylation (Brueggemann *et al.*, 2014c). Furthermore, K_v7.4 homomers are not affected by the β-adrenergic agonist,

isoproterenol, suggesting $K_v7.4$ is insensitive to PKA as well (Mani *et al.*, 2016). It stands to reason that $K_v7.5$ is likely the subunit sensitive to vasoconstrictors and dilators. In spite of this, hypertension induced by the renin-angiotensin-aldosterone cascade also results in downregulation of $K_v7.4$ in the renal artery (Fosmo and Skraastad, 2017).

K_v7 channels are also expressed in the autonomic nervous system innervating the cardiovascular system and there is also evidence that patients with *KCNQ2* mutations presenting with seizures may also present with bradycardia (Weckhuysen *et al.*, 2013), possibly as a result of parasympathetic disinhibition via hyperexcitability of parasympathetic neurons. This is supported by the vagal nerve hyperpolarising in response to retigabine application and detection of Kcnq2 mRNA in the nucleus ambiguus (Passmore *et al.*, 2012, Rouillard *et al.*, 2016).

1.6.4 Bladder Dysfunction

Pan-K_v7 potentiators such as retigabine reduce bladder tone, resulting in urinary retention during treatment, whereas XE-991 and the MAChR agonist carbachol cause bladder constriction and therefore a degree of incontinence (Svalø *et al.*, 2015, Seefeld *et al.*, 2018). Despite often being seen as an adverse effect of K_v7 modulators when used as treatments for other disorders, in patients with bladder dysfunction, K_v7 enhancers and blockers may have a therapeutic role in treating incontinence or retention respectively. However, despite some studies showing expression of K_v7 subunits in the bladder (Svalø *et al.*, 2012, Anderson *et al.*, 2013, Provence *et al.*, 2015a, Svalø *et al.*, 2013), K_v7-like current and retigabine-sensitive K^+ current, was not recorded in mouse bladder smooth muscle cells. Instead, it was suggested that activation of K_v7 channels in the sensory afferents innervating the bladder resulted in retention (Tykocki *et al.*, 2019).

1.6.5 Gastrointestinal Disorders

$K_v7.1$/KCNE3 channel complexes are expressed in the epithelial cells of the gastrointestinal tract, where they are involved in chloride (Cl^-) secretion, which is impaired in cystic fibrosis (due to excessive mucus in the digestive system) (Schroeder *et al.*, 2000b). Intestinal crypt cells express $K_v7.1$/KCNE3 complexes and $K_v7.1$ has been localised to colonic epithelial cells and parietal cells of the stomach alongside KCNE2 and KCNE3. In addition, $K_v7.1$-like currents stimulated by cAMP have been identified and reported as being essential for gastric acid and Cl^- secretion (Warth *et*

al., 1996, Grahammer *et al.*, 2001, Heitzmann *et al.*, 2004). Expanding on this idea, $K_v7.1$/KCNE3 complexes are essential for recycling potassium back out of the cell after being transported into the cell by NKCC transporters that bring in K^+ along with Cl^- (Dedek and Waldegger, 2001). In doing so, the intracellular membrane remains polarised, increasing the electrical driving force for Cl^- to move into the cell as well as recycling the substrate required to transport Cl^- into the cell (Dedek and Waldegger, 2001). The increase in Cl^- concentration inside the cell allows for strong secretion of Cl^- to drive the secretion of water, hydrating the GI (and airway) tracts (Dedek and Waldegger, 2001, Abdullah *et al.*, 2017). When Cl^- secretion is reduced, the lumen is dehydrated and mucous build up occurs, as is the case in cystic fibrosis (Abdullah *et al.*, 2017).

$K_v7.4$ and $K_v7.5$ are expressed in the smooth muscles (circular muscle layer of the muscularis) of the intestine responsible for peristaltic movement. Indeed, blocking K_v7 channels in the circular muscle with XE-991 increased contractility of the muscle, increasing peristaltic movement (Jepps *et al.*, 2009). This is one of the few cases explored in section 1.6 where inhibition of K_v7 channels may have a therapeutic effect, alleviating constipation, a common symptom of irritable bowel syndrome. Although, the sequential contractility of the circular muscle is required for peristalsis to occur and increasing contractility of these muscles may interfere with the sequence of movement, this did not seem to be affected when inhibiting K_v7 channels in isolated sections of intestine but the effect of inhibiting K_v7 was not studied *in vivo* (Jepps *et al.*, 2009).

1.6.6 Pulmonary Disorders

Unsurprisingly, K_v7 channels are also expressed in the smooth muscle of the pulmonary arteries, bronchial tubes and bronchial epithelia, as well as sensory inputs innervating the lung from the nodose ganglia and autonomic neurons. As one may expect, activation and inhibition of K_v7 channels exerts a bronchorelaxant or bronchoconstrictive effect, respectively (Brueggemann *et al.*, 2014b, Haick *et al.*, 2017). Histamine release is the primary result of allergic reactions with one of the effects of histamine release being bronchoconstriction, where the airways constrict and impair breathing. As H1 histamine-activated receptors are $G_{q/11}$ coupled, part of the constricting effect of histamine is $K_v7.5$ channel inhibition via PKC (Haick *et al.*, 2017). In the epithelial cells of the airway, $K_v7.1$ aids in secretion of Cl^- by co-secretion

of K^+ (Mall *et al.*, 2000, Mondejar-Parreño *et al.*, 2020). Therefore, any lung associated, muscle or epithelia related disorder may implicate K_V7 subunits in the disease-state or may be employed as a therapeutic target.

1.7 Somatosensory Nervous System

The sensory nervous system includes the combination of peripheral and central components of the nervous system. In brief, first order neurons have axon terminals in the skin for somatosensation or in the organs for visceral sensation that sense a variety of sensory stimuli. Stimulation generates action potentials at these peripheral terminals; these potentials then propagate toward the cell bodies of these neurons and further, through the dorsal roots to the first synapses in the dorsal spinal cord or brainstem. The first order neurons are pseudo-unipolar and have their cell bodies present in a peripheral ganglion. The ganglia innervating the body are present just outside the dorsal spinal cord between the vertebrae, thus are known as the DRG. The same type of ganglia exists in and below the brain, the largest innervating the face and mouth/teeth are located underneath the brain is the TG, though various others are also present. The main visceral ganglia are also located near the base of the brain and include the Geniculate, Petrose and Nodose ganglia. Second order neurons decussate and ascend the spinal cord through specific tracts carrying different types of sensory signal. The dorsal column tract (fasciculus Gracilis and Cuneatus) carries information on fine touch and vibration to the Gracilis and Cuneatus nuclei in the medulla. Lateral and anterior spinothalamic tracts carry pain, temperature (lateral tract) coarse touch and pressure (anterior tract), synapsing in the periaqueductal gray (PAG) in the brainstem and the reticular nucleus and ventral posterolateral nucleus (VPL) in the thalamus. The anterior and posterior spinocerebellar tracts carry proprioceptive fibres to the anterior and posterior tract of the medulla and into the cerebellum. The other tracts continue to ascend the brain to the sensory cortex where animals become consciously aware of the sensory stimulus. The various sensory tracts and primary nuclei are outlined in **Figure 1.12**.

Further focussing on the peripheral somatosensory neurons, there are distinct sub-populations of neurons that detect various stimuli. Sensory neurons with the largest cell-bodies have the fastest signal velocity due to having thickest myelination, these are Aα fibres and carry proprioceptive signals, relaying information on muscle movement. Medium sized, myelinated fibres are separated into larger Aβ fibres and

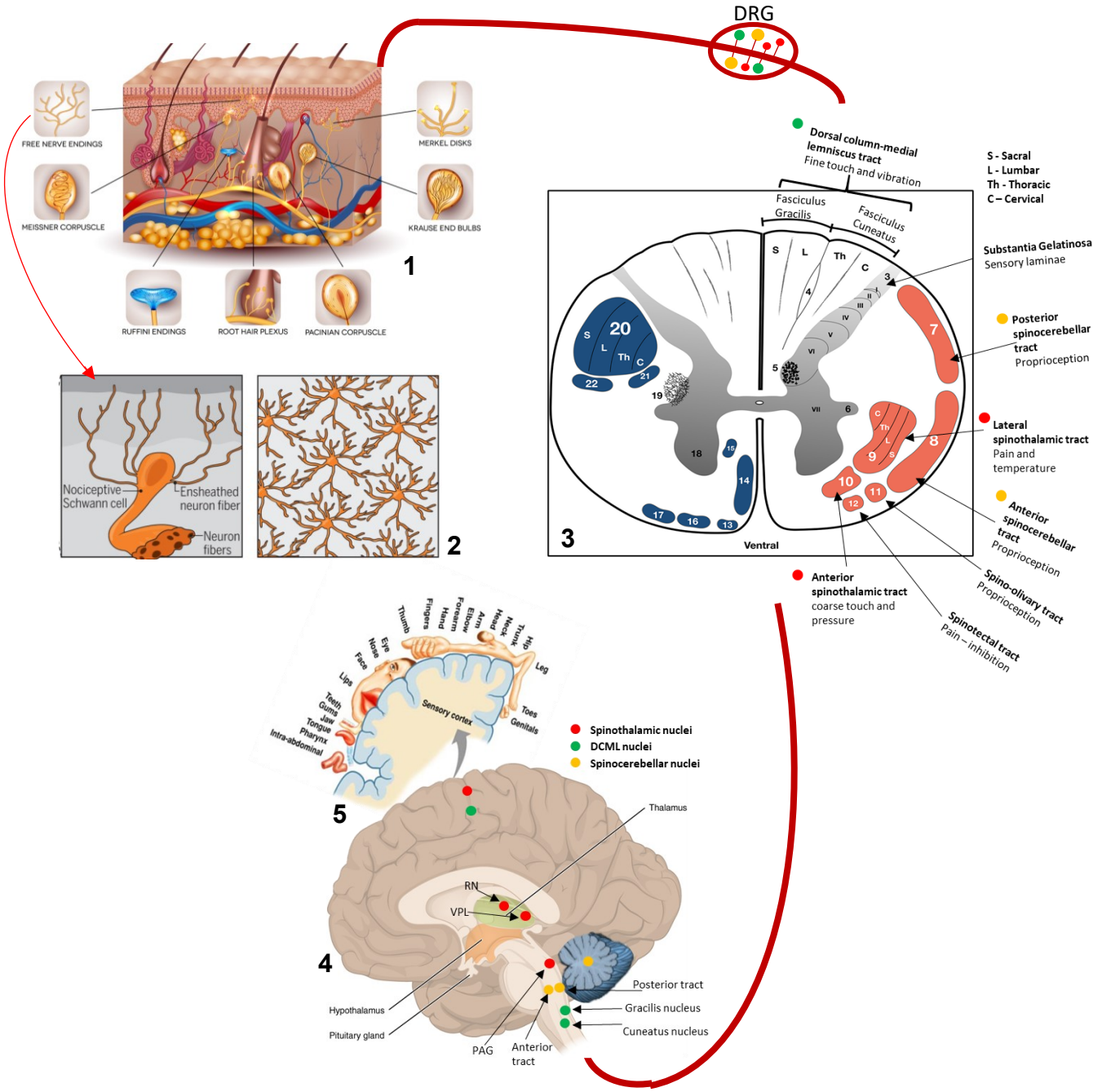

Figure 1.12 Somatosensory pathways. **(1)** Skin sensory receptors detect various types of stimuli, each stimulus is detected by a different type of terminal structure; Meissner's corpuscles (light touch), Merkel discs (pressure and texture), Ruffini cells (stretch), Pacinian corpuscles (vibration and pressure), End bulbs of Kraus (Cold) and free-nerve endings (Pain and heat). arrow indicates new research showing free-nerve endings surrounded by a network of Schwann cells that may be deemed a structure **(2)**. These structures/receptors have fibres that pass through the dorsal root ganglia (DRG), into the spinal cord. **(3)** Organisation of the spinal cord white matter into sensory tracts, each tract relaying different sensory information. **(4)** The sensory spinal tracts synapse with third order neurons in specific nuclei in the brainstem and midbrain. (5) Termination of the third order neurons in the sensory cortex, where neuron terminals are organised by the area of the body innervated. Key: tracts and the related brainstem/thalamic nuclei and termination areas are indicated with Green (dorsal column-medial lemniscus tract), Orange (spinocerebellar tract) or Red (spinothalamic). The sensory information each tract relays is noted under each tract name in **(3)**. Base graphics adapted from (1) (Nishio *et al.*, 2016), (2) (Doan and Monk, 2019), (3) (de Souza *et al.*, 2018), (5) adapted from (Penfield and Boldrey, 1937), (4) (DeSaix *et al.*, 2013).

smaller Aδ fibres, both Aβ and Aδ have populations that respond to innocuous touch and pressure, otherwise known as low-threshold mechanoreceptors. Although, Aδ fibres also have populations of nociceptive neurons that respond to fast nociceptive signalling, particularly fast sharp pain such as pin prick. The smallest neuronal cell bodies are unmyelinated C fibres, predominantly carrying nociceptive, pruriceptive (itch) and temperature signals, though temperature is also carried by some Aδ fibres (Table 1.4) (Siegel and Sapru, 2011). Conduction velocity is also reduced as myelination and fibres diameter reduces (Table 1.4) (Siegel and Sapru, 2011). Different modalities of sensory neurons also have specialised formations at the terminals to aid in transmission of specific stimuli. Meissner's corpuscles are rapidly adaptive receptors responsible for the detection of light touch, Merkel's discs are slowly adapting mechanoreceptors that provide information on pressure and texture. Ruffini endings are another type of mechanoreceptor in the deeper skin layers that detect stretch in the skin, Pacinian corpuscles are also found deeper in the skin and detect vibration and pressure **(Figure 1.12)**. Cold sensation is detected by the endbulbs of Kraus and nociception has long been said to be detected by free nerve endings, though new evidence suggests that specialised mechanosensitive Schwann

Table 1.4: Sensory Neuron Classification

Nomenclature	Function	Receptor Type	Myelination	Axon Diameter (μM)	Conduction Velocity (m/s)
Aα (type 1 and 2)	Proprioception	Muscle spindles	High	13-20	80-120
Aβ	Touch, Pressure	Meissner, Merkel, Pacinian and Ruffini receptors	Medium	6-12	35-75
Aδ	Touch, Pain, Temperature	Free Nerve Endings (Aided by surrounding glia)	Low	1-5	5-30
C	Pain, Itch, Temperature	Free Nerve Endings (Aided by surrounding glia)	None	0.2-1.5	0.5-2

cells surround the terminals and form interlacing networks **(Figure 1.12)** (Abdo *et al.*, 2019).

This broad classification has been separated into further populations of sensory neurons using RNA-seq, as it has become clear that there are distinct populations of neurons responding to very different stimuli that are not identifiable just by cell body size. Using single-cell RNA-seq two groups separately classified sensory neurons into 11 or 10 populations of neurons based on unique expression of markers that identify that population. Usoskin and colleagues initially categorised three populations of low threshold mechanoreceptors, two proprioceptors, three populations of unmyelinated, non-peptidergic neurons, two peptidergic populations, one unmyelinated and one myelinated and finally a thymidine kinase expressing population of unmyelinated low threshold mechanoreceptors (Usoskin *et al.*, 2015) **(Figure 1.13A)**. Li and colleagues identified 10 populations of sensory neurons into 17 sub-populations. Some markers were shared across the two studies and some were not. TrkA was identified in one but not the other studies, TrkB and TrkC was suggested in two studies but as markers for different cell types, but MrgprD consistently identified non-peptidergic neurons, further complicating how to separate these populations. This study was able to also examine the stimuli that these sub-populations respond to (Li *et al.*, 2016) **(Figure 1.13B)**. Using the approach of fluorescently tagging the unique markers to each population and FACS sorting based to create a homogenous population, Zheng and colleagues were able to separate 8 populations of neurons and assess the mRNA expression and functional phenotype of each population (Zheng *et al.*, 2019) **(Figure 1.13C)**. Being able to identify these different populations is a very useful research tool, allowing for increased specificity and accuracy when analysing sensory neurons, though sorting populations by marker is still difficult to do before functionally assessing those neurons and there is not a consensus on the exact markers to use.

Sensory neuron action potentials are similar to other neuronal action potentials with the depolarising phase largely due to the activation of Na_V channels and the repolarisation and hyperpolarisation phase mediated by K_V channels. Unlike most neurons that communicate through chemical neurotransmitter synapses, the main stimuli for peripheral sensory neurons are environmental cues, such as touch, pressure, sound, movement, light, nociception or non-neurotransmitter type chemicals. This means that specialised receptors are required at the terminals of

A **Usoskin *et al* 2015**

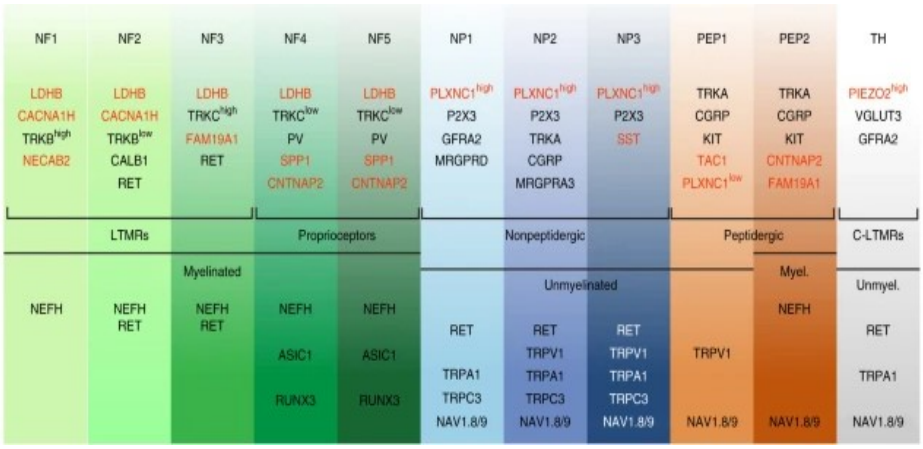

B **Li *et al* 2016**

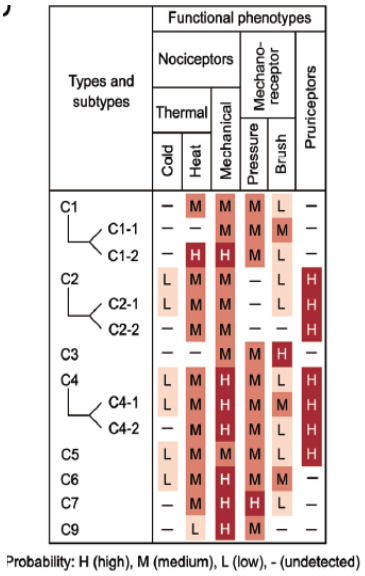

C

Zheng *et al* 2019

Neuronal Subtypes	Labeling Strategy
Nonpeptidergic Nociceptors	*MrgD*^{EGFP}
Peptidergic Nociceptors	CGRPα-EGFP
C-LTMRs	*TH*$^{2A\text{-}CreER}$;*R26*$^{LSL\text{-}tdTomato}$ TAM@P13.5-14.5
Aδ-LTMRs	*TrkB*^{CreER};*R26*$^{LSL\text{-}tdTomato}$ TAM@E12.5-14.5
Aβ RA-LTMRs	Npy2r-GFP
Aβ SA1-LTMRs	*TrkC*^{CreER};*Ret*^{tfGFP} TAM@E12.5
Aβ Field-LTMRs	*TrkC*^{CreER};*Ret*^{tfGFP} TAM@P12.5-14.5
Proprioceptors	*PV*^{IresCre};*R26*$^{LSL\text{-}tdTomato}$

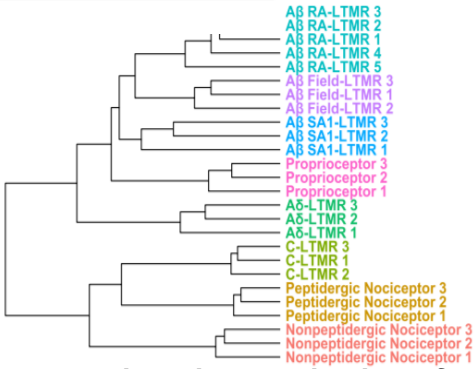

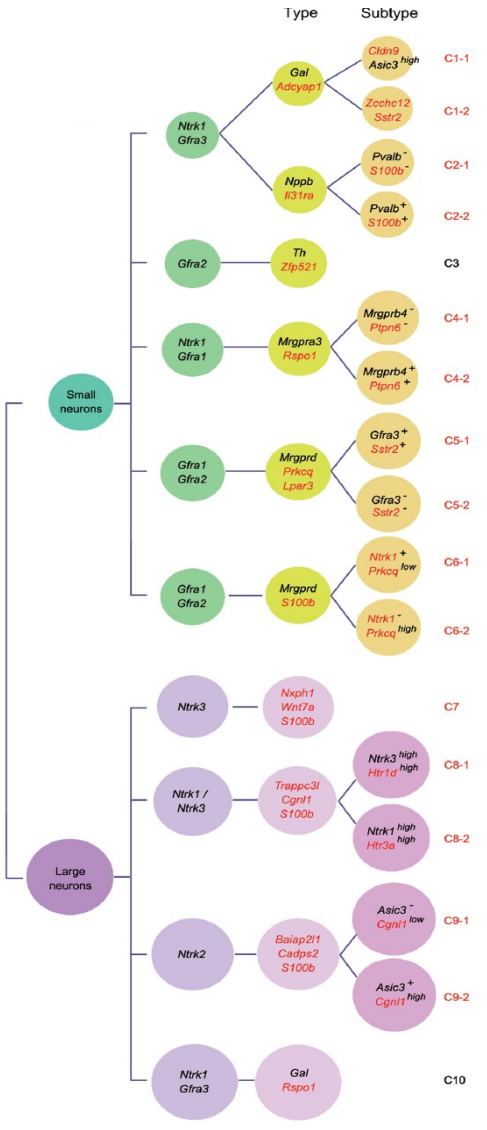

Figure 1.13 RNA-sequencing characterisation of sub-populations of sensory neurons in the DRG. **(A)** Identification of 11 sub-populations of sensory neurons using single-cell RNA-seq taken from (Usoskin *et al.*, 2015). **(B)** Identification of 10 populations of sensory neurons, further separated into 15 sub-populations using single-cell RNA-seq and identification of stimulus type each population responded to, including cold, heat, light touch, noxious touch, pressure and proprioception, taken from (Li *et al.*, 2016). **(C)** Separation of 8 populations of sensory neurons by GFP-tagging genes shown in the table and sorted based on the fluorescence (FACS) then mRNA expression assessed using RNA-seq, taken from (Zheng *et al.*, 2019). Studies agree there are a number of sub-populations but markers for each population are not clear.

sensory neurons to transduce non-electrical stimuli into action potentials, rather than just transmitting. For this, there are specialised ion channels and GPCRs that respond to mechanical, thermal and chemical stimuli, there are also differences in those that respond to innocuous and noxious stimuli of the same physical nature. The ion channels that transduce the stimulus into ionic current are usually non-selective cation channels that cause the initial depolarisation that can then be propagated along the axon by Na_v channels.

Focussing on noxious stimuli, receptors such as TRPV1 (one of the principal heat sensing ion channels), cold sensitive channel TRPM8 and mechanosensitive channel, Piezo2, are identified in sensory neurons. In addition, there are a number of chemically sensitive channels such as TRPA1 and GPCRs that respond to chemicals (e.g. released by immune cells or tissue damage), such as interleukins, prostaglandins, serotonin, histamine and bradykinin **(Figure 1.14)**. This has the effect of sensitising the neuron, to reduce the level of stimulus required for activating the neurons or generating action potentials directly. The sensitising process can be augmented or caused by the nociceptor releasing substance P or CGRP (calcitonin gene-related peptide) at the injury site (Russell *et al.*, 2014) **(Figure 1.14)**. In turn leading to the allodynia (innocuous stimuli becoming noxious) and hyperalgesia (an increased response to already noxious stimuli) that accompanies inflammatory pain.

Most treatments for mild to moderate pain in fact target these inflammatory factors to reduce the sensitisation of the nociceptors; these treatments include either steroidal or non-steroidal anti-inflammatories (NSAIDs) (Tomić *et al.*, 2017). Paracetamol, aspirin and propionic acids such as ibuprofen and naproxen all inhibit cyclooxygenases, COX-1 and COX-2 (Tomić *et al.*, 2017). COX-1 and COX-2 inhibition prevents the synthesis of prostaglandins with COX-1 found in kidney's, blood vessels and stomach and COX-2 present in inflammatory cells (Hawkey, 2001). Therefore, COX-2 inhibition has an analgesic effect; COX-1 inhibition leads to the main side effects of NSAIDs, such as gastrointestinal damage such as ulcers (Hawkey, 2001). NSAIDs are currently the first analgesics of choice, pain not treatable with NSAIDs is treated with painkillers with potentially worse side effects, as they have a strong effect in the central nervous system (opioids and cannabinoids) or suppressing the immune system (steroidal anti-inflammatories SAIDs).

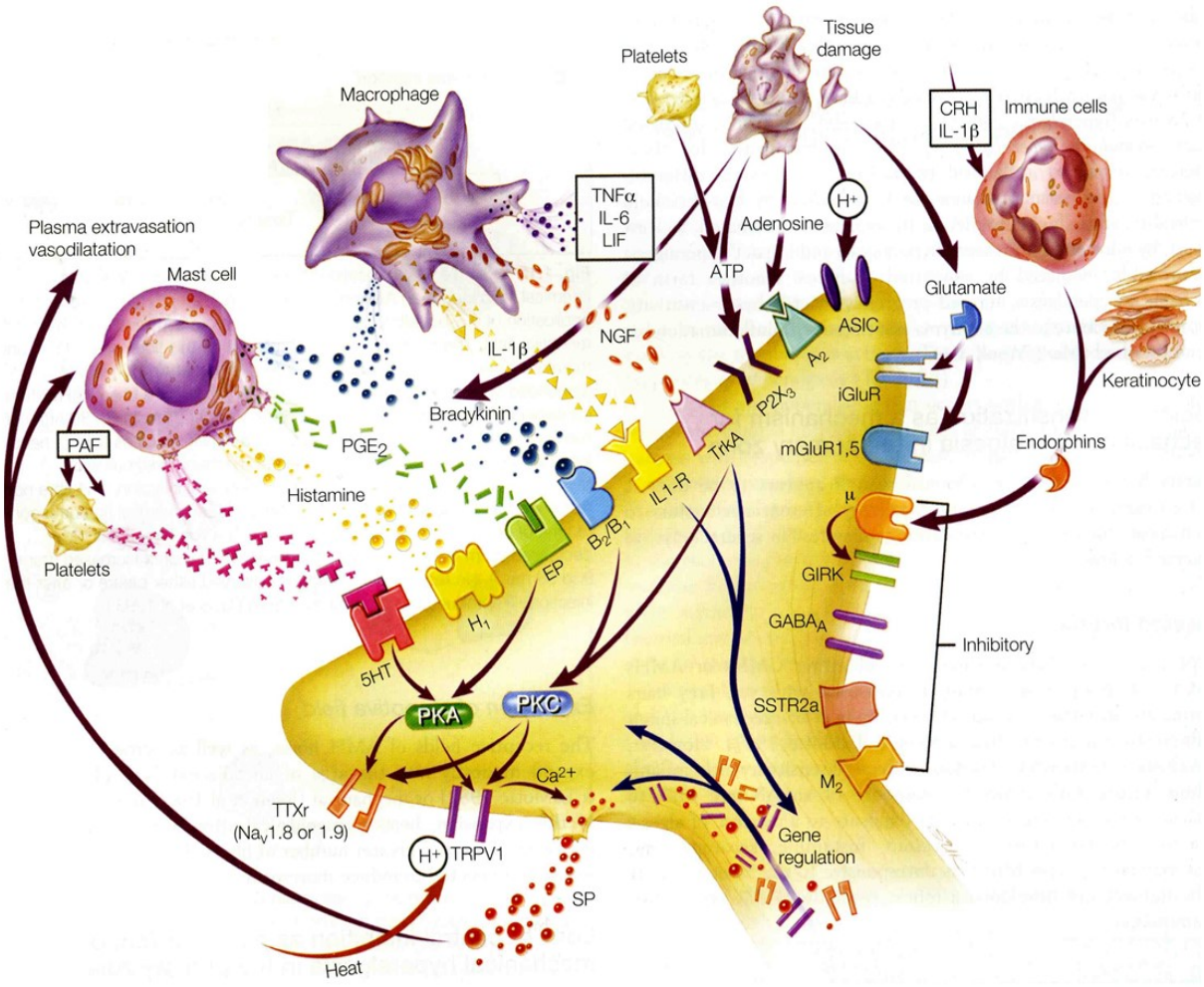

Figure 1.14 Interface between immune cells and sensory nerve terminals releasing inflammatory mediators. Taken from *Wall and Melzack's Textbook of Pain (McMahon et al., 2013)*

SAIDs are a class of therapeutics that increase the level of adrenal steroids such as corticosterone or mimic their action with synthetic compounds such as hydrocortisone and dexamethasone (Ramamoorthy and Cidlowski, 2016). SAIDs are immunosuppressants, suppressing the immune system, thereby preventing the inflammatory response occurring and therefore inhibiting sensitisation at the source. The adverse effect being that the patient is immunocompromised and thus less likely to be able to fight off infection (Coutinho and Chapman, 2011). There is also a negative feedback loop that prevents humans over-producing steroid hormones, mimicking these steroids supress endogenous corticosteroid synthesis (Coutinho and Chapman, 2011).

As well as SAIDs and NSAIDs, opioids and cannabinoids can be used as analgesics, with opioids still very widely used and medical cannabis (and cannabinoids) being increasingly prescribed as analgesics (Levinsohn and Hill, 2020). Both types are active in the descending inhibitory pathway that inhibits pain response and the dopaminergic reward pathways that result in addiction and euphoria through binding to GiPCRs that reduce adenylyl cyclase and cAMP activation (Kendall and Yudowski, 2017, Al-Hasani and Bruchas, 2011). Thus, both have significant side effects, in the central nervous system and in the body. The most efficacious opioids are also very addictive and lead to tolerance and dependence, also producing a euphoric 'high' effect in the brain and causing significant respiratory depression (Allouche *et al.*, 2014). Although seemingly less addictive, some cannabinoids still have a strong psychoactive component and increase appetite, both of which are unwanted effects for an analgesic(Degenhardt and Hall, 2008). Research into the addictive impact of cannabinoids and the therapeutic benefit has been hindered by the legal status of cannabis in the majority of places that pain research occurs.

Therefore, there is still space for better analgesics and further understanding of different types of pain and areas that can be targeted for pain relief.

1.8 The Role of K_v7 in Pain

1.8.1 K_v7 and Physiological Pain

K_v7 channels are expressed through central and peripheral neurons involved throughout the pain pathway, in peripheral sensory neurons, in the spinal cord and in various regions of the brain. Retigabine-sensitive K_v7 current has been recorded from

peripheral sensory neuron cell bodies in cultured DRG neurons preparations (Linley *et al.*, 2008, Liu *et al.*, 2010, Passmore *et al.*, 2003, Mucha *et al.*, 2010) and acute DRG slices. Furthermore, the presence of K_v7 protein has also been detected in axons and terminals of sensory neurons, as well as increases in spike frequency after XE-991 and decreases in spike frequency in response to retigabine, when these compounds were applied to a bath containing the skin and distal portion of the nerve (Rose *et al.*, 2011, Roza *et al.*, 2011, Passmore *et al.*, 2012). In capsaicin responsive sensory neurons, retigabine hyperpolarises resting membrane potential whereas the K_v7 inhibitor, XE-991 leads to depolarisation of neurons (Liu *et al.*, 2010, Passmore *et al.*, 2003, Du *et al.*, 2014); this suggests that K_v7 channels are involved in controlling the excitability of heat sensitive nociceptors. Mechano-heat sensitive Aδ fibres and a portion of C-fibres also responded to retigabine when applied to the receptive field on the skin by local injection to the paw by hyperpolarising the resting membrane potential. Retigabine application also reduced the response of the neurons to noxious heat and in accordance with a role for K_v7 channels controlling nociceptor activity, application of XE-991, after prolonged retigabine application, reversed the effect and led to sensitisation of the neurons to heat (Passmore *et al.*, 2012). The functional effect of non-specific K_v7 modulators has been accompanied by demonstration of the expression of $K_v7.2$ in NF200 positive (myelinated) and negative cutaneous sensory nerve endings using immuno-fluorescence. Interestingly, XE-991 application was able to elicit responses to heat in apparent heat-insensitive Aδ neurons, whereas an increased response to heat was rarely seen in C-fibres after XE991 application (Passmore *et al.*, 2012). However, it is important to note that the receptive fields for heat sensitive C-fibres are made up of multiple C-fibre neurons and require a larger surface area to be heated compared to mechanical or cold stimuli (Stevens *et al.*, 1974, Paricio-Montesinos *et al.*, 2020), thus, the effect on C-fibres may be lost here. Passmore and colleagues also demonstrated that changes in M current are able to alter excitability in some unmyelinated neurons (Passmore *et al.*, 2012).

K_v7 channels are also important in the detection of cold both in the DRG and in the TG neurons. In DRG neurons, XE-991 amplified the response to cold in mechano-cold C-fibres, which were also responsive to menthol and camphor (cold sensing neuron activators) and increased the temperature (warmer temperatures) at which those neurons responded to cold (Vetter *et al.*, 2013). In TG, $K_v7.2$ immuno-reactivity is

strong, particularly in small-diameter neurons. Research done using behavioural studies, demonstrated that XE-991 application increased sensitivity to oro-facial cold, this was achieved by placing a drinking reward that is reached through an aperture with a thermal element present. Oro-facial cold sensitivity was measured by cooling the element, then analysing the amount of time and number of times an infra-red beam was broken by the head reaching the reward (Ling *et al.*, 2018). Interestingly, retigabine did not affect oro-facial cold response in naïve animals but after nerve constriction injury, retigabine significantly attenuated neuropathic cold sensitivity and this was accompanied by an upregulation of $K_v7.2$ after injury (Ling *et al.*, 2018). In contrast, $K_v7.2$ was downregulated in V2 trigeminal neurons after chemotherapy-induced neuropathic pain. This was accompanied by increased sensitivity to mechanical stimuli in the oro-facial region and hindpaw, which was reversed by the analgesic effect of retigabine (Ling *et al.*, 2017).

K_v7 channels are also affected as part of the inflammatory pain process. Inflammatory mediators that activate $G_{q/11}$PCRs such as bradykinin and proteases inhibit K_v7 channels through the IP3-calcium/calmodulin pathway detailed in section 1.2.4. Accordingly, local hindpaw injection of retigabine reduces thermal hyperalgesia after bradykinin injection (Liu *et al.*, 2010). Injecting retigabine directly into L5 lumbar DRGs also reduces thermal hyperalgesia and nocifensive behaviour after hindpaw bradykinin injection (Du *et al.*, 2014). However, injecting flupirtine into afferent fibres only reduced thermal hyperalgesia in injured animals; the response of unsensitised animals to thermal stimuli was unchanged with flupirtine injection (Rose *et al.*, 2011), suggesting that flupirtine is able to reverse the inhibition of the channels.

Whilst the evidence for the involvement of K_v7 channels in the sensory response to thermal stimuli is compelling, the effect on mechano-transduction is less clear. In skin-nerve preparations where extracellular recordings are made from intact skin-nerve samples, retigabine had no significant effect on firing-rate of mechano-sensitive neurons (Passmore *et al.*, 2012). Yet in axotomized mechano-sensitive nociceptors, XE-991 increased the response to mechanical stimulation whereas retigabine resulted in inhibition suggesting that activating K_v7 channels can alleviate the hyper-excitability of axotomized LTMR neurons (Roza and Lopez-Garcia, 2008). In addition, *Kcnq2* knockout mice have increased thermal and mechanical sensitivity based on hindpaw withdrawal when heating (Hargreaves) or applying mechanical pressure (von Frey) to

the hindpaw while locomotion was unaffected in the rotarod test (King *et al.*, 2014). Unfortunately, no further behavioural observations were made, so the impact of knockout on other pain behaviours is unknown (King *et al.*, 2014).

A related process to pain, pruritus (itch) is also enhanced by the inhibition of K_v7 channels and retigabine supresses' pruriceptor excitability and itch related behaviour (Zhang *et al.*, 2020a).

1.8.2 K_v7 and Pathological Pain

As K_v7 channels are so heavily regulated by GPCRs, it stands to reason that chronic release of inflammatory mediators, especially those acting via the $G_{q/11}$ signalling cascade, leads to longer term inhibition of K_v7 channels. In animal models of chronic inflammation, retigabine and flupirtine significantly attenuated hyperalgesia whereas XE-991 enhanced the hyperalgesia, as expected (Blackburn-Munro and Jensen, 2003). This demonstrates that there is residual K_v7 current, and the channels are still present; $K_v7.2$ expression is seemingly unchanged after chronic CFA induced inflammation (Cisneros *et al.*, 2015) however, other longer-term inflammatory conditions have not been studied. Retigabine is also effective in alleviating hyperexcitability associated with neuroinflammation when induced by liposaccharides (Tzour *et al.*, 2017). Other chronic inflammatory disorders are also alleviated by K_v7 enhancers such as gout arthritis which is characterised by periods of excessive inflammation that causes severe acute pain (Zhang *et al.*, 2020b). Inducing Gout arthritis by injecting monosodium-urate into the ankle joints of rats resulted in strong hyperalgesia which was reversed by retigabine or flupirtine (Zhang *et al.*, 2020b).

Neuropathic pain is also a type of chronic pain but produced by nerve injury; the definition of neuropathic pain is 'pain caused by a lesion or disease of the somatosensory nervous system and develops due to mechanistic sustained hyperexcitability of nociceptive afferents' (Murnion, 2018). This can be due to nerve damage by crushing or cutting such as in amputation or in degeneration as in diabetic neuropathy (Rose *et al.*, 2011, Djouhri *et al.*, 2019). Depending on the type of injury and the subsequent downstream effects that occur, the pain can be oriented to the side of the injury only or can also appear on the contralateral side to the injured region (Seltzer *et al.*, 1990), usually due to changes in the spinal cord and/or brain (Dickenson and Sullivan, 1987). 'Wind up' of the spinal cord is a form of plasticity whereby changes in transcription and translation of proteins due to excessive release of

neuromodulators and prolonged presence of glutamate lead to the amplification of peripheral nociceptive input by the spinal circuits (Dickenson and Sullivan, 1987). NMDA receptor upregulation is commonly identified as one of such wind-up mechanisms. NMDAR activation allows the influx of Ca^{2+} in response to glutamate, this influx activates calmodulin-dependent kinases, CaMKI and CaMKII (Malinow *et al.*, 1988, Malinow *et al.*, 1989), resulting phosphorylation of proteins promotes the activation and insertion of proteins involved in increasing firing frequency, such as AMPA receptors (short term potentiation) (Kerr *et al.*, 1998, Polgár *et al.*, 2008). The downstream effect of this is long-term potentiation due to second messenger induced changes in translation and transcription, which maintains the increased response to glutamate (Malinow *et al.*, 1989, Rygh *et al.*, 2006). This is similar to the synaptic plasticity that occurs in memory formation, but in this case has the detrimental effect of amplifying nociceptive signalling (reviewed in (D'Mello and Dickenson, 2008).

However, often the wind-up that occurs is due to the initial changes in damaged peripheral neurons so preventing the hyperexcitability of the peripheral neurons reduces the extent of spinal cord wind-up and neuropathic pain. Therefore, the changes that occur in peripheral afferents during neuropathic pain are particularly important.

In the peripheral afferents, severing the nerve results in a swelling that forms an endbulb that sprouts axons to attempt to regenerate nerve endings (Terenghi, 1999). Obstruction of this process causes the endbulb, sprouts and glia as well as other important cells aiding in the regeneration process to create a mass known as a neuroma (Laing *et al.*, 2015). The neuroma and the cell bodies in the DRG generate ectopic firing (spontaneous action potentials from somewhere other than the nerve terminal). As nociceptors are usually silent unless receiving noxious stimulation, the spontaneous firing of these neurons leads to spontaneous pain associated with neuropathy (Laing *et al.*, 2015).

Changes in K_V7 channel expression is observed in the peripheral neurons after neuropathy occurs. The expression of *Kcnq2* in the DRG is significantly reduced after neuropathic injury *in vivo* (Rose *et al.*, 2011, Roza *et al.*, 2011) and after axotomy, *Kcnq5* expression was abolished (King and Scherer, 2012). Despite the downregulation of *Kcnq2*, retigabine was able to inhibit the ectopic firing of axotomized

neurons when applied to the neuroma (Roza and Lopez-Garcia, 2008). Later, the same group identified that the downregulation of $K_v7.2$ in the cell bodies was accompanied by an upregulation of $K_v7.2$ in the neuroma, a process that did not occur when axonal transport was interrupted (Cisneros *et al.*, 2015). This suggests that K_v7 downregulation contributes to the development of neuropathic pain but that diverting expression to the neuroma can reduce the likelihood of spontaneous firing (Cisneros *et al.*, 2015). There is also evidence that in other neurons, K_v7 channels at the axon initial segment, migrate down the axon after prolonged periods of inhibition (Lezmy *et al.*, 2017). One of the most prevalent neuropathies is diabetic neuropathy that can affect up to 50% of patients; the pain associated with diabetic neuropathy can be alleviated by retigabine (Djouhri *et al.*, 2019) and may also involve changes to K_v7 expression (Djouhri *et al.*, 2020), though suggested, strong evidence of this is currently lacking. Additionally, in a rat model of bone cancer, $K_v7.2$ and $K_v7.3$ expression was reduced in the DRG as did K_v7 current recorded from DRG neurons and retigabine reversed the hyperexcitability of the neurons induced by bone cancer (Zheng *et al.*, 2013).

KCNQ2, *KCNQ3* and *KCNQ5* all share an RE1 binding site for REST (repressor element 1-silencing transcription factor), *KCNQ1* and *KCNQ4* were seemingly less likely to bind REST (Mucha *et al.*, 2010). This was identified through a gel mobility assay, whereby *KCNQ* DNA oligonucleotides with the RE1 sequence present (or closest homology) were incubated with the complex. If the RE1 site was present and able to bind REST, it competed off the radiolabelled RE1 sequence added prior, resulting in loss of the band produced by radiolabelled RE-1 (Mucha *et al.*, 2010). REST downregulates gene expression, often supressing neuronal genes in non-neuronal tissues. Therefore, tonic expression of REST is low in sensory neurons, but is drastically increased during inflammation (Mucha *et al.*, 2010) or neuropathic injury (Rose *et al.*, 2011, Zhang *et al.*, 2019). Because of the RE1 binding sites, REST is able to affect K_v7 channels, presumably reducing the level of expression in chronic conditions. Inducing chronic pain either by sciatic nerve ligation or in a rat bone cancer model, leads to a strong reduction in *KCNQ2* (Rose *et al.*, 2011, Zheng *et al.*, 2013) and *KCNQ3* (Zheng *et al.*, 2013). Furthermore, REST knockout animals do not develop neuropathic pain (Zhang *et al.*, 2018, Zhang *et al.*, 2019) and genes such as *KCNQ2* are not downregulated (Zhang *et al.*, 2019). In contrast, viral overexpression

of REST resulted in neuropathic-like hyperalgesia in uninjured animals (Zhang *et al.*, 2019), suggesting a link between neuropathic pain, K_v7 channels and increased REST expression.

Thus, K_v7 channels are important for controlling the excitability of cells, resulting in changes to the contractility of muscles or the activity of neurons and therefore are highly modulated by intracellular processes. In the case of pain, many of the pro-inflammatory modulators exert some inhibition of K_v7 channels to increase the pain response. Changes to K_v7 activation and expression are also a key factor in chronic pain, including neuropathic and cancer pain. Indeed, potentiating K_v7 channel current, alleviates pain in rodent models and in humans. However, the wide-ranging expression of K_v7 channels presents a problem in targeting K_v7 channels for pain therapies. Though understanding the subunits involved in pain response compared to subunits involved in other tissues and processes may provide a new avenue to explore for therapy.

1.9 Aims and Objectives

Much of the work looking at modulating K_v7 channels to reverse the effects of a variety of illnesses result in improvements in that condition, meaning K_v7 channels seem to be an adequate target for treatment of various conditions. However, what is also demonstrated here is the wide-ranging expression of K_v7 channels and the importance of them functioning within the correct range of activity for the given tissue. For example, by increasing K_v7 current in hyperexcitable neurons to treat epilepsy will also lead to an increase in K_v7 current in correctly functioning tissues, which could possibly result in impaired functionality of that tissue. Indeed, this is the case when treating epilepsy with retigabine; bladder retention and reduced blood pressure can occur due to the inhibition of smooth muscle contractility and peripheral neurons.

Therefore, targeting the entire repertoire of K_v7 channels in the body as a whole may not be an acceptable target for many conditions. In order to determine whether K_v7 channels are potentially a viable target for treating pain conditions, we assessed K_v7 subunit expression in the rodent DRG to better understand the distribution of K_v7 subunits in different sensory neurons with an aim to identify if K_v7 expression pattern that would distinguish sensory neurons from non-neuronal cells, such as smooth muscle cells or cardiomyocytes We also sought to understand the functional

implication of the expressed subunits on K_v7 current in sensory neurons and the impact the subunits had on neuronal excitability *in vitro* and on pain behaviour *in vivo*. We also thought to obtain further clarity on the contribution of K_v7 channels in peripheral sensory neurons to the development of pain responses compared to K_v7 channels expressed in the central neurons of the pain pathway. The overall aim of this study is to understand the distribution and functional contribution of all five K_v7 subunits in peripheral sensory neurons and their effect on nociception and pain response.

Aim 1: To determine the pattern of K_v7 subunit expression in myelinated and unmyelinated peripheral somatosensory neurons of rats and mice by employing measures of gene and protein expression to analyse the whole-DRG and individual neuron expression of K_v7 subunits.

Aim 2: Characterise the functionality of expressed subunits in different populations of somatosensory neurons through electrophysiological recordings of potassium current in sensory neurons with the aid of pharmacological and gene-interference compounds.

Aim 3: Assess the contribution of subunits expressed in the DRG to pain response *in vivo* via administration of pharmacological and gene-interference compounds in the presence of acute and inflammatory noxious stimuli.

Chapter 2: Materials and Methods

2.1 Reagents and Resources

Table 2.1A: Antibodies

Antibodies	Concentration	Source	Code
Mouse anti-NF200	1:2000	Sigma	N2912
Rabbit anti-NF200	1:1000	Sigma	N4142
Chicken anti-Peripherin	1:500	Abcam	ab39374
Mouse anti- K_v7.1	1:200	Santa Cruz	sc-365186
Mouse anti- K_v7.2	1:200	Santa Cruz	sc-271852
Rabbit anti- K_v7.3	1:500	Alomone	APC051
Rabbit anti- K_v7.4	1:500	Neuromab	75-082
Rabbit anti- K_v7.5	1:200	Abcam	ab19319
Donkey anti-Rabbit AF488	1:1000	Invitrogen	A21206
Donkey anti-Mouse AF488	1:1000	Invitrogen	A21202
Donkey anti-Rabbit AF555	1:1000	Invitrogen	A-31572
Donkey anti-Mouse AF555	1:1000	Invitrogen	A-31570
Goat anti-Chicken AF555	1:1000	Invitrogen	A21437
eYFP	1:1000		
NeuroTrace Alexa Fluor 555 paste	Neat	Invitrogen	N22883
Cholera toxin B-AF488	0.1 % w/v	Invitrogen	C34775

Table 2.1B: Compounds

Compounds	*In vitro* Concentration (I.P concentration) [I.plantar concentration]	Source	Code
ICA-27243	2 µM (30 mg/kg) [500 µM]	Alomone	I-130
Retigabine	10 µM (15 mg/kg) [500 µM]	Abcam	ab145545
XE-991	10 µM	Sigma	X2254
Capsaicin	1 µM [300 µM]	Sigma	M2028
Freund's adjuvant	[Neat]	Sigma-Aldrich	F5881

Table 2.1C: Plasmids

Plasmids	Concentration	Source
KCNQ1+eYFPc	400ng	Kindly provided by Mark Shapiro, University of Texas Health Science Center at San Antonio, Texas, USA
KCNQ2+eYFPc	400ng	Kindly provided by Mark Shapiro, University of Texas Health Science Center at San Antonio, Texas, USA
KCNQ3+eYFPc	400ng	Kindly provided by Mark Shapiro, University of Texas Health Science Center at San Antonio, Texas, USA
KCNQ4+eYFPc	400ng	AF105202
KCNQ5+eYFPc	400ng	Kindly provided by Mark Shapiro, University of Texas Health Science Center at San Antonio, Texas, USA
KCNQ2/3 concatemer	400ng	Kind gift from Snezana Maljevic, Tubingen University, Germany (Gao *et al.*, 2017)

DNA was delivered in a pcDNA3 plasmid. eYFPc denotes an eYFP tagged to the C-terminus of the channel. KCNQ2/3 concatemer contains the sequence for both subunits to produce a KCNQ2/3 dimer.

Table 2.1D: Specialist reagents and kits

Specialist reagents and kits	Source	Code
FuGENE	Promega	E2311
Taqman qPCR mix	Thermo Fisher	4444557
RNeasy	Qiagen	74104
Taqman MultiScribe RT	Invitrogen	N8080234
Sensiscript	Qiagen	205211
Fast Gene scriptase II	Nippon	LS63
GoTaq green	Promega	M7121
Vectashield	Vector Labs	H-1200
Amaxa rat neuron nucleofector	Lonza	VPG-1003
Purelink RNA Kit	Invitrogen	12183018A

Table 2.1E: Primers and siRNA

Primers and siRNA	Sequence	Source	Code
Taqman Rat KCNQ1	proprietary information	Invitrogen	Rn00583376_m1
Taqman Rat KCNQ2	proprietary information	Invitrogen	Rn00591249_m1
Taqman Rat KCNQ3	proprietary information	Invitrogen	Rn00580995_m1
Taqman Rat KCNQ4	proprietary information	Invitrogen	Rn01518851_m1
Taqman Rat KCNQ5	proprietary information	Invitrogen	Rn01512013_m1
Taqman Rat HPRT1	proprietary information	Invitrogen	Rn01527840_m1
KCNQ2 siRNA1 (Stealth)	sense (5'-3'): GCUUUGCCCUGAAAGUCCAAGAGCA antisense (3'-5'): UGCUCUUGGACUUUCAGGGCAAAGC	Invitrogen	Kcnq2RSS301288
KCNQ2 siRNA2 (Stealth)	sense (5'-3'): AGGUCAGUUUGAAAGAUCGUGUCUU antisense (3'-5'): AAGACACGAUCUUUCAAACUGACCU	Invitrogen	Kcnq2RSS301289
KCNQ2 siRNA3 (Stealth)	sense (5'-3'): CCUCCAGACUCAUUCCGCCUCUGAA antisense (3'-5'): UUCAGAGGCGGAAUGAGUCUGGAGG	Invitrogen	Kcnq2RSS350743
Non-coding RNA (Stealth)	Medium GC Duplex Sequence is proprietary information	Invitrogen	12935112
Cholesterol tagged KCNQ2 siRNA 1	sense (5'-3'): GCUGUAUUAUUAAGAUUGU antisense (3'-5'): CGACAUAAUAAUUCUAACA	Dharmacon	A-092568-13
Cholesterol tagged KCNQ2 siRNA 2	sense (5'-3'): CGUGUUUCUUUUAGUCUUC antisense (3'-5'): GCACAAAGAAAAUCAGAAG	Dharmacon	A-092568-14
Cholesterol tagged KCNQ2 siRNA 3	sense (5'-3'): CCUUUAUCCAAUAGUAGGU antisense (3'-5'): GGAAAUAGGUUAUCAUCCA	Dharmacon	A-092568-15
Cholesterol tagged KCNQ2 siRNA 4	sense (5'-3'): CGUUUACCCUCAUUGGUGU antisense (3'-5'): GCAAAUGGGAGUAACCACA	Dharmacon	A-092568-16
Cholesterol tagged non-targeting siRNA pool	proprietary information	Dharmacon	D-001910-10
Cholesterol tagged KCNQ5 siRNA 1	sense (5'-3'): CCAUUGUUCUUAUCGCUUC antisense (3'-5'): GGUAACAAGAAUAGCGAAG	Dharmacon	A-082545-13

Cholesterol tagged KCNQ5 siRNA 2	sense (5'-3'): UUUUCAACAUAUGCGGAUG antisense (3'-5'): AAAAGUUGUAUACGCCUAC	Dharmacon	A-082545-14
Cholesterol tagged KCNQ5 siRNA 3	sense (5'-3'): GCCUGGUACAUUGGAUUUC antisense (3'-5'): CGGACCAUGUAACCUAAAG	Dharmacon	A-082545-15
Cholesterol tagged KCNQ5 siRNA 4	sense (5'-3'): UCACUACGCCUCAAGAGUU antisense (3'-5'): AGUGAUGCGGAGUUCUCAA	Dharmacon	A-082545-16
***In vivo* purity cholesterol tagged KCNQ2 siRNA 4**	sense (5'-3'): CGUUUACCCUCAUUGGUGU antisense (3'-5'): GCAAAUGGGAGUAACCACA	Dharmacon	CTM561931
***In vivo* purity cholesterol tagged KCNQ5 siRNA 1**	sense (5'-3'): CCAUUGUUCUUAUCGCUUC antisense (3'-5'): GGUAACAAGAAUAGCGAAG	Dharmacon	CTM-669535
***In vivo* purity cholesterol tagged non-targeting siRNA**	sense (5'-3'): UGGUUUACAUGUCGACUAA antisense (3'-5'): AGUCGACAUGUAAACCAUU	Dharmacon	CTM561931

Table 2.1F: Software

Software	Source
Zen	Zeiss
Patchmaster	HEKA
Fitmaster	HEKA
Fiji	ImageJ
Origin pro	Origin
Prism 8	Graphpad
Python	Credit P. Mullen

2.2 Cell line experimentation

2.2.1 HEK293 Cell Culture and Transfection

Human embryonic Kidney line 293 (HEK293) cells were cultured to 80% confluency before passaging and used for experimentation between P10 and P60. Cells were grown in Dulbecco's modified Eagle's medium (DMEM Gibco) containing penicillin (100 U/mL) (Sigma), streptomycin (100 µg/mL) (Sigma) and 10% foetal calf serum (Sigma).

For both immuno-fluorescence studies and patch clamp HEK293 cells were cultured in 24 well plates for 24 hours prior to transfection, transfected with 400 ng of plasmid (Table 2.1C) using 1.5 µL of FuGene and made up to a 25 µL reaction mix with cell grade culture water (HyClone). Cells were treated with reaction mix for 16-18 hours before being washed from the wells, pelleted and re-plated onto 10 mm glass coverslips at varying dilutions. In most cases eYFP (enhanced yellow fluorescence protein) was used to detect transfected cells as the transfected cells were fluorescent when the DNA was translated to protein.

2.2.2 Immuno-fluorescence

Fluorescence studies on HEK293 cells were carried out as target validation for antibodies. Target validation was assessed as both positive controls and negative controls. HEK293 cells transfected with an eYFP tagged plasmid (or untransfected) were fixed in 4% paraformaldehyde (PFA Sigma) for 10 minutes, washed with PBS, blocked and permeabilised with 5% donkey serum, 0.05% Tween20 and 0.25% Triton X (Sigma) in PBS for 30 minutes and treated with primary antibodies for eYFP and a K_v7 antibody (Table 2.1A) for 2 hours. Cells were washed with PBS and treated with secondary antibodies for 1 hour 15 minutes then mounted onto slides using Vectashield. Specificity of antibody was assessed both on co-expression with eYFP in conditions where the complementary subunit was eYFP tagged and in conditions where eYFP was tagged to a KCNQ subunit not complementary to the antibody (in this case only eYFP fluorescence was expected). Images were taken using the LSM880 confocal microscope (Zeiss).

2.2.3 Voltage Clamp Electrophysiology

KCNQ transfected HEK293 cells were used to isolate the K_v7 potassium currents and study them independently of other ion channels. K_v7 current was recorded using a

HEKA EPC10 amplifier and Patchmaster V2 (HEKA instruments) using an inverted step protocol where cells were held at -20 mV, a deactivating 600 ms square voltage pulse to -60 mV was applied, the voltage was then restored to -20 mV. Voltage-dependence of activation was investigated using a standard IV protocol consisted of a train of square voltage pulses (1000 ms) from -80 mV to +40 mV in 10 mV increments with a deactivating pulse of 600 ms to -80 mV. In this protocol, the tail current elicited by the step to -80 mV is measured to remove the impact of driving force on the recording. Pipettes were pulled using a horizontal puller (Sutter P-97) and fire polished to typically 2-4 MΩ resistance. Upon entering whole-cell configuration, cell capacitance was nulled and series resistance was typically below 10 MΩ.

Experimental compounds were dissolved using DMSO as a vehicle in extracellular solution and control recordings were taken with DMSO present.

Intracellular solution (310 mOsm) contained: 160 mM KCl, 5 mM $MgCl_2$, 5 mM HEPES, 0.1 mM BAPTA, 3 mM K-ATP, 0.1 mM GTP; pH adjusted to 7.4 using NaOH (all from Sigma).

Extracellular solution contained (320 mOsm): 160 mM NaCl, 2.5 mM KCl, 1 mM $MgCl_2$, 10 mM HEPES, 2 mM $CaCl_2$ and 10 mM Glucose; pH adjusted to 7.4 with NaOH (all from Sigma).

Quantification and statistics

To analyse voltage dependence, voltage clamp recordings were quantified in Fitmaster V2 (HEKA instruments) by measuring the tail current from each voltage step immediately after the return step to -80 mV, as at this point the impact of electrical driving force is removed. Fitting the tail currents with a Boltzmann equation showed a sigmoidal current voltage relationship as expected for voltage-dependent potassium channels. Steady state outward current amplitude was measured at -20 mV and -60 mV and currents measured during compound applications were normalised to baseline current within that same cell to reduce inter-cellular differences. Repeated measures ANOVAs were used to identify a statistical difference between treatment groups.

2.3 *In vitro* Sensory Neuron Experimentation

2.3.1 Animal Information

Juvenile (bred in house in Leeds) and adult Wistar rats obtained from Charles River were housed on site at either Erl Wood (Lilly) or Leeds. Animals were housed in groups of three or four, exposed to a normal 12-hour light-dark cycle at 21°C with free access to food, water and environmental enrichment ad libitum. The health and welfare of all animals was monitored daily by trained unit staff and the investigator of this study. Experimenters were blinded to treatment conditions during testing and administration and sterile procedures were observed during intrathecal injections. Male Wistar rats were used for experiments in this study unless otherwise stated. Mice used here are sensory neuron specific *Kcnq2* knockouts, strain C57BL housed in Indianapolis and extracted tissue delivered either frozen or in hibernation media. Mice were housed 5 to a cage in a 12-hour light-dark cycle with food and water available *ad libitum*. All procedures were performed by personal licence holders (I93F8B0AF) under project licences (P40AD29D7, GG P6817644) as in accordance with the UK Animals (Scientific Procedures) Act 1986 and the EU directive.

Kcnq2 knockout mice were generated by flanking exons 2-5 with LoxP. Cutting out exons 2-5 removed the pore region and introduced a frameshift mutation, rendering the channel non-functional. LoxP mice were crossed with Cre mice with the Cre promoter on the *Pirt* (Phosphoinositide-interacting protein) gene, to produce a sensory neuron specific knockout.

2.3.2 DRG Preparation, Culture and Transfection

Juvenile or adult rats were sacrificed with overdose of Isoflurane or CO_2 and confirmed with cervical dislocation or severing of the femoral artery (Schedule 1 protocol). Spinal columns are extracted and to save spinal cords they were removed by pushing PBS through the intrathecal space to remove the spinal cord in an intact fashion. The spine was then cut sagittally to expose the DRGs down the left and right side in inter-vertebral spaces. They were extracted from these spaces and stored in ice-cold Hanks Balanced Salt Solution (HBSS HyClone) during extraction. From this stage DRGs were either taken for dissociation (to generate primary DRG culture) of for fixation (in order to perform immunostaining). To fix, DRGs were incubated in 4% paraformaldehyde (PFA Sigma) for one hour on ice and washed thoroughly in PBS

before being embedded in 10% gelatine for immuno-fluorescence. DRGs taken for dissociation were transferred to 37^{o}C HBSS containing 1 mg/mL Collagenase type 1A and 10 mg/mL Dispase (Sigma). DRGs were incubated in this dissociation solution at 37^{o}C for 13 minutes before gently triturating to mechanically dissociate the DRGs somewhat before incubating for a further 3 minutes. After incubation DRGs were triturated again before transferring the whole mixture into ice-cold Dulbecco's modified Eagle's medium (DMEM; Gibco) containing Glutamax, penicillin (100 U/mL; Sigma), streptomycin (100 µg/mL; Sigma) and 10% foetal calf serum (Sigma) to terminate the dissociation process through enzyme deactivation. Cells were pelleted by centrifuging at 64 g (G-force) for 5 minutes at 4^{o}C, resuspended in ice-cold DMEM and pelleted again. The pellet was resuspended in an appropriate volume of warm DMEM and plated onto 10 mm coverslips coated with poly-D-Lysine + laminin (10% poly-D-Lysine, 10% Laminin in cell grade culture water). Once plated cells were incubated at 37^{o}C in a humidified chamber (5% CO_2) for 4 hours to allow cell adhesion to the coverslip surface before having the wells flooded with prewarmed DMEM-Glutamax. Wells were cultured for a minimum of 2 days before experimentation and used for up to 5 days in vitro.

For transfection with siRNA oligonucleotides lacking any additional conjugations, (such as a cholesterol tag), DRGs followed the same preparation as described above, until the cell pellet was formed. Once the pellet was obtained it was resuspended in 100 µL of rat neuron nucleofection buffer (Lonza) with siRNA or non-targeting RNA for a final RNA concentration of 400 nM. This suspension was transferred to a Lonza-certified cuvette and transferred to a Lonza nucleofector I console where an electroporating 30 ms pulse was delivered to the cells in order to deliver the RNA to the cells. Once complete the suspension was extracted from the cuvette and added to 500 µL of DMEM-Glutamax and the culture process laid out above was completed. Cells were only used 2-4 days in vitro. Cholesterol-conjugated siRNA oligonucleotides were delivered to cultured neurons 24 hours after culturing, where DMEM was aspirated and replaced with DMEM containing 2% foetal calf serum and 1 µM siRNA conjugate (in 100 µL buffer), 1 µM NTC (in 100 µL buffer) or buffer control (Dharmacon) and allowed to culture a further 72 hours (optimised as minimum time for knockdown).

2.3.3 siRNA Preparation

The core active sequences for the siRNA used in this study were either Invitrogen stealth siRNA or Cholesterol conjugated siRNA from Dharmacon. In both cases the *in vivo* modifications to these siRNAs do not change the active sequence. Non-targeting controls were used to assess the specificity of knockdown, mRNA transcripts from closely related subunits were also examined as was sequence homology as a predictor of likely off-target knockdown. All siRNA sequences and information are presented in Table 2.1E.

2.3.4 Quantitative Polymerase Chain Reaction (qPCR)

In this work qPCR was utilised for whole DRG RNA expression and for quantifying the efficacy of siRNA knockdown in DRGs. For *in vitro* experiments RNA extraction was done from cultured cells from DRGs and the RNeasy (Qiagen) RNA extraction kit was used to extract and purify RNA. The concentration was measured with the Nanodrop 2000 (Thermo Scientific) in order to standardise the amount of RNA converted to cDNA. One µg of RNA was added to all cDNA synthesis reactions (Sensiscript RT Qiagen) with DNA polymerase and OligoDT and incubated at 37°C for 60 minutes.

Table 2.2: Quantitative PCR protocol

	1	**2**	**3**	**4**	**5**	**6**
Temperature (°C)	50	95	95	60	Run cycle (3-4) 40 times	4
Time (mins)	2:00	10:00	0:15	1:00		∞

cDNA (1 µL) was added to 20 µL reactions in 96 well plates using TaqMan master mix (10 µL) and TaqMan primers (0.5 µL per primer; Thermo Scientific), made up with RN-ase free water. qPCR was ran using a CFX96 Touch Deep Well Real-Time PCR Detection System (Bio-Rad), specific cycle outlined in Table 2.2. Prior to quantification using CT values, all curves were quality controlled to ensure they fit an expected sigmoid shape.

Quantification and statistics

Mean Ct (cycle threshold) value calculated for housekeeper gene transcript (*Hprt*1) and experimental gene (*Kcnq*1-5). These values were used to calculate ΔCt (gene Ct

– housekeeper Ct). ΔΔCt was then calculated by compared mean ΔCt to the vehicle control animals before calculating the fold change (2^ΔΔCt) and percentage knockdown (%). Statistical analysis (independent or repeated measures one-way ANOVA) was completed on ΔCt but results displayed as percentage knockdown for ease of understanding.

2.3.5 Voltage Clamp Electrophysiology

Recordings were obtained using EPC10 amplifier controlled by the Patchmaster V2 software (HEKA instruments), using an inverted hyperpolarising step protocol in order to isolate the K_v7/M current from other voltage-dependent potassium currents in sensory neurons. The protocol was similar to that used for HEK293 cell recordings (see Section 2.2.3). Cells were held at -20 mV and 600 ms steps to -60 mV were applied in order to deactivate the potassium current, the voltage was then returned to -20 mV. This is advantageous as most voltage-dependent potassium currents are negligible at these voltages due to the channels being inactivated in this range of voltages and K_v7 current has a characteristic slow time of deactivation and activation. These biophysical properties combined are not well conserved between other voltage-dependent potassium channels, so this protocol allows for enrichment of the M current without relying on pharmacological block of other potassium currents. Measurements were taken from steady state currents at -20 and -60 mV. Pipettes were pulled using a horizontal puller (Sutter P-97) and fire polished to typically 2-4 MΩ resistance. Upon entering whole-cell configuration, cell capacitance was nulled and series resistance at typically under 10 MΩ.

Experimental compounds were dissolved using DMSO as a vehicle in extracellular solution and control recordings were taken with DMSO present.

Intracellular solution (310 mOsm) contained: 160 mM KCl, 5 mM $MgCl_2$, 5 mM HEPES, 0.1 mM BAPTA, 3 mM K-ATP, 0.1 mM GTP; pH adjusted to 7.4 using NaOH (all from Sigma).

Extracellular solution (320 mOsm) contained: 160 mM NaCl, 2.5 mM KCl, 1 mM $MgCl_2$, 10 mM HEPES, 2 mM $CaCl_2$ and 10 mM Glucose; pH adjusted to 7.4 with NaOH (all from Sigma).

Quantification and statistics

Steady state outward current amplitude was measured at -20 mV and -60 mV and currents measured during compound applications were normalised to baseline current within that same cell to reduce inter-cellular differences. In the same way siRNA and non-targeting control currents were normalised to the average baseline current of the buffer/negative control. Independent and repeated measures One-Way ANOVAs were used for statistical analysis and mixed Two-Way ANOVAs used for voltage clamp *Kcnq2* siRNA experiments to compare between siRNA groups and compare compound effect within each group.

2.3.6 Current Clamp Electrophysiology

Sensory neurons were prepared and recorded in the whole-cell configuration, as described above but in current-clamp mode. Analysis of action potentials was done using Python coding to automatically measure components of the action potential and after-hyperpolarisation, detailed below. Cells were held with 0 pA of current to allow recordings from the resting membrane potential of the cell not an artificial holding potential. Cells with resting membrane potentials above -40 mV were excluded, input resistances for each condition are detailed in Table 2.3 and were consistent with previous reports (Zheng *et al.*, 2012, Kanda and Gu, 2017, Gold and Traub, 2004). The protocol used for recording was a current clamp step protocol with an initial 1000 ms -50 pA step to allow for determination of cellular properties. Following this initial step, 50 pA increments (of the same 1000 ms duration) were applied up to 1 nA of current, with a returning step to 0 pA between increments. This protocol was used for action potential properties and firing patterns and was ran 3 times per cell to get a range of when the first action potential was fired. To measure the rheobase a second protocol was used that spanned from 50 pA below to 50 pA above the current at which the first action potential was fired and increased current injection by increments of 5 pA. For example, if in protocol one, the cell fired and action potential at 200 pA of current, protocol two would have 5 pA increments from 150 pA to 250 pA to establish the current required to elicit an action potential more precisely. To standardise the level at which action potential properties were measured, action potentials from rheobase + 200 pA were analysed. For example, a rheobase of 200 pA would mean action potential properties from those at 400 pA were measured from that cell. The final protocol used was a continuous gap free recording of the cell with 0 current

injected to measure spontaneous depolarisation and action potential firing. This protocol was used to assess whether these cells responded to Capsaicin stimulation. If so, cells should spontaneously fire bursts of action potentials. Pipettes were pulled using a horizontal puller (Sutter P-97) and fire polished to typically 2-4 MΩ resistance.

Intracellular solution (310 mOsm) contained: 160 mM KCl, 5 mM $MgCl_2$, 5 mM HEPES, 0.1 mM BAPTA, 3 mM K-ATP, 0.1 mM GTP; pH adjusted to 7.4 using NaOH; (all from Sigma).

Extracellular solution (320 mOsm) contained: 160 mM NaCl, 2.5 mM KCl, 1 mM $MgCl_2$, 10 mM HEPES, 2 mM $CaCl_2$ and 10 mM Glucose; pH adjusted to 7.4 with NaOH; (all from Sigma).

Table 2.3: Input resistances for sensory neurons in rat DRGs

Condition	Buffer	NTC	Kcnq2 siRNA	Buffer	NTC	Kcnq5 siRNA
Input resistance MΩ (mean±sem)	684±35	701±49	637±33	533±23	570±41	698±34

Quantification and statistics

All analysis was done through a python script designed to measure action potential parameters and firing frequency. The software detected the action potential (AP peak and hyperpolarisation (AHP) peak using the find peaks function in the SciPy python module. The prominence, that is how much a peak stands out from the local signal, was set at a threshold of 20 mV and 5 mV for detection of AP and AHP peaks respectively. The width of the action potential at half the height of the AP peak to AHP peak amplitude (half-height width) was measured and refined to define the start and end of the AP peak and the start of the AHP. The end of the AHP was defined as the point when the signal returned to baseline. From these markers, depolarisation, repolarisation, AP width and AHP duration could be calculated. Firing frequency was calculated by the number of AP peaks in the one second current step and inter-spike interval by the time between AP peaks. M current (obtained in voltage clamp) and the threshold injected current required to elicit action potentials (rheobase) were

measured manually. Independent measures One-Way ANOVAs were used for current clamp statistical analysis.

2.3.7 Immuno-fluorescence

Protein expression was examined using immuno-fluorescence; the method also allowed to characterize neuronal types by the expression of appropriate markers (see below) and the methodology was similar for both rats and mice.

DRGs were fixed in 4% paraformaldehyde (PFA) for one hour on ice, washed and embedded in 10% w/v porcine gelatine (Sigma) and allowed to set at 4°C overnight. After setting, gelatine was cut into roughly 1 cm cubes with a single DRG in the centre and submerged in 4% PFA for 4-5 hours at 4°C until sufficiently hard, washed and stored in 0.1 M phosphate buffer (PB). Cubes of single DRGs were cut into 30 µm sections in PB using a VT1000s microtome (Leica) and washed in PBS. Sections were placed into a 24 well plate, 4 per well and treated with a 0.05% trypsin (Sigma) 1% Calcium chloride (Sigma) solution in PBS for 10 minutes at 37°C for enzymatic antigen retrieval. Sections were washed thoroughly in PBS and blocked and permeabilised with 5% donkey serum, 5% goat serum, 0.05% Tween20 and 0.25% Triton X (all Sigma) in PBS for 2 hours. As a sequential method was employed, the sections were incubated for 2 hours (or overnight at 4°C) in the first primary antibody (always the K_v7 antibody and if multiple subunits were analysed, $K_v7.2$ or $K_v7.4$ antibodies were applied first, as these were the antibodies most benefiting from the antigen retrieval step). Sections were washed in PBS and treated with the corresponding fluorescently conjugated secondary antibody for 1.5 hours at room temperature. Sections were washed again and incubated with the second primary antibody for 2 hours (or 4°C overnight), washed and incubated with the corresponding secondary antibody for 1.5 hours. Sections were washed prior to mounting and mounted on double frost slides using Vectashield mounting media with DAPI and glass coverslips and imaged with an LSM880 confocal microscope (Zeiss). Table 2.1A contains information on antibodies used in this study.

Quantification and statistics

Neuronal immuno-fluorescence was quantified by taking the non-neuronal background fluorescence and neurons with more than double this average fluorescence were deemed positive for that protein. Using this average was a way to

normalise the difference in fluorescence between samples. The border of each neuron was recognised, and the average fluorescence intensity of that area calculated using Zen software. The fluorescence would either be more than double or less than double the average fluorescence thus the neuron marked positive or negative for that protein. Percentage of neurons is reported for ease, but statistical analysis was completed using a non-parametric Fishers test of proportion as this test identifies differences in the proportion of neurons positive for one protein compared to another. For example, if protein A is expressed in 100 out of 500 total neurons and protein B is expressed in 200 out of 700 total neurons, Fisher's test determines a significant difference based on these proportions. Fluorescence intensity was quantified by subtracting a non-neuronal area used as background subtracted from the whole field of view fluorescence and statistical difference determined with a non-parametric Wilcoxon signed rank test.

2.4 *In vivo* Experimentation

2.4.1 *In vivo* Pharmacology Studies

Animals were sensitised using intra-plantar injections of either complete Freund's adjuvant as a sustained inflammatory model or Capsaicin for acute pain sensation. Analgesic compounds were delivered either intra-peritoneally for systemic delivery or intra-plantar for local delivery. After dosing, behavioural testing was employed to evaluate the effectiveness of analgesic compounds as compared to each other and a vehicle control. For systemic delivery, Retigabine was administered at 15 mg/kg and ICA-27243 at 30 mg/kg at a volume of 2 mL/kg suspended in 1% HEC (1% hydroxyethylcellulose, 0.25% Tween80, 0.05% antifoam) as a vehicle. Local administration of these compounds was achieved by intra-plantar injection of 100 µg in 50 µL of 1% HEC.

2.4.2 *In vivo* Knockdown of *Kcnq2* and *Kcnq5* with siRNA

siRNA knockdown of *Kcnq2* was achieved via intrathecal injection into the subarachnoid space in adult rats. Intrathecal injection was performed under general anaesthesia (4% isoflurane in oxygen at 2.5 L/min) in surgically aseptic conditions. A ~6 cm^2 area of fur was removed from the posterior of the rat, ascending from the base of the tail to facilitate accurate needle insertion. For the duration of the procedure rats

were placed on heating mats and anaesthesia maintained through a surgical mask at 2% isoflurane in oxygen with a flow rate of 0.6 L/min.

The L5-L6 vertebral junction was located using the finger, easily identified by a much deeper crevice than those above or below. A 26G x 1" (0.45x25mm) NR.18 needle (Fine-Ject) attached to a Luer lock Hamilton syringe was inserted into the groove between L5 and L6 and positioned in the subarachnoid space. A characteristic tail flick occurs when the needle is positioned correctly in the space, incorrect positioning is accompanied by a characteristic foot twitch and no tail flick. Upon observation of the tail flick, 10 µL volume was injected, the needle held in position for 30 seconds and then rotated and carefully removed. In all cases the injection vehicle contained 10% lidocaine as a further confirmation of successful injection. A successful intrathecal injection was accompanied by temporary hindlimb paralysis for 10 minutes and full recovery. Unsuccessful injections would result in no paralysis or a much more sustained, often unilateral paralysis of the hindpaw if injection was into the muscle.

After injections, rats were placed in heated recovery boxes for 30 minutes and observed at 4 intervals post-injection. Intrathecal injections were delivered as 100 µg of NTC or siRNA in PBS (with 10% lidocaine) once a day for 4 consecutive days before behavioural testing and tissue harvesting (DRGs, spinal cord and brain) to confirm the extent and location of knockdown.

2.4.3 Behavioural Testing

Von Frey Test

Assessment of mechanical hyperalgesia was performed using the Von Frey test, whereby dull, flexible filaments of increasing thickness are applied to the paw until the filament yields or the paw is withdrawn, the Dixon method was employed for analysis (Dixon, 1980, Chaplan *et al.*, 1994). Animals were habituated in the apparatus over two 30-minute sessions prior to taking measurements. Two consecutive baseline measurements were performed on the animals after two 30-minute habituation sessions, to assess the naïve mechanical pain thresholds and ensure consistency between trial days. In hyperalgesia studies, 24 hours before the test animals received an intra-plantar injection of complete Freund's Adjuvant (CFA) into the left paw and 30 minutes prior to testing, analgesics or vehicles were administered intra-peritoneally at 2 mL/kg **(Figure 2.1A)**. During assessments of normal pain threshold after *Kcnq2*

Experimental flow for analgesic behavioural testing

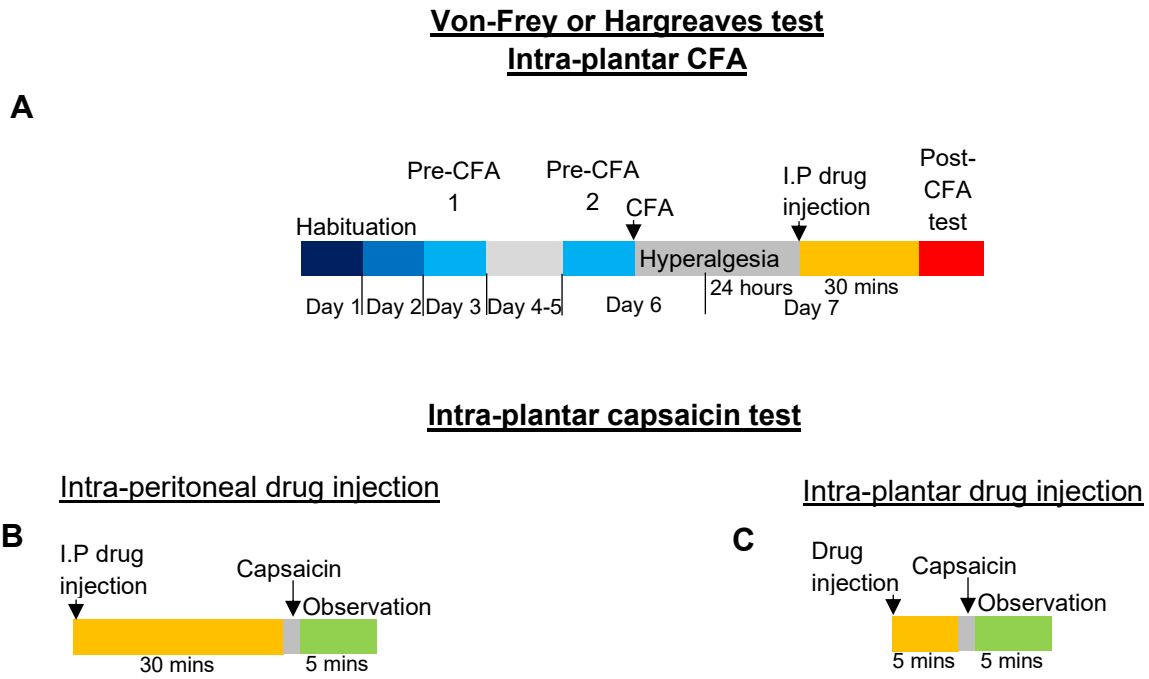

Figure 2.1 Experimental flow for analgesic behavioural testing. **(A)** Schedule for Von-Frey and Hargreaves tests; two 30-minute sessions of habituation, two baseline tests, followed by a hindpaw intra-plantar injection of CFA. Animals were left for 24 hours to allow development of hyperalgesia. 30 minutes prior to Von-Frey or Hargreaves tests, animals received an intra-peritoneal injection of retigabine, ICA-27243 or vehicle. **(B)** Intra-peritoneal injection of retigabine, ICA-27243 or vehicle 30 minutes prior to intra-plantar injection of capsaicin. Extent of nocifensive behaviour observed for 5 minutes post-capsaicin. **(C)** Intra-plantar injection of retigabine, ICA-27243 or vehicle 5 minutes prior to intra-plantar injection of capsaicin either into the same or opposite paw. Extent of nocifensive behaviour observed for 5 minutes post-capsaicin.

knockdown, intrathecal injections were delivered as described previously, no other injections were made **(Figure 2.2A)**. Baselines and testing were performed on both paws (in the case of CFA, the injured and uninjured paw) and involves ascending up through filament force until a painful withdrawal response was observed. This includes rapid withdrawal of the paw from the stimulus, often accompanied by licking or prolonged elevation of the paw. Once a painful response occurred, filament force was reduced and then reduced or increased depending on the resulting response as described in the Dixon method (Dixon, 1980, Chaplan *et al.*, 1994). The Dixon method (also known as 50% threshold method) gives a value for the withdrawal threshold that accounts for the pattern of positive and negative responses using the up and down method. The 50% threshold value was determined according to the following equation: 50% withdrawal threshold (10[Xf + Kδ])/10,000; where Xf is a value (in log units) of the final von Frey filament used; k is a tabular value for the pattern of positive/negative responses; and δ is a mean difference (in log units) between stimuli. The value is then converted from log back to grams. Following this method adjusts for the pattern of response to provide a more accurate paw withdrawal threshold and allows researchers to spot anomalies and inconsistencies in response. Such as in the case of a response, followed by 3 no response marks, the initial response is deemed a false positive. Animals were randomised and mean baseline thresholds compared to ensure each group had comparable means. Researcher was blinded as to which group received which treatment or vehicle.

Hargreaves Test

Thermal hyperalgesia was assessed by using a Hargreaves method (Hargreaves *et al.*, 1988) which utilises a progressively heating radial heat source positioned under animal hindpaw. The apparatus is equipped with an infrared sensor allowing to accurately record time to paw withdrawal (withdrawal latency); the shorter the latency the lower thermal pain threshold. Animals were habituated in the Hargreaves boxes over two 30-minute sessions prior to baseline measurements. Two consecutive trials were taken consisting of 4 replicates per paw per trial. In the hyperalgesia studies, 24 hours before test day animals received an intra-plantar injection of CFA into the left paw and 30 minutes prior to testing, analgesics or vehicles were administered intra-peritoneally at 2 mL/kg **(Figure 2.1A)**. During assessments of baseline pain threshold after *Kcnq2* knockdown, intrathecal injections were delivered as described previously,

Schedule for siRNA knockdown studies

A

Pain Threshold measurements: Von-Frey and Hargreaves tests

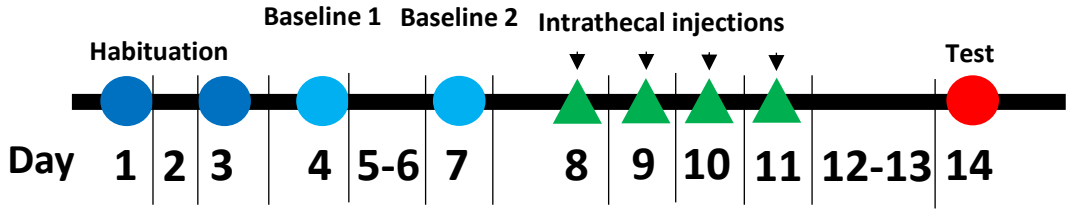

B

Intra-plantar capsaicin test

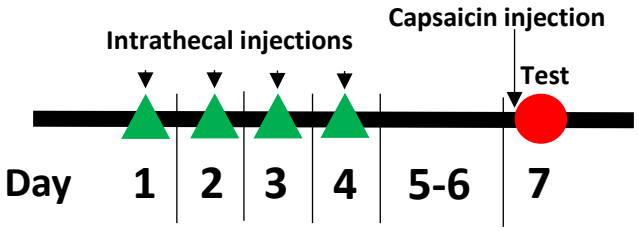

Figure 2.2 Schedule for siRNA knockdown studies. **(A)** Measurements of mechanical (Von-Frey) and thermal (Hargreaves) pain threshold performed on the same day. Two 30-minute sessions of habituation, two baseline tests followed by four consecutive intrathecal injections and two days of recovery. Post-intrathecal injection pain threshold tests were completed on day 14. **(B)** Four consecutive intrathecal injections followed by two days of recovery. Finally, extent of nocifensive behaviour observed for 5 minutes post intra-plantar capsaicin injection.

no other injections were made **(Figure 2.2A)**. Both paws (in the case of CFA, the injured and uninjured paw) were assessed in 4 replicates again to ensure consistency and to spot anomalies.

Nocifensive Behaviour

Nocifensive behaviour tests are often used for acute short acting algogens such as capsaicin and for intense sensitizers such as formalin which has two distinct phases of action: an acute (1^{st}-phase) and longer lasting (2^{nd}-phase) response. Observing nocifensive behaviour through how the animal tends to the paw is advantageous in these conditions because these pro-algesic compounds cause the animals to elevate the paw or tend to it for the duration of its effect. This makes tests of pain threshold like Hargreaves and Von Frey test hard to complete in a consistent way as these tests can take longer than the effect lasts (as e.g., for the case of capsaicin) or the paw is not accessible to the apparatus due to licking and elevating the paw (e.g., in the case of capsaicin and formalin injections). In this study, the Capsaicin test were used for to induce acute nocifensive behaviour.

The capsaicin test involved hindpaw injection of 100 µL capsaicin solution (300 µM) and quantification of the following parameters: i) the time taken to first lick of the paw; ii) the number of bouts of licking; iii) the total time spent licking over the 5-minute period and iv) the time the animal last licked the paw. The test always followed the same pattern of a 5-minute period of observation following the injection. During pharmacology studies, systemic intra-peritoneal injections of 2 mL/kg were given 30 minutes prior to the intra-plantar injection **(Figure 2.1B)** and during local application 100 µg in 50 µL of compound was injected intra-plantar 5 minutes prior to a 50 µL intra-plantar injection of 300 µM capsaicin **(Figure 2.1C)**. During assessments of baseline pain threshold after *Kcnq2* knockdown, intrathecal injections were delivered as described previously, the capsaicin test involved only the intra-plantar injection of 300 µM and observation **(Figure 2.2B)**.

Quantification and statistics

Von Frey and Hargreaves tests were quantified by normalising the test result for each animal to the same animal's baseline results to remove inter-animal differences. The baseline periods of observation for nocifensive behaviour always showed no to negligible nocifensive behaviour so normalising was not necessary. Independent

measures one-way ANOVA was used to analyse either differences between pharmacological compounds or between siRNA groups.

2.5 *Ex vivo* Analysis

2.5.1 Measuring mRNA Expression

Tissue Extraction

For studies involving siRNA knockdown of *Kcnq2* or *Kcnq5 in vivo*, tissue was harvested post behavioural experimentation, flash frozen on dry-ice and stored at -80ºC to preserve in order to measure the level of *Kcnq2* or *Kcnq5* at the time of behavioural testing. Animals were sacrificed in accordance with UK Animals (Scientific Procedures) Act 1986 and the EU directive. Heads were removed and skin opened up down the spinal column. Brains were removed from the skull and the cortex and hippocampus removed, placed in a 1.5 mL Eppendorf tube and flash frozen on dry-ice. Lumbar spines were removed from the body and the spinal cord removed by passing RNase free PBS into the central cavity where the spinal cord resides using a 10 mL syringe and blunted needle wide enough to reduce the chance of liquid coming back past the sides of the needle. The Lumbar spinal cord was collected in an Eppendorf and flash frozen, and the spine split into left and right halves by cutting up the dorsal and ventral portion of the spine. The DRGs lie in the spaces between the vertebrae in these two halves of the spine and were removed under a microscope and again flash frozen in a 1.5 mL Eppendorf.

From this point all tissues were treated identically.

RNA Extraction

In order to extract RNA from the tissue it first was first homogenised using a TRIzol and chloroform methodology. The tissue was placed into a small volume of TRIzol in an Eppendorf tube and homogenised using an electric pestle for a few seconds. The TRIzol volume was then adjusted to a total of 1 mL volume and the homogenate incubated for 10 minutes. Chloroform (0.2 mL) was then added and the mix shaken vigorously for 15 seconds and incubated for 5 minutes. Samples were centrifuged at 12,000g for 20 minutes at 4ºC to separate the mix into three levels, a bottom red phenol-chloroform phase, a sediment/tissue interphase and a clear layer on top containing the RNA in suspension. This RNA suspension was transferred to a new tube and 100% ethanol added for a final concentration of 35% ethanol.

From this stage the solution was added to a spin cartridge and the PureLink RNA isolation kit (ThermoFisher 12183018A) protocol followed to produce RNA in RNase free water. RNA was isolated following the manufacturer's supplied protocol with the following modification. After the first wash step the RNA column was treated with 80 µL PureLink DNAse (ThermoFisher 12185010) for 15 minutes and washed through with an extra wash step.

RNA concentration was determined via a nanodrop 2000 (Thermo Scientific) a 260/230 absorbance ratio close to 2 indicates a low level of non-RNA contamination. This is particularly important as TRIzol contamination would become apparent here and TRIzol would interfere with the qPCR.

cDNA Synthesis and Quantitative Polymerase Chain Reaction (qPCR)

For a 100 µL final volume 41 µL of master mix (Table 2.4), made up of Taqman MultiScribe reagents, was added at 2.5x final concentration. RNA was added for a final of 1 µg/ul (in total of 100 uL, including the mastermix) and incubated in a MiniAmp plus thermal cycler to synthesise cDNA.

Thermal cycler protocol: 25°C for 10 mins, 37°C for 60 mins, 75°C for 5 mins, 4°C infinite hold.

Table 2.4: Contents of reverse transcription reaction mixture

Taqman MultiScribe master mix contents	
Stock reagents	**Final concentration**
10x Buffer	1x
25 mM $MgCl_2$	1.75 mM
10mM dNTPs	1 mM
50µM random hexamer	2.5 µM
20U/µL RNase inhibitor	0.4 U/µL
50U/µL MMLV reverse transcriptase	1.5 U/µL

qPCR was performed using a standard TaqMan protocol. Briefly, the cDNA created in the RT reaction is added to a TaqMan solution containing master mix, the relevant Rat Fam primers, in this case rat *Kcnq2* primer, *Kcnq5* primer or *Hprt1* primer. This mix

was sealed with a thermostable seal (Micro Amp optical adhesive film) spun down and placed in the QuantStudio qPCR machine along with negative controls. The qPCR cycle was as previously (Table 2.2).

Quantification and statistics

Mean Ct value calculated for housekeeper (*Hprt1*) and experimental gene (*Kcnq2* or *Kcnq5*). These values were used to calculate ΔCt (gene Ct – housekeeper Ct). ΔΔCt was then calculated by compared mean ΔCt to the vehicle control animals before calculating the fold change (2^ΔΔCt) and percentage knockdown (%). Statistical analysis (independent or repeated measures one-way ANOVA) was completed on ΔCt but results displayed as percentage knockdown for ease of understanding.

Chapter 3: Assessing the mRNA and Protein Expression profiles of K_v7 Subunits in the Dorsal Root Ganglion (DRG)

3.1 Introduction

In Mammals K_v7 subunits are broadly expressed in excitable (e.g. neurons, muscles, neuroendocrine cells) and non-excitable (e.g. epithelia) tissues (see Chapter 1). Given the i) the broad expression of K_v7 subunits, ii) the range of diseases arising from Kv7 subunit malfunction, and iii) therapeutic potential of K_v7 modulating drugs, it is imperative to ascertain the Kv7 subunit expression profiles in various cell and tissue types.

Indeed, different tissues have distinct K_v7 subunit expression patterns, thus, $K_v7.1$ is hardly detectable in nervous system (Uhlén *et al.*, 2015) but it is the main cardiac K_v7 subunit (it forms the I_{Ks} channel, co-assembling with the KCNE1 auxiliary subunit). More recently, $K_v7.4$ has been identified in a significant portion of cardiomyocytes specifically in the mitochondria (Testai *et al.*, 2015). It has been suggested to have cardioprotective effects in ischemia (Testai *et al.*, 2015), however the role it plays is not fully understood. $K_v7.4$ is expressed in the outer hair cells, inner hair cells and the afferent spiral ganglia and is required for normal functioning of the ear (Kubisch *et al.*, 1999, Kharkovets *et al.*, 2000, Beisel *et al.*, 2000, Lv *et al.*, 2010, Carignano *et al.*, 2019, Kharkovets *et al.*, 2006). Smooth muscle cells in general express $K_v7.1$, $K_v7.4$ and $K_v7.5$ channels and at least $K_v7.4$ and $K_v7.5$ are important for changes in the level of contractility (Ng *et al.*, 2011), while $K_v7.2$ and $K_v7.3$ are not expressed or expressed at low levels (Tsai *et al.*, 2020).

The traditional neuronal K_v7 channels, $K_v7.2$ and $K_v7.3$, are expressed throughout the higher brain regions in the cortex, olfactory regions, hippocampus, amygdala and basal ganglia where mutations to $K_v7.2$ have resulted in changes to potassium current or retigabine-sensitive potassium currents have been identified (Biervert *et al.*, 1998, Schroeder *et al.*, 1998, Uhlén *et al.*, 2015). Increasingly, $K_v7.5$ is also being identified in the same regions, generally at lower expression levels, with the exception of the basal ganglia and pons and medulla. In the basal ganglia, $K_v7.5$ is found at levels comparable to these of Kv7.2 and Kv7.3 (Uhlén *et al.*, 2015), while in the medulla and

pons $K_v7.5$ is expressed very highly compared to $K_v7.2$ and $K_v7.3$ (Tzingounis *et al.*, 2010). Changes in neuronal excitability upon retigabine application have been identified throughout the dopaminergic systems of the brain including the basal ganglia (Baculis *et al.*, 2020). However, to the best of my knowledge there have been no reports of K_v7/retigabine-sensitive potassium currents in these areas.

This begs the question: what is the functional significance of specific subunit expression in different tissue types? Although the subunits are similar in functionality, understanding the specific expression of the subunits becomes important in tissues such as the sensory ganglia as there are multiple sensory processes occurring which could be controlled by different subunits.

Although functional significance of different K_v7 subunits in somatosensory neurons have not been comprehensively evaluated yet, there are various data reporting the expression of various *Kcnq* transcripts and K_v7 proteins. Initially by Passmore and colleagues (Passmore *et al.*, 2003) identified mRNA expression of *Kcnq2*, *Kcnq*3, and *Kcnq*5 in small and large diameter neurons and *Kcnq4* in large diameter neurons of rat DRG. They also confirmed co-expression of $K_v7.2$, $K_v7.3$ and $K_v7.5$ protein in various combinations. Since then, there have been reports of $K_v7.5$ being the dominant subunit in small-diameter neurons (King and Scherer, 2012) and $K_v7.2$ being dominant in small-diameter nociceptive neurons both in the DRG (Rose *et al.*, 2011) and trigeminal ganglia (Ling *et al.*, 2017, Ling *et al.*, 2018). Interestingly, in nodose ganglion sensory neurons that innervate somatosensory organs and visceral organs; $K_v7.2$ was expressed in TRPV1 positive and negative C-fibre neurons innervating somatosensory organs but preferentially expressed in TRPV1 negative neurons innervating the visceral neurons (Sun *et al.*, 2019). $K_v7.5$ was expressed in a small number of both types. In mouse DRG neurons, single-cell RNA-seq suggests that *Kcnq2* is expressed in nociceptors and larger low-threshold mechanoreceptors, whereas *Kcnq5* was mostly expressed in low threshold mechanoreceptors, with some limited expression in peptidergic nociceptors (Zheng *et al.*, 2019). This study also marked *Kcnq4* expression in a subpopulation of Aβ low threshold mechanoreceptors, which is in line with immuno-reactivity of $K_v7.4$ previously reported (Heidenreich *et al.*, 2012).

In this chapter, we seek to obtain a comprehensive expression pattern for all 5 K_v7 subunits in sensory neurons of different size and sensory modality from DRG of rats and mice.

3.2 Results

3.2.1 Confirming *Kcnq* Gene Expression in Rat DRGs

Although there are previous reports of *Kcnq* mRNA expression in the DRG, we felt it is important to confirm the mRNA expression of all five *Kcnq* subunits as a stepping-stone for building more specific expression profiles. Gene expression analysis was completed using TaqMan quantitative polymerase chain reaction (qPCR). The genes encoding the reported neuronal type K_v7 channels, $K_v7.2$ (*Kcnq2*), $K_v7.3$ (*Kcnq3*) and Kv7.5 (*Kcnq5*) were well expressed in the DRG **(Figure 3.1)**. *Kcnq4* showed minimal but detectable expression levels whereas the *kcnq1* gene, encoding the cardiac channel $K_v7.1$, was undetectable in the DRG **(Figure 3.1)**.

3.2.2 Optimising Antibody Utility and Specificity

Having confirmed gene expression to be similar to other studies and other species it was important to evaluate protein expression in the DRG. There is still not a complete consensus on which subunits are expressed in different types of sensory neurons, e.g., whether it is $K_v7.2$ or $K_v7.5$ being the major subunit in small diameter neurons (Passmore *et al.*, 2003, King and Scherer, 2012, Rose *et al.*, 2011). We reasoned that one source of disparity could be in antibody specificity issues. In light of this, we felt it appropriate to thoroughly test and optimise the antibodies to be used in this study. To do this, each of five K_v7 subunits were individually expressed as eYFP-fusion proteins in HEK293 cells and treated with the corresponding antibody at concentrations of 1:1000, 1:500 and 1:200. Confocal imaging was then performed to confirm overlap of the antibody staining with eYFP **(Figure 3.2A)**. This confirmed that all the antibodies shown bound to the correct subunit as the cells showing antibody reactivity were also expressing eYFP **(Figure 3.2A)**. Cells not expressing eYFP and cells in untransfected conditions **(Figure 3.2B)** showed no antibody reactivity, suggesting the antibodies are not reacting with unrelated proteins **(Figure 3.2A/B)**. However, the close homology of the subunits presents the possibility of cross-reactivity between the antibodies and other subunits. As this study attempts to separate out the different K_v7 subunits, it was also important to examine this potential cross-reactivity. To this end, HEK cells

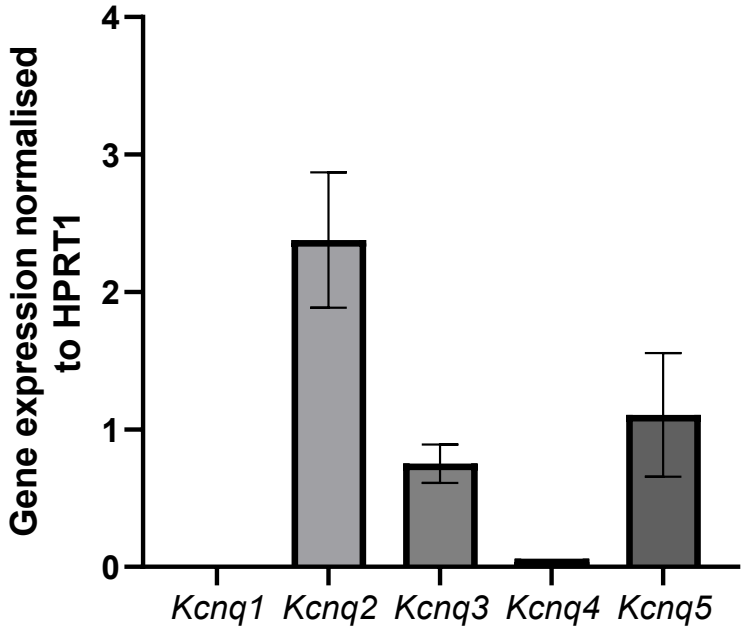

Figure 3.1 Kcnq2-5 but not Kcnq1 are expressed in rat dorsal root ganglia (DRG) Gene expression of *Kcnq1-5* in rat DRGs normalised to *Hprt1* expression (Y-axis) Mean ±S.E.M (N=4 animals).

transfected with individual eYFP-tagged K_v7 subunits were cross-stained with non-corresponding antibodies, which showed no signal **(Figure 3.2C)**. For example, eYFP-tagged $K_v7.2$ was transfected into HEK cells but treated with the antibody for $K_v7.3$. Reasoning that if the antibody, labelled red, co-expressed with the eYFP in green, it would suggest that the antibody displayed cross-reactivity with the other subunit, the full list of antibody-plasmid combinations presented in **(Figure 3.2C)** are outlined in Table 3.1 for clarity. Taken together, this data suggests that using the optimised conditions our K_v7 antibodies recognised only the subunit they were designed to recognise. Other antibodies did show cross-reactivity with other subunits (data not shown), therefore no further work was completed with these antibodies.

Table 3.1: Antibody-plasmid combinations explored in Figure 3.2C

eYFP tagged plasmid (Green)	**Antibody (Red)**
$K_v7.2$	$K_v7.3$
$K_v7.3$	$K_v7.2$
$K_v7.2$ and $K_v7.3$	$K_v7.4$
$K_v7.2$ and $K_v7.3$	$K_v7.5$
$K_v7.4$	$K_v7.2$
$K_v7.4$	$K_v7.3$
$K_v7.4$	$K_v7.5$
$K_v7.5$	$K_v7.2$
$K_v7.5$	$K_v7.3$
$K_v7.5$	$K_v7.4$
$K_v7.2$ and $K_v7.3$	$K_v7.1$
$K_v7.4$ and $K_v7.5$	$K_v7.1$

To provide some optimisation to our protocol, DRG slices were also treated with experimental antibodies under a number of different conditions to provide the most accurate results; this included preserving the neuron morphology. K_v7 antibodies can interact poorly with fixatives such as PFA and indeed was particularly the case for $K_v7.2$ and $K_v7.4$. Thus, the approach to flash-freeze the DRGs without fixation and embed in OCT (optimal cutting temperature compound) for cutting was employed. This

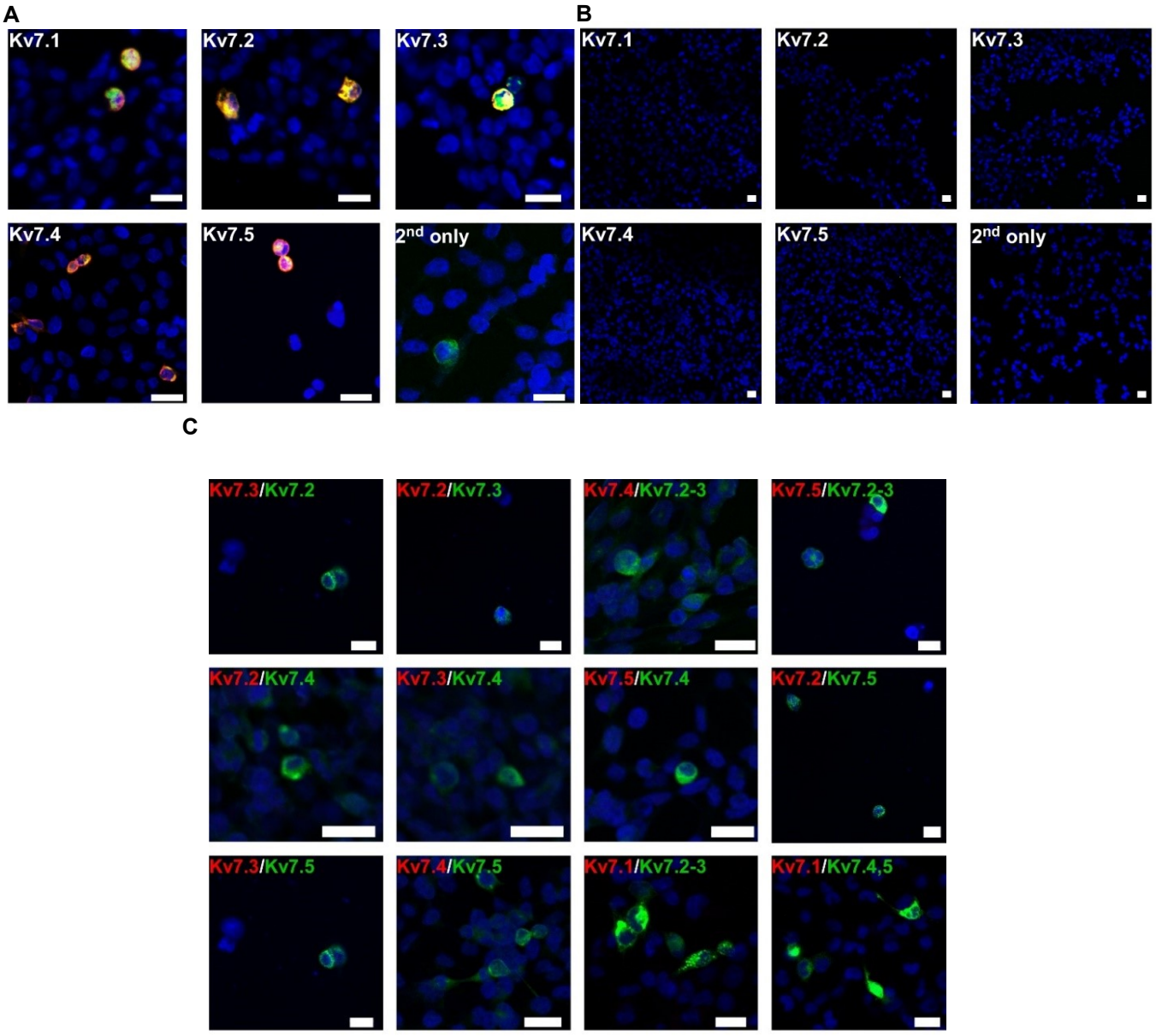

Figure 3.2 Evaluation of K_v7 antibodies in Human Embryonic Kidney cells (HEK293). **(A)** eYFP tagged *Kcnq1-5* transfected HEK293 cells (green) stained with the corresponding K_v7.1-7.5 antibody (red). Cells fluorescing green and red indicates that the antibody recognises cells expressing the correct subunit (N=3 experiments). **(B)** Untransfected HEK293 cells treated with K_v7.1-7.5 antibodies (red). A lack of red fluorescence indicates that the antibodies do not bind non-specifically to HEK cells (N=3 experiments). **(C)** eYFP tagged *Kcnq1-5* transfected HEK293 cells (green) treated with various non-corresponding K_v7 subunit antibodies (red). Cells fluorescing green express the eYFP tagged subunit labelled in green on the panel. Cells were treated with the antibody for a different subunit to that expressed in the cell, a lack of red fluorescence indicates that the antibody does not bind to the incorrect subunit (N=3 experiments) The various combinations of transfected subunit and non-corresponding antibody used are outlined in Table 3.1. Scale bars = 20 μm.

resulted in very fragile DRGs with poorly preserved morphology of the neurons. Theorising that this was due to length of time the slices are bathed in antibody solutions before mounting, an attempt was made to post-fix the slices in PFA after cutting for 10-20 minutes to preserve morphology, this improved morphology somewhat but still not to the level of fixing in PFA immediately and was not optimal for antibody binding.

As the fresh-frozen approach produced worse morphology than fixing the DRGs in PFA and embedding in gelatine. Therefore, the original method was reverted to but with modifications to improve antibody binding. Two antigen retrieval methods were attempted after cutting of the samples to break the cross-links formed by PFA. The first, heat antigen retrieval, heating the samples to 80^{o}C in a citric acid solution, this was unsuccessful because the antibodies were embedded in gelatine, the heat caused the gelatine to lose its structure, becoming 'floppy' and thus too fragile to work with efficiently. The second, chemical antigen retrieval, applying a trypsin-calcium chloride solution to the samples at 37^{o}C. This also made the gelatine more fragile, but to a lesser extent, the extent of loss of structural integrity was time dependent, 10 minutes was sufficient to improve antibody binding without making the samples too difficult to work with.

Finally, despite the K_v7 antibodies benefiting from antigen retrieval, it was discovered that when applying K_v7 antibodies simultaneously with the peripherin antibody, as is convention, this compromised the binding of one or both antibodies with regular enough occurrence to be of concern. Thus, a sequential approach to antibody application was tested. Whereby, one primary antibody was applied alone, then the corresponding secondary antibody, followed by the primary then secondary antibody of the second antibody. This approach prevented the antibodies interfering with the binding of each other, so was combined with the antigen retrieval to optimise the protocol fully.

It was found that morphology was best preserved using 4% PFA as a fixative and the K_v7 antibodies benefited from individual application (sequential) to the slices rather than with another antibody. Furthermore, $K_v7.2$ and $K_v7.4$ antibodies benefited from trypsin antigen retrieval after fixing. Thus, for all further staining, PFA was employed as the fixative followed by antigen retrieval using trypsin. All antibodies were added

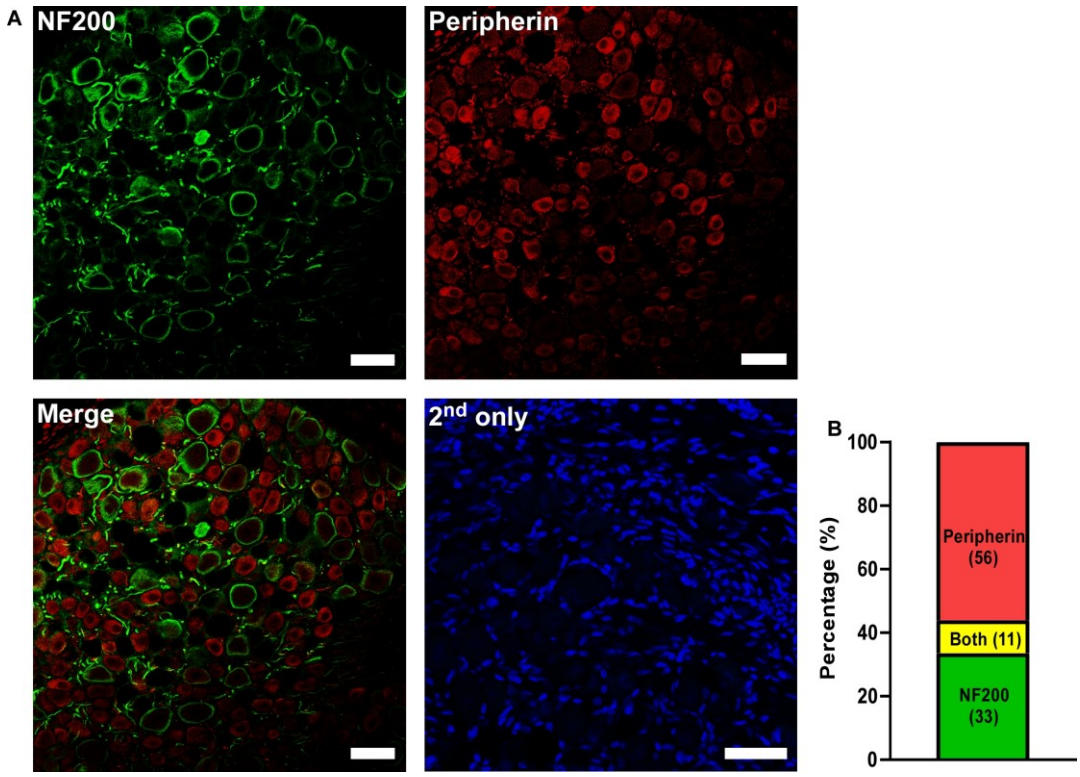

Figure 3.3 NF200 and peripherin only co-express in a minority of rat sensory neurons. **(A-B)** Co-expression of NF200 and peripherin in rat DRGs (N=4 animals) (n=4^{+} DRGs per animal). Data presented is **(A)** representative examples and **(B)** percentage co-expression as parts of a whole. Scale bars = 50 μm.

sequentially ensuring those that benefited from antigen retrieval were applied first and testing increasing concentrations from 1:1000 to 1:200.

In addition to confirming experimental antibody specificity, rat DRG slices were probed for with markers for different sensory neuron types to assess how well cell types could differentiated. To distinguish myelinated 'A-type' and non-myelinated 'C-type' neurons we used two widely used markers: neurofilament 200 (Perry *et al.*, 1991) and peripherin (Sleigh *et al.*, 2017), abundantly expressed by either A or C fibre, respectively. Probing with anti-NF200 and anti-Peripherin antibodies identified a large portion of neurons and revealed two distinct populations **(Figure 3.3A)**, with co-expression of both proteins in only 11% (39 of 337 neurons) of DRG neurons **(Figure 3.3B)**, suggesting that using these markers we could sufficiently differentiate between A-type (NF200) and C-type (peripherin) sensory neurons.

3.2.3 Assessing K_v7 Protein Distribution in Rat DRGs by Neuron Type

Using optimised conditions and antibodies verified above we performed immuno-fluorescence experiments to identify populations of sensory neurons in the DRG that may express K_v7 channels. Broad separation into A- and C-type neurons was achieved by co-immunolabelling with NF200 and peripherin. separating NF200-positive alpha type sensory neurons (Aβ and Aδ), often low-threshold mechanoreceptors (some fast nociceptors) and peripherin-positive C type sensory neurons, often nociceptors and pruriceptors.

Initial observations show a similar global pattern of K_v7 gene and protein expression in the DRG: $K_v7.2$, $K_v7.3$ and $K_v7.5$ constitute most of the K_v7 in the DRG with $K_v7.4$ expression limited to small subpopulation of neurons and no expression of $K_v7.1$ in NF200 **(Figure 3.4A)** or peripherin positive neurons **(Figure 3.5A/3.6A)**. A further analysis of the $K_v7.4$ expression revealed that it is localised to a subpopulation of NF200 positive neurons (17%±3.5) **(Figure 3.4D/3.6D)**; this constituted 11% of total neurons counted. These findings are in agreement with previous findings whereby $K_v7.4$ was found to specifically express in a subset of mechanosensitive neurons (Heidenreich *et al.*, 2012). $K_v7.2$, $K_v7.3$ and $K_v7.5$ were expressed in at least 50% of both types (NF200+ or Peripherin+) of neurons **(Figure 3.4-3.6)**. $K_v7.2$ and $K_v7.3$ were expressed in significantly higher proportions of the peripherin-positive neurons (816 of 980 or 83% and 1079 of 1519 or 71%, respectively N=5) **(Figure 3.5B-C/3.6B-F)**

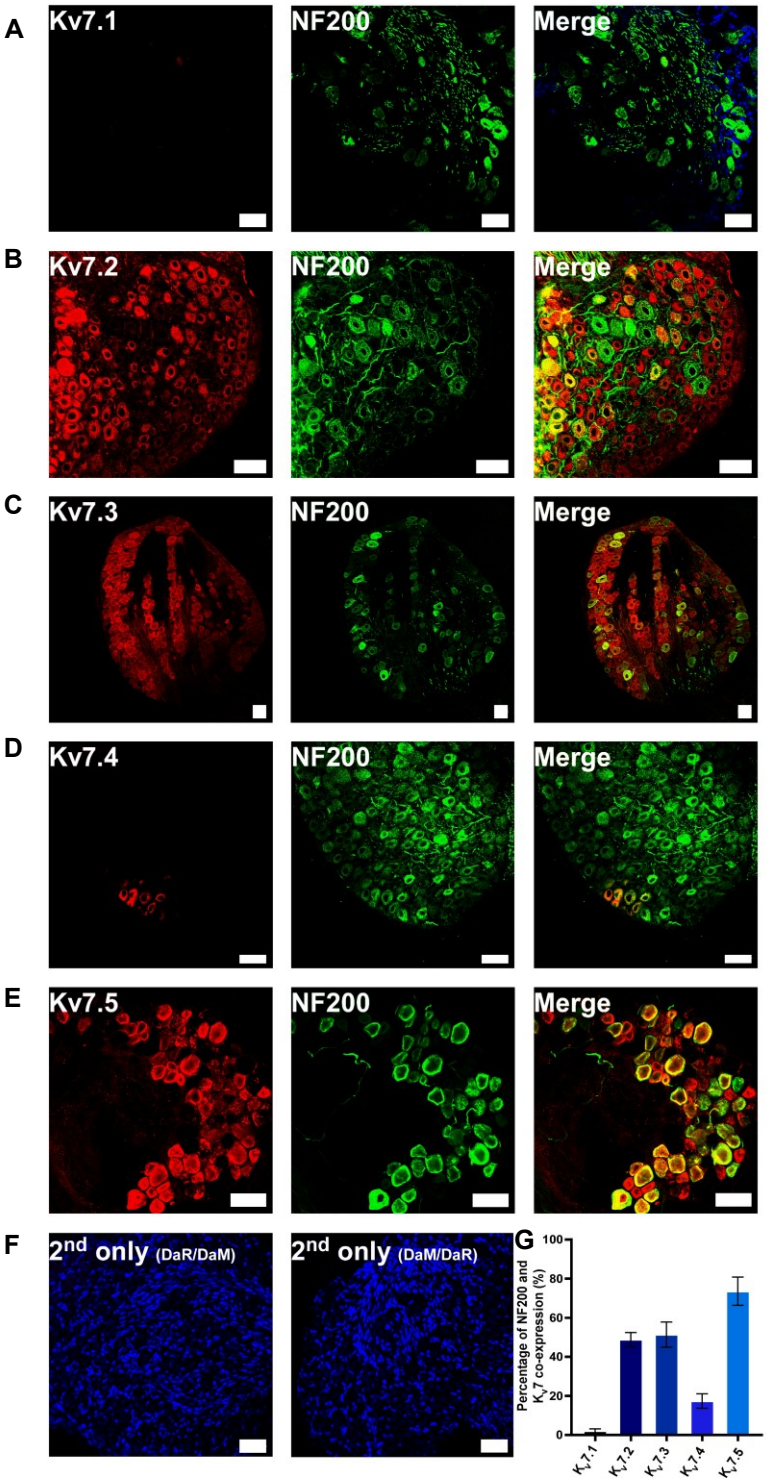

Figure 3.4 K_v7.2-7.5 but not K_v7.1 are differentially expressed in myelinated rat sensory neurons in the DRG. **(A-E)** Representative examples of K_v7 expression in NF200 positive neurons of **(A)** K_v7.1, **(B)** K_v7.2, **(C)** K_v7.3, **(D)** K_v7.4 and **(E)** K_v7.5. **(F)** Representative controls for NF200. **(G)** The percentage of NF200 positive neurons also expressing K_v7 subunits. N=4 rats, n=5$^+$ DRGs per rat per group. Scale bars = 50 µm.

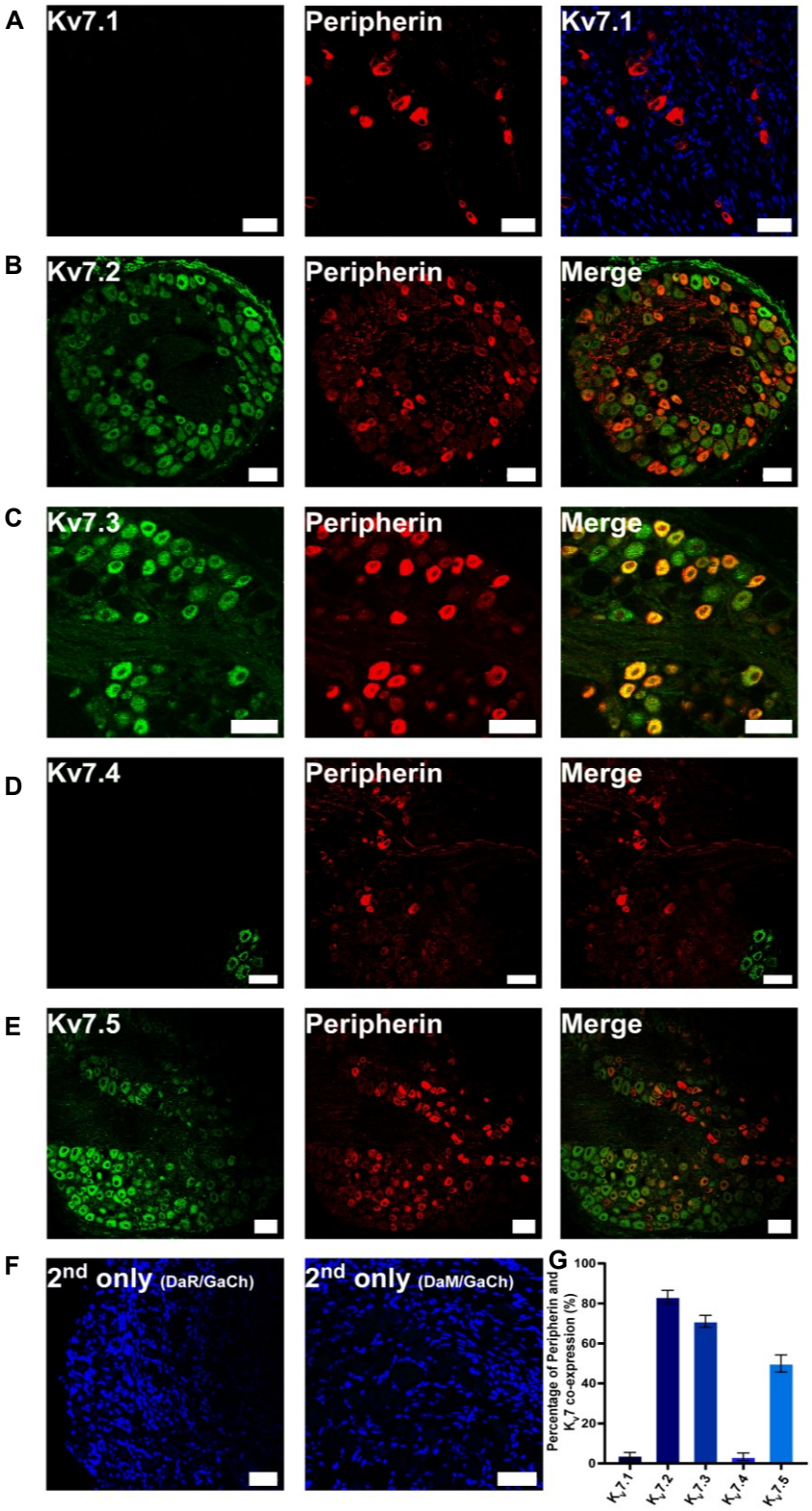

Figure 3.5 K_v7.2-7.5 but not K_v7.1 are differentially expressed in unmyelinated rat sensory neurons in the DRG. **(A-E)** Representative examples of K_v7 expression in peripherin (Pn) positive neurons of **(A)** K_v7.1, **(B)** K_v7.2, **(C)** K_v7.3, **(D)** K_v7.4 and **(E)** K_v7.5. **(F)** Representative controls for Pn. **(G)** The percentage of Pn positive neurons also expressing K_v7 subunits N=4 rats, n=5^+ DRGs per rat per group. Scale bars = 50 µm.

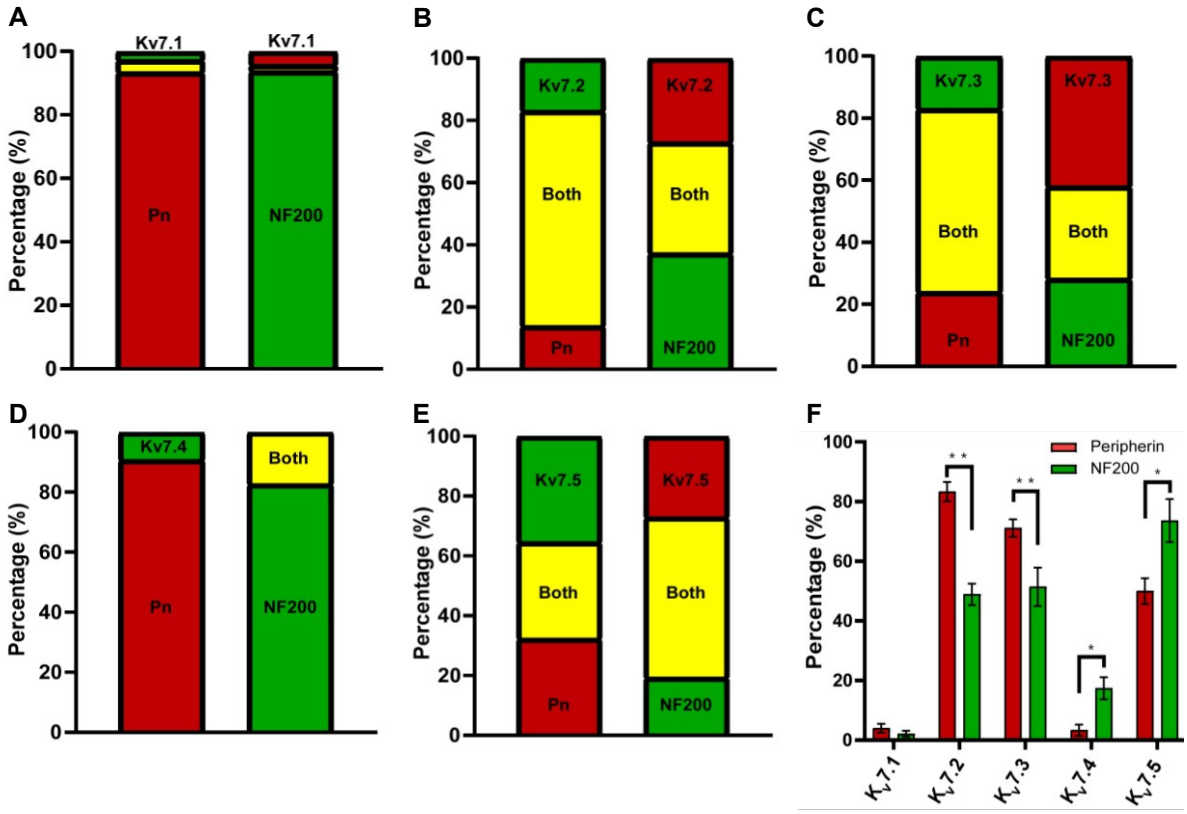

Figure 3.6 Quantitative analysis of K_v7 expression in rat sensory neurons in the DRG. **(A-E)** Expression percentage in NF200 and peripherin (Pn) positive neurons of **(A)** $K_v7.1$, **(B)** $K_v7.2$, **(C)** $K_v7.3$, **(D)** $K_v7.4$ and **(E)** $K_v7.5$. **(F)** Comparison of co-expression between NF200 and peripherin. Data presented as mean percentage co-expression ±S.E.M but statistically evaluated as proportions using Fisher's exact test for proportion, multiple comparisons manually adjusted with Bonferroni correction *P<0.05, **P<0.01. N=4 rats, $n=5^+$ DRGs per rat per group.

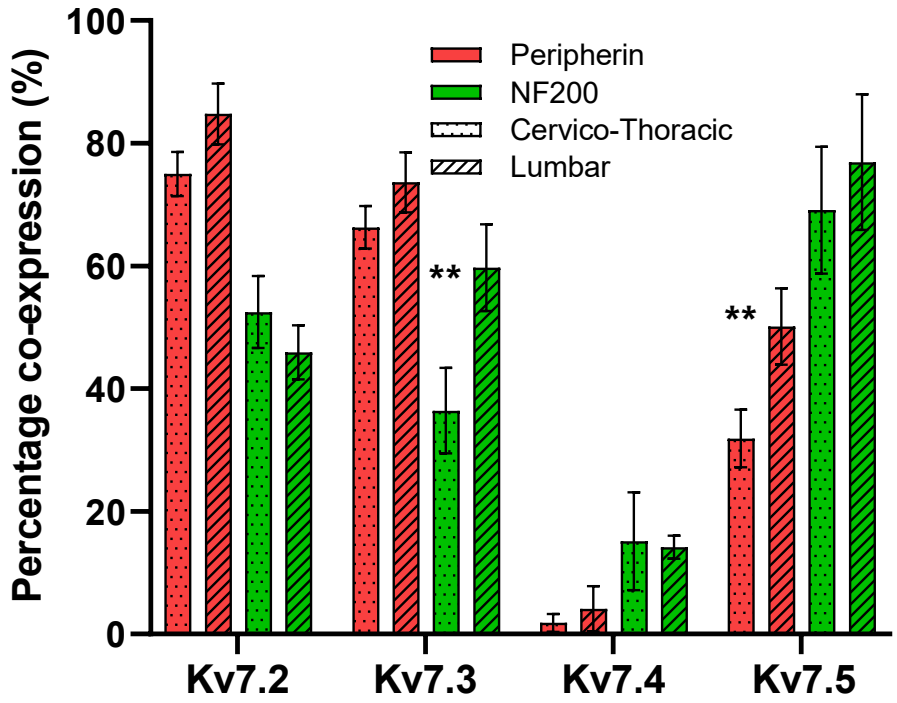

Figure 3.7 Only K_v7.3 and K_v7.5 expression differs significantly between rat Lumbar and cervical-thoracic DRGs. Co-expression of K_v7.2-7.5 and peripherin (red) or NF200 (green) in Lumbar DRGs ($n=5^+$) innervating the hindpaw and cervical and thoracic DRGs (Cervico-Thoracic) ($n=5^+$) innervating the forepaws and trunk. Data presented is representative examples and Mean ±S.E.M, statistical evaluation with Fisher's exact test, multiple comparisons manually adjusted with Bonferroni correction (**P<0.01) (N=4 animals).

compared to 49% (289 of 592) and 51% (231 of 450) of NF200-positive neurons (N=4 P<0.01) **(Figure 3.4B-C/3.6B-F)**. K_v7.5 showed the opposite expression pattern with significantly higher expression in A-type, NF200-positive neurons at 73.5% (303 of 412 neurons) compared to 50% (286 of 573) of peripherin-positive neurons (N=4 P<0.05) **(Figure 3.4E/Figure 3.5E/Figure 3.6E-F)**. This data suggests that K_v7.2, K_v7.3 and K_v7.5 are highly expressed across a broad range of sensory neurons, however, there is a bias towards small-diameter, peripherin-positive neurons for K_v7.2 and for large-diameter, NF200-positive neurons for K_v7.5 to medium-diameter neurons. As the quantification here is taken from the whole-cell expression of K_v7 channels, the results are based on the total protein in the cell membrane and cytoplasm, not the surface expression of the channels on the membrane. In addition, we compared the pattern of expression of the subunits in the neurons innervating the hindlimbs (lumbar, Lu) to DRGs innervating the trunk and forepaws (cervical and thoracic, CT). Overall, we found that the pattern of expression was unchanged throughout the DRGs **(Figure 3.7)**.

3.2.4 Evaluation of K_v7 Expression in Rats and Wild-Type or *Kcnq2* Knockout Mice

Due to such a high level of neuronal expression and the ability of various K_v7 subunits to co-assemble and heteromerise, it was important to understand the co-expression of subunits. K_v7.2 and K_v7.3 co-localised in 50% of rat and mouse neurons and K_v7.2 and K_v7.5 co-localised in 18% of rat and mouse neurons, the difference between K_v7.2-K_v7.3 and K_v7.2-K_v7.5 was significant in rat (P<0.001) and mice (P<0.01) but the difference in co-expression between rats and mice was not significant **(Figure 3.8A/B-D/E)**. Of the neurons expressing at least one of K_v7.2, K_v7.3 or K_v7.5 channels, K_v7.2 constituted 50%, K_v7.3 30% and K_v7.5 20% in rat, with qualitatively similar results in mice **(Figure 3.8C/F)**. This confirmed that i) K_v7.2 and K_v7.5 localise to largely different subpopulations of neurons and ii) Kv7.2 is the most abundantly expressed Kv7 subunit in the DRG. Unfortunately, K_v7.5 and K_v7.3 co-expression could not be evaluated due to antibody constraints (both raised in the same species).

We had limited access to the fixed DRG tissue from the sensory-neuron-specific *Kcnq2* knockout mice (provided by collaborator Lilly & Co), thus, we tested the co-expression of K_v7.2 with K_v7.3 and K_v7.5 in both, the Wild-Type and *Kcnq2* knockout mice. We confirmed broad expression of K_v7.2 in the Wild-Type mouse DRGs

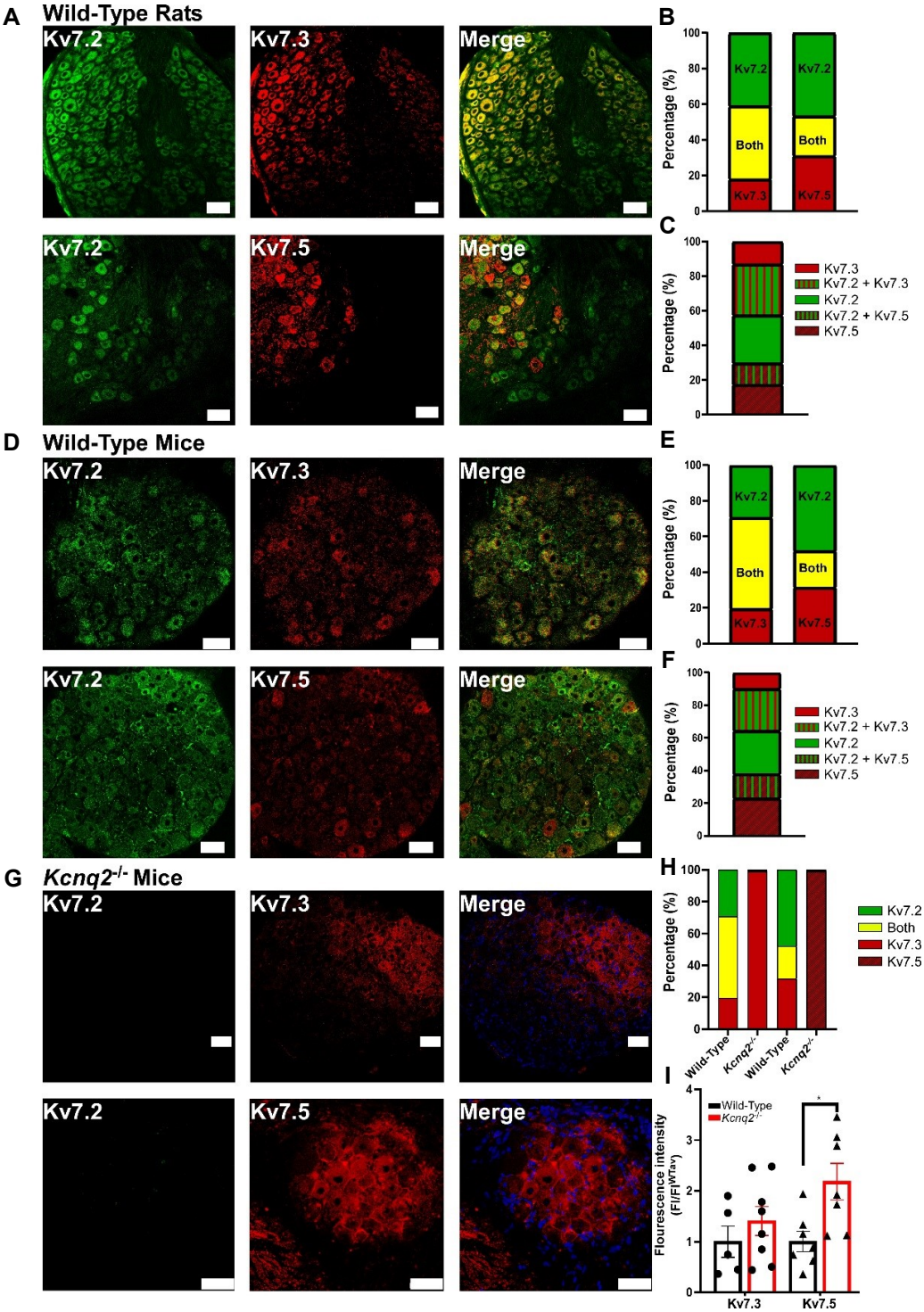

Figure 3.8 K_v7 subunits co-localise in rat and mouse sensory neurons, knocking out Kcnq2 causes loss of $K_v7.2$ expression and potential compensation. **(A)** Representative examples of $K_v7.2$ co-localisation with $K_v7.3$ or $K_v7.5$ in rat. **(B)** Percentage co-localisation of $K_v7.2$ and $K_v7.3$ and $K_v7.2$ and $K_v7.5$ in rats. **(C)** Percentage of K_v7 positive neurons expressing $K_v7.2$, $K_v7.3$ or $K_v7.5$ in rats. **(D)** Representative examples of $K_v7.2$ co-localisation with $K_v7.3$ or $K_v7.5$ in mice. **(E)** Percentage co-localisation of $K_v7.2$ and $K_v7.3$ and $K_v7.2$ and $K_v7.5$ in mice. **(F)** Percentage of K_v7 positive neurons expressing $K_v7.2$, $K_v7.3$ or $K_v7.5$ in mice. **(G)** Representative examples of $K_v7.2$, $K_v7.3$ and $K_v7.5$ in *Kcnq2* knock-out mice. **(H)** Percentage co-expression of $K_v7.2$, $K_v7.3$ and $K_v7.5$ in Wild-Type and knock-out mice. **(I)** Fluorescence intensity of $K_v7.3$ and $K_v7.5$ in Wild-Type and knock-out mice normalised to average Wild-Type fluorescence intensity (FI/FI^{WTav}). Data presented as mean percentage co-expression ±S.E.M, statistical evaluation by Kruskal-Wallis test (non-parametric ANOVA) *P<0.05. N=4 rats, n=5$^+$ DRGs per rat, N=3 Wild-Type mice, N=3 *Kcnq2* knockout mice, n=5$^+$ DRGs across all mice. Scale bars = 50 μm.

however, no detectable expression of $K_v7.2$ was seen in the *Kcnq2* knockout DRGs **(Figure 3.8G-I)**. This confirms the knockout of $K_v7.2$ in the DRG and, importantly, further validates the $K_v7.2$ antibody used in this study. The patterns of $K_v7.2$, $K_v7.3$ and $K_v7.5$ subunit expression in the Wild-Type mice DRG was qualitatively similar to these in rats **(Figure 3.8)**. In addition to this, there was a significant increase in $K_v7.5$ expression in the knockout animals (2.88±0.26-fold increase) **(Figure 3.8H/J)**. This perhaps represents a compensatory mechanism to circumvent M current loss-of-function. In contrast, $K_v7.3$ fluorescence intensity was not significantly increased (1.4±0.2-fold increase) **(Figure 3.8G/J)**.

3.3 Discussion

In this study we confirm the differential expression of K_v7 subunits in sensory neurons of the DRG in rats and mice, we also used well known markers for A- and C-type neurons in order to reveal potential sensory modality-specific differences in expression. $K_v7.1$ was virtually undetectable in rat sensory neurons, which is consistent with other studies on rodent protein and mRNA expression of $K_v7.1$ in sensory neurons (Passmore *et al.*, 2003, Zheng *et al.*, 2019).

$K_v7.4$ was expressed almost entirely in large NF200 positive neurons, equating to around 10% of total sensory neurons, which is in good agreement with the original study identifying $K_v7.4$ in a small subset of mechanosensitive Ab fibres (Heidenreich *et al.*, 2012). The majority of K_v7 expression is relayed by $K_v7.2$, $K_v7.3$ and $K_v7.5$, again in agreement with previous work (Passmore *et al.*, 2003, King and Scherer, 2012). Previously, there has been conflicting results as to what is the major K_v7 subunit in small diameter neurons. It has been demonstrated that $K_v7.2$ is the predominant subunit in small sensory neurons by Rose and colleagues (Rose *et al.*, 2011) however, King and Scherer showed $K_v7.5$ being the predominant subunit in small-diameter neurons (King and Scherer, 2012). This was further complicated by the Brown lab who proposed that there was a mix of the two subunits in small diameter neurons (Passmore *et al.*, 2003). Here we demonstrate a significant bias of $K_v7.2$ to small-diameter neurons and $K_v7.5$ to large-diameter neurons. We also found that only 18% of neurons co-express both $K_v7.2$ and $K_v7.5$ in rats. $K_v7.3$, on the other hand, is more evenly expressed with some bias to small-diameter neurons. Interestingly, we see $K_v7.2$ in more small-diameter neurons than $K_v7.3$, suggesting that there may be a subset of neurons with M current controlled entirely by $K_v7.2$. This comprehensive

study provides a full characterization of expression patterns of all five K_V7 subunits performed under the same experimental conditions using thoroughly verified antibodies, which provides an advantage over the previous reports where only certain subunits were analysed.

However, it is important to note that this study accounts for total protein expression within the cell, this includes the plasma membrane and cytoplasm so includes channels that were likely functionally available (plasma membrane) and those that were being trafficked in vesicles, still in the ER or Golgi or otherwise not functioning as channels at the time of fixation. Therefore, we do not infer surface expression or the level of expression in the cell from this data. Thus, this data comes with the caveat that the level of surface expression of the K_V7 subunits and in turn, macroscopic current, is likely to vary between cells and has not been reported here. There are indeed ways to assess the surface expression of proteins, in its simplest form of only measuring fluorescence in the very outer region of the cell, although to only include the membrane accurately would be difficult and with an ion channel such as K_V7 channels, the C-terminus is long and extends into the cytoplasm, this is also where many of the antibodies bind along with the intracellular loops as these areas are more exposed for antibody binding. There is also evidence for the ER and plasma membrane being close together to allow for efficient calcium transfer (Hogea *et al.*, 2021), further clouding what the actual surface expression is. Another possible approach would be to do a membrane extraction on the DRG cells, this works by separating the components of the cell by centrifuging at very high rates, producing a membrane layer, which can be collected in isolation and used for western blotting or proteomic analysis (Smalley *et al.*, 2020, Smolders *et al.*, 2015). The limitation of this method for the present study would be in separating out different neuron types to analyse, current technology does not allow for single-cell analysis with this method so the only way to separate neuron types and obtain enough sample would be to generate transgenic mice, each with different neuronal markers fluorescently tagged. In this way, cells of a particular type could be FACS sorted by fluorescence and then collected for membrane separation. Although, this approach would have been difficult to justify to study surface expression due to the cost, time constraints and the use of a different species.

Our data is in consensus with previously identified expression profiles for $K_v7.2$ in both DRG and in the axons of sensory neurons (Rose *et al.*, 2011, Passmore *et al.*, 2012, Roza *et al.*, 2011). Moreover, it is largely agreeing with the mRNA expression profiling identified in RNA-seq for mouse DRG neurons (Zheng *et al.*, 2019). Broadly, the latter study demonstrated moderate *Kcnq5* expression in non-peptidergic, peptidergic and mostly low-threshold mechanosensitive Aβ fibres. *Kcnq3* was expressed at low levels across most neuron types and *Kcnq2* was expressed at high levels in peptidergic and non-peptidergic C-fibres and Aβ fibres at high levels. The RNA-seq data generally match the protein expression data shown in the current study. However, there are also important differences in the expression data between Zheng and colleagues and the data presented here: i) Zheng and colleagues reported transcript levels while here protein expression was analysed; ii) Here, the expression patterns were calculated based on whether any given neuron was positive or negative for a particular protein, the mRNA data is based on number of transcript counts from an entire population of that neuron type. In addition, larger neurons are likely to require larger amounts of mRNA and protein, but we did not take level of expression in individual neurons into account, only whether it was positive or negative for a certain protein. We did not compare different K_v7 subunit expression levels based on fluorescence intensity because different antibodies would have different affinities for their specific epitopes, which is hard to normalise meaningfully. Therefore, the levels of expression in these two studies are not exactly comparable but do show a similar pattern nevertheless.

My work has also paid particular focus on verifying the specificity of the antibody used on the correct subunit, but also ensuring no cross-reactivity with the other subunits. This allowed us to co-label the subunits to assess their co-expression. There was a strong overlap between $K_v7.2$ and $K_v7.3$ in Rat and Mouse DRGs but this was not complete. It is likely that the neurons in which $K_v7.3$ was detected but not $K_v7.2$ would also co-express $K_v7.5$ since heterologously expressed $K_v7.3$ homo-multimers produce very little current (Zhang *et al.*, 2003). Unfortunately, antibody specification constraints prevented us from confirming this hypothesis. In contrast, $K_v7.2$ and $K_v7.5$ co-expressed to a much smaller degree in either type of rodent DRGs suggesting that there are a significant portion of neurons that express $K_v7.2$ alone. The importance of such a phenomenon could be in potentially controlling a particular population of sensory neurons via manipulating $K_v7.2$ activity specifically. This question is beyond

the scope of this study but is certainly an avenue for further research. Despite K_v7.2 and K_v7.5 subunits not co-assembling into heteromers, there is still some clear co-expression in some 16-18% of sensory neurons. This is of interest as it could suggest the formation of two separate homomeric K_v7 channels in these cells, or if these cells were to express K_v7.3 as well, that there could be the formation of K_v7.2, 7.3 and 7.5 heteromers, something that has been reported previously (Zhang *et al.*, 2016a).

Previous studies have knocked out *Kcnq2* in mice and reported only a mild reduction to pain response in these animals, although this knockout was not sensory neuron but neural crest specific (King *et al.*, 2014). Moderate reductions were seen on induced painful behaviour but only a small decrease in thermal and mechanical pain threshold was observed in a sensory neuron specific (not conditional) knockout mouse line generated by Eli Lilly & Co (data currently confidential). On DRG samples from this same mouse line we were able to validate the *Kcnq2* antibody and knockout. Interestingly, there was an apparent increase in K_v7.5 immunoreactivity in the knockout mice compared to the Wild-Type mice, something not seen with K_v7.3. This may suggest a compensatory mechanism in the knockout mice via this related protein; this is not surprising given recent publications suggesting that related proteins can often compensate in situations of chronic downregulation or knockout (El-Brolosy and Stainier, 2017). We were unable to study this potential compensation in K_v7 channel expression further in this work, however these findings indicate that a conditional and inducible sensory neuron specific *Kcnq* knockout or knockdown approach is required to properly evaluate the functional impact of a given K_v7 subunit expression *in vivo*.

To summarise the data presented in this chapter, we can subdivide K_v7 subunits in two categories. Category-1: low incidence expression (K_v7.1 and K_v7.4); K_v7.1 expression was not detectable in the DRG neurons and K_v7.4 was restricted to a small (~10%) subpopulation of myelinated neurons. Category-2: high-incidence expression (K_v7.2, K_v7.3 and K_v7.5). Amongst the subunits in this category, K_v7.2 was the most abundant and had a bias towards the small-diameter C-fibres. K_v7.3 was broadly expressed with slight bias towards the small-dimeter C-fibres. K_v7.5 was the least abundant in the category-2 and had a bias towards the large-diameter, myelinated neurons. However, there are some important points left to make; this data shows neurons as positive or negative for any given protein, the difference in expression within individual cells was not studied due to the inherent difficulty of comparing

staining produced by different antibodies (as discussed above). Therefore, the same cell may be positive for two types of protein but at differing expression levels and this may not necessarily be picked up in our analysis. More importantly, from a physiological point of view, expression of a protein does not necessarily translate to relative effects on the current or cell excitability overall i.e., more protein expression may not produce more current. Therefore, to further understand the functional effects of individual K_v7 subunits, the next chapter will focus on the contribution of $K_v7.2$ and $K_v7.5$ to neuronal excitability and nociceptive behaviour. These two subunits were chosen for further investigation because both display high-incidence expression with reciprocal bias towards A- and C-type sensory neurons.

Chapter 4: Pharmacologically Profiling the Subunit Expression of K_v7 Channels in Peripheral Sensory Neurons

4.1 Introduction

Analysis of gene and protein expression alone does not necessarily transfer to what is functionally important in both the cell and at the level of the sensory system. Thus, understanding the functional importance of $K_v7.2$, $K_v7.3$ and $K_v7.5$ is required to fully evaluate the contribution of specific channels to various sensory processes. Previously, K_v7 current has been functionally identified in the soma (Passmore *et al.*, 2003, King and Scherer, 2012, Zheng *et al.*, 2013, Du *et al.*, 2014), in the peripheral axons and terminals (Rose *et al.*, 2011, Roza *et al.*, 2011, King and Scherer, 2012, Passmore *et al.*, 2012, Peiris *et al.*, 2017, Linley *et al.*, 2008, Liu *et al.*, 2010, Vetter *et al.*, 2013) and the dorsal root and central terminals (Rivera-Arconada and Lopez-Garcia, 2006). Some of these studies have been linked to $K_v7.2$ expression specifically (Rose *et al.*, 2011, Roza *et al.*, 2011, Passmore *et al.*, 2012), based on the expression data, however the subunit identity in these functional studies was not specifically tested. One reason for this is largely owing to the lack of subunit specificity of traditional K_v7 potentiators, retigabine and flupirtine, and the blocker, XE-991. Although, XE-991 is effective in the range of $K_v7.2$-7.4 sensitivity in sensory neurons, this goes against a strong contribution of $K_v7.5$ as it is far less sensitive to XE-991 than the other subunits (Schroeder *et al.*, 2000a, Wang *et al.*, 1998, Jensen *et al.*, 2005).

Retigabine and flupirtine belong to the triaminopyridine class of compounds and are strong pore-binding, relatively non-selective potentiators of K_v7 channels. These triaminopyridines bind to a tryptophan in the cytosolic portion of the pore region (S5-S6) present in all $K_v7.2$-7.5 but not in $K_v7.1$ (Tatulian *et al.*, 2001b) (Chapter 1.3). Triaminopyridines produce negative shifts in voltage-dependence as well as augmenting macroscopic steady-state potassium conductance at saturating voltages. This makes these compounds efficacious pharmacological tools to combat excitability disorders such as epilepsy (retigabine) and pain flupirtine) **(Figure 4.1)**, but have proven to be clinically non-viable, with the risk/benefit ratio being poor due to bladder retention, sedation and blue skin discoloration (retigabine), and liver toxicity (flupirtine) among other side effects (Clark *et al.*, 2015, Harish *et al.*, 2012). As a result, retigabine

was only approved for short term drug-resistant, partial onset seizures and flupirtine for short term non-opioid pain management. Both have now been discontinued for clinical use (Clark *et al.*, 2015, Harish *et al.*, 2012).

Increasingly, compounds are being developed with the hope of obtaining selectivity for the different subunits/subunit compositions. $K_v7.4$ and $K_v7.5$ have remained quite elusive with respect to selective compounds, though Fasudil has been shown to selectively potentiate $K_v7.4$ (Zhang *et al.*, 2016b) and Go-Slo-SR potentiating $K_v7.4$ and $K_v7.5$ (and BK) **(Figure 4.1)** (Zavaritskaya *et al.*, 2020). Benzamides such as ICA-27243 and ztz240 have been developed that are generally $K_v7.2/3$ selective compounds, with Kv7.2 being particularly sensitive to such compounds. In the case of ICA-27243, the compound binds to the voltage sensing domain in the S3-S4 region to stabilise the open conformation **(Figure 4.1)**. Furthermore, ICA-27243 has the added advantage of not having an effect on GABAa or NaV1.2 channels, something that has been previously reported for retigabine (Otto *et al.*, 2002). Benzimidazole compounds (B1) are also selective for $K_v7.2$ over other K_v7 subunits (Zhang *et al.*, 2011a).

Given the importance to establish the identity of functionally active M channel subunit in sensory neurons and the availability of chemical modulators with reasonable selectivity, this chapter focuses on the evaluation of functional activity of K_v7 subunits most abundantly expressed in the DRG neurons: $K_v7.2$, $K_v7.3$ and $K_v7.5$. To do this we employed the following compounds: ICA-27243 (potentiates Kv7.2 homomers and $K_v7.2/7.3$ heteromers but not $K_v7.3$ or $K_v7.5$ homomers) (Wickenden *et al.*, 2008, Padilla *et al.*, 2009), the prototypic K_v7 potentiator, retigabine (potentiates all K_v7 homo- and heteromers, except the $K_v7.1$) (Wickenden *et al.*, 2001, Schenzer *et al.*, 2005b) and the blocker XE-991 (strongly inhibits $K_v7.1$-$K_v7.4$, less potent for $K_v7.5$) (Schroeder *et al.*, 2000a, Wang *et al.*, 1998, Jensen *et al.*, 2005). Knowing that $K_v7.2$ and $K_v7.5$ can heteromultimerize with $K_v7.3$ but not with each other, we reasoned that sequential application of ICA-27243 and retigabine to a DRG neuron (while continuously recording M current amplitude) would allow us to estimate relative contribution of $K_v7.2$ and $K_v7.5$ to the M current recorded. We reasoned that if retigabine induces additional M current increment after ICA-27243, this would indicate presence of functional $K_v7.5$- and $K_v7.3$- containing channels, which do not contain

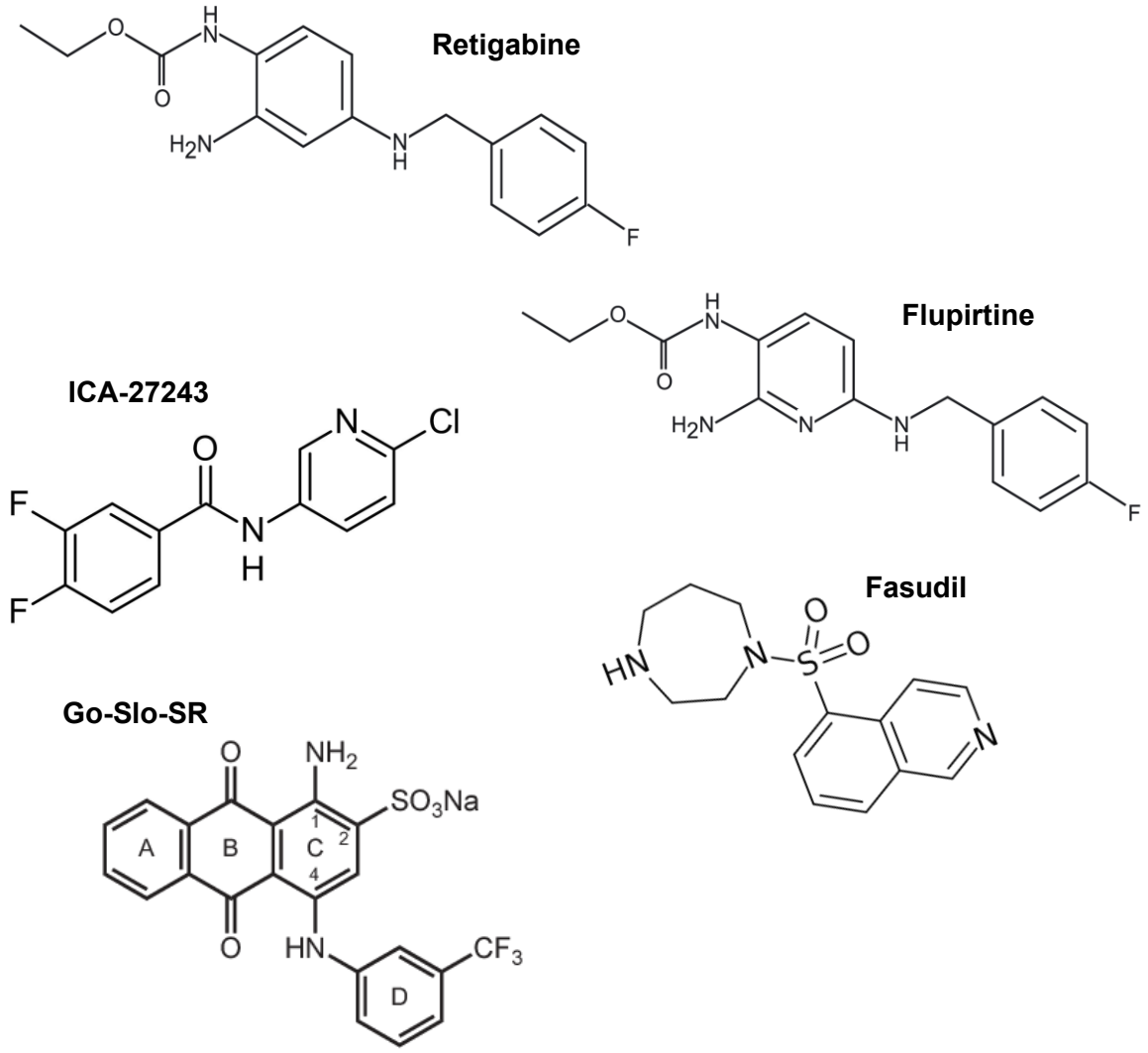

Figure 4.1 Chemical structures of K_v7 channel potentiators.

K_v7.2. On the contrary, if retigabine produces no further increment, this would suggest that all (or most) functional M channels to contain K_v7.2.

We first aimed to confirm the selectivity of ICA-27243 for different subunit compositions and compare the efficacy of ICA-27243 and retigabine. The second aim was to identify the functionality of K_v7 subunits in individual sensory neurons *in vitro*, with our third aim to assess the translation of this to the *in vivo* condition. The final aim was to determine the analgesic effect of local application of K_v7 potentiators compared to systemic application *in vivo*.

4.2 Results

4.2.1 Assessing the Selectivity and Efficacy of K_v7.2/3 Potentiator, ICA-27243

In order to identify the predominant subunits contributing to K_v7 (M) current in peripheral sensory neurons, we first had to clarify the specificity of K_v7.2/3 potentiator ICA-27243 and compare its efficacy to retigabine. To do this, HEK293 cells were transfected with either a *Kcnq3/2* concatemer, *Kcnq5* alone or *Kcnq5/3* to give cells expressing K_v7.2/3 heteromers, K_v7.5 homomers or K_v7.5/3 heteromers, respectively, and the resulting slow activating and deactivating potassium currents were recorded through a voltage clamp patch.

The slow activating and deactivating properties of the exogenous outward current and the negative voltages at which it is active, make it easily distinguishable from the fast activating and deactivating endogenous potassium currents in HEK293 cells (Gamper *et al.*, 2002). Nonetheless, in all cases, an inverted voltage step from -20 mV to -60 mV was employed to minimize the contribution of the endogenous K^+ current in the cell being recorded, in addition, XE-991 (10 μM) was routinely applied at the end of the recording to confirm current identity. Due to the fact that outward current at -20 or -60 mV was negligible in HEK293 cells, the presence of a slow activating and deactivating current between these two voltages indicated a cell functionally expressing K_v7 channels (hence K_v7/M current).

With this established, the impact of our pharmacological tools was assessed the protocol to evaluate voltage-dependence: a train of square 1000 ms voltage pulses from -80 to +40 mV in 10 mV increments from a holding potential of -80 mV. After each

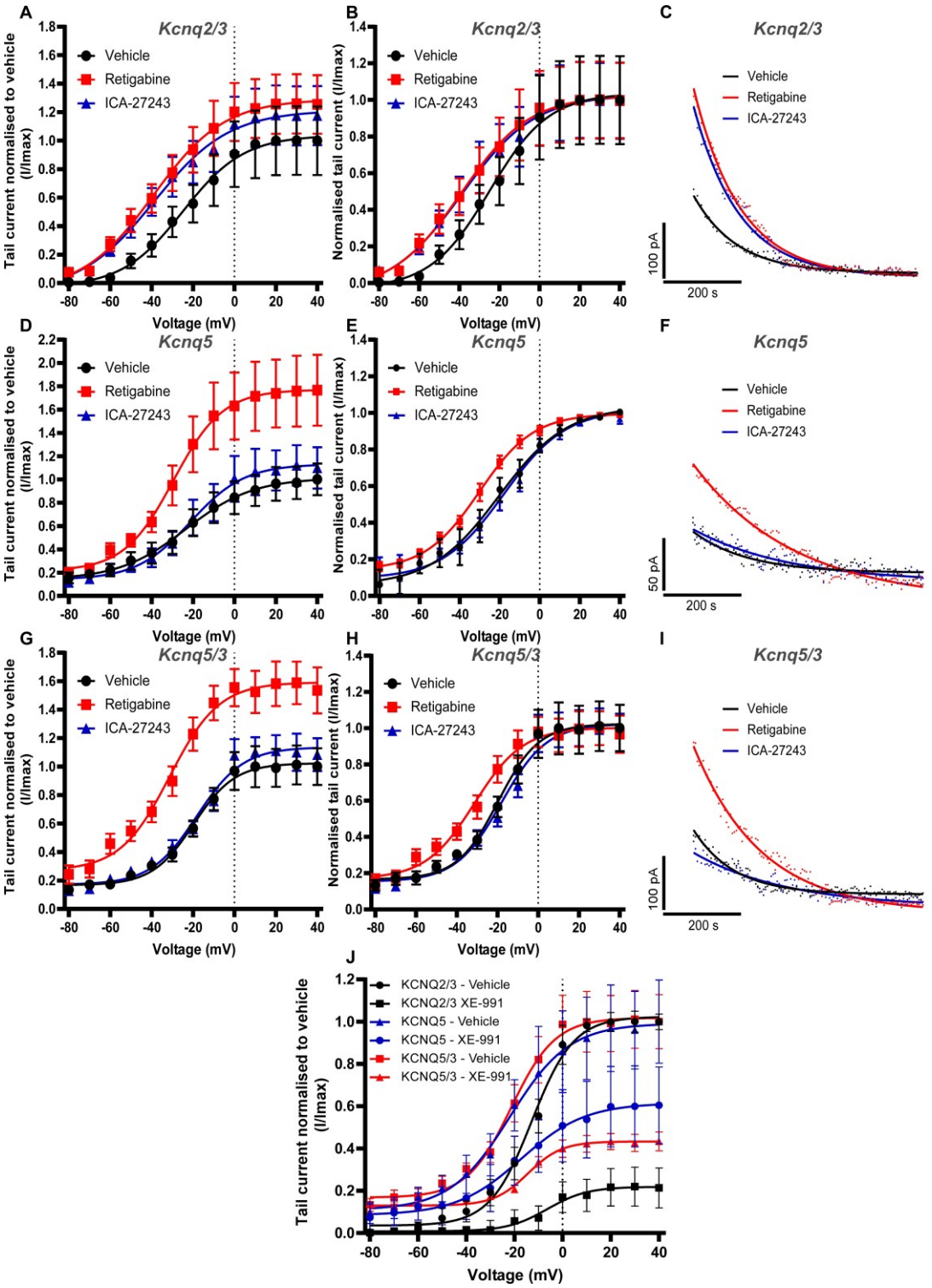

Figure 4.2 ICA-27243 is selective for K_v7.2/7.3 heteromers and has comparable efficacy to retigabine in HEK293 cells. IV curves generated by 2 μM ICA-27243 and 10 μM retigabine in HEK293 cells transfected with **(A-C)** *Kcnq2/3* (n=12), **(D-F)** *Kcnq5* (n=8) or **(G-I)** *Kcnq5/3* (n=10). **Left panels** show tail currents normalised to vehicle (I/Imax) to measure overall current change. **Middle panels** show tail current normalised to the maximum current in that condition (I/Imax) to measure open probability (Po) and voltage shift. **Right panels** are representative examples of the tail current after return to baseline potential (-70 mV). **(J)** Tail current IV curves for *Kcnq2/3*, *Kcnq5* and *Kcnq5/3* response to 10 μM XE-991 normalised to vehicle. IV data presented is Mean ±S.E.M fitted with Boltzmann curves.

step voltage was returned to -80 mV for 600 ms to allow measurement of the tail current amplitudes at different pre-pulse voltages. Representative examples of these tail currents are shown in **Figure 4.2 C, F and I**.

In our hands, 2 μM ICA-27243 and 10 μM retigabine, had a similar impact on increasing the overall outward current **(Figure 4.2A-C)** and in shifting the voltage-dependence of K_v7.2/3 heteromers to more negative voltages **(Figure 4.2B)**. ICA-27243 significantly negatively shifted V50 (half-maximal voltage) by -14.03±1.50 mV from -23.9±2.2 mV to -37.9±1.5 mV (n=12, P<0.001) and retigabine shifted voltage-dependence negatively at V50 by -18.7±3.1 mV (-42.6±3.1 mV; n=12 P<0.01), the difference between ICA-27243 was not significant (Table 4.1) **(Figure 4.2B)**. Retigabine showed a similar increase in current and shift in voltage-dependence on K_v7.5 homomers, with a ΔV50 (average change in half-maximum voltage) of 8.9±1.8 mV (V50 vehicle -20.4±4.0 mV compared to retigabine -29.2±1.8 mV; n=8 P<0.05) and K_v7.5/3 heteromers with ΔV50 of 12.5±3.7 mV (V50 vehicle -19.8±4.9 mV compared to retigabine -32.3±3.7 mV; n=10 P<0.01) (Table 4.1) **(Figure 4.2E/H)**, whereas at 2 μM, ICA-27243 had little impact on the current produced by K_v7.5 homomers (ΔV50 0.07±2.71 mV, V50 -17.9±2.7 mV; n=8) (Table 4.1) **(Figure 4.2D-F)** or K_v7.5/3 heteromers (ΔV50 0.2±4.0 mV, V50 -19.5±4.0 mV; n=10) (Table 4.1) **(Figure 4.2G-I)**. This data suggests that at 2 μM, ICA-27243 is selective for K_v7.2/3 heteromers and has a similar efficacy to that of 10 μM retigabine on these subtypes. XE-991 at 10 μM inhibited outward current of all these subunit combinations, though the level of current blocked by this concentration was variable among the subunits **(Figure 4.2J)**. XE-991 inhibited 85% of tail current K_v7.2/7.3 heteromers at -20 mV (vehicle 38.9±10.1 pA, XE-991 5.8±6.2 pA; n=12 P<0.0001), inhibited K_v7.5 current 43% (vehicle 12.6±2.5 pA, XE-991 7.1±2.4 pA; n=8) and XE-991 intermediately inhibited K_v7.5/7.3 channels by 66% (vehicle 38.5±5.5 pA, XE-991 12.9±0.7 pA; n=8 P<0.001) **(Figure 4.2J)**. This is consistent with K_v7.5 being much less sensitive to XE-991 with an IC_{50} of around 60 μM (Schroeder *et al.*, 2000a) as compared to 1-5 μM in all other subunits (Wang *et al.*, 1998, Wang *et al.*, 2000, Søgaard *et al.*, 2001a).

Table 4.1: current-voltage relationship of K_v7 channels expressed in HEK293 cells.

K_v7 channel	Compound	V50 ±sem (mV)	ΔV50 ±sem (mV)	Max tail current ±sem (pA)
$K_v7.2/7.3$	Vehicle	-23.9±2.2	0±2.2	127.1±15
	ICA-27243	-37.9±1.5***	-14.03±1.50***	149.9±21
	Retigabine	-42.6±3.1**	-18.7±3.1**	160.8±24
	XE-991	-6.3±1.2***	6.7±1.2***	25.2±11
$K_v7.5/7.3$	Vehicle	-19.8±4.9	3.5±4.9	63.3±8.6
	ICA-27243	-19.5±4.0	-0.2±4.0	69.5±6.9
	Retigabine	-32.3±3.7**	-12.5±3.7**	107.7±9.4
	XE-991	-14.4±0.6	5.4±0.6	27.2±2.8
$K_v7.5$	Vehicle	-20.4±4.0	1.9±4.0	19±2.9
	ICA-27243	-17.9±2.7	0.07±2.71	20.9±4.2
	Retigabine	-29.2±1.8*	-8.9±1.8*	35.9±11.0
	XE-991	-17.30±0.97	3.10±0.97	12.6±3.8

Data is mean±sem of current in the presence of each compound. Significance calculated based on repeated measures One-Way ANOVA *P<0.05, **P<0.01, ***P<0.001

4.2.2 Subunit Selective and Non-selective Drugs are Equally Efficacious in TRPV1 Positive but not TRPV1 Negative Sensory Neurons

Although the expression of K_v7 subunits revealed predominantly $K_v7.2$ expression in small-diameter and $K_v7.5$ in medium diameter neurons, respectively, there was still significant expression in other neuron types and significant subunit overlap. Moreover, properties of the subunits to form heteromers and homomers means that expression alone is not enough to identify the functionally predominant subunit responsible for K_v7 current in various cell types. Here, the focus is on $K_v7.2$ and $K_v7.5$ as active subunits due to $K_v7.3$ being able to heteromize with both subunits and the fact that $K_v7.3$ homomer currents are negligible (Zhang *et al.*, 2003). To this end, we separated TRPV1-positive (presumed polymodal nociceptors) neurons from TRPV1-negative neurons by their response to 1 μM capsaicin to characterise them as TRPV1 positive or negative.

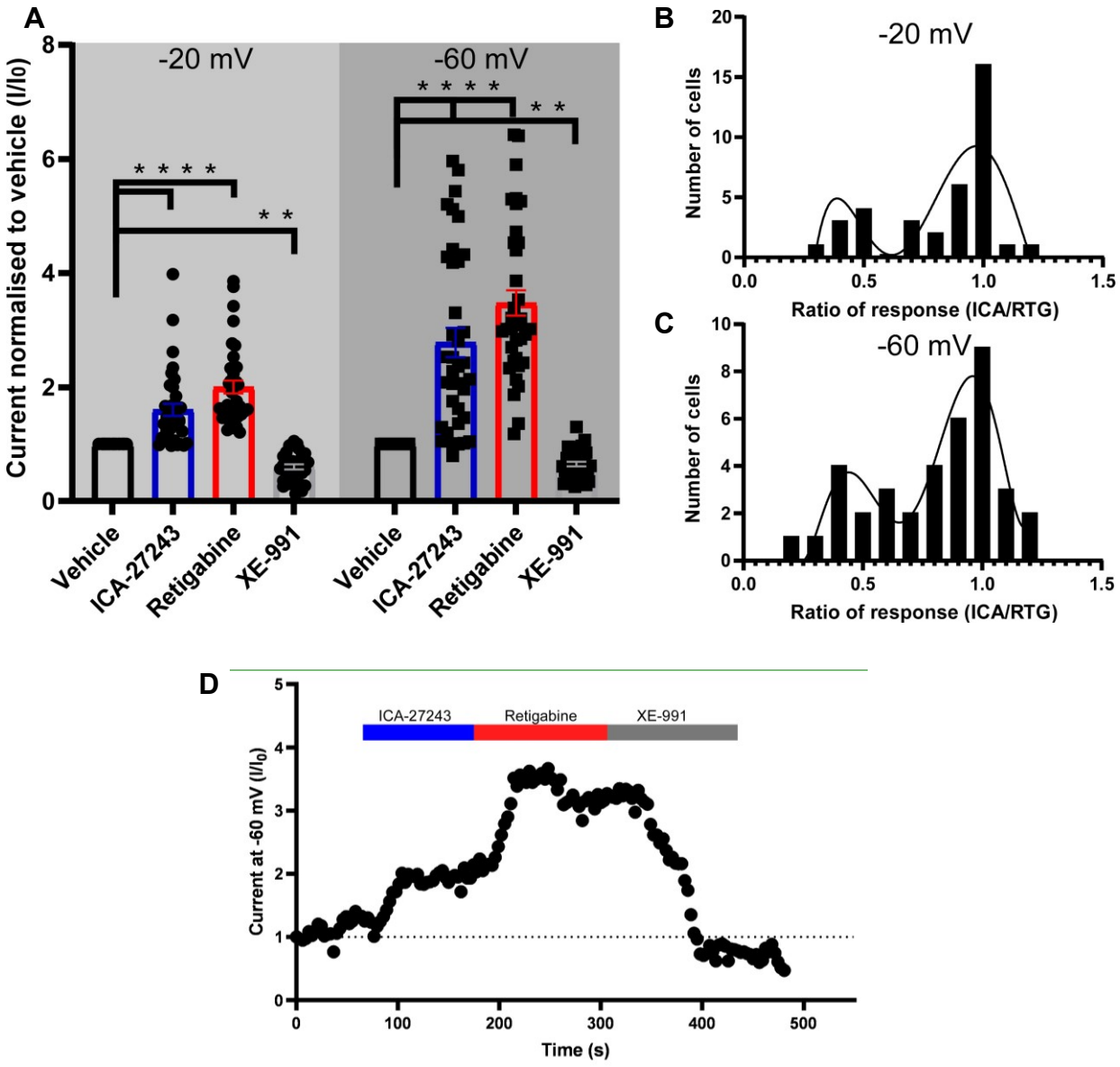

Figure 4.3 The impact of ICA-27243, retigabine and XE-991 on rat sensory neurons. **(A)** Fold-change in response to 2 μM ICA-27243, retigabine 10 μM and 10 μM XE-991 in all sensory neurons recorded from (n=37). Data presented is Mean ±S.E.M. **(B-C)** Distribution histograms for how cells are responding to ICA-27243 compared to retigabine (Ratio of response ICA/retigabine) at **(B)** -20 mV and **(C)** -60 mV. **(D)** representative example of a cell responding to ICA-27243 but responding further to retigabine after ICA-27243 application.

Cultured DRG neurons were patched and an inverted step protocol from -20 mV to -60 mV to -20 mV employed to isolate K_v7 current in neurons non-pharmacologically. This is possible as K_v7 current comprises most of the slow activating and slow deactivating outward current at hyperpolarised voltages. Having confirmed a similar efficacy between ICA-27243 and retigabine **(Figure 4.2)**, one could assume that differences in current between ICA-27243 and retigabine in the same cell could largely be attributed to the presence of a subunit other than $K_v7.2$ or $K_v7.2/3$ heteromers. Therefore, neurons were bath treated until current saturation or for at least 180 s with 2 μM ICA-27243 before a subsequent application of 10 μM retigabine (until saturation or 180 s). XE-991 (10 μM) was applied to confirm the currents were indeed mediated by K_v7 and 1 μM capsaicin was applied to characterise neurons as TRPV1 positive or negative (positive response to capsaicin application would produce negative inflection in current recordings).

Initial analysis suggested that neurons responded similarly to ICA-27243 and Retigabine at -20 mV and -60 mV (responses did not differ significantly at either voltage) **(Figure 4.3A)**; this indicated that $K_v7.2$ contributed to most of the K_v7 current. However, comparing the responses of an M current amplitude to ICA-27243 and Retigabine as a ratio ($I_{ICA\text{-}max}$:$I_{RTG\text{-}max}$) and measuring the frequency distribution, we identified at least two populations of neurons. One population responded very similarly to ICA-27243 and retigabine (ratio ≈1) and a population that responded very differently to the two compounds (ratio <0.5); this multimodal distribution persisted at both voltages **(Figure 4.3B-C)**.

We then analysed M current responses in TRPV1-positive and TRPV1-negative neurons separately. TRPV1 positive and negative neurons showed similar, slow activating and deactivating currents in response to -20 to -60 mV voltage steps **(Figure 4.4A-B inset)** with all cells responding robustly to retigabine and XE-991 **(Figure 4.4A-D)**. However, two populations displayed markedly different responses to ICA-27243. Overall, ICA-27243 significantly increased outward current in TRPV1 positive neurons by nearly 2-fold at -20 mV (1.9±0.15-fold change; n=20 N=5 P<0.0001) and 3.2-fold at -60 mV (3.23±0.31-fold change; n=20 N=5 P<0.0001), this increased outward current was not significantly further increased by retigabine which showed a 2-fold increase (compared to baseline) at -20 mV (2.1±0.15-fold change; n=20 N=5 P<0.0001) and 3.6-fold at -60 mV (3.57±0.3-fold change; n=20 N=5 P<0.0001) **(Figure**

4.4C). The higher efficacy of the drugs (higher relative current increase) at -60 mV, as compared to that at -20 mV is likely to reflect the fact that at more negative voltage (-60 mV) the effect of negative shift in channel voltage dependence is more impactful than at voltage that is nearer to saturation (-20 mV). In TRPV1-negative neurons effect of ICA-27243 was much weaker. At -20 mV there was a small but significant 1.22-fold increase in current (1.22±0.07-fold change; n=17 N=5 P<0.05) and there was a 2.25-fold increase at -60 mV (2.25±0.4-fold change; n=17 N=5 P<0.05). This overall increase was significantly smaller than the 2-fold increase at -20 mV (1.9±0.16-fold change; n=17 N=5 P<0.01) and over 3-fold increase at -60 mV (3.36±0.34-fold change; n=17 N=5 P<0.01) elicited by retigabine **(Figure 4.4D)**. This suggests that K_v7.2, although contributing to K_v7 current in these types of cells, is not the only subunit involved; most likely K_v7.5 or K_v7.5/7.3 channels responding to retigabine and not ICA-27243. XE-991 (10 μM) significantly reduced the current compared to the vehicle in all conditions (TRPV1-positive P<0.0001; TRPV1 negative P<0.01) **(Figure 4.4C-D)**. However, XE-991 had a lesser effect in TRPV1 negative neurons, reducing current compared to vehicle by around 25% (mean 0.7±0.056-fold; n=20 N=5) compared to nearly a 55% (mean 0.47±0.05-fold; n=17 N=5) reduction in TRPV1 positive neurons at -20 mV **(Figure 4.4C-D)**. This further supports the hypothesis higher contribution of Kv7.5-containing channels to the M current in TRPV1 negative neurons, as Kv7.5 is less sensitive to XE-991.

Comparing the difference in currents elicited by the two potentiators in TRPV1 positive neurons revealed that the response to ICA-27243 and retigabine was very similar in the majority of cells. Retigabine increased current more than ICA-27243 in 8 of 20 cells at -20 mV and 10 of 20 cells at -60 mV **(Figure 4.4E-F green line)**. Retigabine increased outward current more than ICA-27243 in 12 of 17 and 14 of 17 TRPV1 negative neurons at -20 mV and -60 mV, respectively **(Figure 4.4E-F green line)**. This paired data suggests that in most TRPV1 positive neurons M current is dominated by K_v7.2 or K_v7.2/3 channels with some residual current carried by channels lacking Kv7.2 (i.e., K_v7.5, K_v7.5/7.3 or K_v7.3) in some cells. However, in TRPV1-negative the situation was rather more complicated compared to TRPV1 positive neurons. Examining TRPV1 negative results more closely suggests there are three sub-populations of neurons with regards to K_v7 current. One sub-population showed no response to ICA-27243 at all (7 of 17 cells) **(Figure 4.4B/D)**. Another sub-population

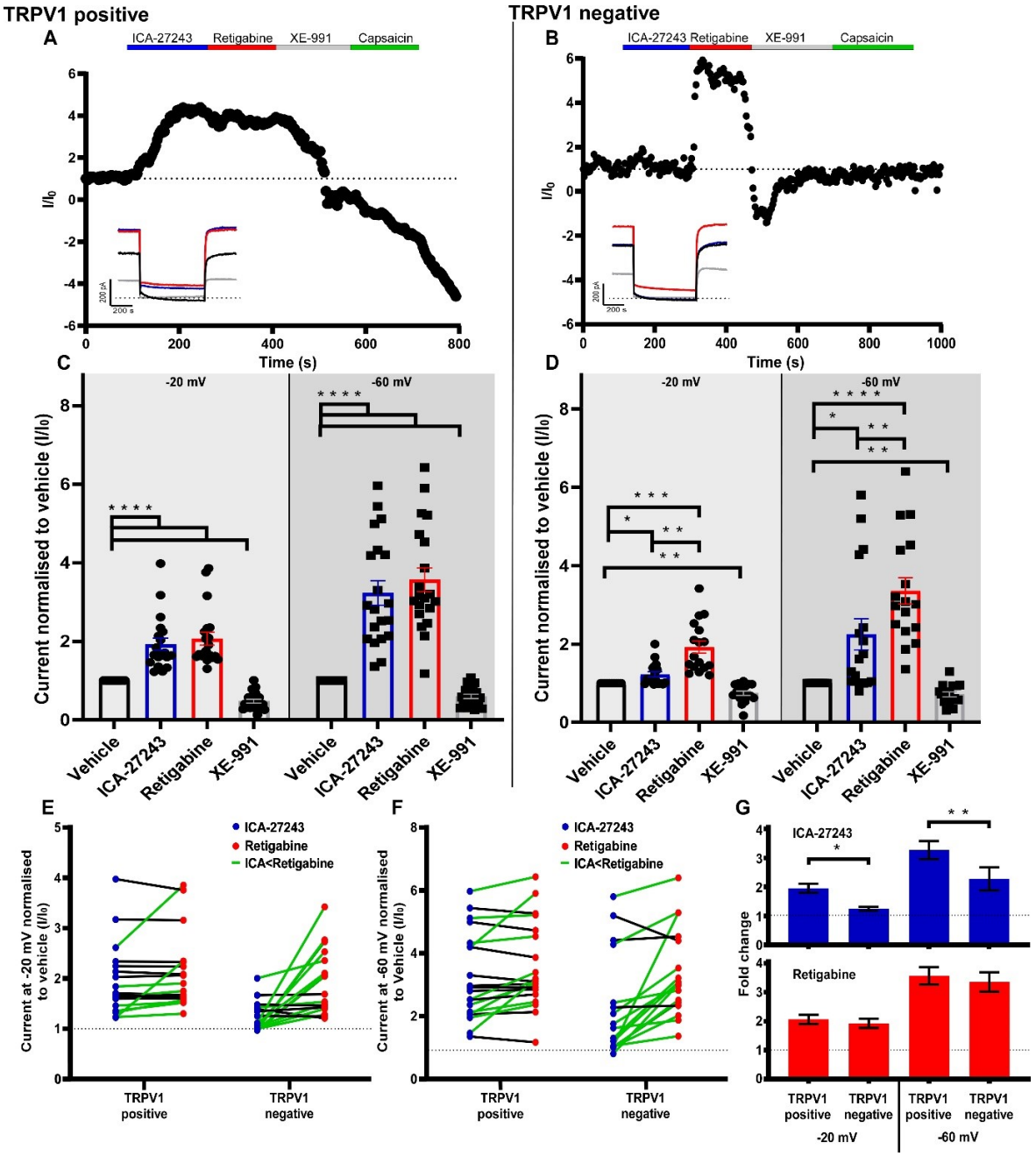

Figure 4.4 Pharmacological profiling suggests $K_v7.2$ is the principal subunit controlling M current in TRPV1 positive mechano-heat nociceptors. **(A-B)** Representative examples of time-courses in TRPV1 positive and TRPV1 negative neurons at -60 mV. Insets are M current traces from the same examples. **(C-D)** Response to 2 μM ICA-27243, 10 μM retigabine and 10 μM XE-991 at -20 mV and -60 mV in **(C)** TRPV1 positive (n=20) and **(D)** TRPV1 negative neurons (n=17) normalised to vehicle for the same cell (I/I_0). **(E-F)** Paired comparison of 2 μM ICA-27243 and 10 μM retigabine in TRPV1 positive and TRPV1 negative neurons at **(E)** -20 mV and **(F)** -60 mV, green lines indicate cells with a higher fold-change in response to retigabine than ICA-27243. **(G)** comparison of ICA-27243 and retigabine fold change between TRPV1 positive and TRPV1 negative neurons at -20 mV and -60 mV. Data presented is Mean ±S.E.M statistical evaluation by repeated measures or independent measures One-Way ANOVA with Tukey's post hoc as appropriate *P<0.05 **P<0.01 ***P<0.001 ****P<0.0001. Animals N=5.

responded to ICA-27243 but showed a further increase in outward current on Retigabine application (5 of 17 cells) and a third sub-population of cells that, similarly to TRPV1 positive cells, responded equally to ICA-27243 and retigabine or only with a small residual increase in current with retigabine compared to ICA-27243 (5 of 17 cells). The first sub-population is likely to express predominantly $K_v7.5$ or $K_v7.5/3$ (or maybe even $K_v7.4$) as there was no response to ICA-27243. Second sub-population had K_v7 current controlled by $K_v7.2$, Kv7.3 and $K_v7.5$ with ICA-27243 potentiating the current of Kv7-2-containing channels in those cells and retigabine potentiating the remaining, most likely $K_v7.5$-containing channels. Finally, there is a population of neurons similar in composition to TRPV1 positive neurons with K_v7 current predominantly controlled by $K_v7.2$ or $K_v7.2/3$. The reason for this is possibly the variety of neurons that would be included in the TRPV1 negative category here. These would include low threshold mechanoreceptor Aβ fibres, some mechano-cold Aδ and C-fibres and two-thirds of non-peptidergic IB4 positive C-fibre nociceptors (Woodbury *et al.*, 2004). These IB4 positive neurons are principally responsible for noxious touch and pruritus, chemosensation and allergy (Emery and Ernfors, 2020).

Overall, ICA-27243 was significantly more effective in increasing K_v7 current in TRPV1 positive neurons compared to TRPV1 negative neurons (1.9±0.15 compared to 1.22±0.07-fold at -20 mV N=5 $P<0.05$; 3.23±0.31 compared to 2.25±0.4-fold at -60 mV N=5 $P<0.01$). In contrast, retigabine had a similar effect in TRPV1 positive and negative neurons **(Figure 4.4G)**. Taken together, these results suggest that $K_v7.2$ is the predominant active subunit in TRPV1 positive neurons but is not the only active subunit in TRPV1 negative neurons.

This heterogeneity in response of TRPV1 negative neurons could be somewhat accounted for by assessing whether cell size correlates with how a TRPV1 negative cell is likely to respond to ICA-27243. Whole cell capacitance (C_{slow}) is a good indicator of cell size in cultured DRG neurons due to their somewhat spherical shape. Analysis of capacitance in TRPV1 positive neurons revealed a normal distribution of lower capacitance suggesting a distribution of smaller sized neurons **(Figure 4.5A)**. Indeed, the whole cell capacitance of TRPV1 positive neurons was lower than TRPV1 negative neurons (14.75±1.4 pF and 20.71±3 pF; n=20, n=17 N=5 $P<0.01$), suggesting a smaller average size of neurons predominantly controlled by $K_v7.2$ **(Figure 4.5B)**. Furthermore, TRPV1 negative neuron capacitance showed a bimodal distribution, with

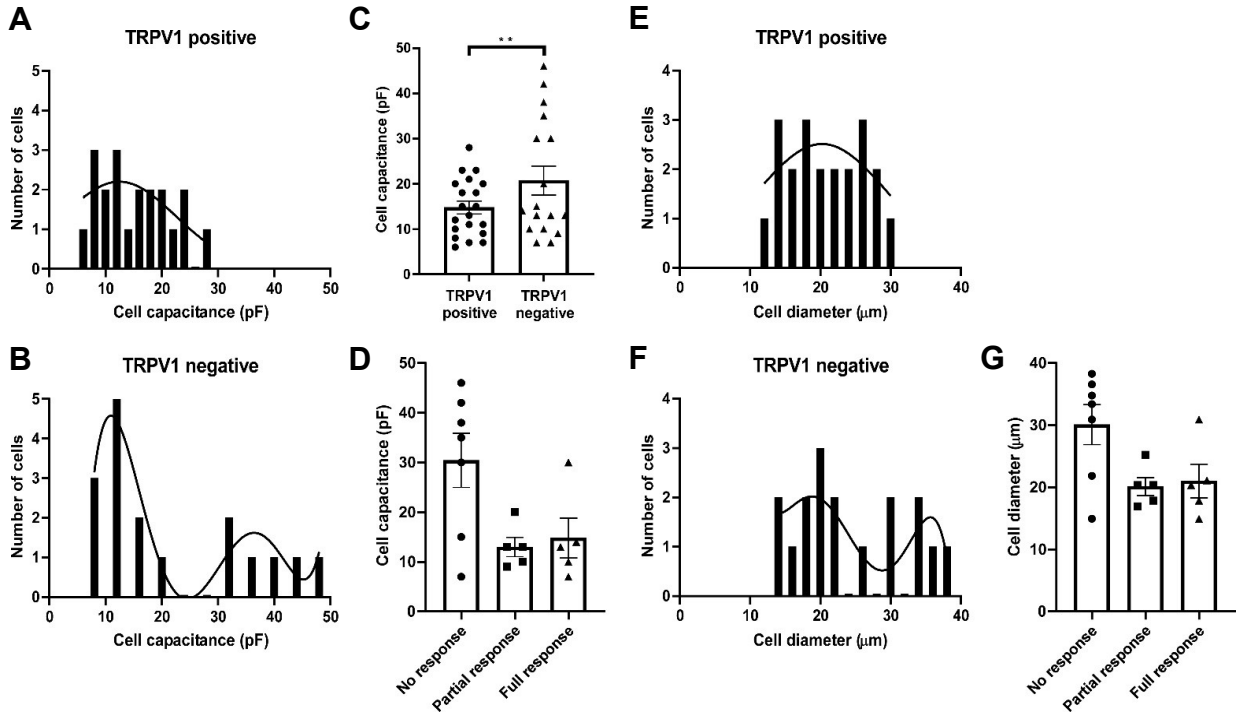

Figure 4.5 Differences in cell size of TRPV1 positive or TRPV1 negative sensory neurons. **(A-B)** Frequency distribution histograms of cell capacitance (pF) in **(A)** TRPV1 positive (n=20) and **(B)** TRPV1 negative neurons (n=17). **(C)** Comparison of cell capacitance (pF) in TRPV1 positive and TRPV1 negative neurons. **(D)** Cell capacitance (pF) of TRPV1 negative neurons that had no response, partial response or full response to 2 μM ICA-27243. **(E-F)** Frequency distribution histograms of cell diameter (μm) based on calculation with capacitance (pF) ($d = 2 \times \sqrt{A \div 4\pi}$) in **(E)** TRPV1 positive and **(F)** TRPV1 negative neurons. **(G)** Cell diameter (μm) of TRPV1 negative neurons that had no response, partial response or full response to 2 μM ICA-27243. Data presented is Mean ±S.E.M. or cell distribution. Independent measures One-Way ANOVA with Tukey's post hoc as appropriate *P<0.05 **P<0.01. N=5.

a population of both lower capacitance and higher capacitance cells, which relates to a mixture of small and large neurons not expressing TRPV1 **(Figure 4.5C)**. Interestingly, the capacitance of TRPV1 negative neurons that did not respond to ICA-27243 was higher (30±5 pF n=7 P<0.05) than neurons that partially (13±1.9 pF n=5) or fully (15±4 pF n=5) responded to ICA-27243, this difference was significantly different (P=0.0387) **(Figure 4.5D)**, suggesting that the size of the neurons that did not respond to ICA-27243 were larger than that of the ICA-27243-responding neurons.

Whole cell capacitance (C_{slow}) can also be used to estimate the diameter of sensory neurons. Previous work has demonstrated that sensory neurons have a membrane capacitance (C_m) of close to 1 μF/cm^2 so this value was used for C_m (Gentet *et al.*, 2000). The area of a cell can be calculated by dividing whole cell capacitance by membrane capacitance ($A = C_{slow} \div C_m$). Area can then be used to calculate the radius by solving the square root of the area divided by 4pi and multiplying by two for cell diameter ($d = 2 \times \sqrt{A \div 4\pi}$). The result of this analysis was very similar to looking at raw capacitance but this estimation of diameter allows us to compare these results to the known diameter of different types of sensory neurons (Tandrup, 2004). TRPV1 positive neurons were normally distributed with an average diameter of 21±1.1 μm (n=20), which is in the range of C-fibre diameter size, as expected **(Figure 4.5E)**. TRPV1 negative neuron diameter was bimodally distributed across 15-40 μm, pertaining to small and medium diameter sensory neurons **(Figure 4.5F)**. The average diameter was 25±2 μm (n=17) which is around the range for C-fibre and Aδ fibre neurons. However, separating the TRPV1 negative neurons by their response to ICA-27243 and comparing size, revealed that neurons responding to ICA-27243, either partially or at the same level as Retigabine, tended to be smaller in size, approximately around C-fibre or Aδ fibre diameter **(Figure 4.5G)**. On the other hand, cells that responded to Retigabine and not ICA-27243 were more likely to be larger in size than those that responded to ICA-27243 with most of these neurons having cell diameters of >30 μm, which is around the size range for Aβ low threshold mechanoreceptors **(Figure 4.5G)** (Tandrup, 2004). This is in accordance with findings in chapter 3.2 where we demonstrated expression of K_V7.5 in Aβ low threshold mechanoreceptors.

It is important to note that this is merely an estimation of cell diameter, as this analysis assumes that C_m is 1 μF/cm^2, although previous reports have shown that the majority of sensory neurons have a C_m of 0.9-1 μF/cm^2 (Gentet *et al.*, 2000), this is not

necessarily the exact value for each cell. This analysis also assumes that the cell is spherical in shape. DRG neurons are indeed largely spherical in culture, however, for cells with many dendritic spines (such as cortical neurons), the shape would not be spherical, and although there are no dendrites, sensory neurons do grow more neurites the longer they are cultured for. Here we assume DRGs are spherical, though it is possible for neurons to grow spines in culture, particularly the longer they are in culture; though cells used in this study were only cultured for 3-5 days. As these are assumptions and not absolutes, the measurement is only an estimate of cell diameter. This approach has previously been shown to be sufficiently accurate, giving confidence in our findings (Hamada *et al.*, 2003), but the values are merely an estimate to compare to the known diameters of sensory neurons. Thus, are perhaps more appropriately interpreted as falling within the range of small, medium and large and should not be taken as the definitive diameter of the neurons.

4.2.3 Analgesic Effect of Systemic Application of ICA-27243 and Retigabine *in vivo*

In individual cultured sensory neurons, we saw a significant increase in K_v7 current with $K_v7.2$ selective compound ICA-27243 and retigabine. It stands to reason that if $K_v7.2$ is indeed the functionally predominant subunit expressed in nociceptive neurons, *in vivo* application of ICA-27243 should provide some analgesic response, possibly similar to retigabine.

We tested this hypothesis both in acute and inflammatory pain conditions to test both common types of acute pain and hyperalgesia. Acute pain was measured by observing behaviour of adult Wistar rats after an intra-plantar injection of 300 µM capsaicin, as capsaicin elicits a strong burning effect with little lasting pain, akin to humans applying capsaicin cream for muscle injury (O'Neill *et al.*, 2012). For a short duration of time the animals displayed nocifensive behaviour of intensely focusing on and licking the paw; these actions were video-recorded and analysed. Accuracy of this method was tested in pilot experiments with two independent researchers (including the author of this work) timing and counting the licking behaviour; this pilot showed good consistency between researchers' results, increasing our confidence in the accuracy of the measurements. Thirty minutes prior to capsaicin injection, animals received an intra-peritoneal injection of 30 mg/kg ICA-27243, 15 mg/kg retigabine or vehicle. These concentrations were selected as they had previously been shown to be the maximal

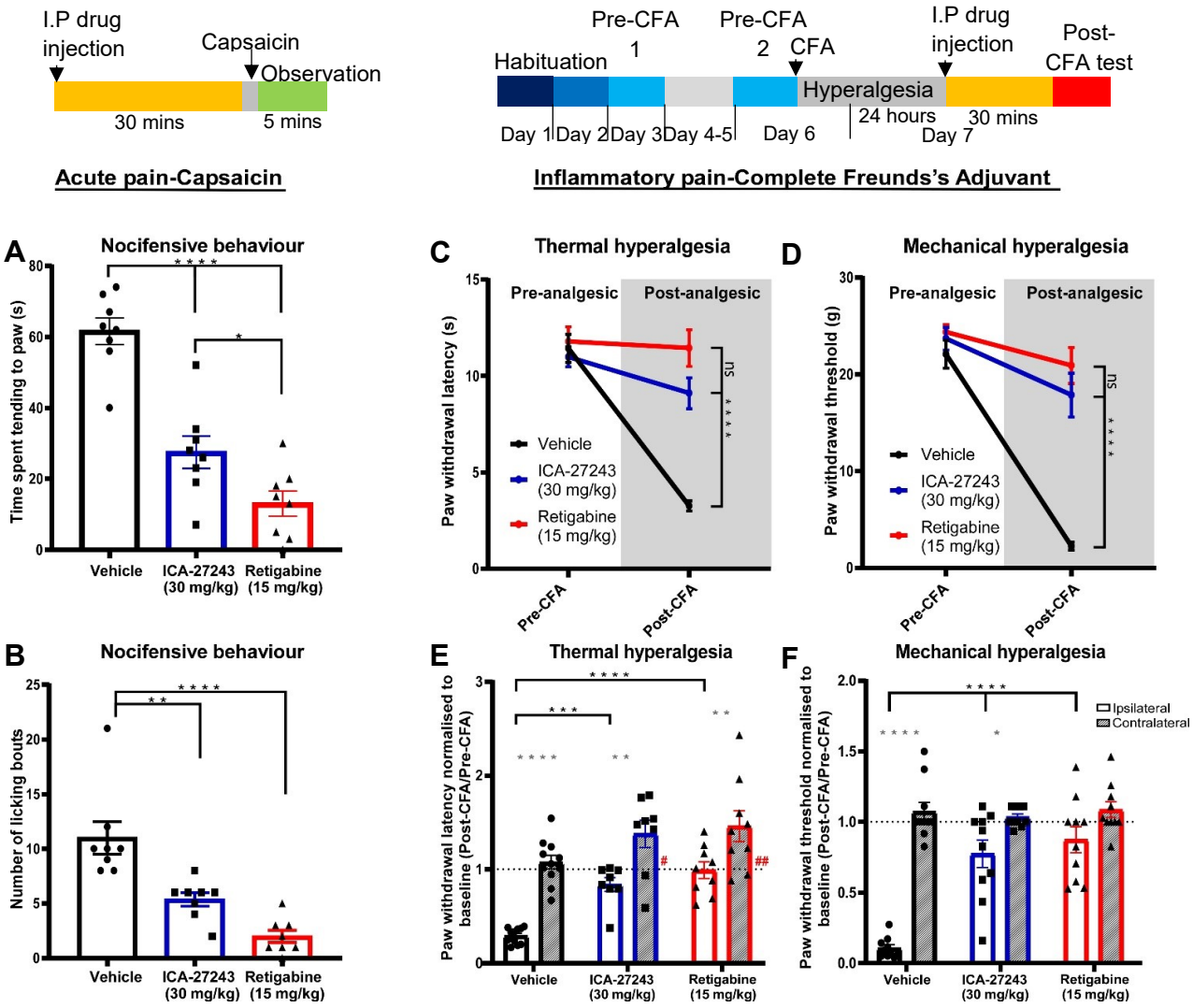

Figure 4.6 Selective activation of $K_v7.2/7.3$ with ICA-27243 promotes a similar analgesic effect to retigabine in acute and inflammatory pain in rats. **(A-B)** Measuring acute hindpaw sensitisation via intra-plantar injection of 300 µM Capsaicin through observing nocifensive type behaviours such as **(A)** the total time spent tending to the paw in a 5-minute period and **(B)** the number of licking bouts during this period. **(C-F)** Inflammatory paw oedema induced by neat Complete Freund's Adjuvant (CFA) intra-plantar injection 24 hours prior to testing. **(C&E)** Changes in thermal hyperalgesia 24 hours after CFA injection assessed using Hargreaves test. **(C)** Change in thermal sensitivity between conditions normalised to pre-CFA injection thermal pain thresholds for each individual (Post-CFA/Pre-CFA). **(D)** Extent of thermal hyperalgesia post-CFA compared to pre-CFA and difference in groups (paw withdrawal latency in seconds). **(D&F)** Mechanical hyperalgesia measured with Von Frey testing. **(E)** Change in mechanical sensitivity between conditions normalised to pre-CFA injection mechanical thresholds for each individual (Post-CFA/Pre-CFA). **(F)** Extent of mechanical hyperalgesia post-CFA compared to pre-CFA and difference in groups (paw withdrawal threshold in grams). Rats in all above tests received an intra-peritoneal injection 30 minutes prior to testing of vehicle, 30 mg/kg ICA-27243 or 15 mg/kg retigabine. Data presented is normalised or raw Mean ±S.E.M, statistical evaluation with independent measures One-Way ANOVA with Tukey's post hoc or Mixed Two-Way ANOVA with Sidak's post hoc as appropriate *P<0.05 **P<0.01 ***P<0.001 ****P<0.0001. (D and F) lined* denotes independent measures significance, *alone (grey) denotes repeated measures significance. Nocifensive behaviour: vehicle N=8, ICA-27243 N=8, retigabine N=8. Thermal threshold: vehicle N=11, ICA-27243 N=9, retigabine N=9. Mechanical threshold: vehicle N=10, ICA-27243 N=10, retigabine N=8.

concentrations that could be administered of the two compounds with minimal sedative and motor effects. Injection of capsaicin after vehicle control elicited an increase in the time spent tending to the paw to 62±3.8 seconds over 11±1.5 bouts (N=8) with this behaviour rarely occurred in the 5 minutes prior to the injection. Both ICA-27243 and retigabine significantly reduced the time and number of licking periods. ICA-27243 treatment reduced time tending to the paw by 65% (27.5±4.57 seconds; N=8; p<0.0001) and licking bouts by 51% (5.38±0.63 bouts; N=8 p<0.001) **(Figure 4.6A-B)**. Retigabine had a further analgesic effect by reducing time tending to the paw by 79% (13±3.5 seconds; N=8), significantly lower than the 65% reduction with ICA-27243 (p<0.05). The number of licking bouts was reduced by 82% (2±0.57 bouts) however this reduction was not significantly different to ICA-27243 treated animals **(Figure 4.6A-B)**.

Inflammatory hyperalgesia involves a complex interplay of secondary messenger mediated protein expression and gene expression changes through release of pro-inflammatory factors (e.g. NGF) (Dray, 1995). These changes extend the hypersensitivity of the inflamed area for a much longer period of time. We induced local inflammation in the hindpaw by intra-plantar injection of complete Freund's Adjuvant (CFA), a widely accepted inflammatory pain model (Gould *et al.*, 1998, Gould, 2000, Fehrenbacher *et al.*, 2012, Hayashi *et al.*, 2014), a PubMed search for CFA returns over 13,000 results. Animals were left for 24 hours to allow the oedema to develop and molecular changes to occur. After 24 hours, mechanical and thermal hyperalgesia were assessed with Von Frey and Hargreaves tests, respectively. Prior to CFA injection animals went through habituation and two baseline tests to identify their pain threshold and these values were used to randomise the groups. Again, 30 mg/kg ICA-27243, 15 mg/kg retigabine and vehicle injected intra-peritoneally 30 minutes prior to post-CFA testing.

Thermal and mechanical hyperalgesia was sufficiently induced in the paw oedema in the vehicle condition. Thermal paw withdrawal latency was reduced from 11.43±0.72 seconds to 3.3±0.26 seconds, a 71% reduction (0.29±0.025 post-CFA/pre-CFA N=11 P<0.0001 compared to baseline) post-CFA injection. Mechanical paw withdrawal threshold was reduced from 22.1±1.4 g to 2.25±0.4 g, a 90% reduction (0.1±0.02 post-CFA/pre-CFA N=10 P<0.0001) **(Figure 4.6C-F)**.

ICA-27243 significantly reduced the change in paw withdrawal latency after CFA. In ICA-27243 treated animals paw withdrawal latency was reduced by 16% (0.84±0.07 post-CFA/pre-CFA N=9 P<0.01 compared to baseline) compared to baseline, with a paw withdrawal latency of 9.1±0.8 seconds (N=9) compared to 3.3±0.26 seconds (N=11) in the vehicle (P<0.001). This analgesic effect was not significantly different to retigabine, where the paw withdrawal threshold was unchanged from baseline (0.99±0.09 post-CFA/pre-CFA, 11.4±0.1 seconds; N=9) **(Figure 4.6C-D)**. Similarly, mechanical hyperalgesia was also reduced in ICA-27243 and retigabine treated animals. Paw withdrawal threshold was significantly higher in ICA-27243 (17.9±2.3 g; N=10 P<0.0001) and retigabine (20.9±1.9 g; N=8 P<0.0001) treated animals compared to vehicle (2.25±0.4 g; N=10) after CFA injection **(Figure 4.6E)**. Furthermore, withdrawal threshold was only reduced by 23% as compared to baseline (0.77±0.1 g post-CFA/pre-CFA; N=10 P<0.05) in ICA-27243 treated animals and retigabine 13% (0.87±0.09 g post-CFA/pre-CFA; N=8) **(Figure 4.6F)**, representing a significant analgesic effect with both treatments (no significant difference between treatments) **(Figure 4.6E-F)**. The contralateral paw did not show any significant change from baseline after CFA injection in Hargreaves (1.08±0.07 post-CFA/pre-CFA; pre- 10.84±0.7 s, post- 11.4±0.7 s; N=11) or Von Frey (1.07±0.07 post-CFA/pre-CFA; pre- 23.9±1 g, post- 25.1±0.6 s; N=10) tests which confirms negligible spinal cord windup effect (Bennett, 2001) **(Figure 4.6D/F)**. Intriguingly, the contralateral paws of animals treated with ICA-27243 and retigabine showed a degree of decreased sensitivity to thermal stimulation. ICA-27243 paw withdrawal latency increased from 11.5±0.64 seconds to 15.46±1.44 seconds (1.38±0.15 post-CFA/pre-CFA; N=9 P<0.05) and retigabine from 10.8±0.4 seconds to 15.5±0.15 seconds (1.46±0.16 post-CFA/pre-CFA; N=9 P<0.01) **(Figure 4.6D)**. This effect was not seen for mechanical stimulation (vehicle pre- 24±1 g, post- 25.1±0.6 g N=10; ICA-27243 pre- 24±1 g, post- 24.8±1 g N=10; retigabine pre- 23.5±0.9 g, post- 25.1±0.6 g N=8) **(Figure 4.6F)**.

This data suggests that systemic injection of ICA-27243 elicits an analgesic effect on acute pain and inflammatory hyperalgesia akin to retigabine, thus implicating $K_V7.2$ (either as homomer or heteromer) as a significant player in nociceptive neurons.

4.2.4 Analgesic Effect of Local Application of ICA-27243 and Retigabine

Systemic application delivers compounds all over the body in the blood and also to the brain if the compound can cross the blood-brain barrier (BBB). As a result of this, the compound can act anywhere the receptors are present. In the case of ICA-27243 and Retigabine, both cross the BBB and can cause sedation as well as other central processes including perhaps CNS-mediated analgesia. Therefore, we also performed behavioural experiments with local application of these analgesics to assess the contribution of peripheral K_v7 channels to analgesia. Wistar rats received a hindpaw intra-plantar injection with vehicle, 500 µM ICA-27243 or 500 µM Retigabine, five minutes prior to an intra-plantar injection of 300 µM capsaicin either into the same paw (ipsilateral) or the opposite paw (contralateral). Here the compounds were delivered at the same concentrations as central effects such as sedation and motor impairment are less of a concern for a local injection (contralateral control still used to test for compounds entering circulation) and this concentration was expected to significantly activate K_v7 channels locally but would be far less effective if entering circulation. Animals that received both analgesic and algogen in the same paw showed a significant reduction in time spent tending to the paw and the number of licking bouts compared to the vehicle control. Vehicle treated animals spent 75±5.4 seconds tending to the paw over 11.33±1 bouts (N=6). ICA-27243 reduced time spent tending to the paw to 34.75±5.4 seconds (N=8, $P<0.001$) over 6.6±1 bouts (N=8, $P<0.05$) and retigabine reduced time spent tending to the paw to 37±6 seconds (N=7, $P<0.001$) over 6.6±1 bouts (N=7, $P<0.05$) (**Figure 4.7A-B**). In contrast, animals that received capsaicin in the opposite paw to the analgesic, showed no significant difference in time spent tending to the paw (vehicle 64.7±8.2 s, N=6; ICA-27243 77.5±5.7 s, N=6; retigabine 72±9 s, N=6) or number of licking bouts (vehicle 11±1.2 bouts, N=6; ICA-27243 11.8±1.4 bouts, N=6; retigabine 12±1.9 bouts, N=6) between any of the groups (**Figure 4.7C-D**). There was no significant difference in the analgesic effects of ICA-27243 and retigabine. This suggests that a significant portion of the analgesic effect of these K_v7 potentiators is peripheral in origin and not entirely central or due to sedation; these data also reinforce the major role $K_v7.2$-containing channels play in analgesic effect of a K_v7 channel potentiator.

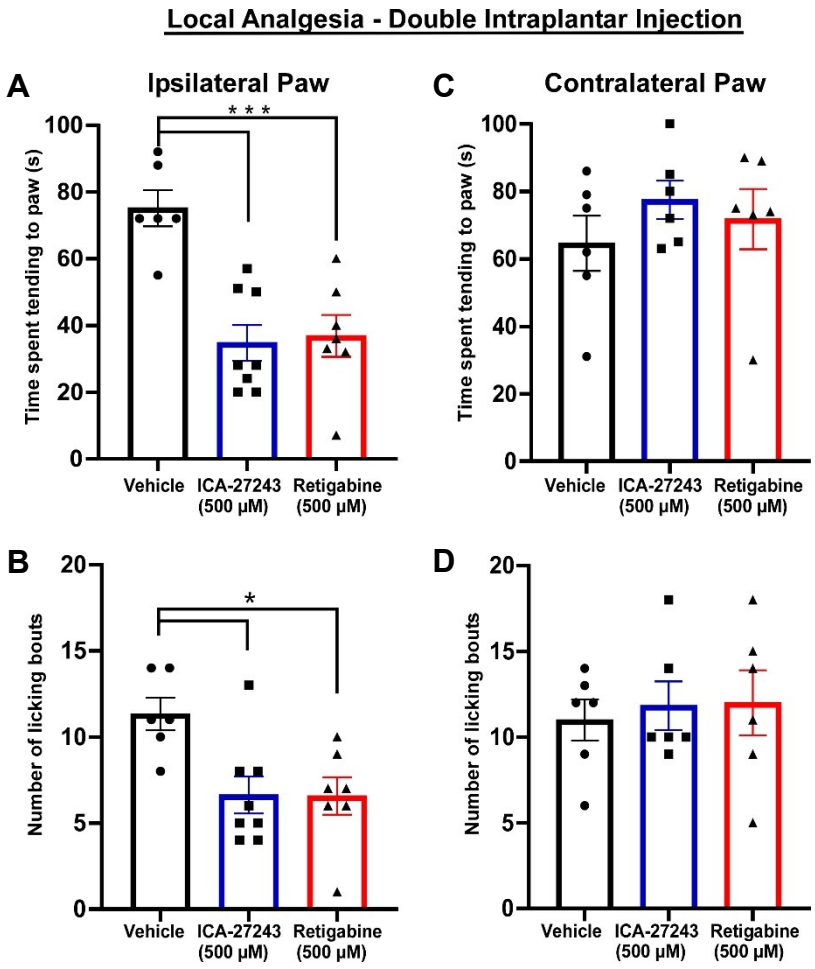

Figure 4.7 Local application of selective K_v7.2/7.3 agonist, ICA-27243 and non-selective Retigabine produce a similar, strong analgesic effect in local, acute pain, in rats. **(A-B**) Measuring acute hindpaw sensitisation via intra-plantar injection of 300 µM Capsaicin, 5 minutes after intra-plantar injection of 500 µM ICA-27243, 500 µM Retigabine or vehicle into the same hindpaw (Ipsilateral to the injection) and observing nocifensive type behaviours such as **(A)** the total time spent tending to the paw in a 5-minute period and **(B)** the number of licking bouts during this period. **(C-D)** Measuring acute hindpaw sensitisation via intra-plantar injection of 300 µM Capsaicin, 5 minutes after intra-plantar injection of 500 µM ICA-27243, 500 µM Retigabine or vehicle into the opposite hindpaw (contralateral to the injection) and observing nocifensive type behaviours such as **(C)** the total time spent tending to the paw in a 5-minute period and **(D)** the number of licking bouts during this period. Data presented is Mean ±S.E.M, statistical evaluation with independent measures One-Way ANOVA *P<0.05 **P<0.01 ***P<0.001. Ipsilateral paw: Vehicle N=6, ICA-27243 N=8, Retigabine N=7. Contralateral paw: Vehicle N=6, ICA-27243 N=6, Retigabine N=6.

4.3 Discussion

The results in this chapter provide a case for $K_v7.2$ being the functionally predominant subunit in TRPV1 positive neurons and a portion of TRPV1 negative neurons. Furthermore, we were able to translate these results into a means to reduce hyperalgesic behaviour in rats suffering from acute pain or inflammatory hyperalgesia. In turn, suggesting that $K_v7.2$ is able to control neuronal hyper-excitability in nociceptive sensory neurons both *in vivo* and *in vitro*.

The *in vitro* pharmacological data shown here agrees broadly with K_v7 subunit expression patterns shown in Chapter 3; $K_v7.2$ is widely expressed and functionally important in a high proportion of neurons with detectible M current. Also, it gives us further insight into which subunits are functionally important in certain types of cells. Previous studies have shown strong effects of retigabine along all compartments of sensory neurons but have been unable to pin down the underlying subunit composition for the current. Our data suggests that when recording from small-diameter (C-fibre) and medium-diameter (Aδ fibre) neurons, it is likely that $K_v7.2$ is carrying a large portion of the K_v7 current, particularly in TRPV1 positive neurons. This is consistent with the RNA-seq analysis showing $K_v7.2$ expression in peptidergic and non-peptidergic C-fibres (Zheng *et al.*, 2019). Notwithstanding, the former study reported an apparent higher mRNA expression of *Kcnq2* in Aβ fibres (Zheng *et al.*, 2019); yet this is not entirely inconsistent with our data as ICA-27243 is still effective in these neurons, but perhaps not the predominant subunit. Additionally, the RNA-seq data is presented as counts of mRNA within a group of neurons, so is not indicative of the level in each individual neuron. These cells are also larger, which may inflate the copy number, a spherical neuron with a 20 μm diameter is around 30 times smaller in volume than a 60 μm neuron, thus the transcripts required to service a large neuron may be significantly higher than for a small neuron.

Importantly, our approach allowed us to some extent overcome the lack of subunit specific K_v7 potentiators and blockers using an ICA-27243/retigabine pair and reasoning that broadly similar responses to ICA-27243 and retigabine would suggest a predominant functional role for $K_v7.2$ in the neuron tested. We can be confident in inferring the contribution of $K_v7.2$ in sensory neurons, however it is more difficult to be accurate in regarding the role of $K_v7.5$, $K_v7.3/5$ or $K_v7.4$. There is still also the possibility that the ICA-27243 responsive current is being controlled by $K_v7.2$

homomers or K_v7.2/3 heteromers which could also be different depending on cell type. As well as the possible functional significance of cells expressing K_v7.2, K_v7.3 and K_v7.5. It is clear that K_v7.2 containing K_v7 channels are important for the function of sensory neurons and the analgesic effect of K_v7 channel potentiators but the contribution of K_v7.3 or K_v7.5 or the heteromers is less identifiable from these tests and are not deducible by the pharmacological tools available at present.

In our hands ICA-27243 was very similar in analgesic efficacy to retigabine *in vivo*. It was also important to test the *in vitro* efficacy of ICA-27243 as the last published efficacy testing was done on the original formulation in 2009 in CHO cells (Padilla *et al.*, 2009). This study showed in the electrophysiological *in vitro* tests, there was a very similar increase in steady-state outward current in transfected CHO cells, as we report, but with a lesser shift in voltage dependence with ICA-27243 compared to retigabine (Padilla *et al.*, 2009). In addition, current literature demonstrates a lack of effect of ICA-27243 on K_v7.5/7.3, K_v7.5 and K_v7.4, consistent with what we report (Wickenden *et al.*, 2008, Padilla *et al.*, 2009). However, there was no published characterisation of the analgesic effect of ICA-27243 from the manufacturers, therefore is limited to one study showing effective analgesia post CFA injection (Hayashi *et al.*, 2014).

We report here that systemic delivery of ICA-27243 produced a strong analgesic effect akin to retigabine, both in acute and inflammatory pain conditions. Though retigabine slightly more efficacious, this suggests a significant role for K_v7.2 in controlling nociception, consistent with our sensory neuron recordings. In addition, local (hind-paw) application of ICA-27243 and retigabine revealed no additive effect of retigabine over ICA-27243, perhaps suggesting the additional effect of systemically delivered retigabine is due to centrally derived analgesia or sedation, rather than the effect of other subunits in the peripheral nerves.

Comparing these K_v7 potentiators to other analgesics, there is a general comparability between retigabine, flupirtine and prescription analgesics for mild to moderate pain. Under acute pain conditions in rats, retigabine was similarly effective to the partial opioid agonist tramadol. After neuropathic injury, retigabine and tramadol were also similarly effective analgesics at comparable concentrations. This was in the same range as the effect of gabapentin despite the concentration of gabapentin being 10 times that of retigabine or tramadol (Dost *et al.*, 2004). In the present study, ICA-27243

was as effective as an analgesic as retigabine, suggesting it would also be akin to tramadol. Flupirtine is usually clinically used instead of retigabine as a post-operative analgesic despite the two only differing by a single nitrogen atom. In the clinical setting flupirtine has an analgesic effect akin to diclofenac and ibuprofen for dental, gynaecological, orthopaedic and craniotomy post-operative pain (Ahuja *et al.*, 2015, Bushra and Aslam, 2010, Yadav *et al.*, 2014). Plus additional muscle relaxation effects and a recently suggested anti-anxiolytic effect (Yadav *et al.*, 2017).

Administered doses used for systemic application were used as the maximal dose that could be delivered with the minimal sedative effect or motor co-ordination impairment (Hayashi *et al.*, 2014). In multiple previous studies at Lilly & Co, ICA-27243 had an advantage over retigabine, inducing sedation at a higher concentration than retigabine (data not disclosable); this was also a consistent observation in pilot studies for this behavioural work with strong sedation in animals treated with 30 mg/kg retigabine (data not shown). However, a previous study suggested less exploratory behaviour in ICA-27243 treated rats than retigabine, suggesting possible sedation (Hayashi *et al.*, 2014). We based the drug concentrations on previous results at Lilly & Co and our pilot observations and even at this concentration a small number of animals treated with retigabine were excluded from the dataset due to signs of sedation during the experiment. This was not the case for rats treated with ICA-27243 or vehicle (studies were blinded, excluded animals were found to be in the retigabine group post experiment).

Interestingly, it appears that potentiating K_v7 channels, particularly $K_v7.2$, reduces noxious heat sensitivity even in the absence of sensitisation, demonstrated by the significant increase in paw withdrawal latency after ICA-27243 or retigabine in the contralateral (non-CFA) paw. This effect was not seen on mechanical sensitivity; however, this could be due to experimental design as there is a maximum limit of 26 grams for Von Frey Filament for adult rats. This data does highlight the possibility that $K_v7.2$ could have a role in setting baseline pain thresholds as well as reducing hypersensitivity.

This data is the first to link $K_v7.2$ pharmacology in sensory neurons *in vitro* to analgesia *in vivo* and to compare ICA-27243 and Retigabine analgesia in acute pain and inflammatory hyperalgesia together. One previous report on behaviour alone did show

similar results for CFA injection (Hayashi *et al.*, 2014), but did not test acute pain or directly compare ICA-27243 with retigabine on the same day with the same conditions and did not analyse the uninjured paw and the effect of the compounds on that paw. Moreover, our data is consistent with other hyperexcitability conditions such as ICA-27243 was shown to have an anti-convulsant effect on induced seizure activity in mice (Roeloffs *et al.*, 2008).

In addition, we show a strong peripheral component to the effect of K_v7 potentiators as analgesics, there was a significant attenuation of pain response after a local injection of either ICA-27243 or retigabine. Hayashi and colleagues also demonstrated K_v7 potentiators analgesic effect is largely peripheral (in contrast to sedation and other such effects), the first inhibiting central K_v7 channels with XE-991 and still demonstrating a significant analgesic effect of systemic analgesia (Hayashi *et al.*, 2014). The team also performed a local application of K_v7 potentiators but in a formalin pain model, they saw a strong attenuation of pain response as we did with capsaicin. However, the concentration of drug delivered to the paw was particularly high at 22 mM, this could lead to lack of specificity of the drugs and systemic penetration. Also, compounds were dissolved in a heavily detergent and alcohol-based vehicle. Whereas here we demonstrate an effect of local application of ICA-27243 and retigabine at a more K_v7 selective concentration, making it the first bona fide test of peripheral analgesic efficacy of these compounds.

In summary, functional pharmacological analysis of K_v7 subunits in sensory neurons provides further clarity to the expression data suggesting that $K_v7.2$ not only is the most abundantly expressed, but also is the predominant functional subunit in TRPV1 positive and a portion of TRPV1 negative neurons. This translates to an important role in controlling pain response to both, acute pain and inflammatory hyperalgesia. However, the lack of specific pharmacological inhibitors prevented us assessing the impact of direct $K_v7.2$ inhibition on M current, neuronal excitability and pain response. There is also the possibility that K_v7 channels may impact the setting of the pain threshold that could not be fully explored. $K_v7.2$ knockdown or knockout in peripheral sensory neurons would provide the means to answer these questions further, which will be explored in subsequent chapters.

Chapter 5: The Impact of Reducing *Kcnq2* and *Kcnq5* Expression in Peripheral Sensory Neurons

5.1 Introduction

Previous chapters have demonstrated: (1) the presence of K_v7 channels in TRPV1-positive DRG neurons, with a predominance of $K_v7.2$ and/or $K_v7.3$; and (2) pharmacological intervention using K_v7 current potentiators that act on these subunits can enhance the M current in this subpopulation of DRG neurons. Taken together, $K_v7.2$ and $K_v7.3$ emerge as functionally predominant subunits underlying the M current in TRPV1 positive DRG neurons. Interestingly, in TRPV1 negative DRG neurons, there is a more variable K_v7 subunit composition. However, pharmacological tools are only an effective means to study ion channels to a point as they can easily have hidden effects or cross-reactivity that are not obvious or easily identifiable (Romano *et al.*, 2005). For example, as mentioned earlier, there is some evidence that suggests that retigabine has off target effects on other ion channels which could impact our results (Otto *et al.*, 2002).

Rather than targeting the channel at the membrane with pharmacological compounds, it is possible to alter the properties of the channel through mutagenesis or controlling expression levels of the protein in the membrane (Hogea *et al.*, 2021, Singh *et al.*, 2008). Both come with advantages and disadvantages and can be achieved in various ways.

Focussing on mutation of the protein to change the function, most commonly, transgenic knock-in approaches, can be used for the animal to express the gene of interest or the mutated protein can be delivered in excess of the endogenous protein. This delivery approach is generally used for dominant-negative versions of a protein to cause a loss of function or gene editing to recapitulate the effect of human mutations in rodent models (Singh *et al.*, 2008, Doyle *et al.*, 2012). Knockout animals would be appropriate for removing *Kcnq* genes to analyse the impact, to avoid compensation and prevent likely fatality in early life, a sensory neuron specific, inducible knockout would be most appropriate.

These methods have particular disadvantages, in the case of transgenic animals, mice are the most common transgenic animals used due to ease, time and cost-effectiveness (Gurumurthy and Lloyd, 2019). Delivering mutated versions of proteins

are often delivered to immortalised cell lines but not easily delivered *in vivo* to assess changes in the live animal, without using the transgenic approach. Significant problems with knockouts are often unknown until it has been generated, such as fatality and compensation (Watanabe *et al.*, 2000, El-Brolosy and Stainier, 2017).

RNA interference (RNAi) describes a class of useful alternatives to knocking out genes with the transgenic approach that can be utilized in cell lines through to the live animal and can also be used in acute or chronic applications. RNAi is a short RNA sequence but rather than being translated like mRNA, they instead form hydrogen bonds with complementary mRNA for a specific protein, forming double-stranded RNA that cannot be translated and is instead, degraded. Acute gene silencing occurs through small interfering RNA (siRNA) and microRNA (miRNA) via the same process and both exist naturally and as synthetic tools. The main differences currently identified are that miRNA is generally synthesised in the cell nucleus whereas siRNAs are introduced by exogenous means (in natural circumstances); siRNAs selectively silence a specific gene compared to the less specific but more wide-ranging effects of miRNAs. RNAis are introduced into the cell as double stranded precursors that are cleaved into short 19-24 nucleotide RNAs by the endonuclease, Dicer. The guide strand of the cleaved RNA is bound to an argonaute protein that stabilises this ‘active’ strand whilst the PIWI domain cleaves the passenger strand; the complex minus the passenger stand is named the RNA induced silencing complex (RISC). Through the single-stranded RNA present, RISC binds to complementary mRNA (in the case of siRNA this is specific), which is then cleaved by the PIWI domain in RISC and degraded via the usual mRNA degradation processes such as in P-bodies (Parker and Sheth, 2007). These processes are acute (effect can last up to 4 days from maximum knockdown, usually occurring after 72-96 hours) as siRNA is degraded over time and protein levels return to normal **(Figure 5.1)**.

Longer term RNAi is mediated by short hairpin RNA (shRNA), for experimental manipulation, shRNA is inserted into a DNA vector delivered through viral transduction or transfection. This type of RNAi can integrate into the genome or be transcribed from a plasmid (extra-chromosomal) for generation of stable cell lines and long-term downregulation of genes *in vivo* (Brummelkamp *et al.*, 2002). Designs for shRNA include Stem-Loop shRNA and adapted shRNA. Stem-Loop are microRNA precursors that get cloned into viral vectors. They are single-strand molecules of 50-70

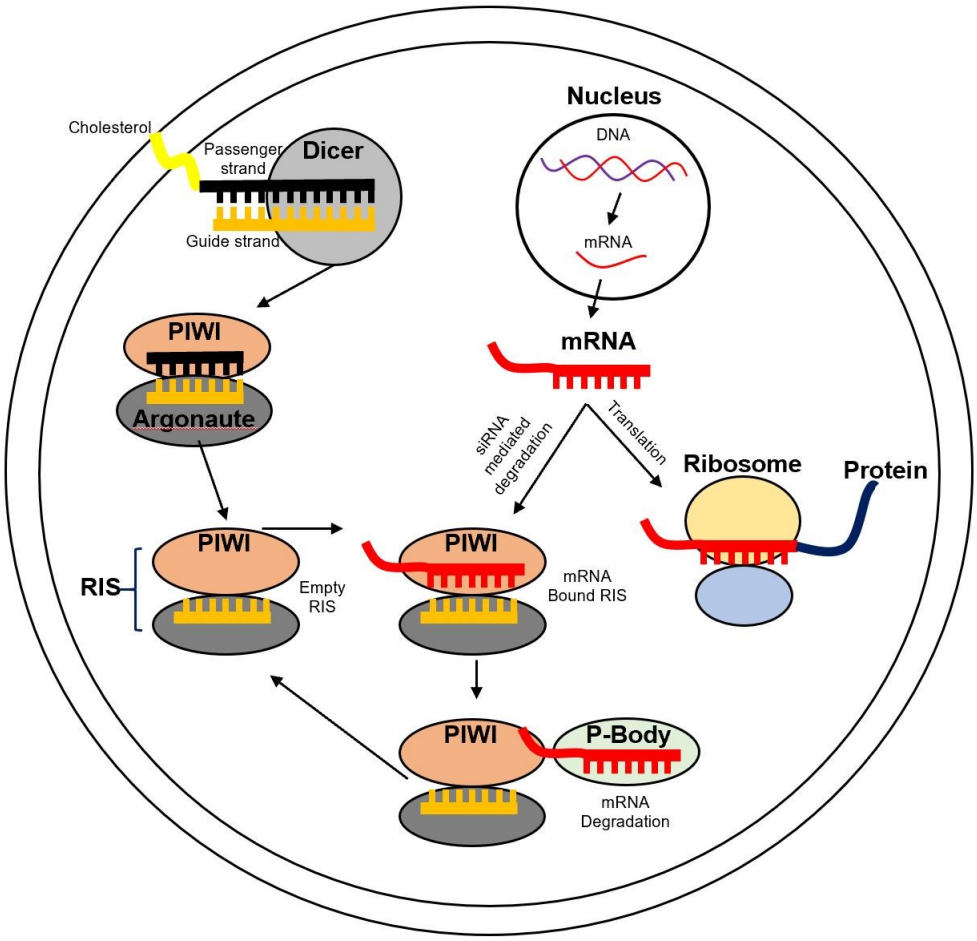

Figure 5.1 Mechanism of action of cholesterol-conjugated siRNA. siRNA is initially double-stranded, consisting of a guide strand, which targets the mRNA and a passenger strand. The siRNA is conjugated to a lipophilic cholesterol. Once in the cell, argonaute proteins stabilise the guide strand as the passenger strand is cleaved by the PIWI domain. The argonaute-guide strand-PIWI complex (minus the passenger strand) is the RNA induced silencing complex (RISC). mRNA transcribed from DNA in the nucleus is normally translated to protein in ribosomes but instead is captured by RISC and degraded in P-bodies. The empty RISC is able to repeat the process.

nucleotides that form a double-strand RNA (stem) bridged by single stranded RNA (loop) plus a 3' overhang. The shRNA is transcribed and exits the nucleus and are then cleaved at the loop by Dicer and follows the RISC process stated above.

Another synthetically produced RNAi used for experimental manipulation is adapted microRNA shRNA. This RNA has the same shRNA stem structure as normal shRNA but surrounded by endogenous microRNA. This type also follows the Dicer RISC process, but the microRNA attachment can improve efficiency and reduce toxicity for *in vivo* application (McBride *et al.*, 2008).

With the vast range of gene silencing techniques available, we decided to take advantage of siRNA to enable the study of the acute effects of *Kcnq* knockdown in both *in vitro* and *in vivo* settings. The use of siRNA will minimise the impact of compensatory increases in other related genes and allows paired comparison of behavioural responses in the same animals before and after the knockdown.

5.2 Results

5.2.1 Assessing the Efficacy of Various *Kcnq2* siRNAs in Cultured Sensory Neurons

To provide the best chance for strong mRNA knockdown, three *Kcnq2* siRNAs were transfected into cultured rat DRGs by electroporation (Lonza), both separately and in combination, followed by qPCR to assess the level of knockdown compared to a non-targeting control (NTC) and naïve cells.

RNA was extracted from *Kcnq2* siRNA transfected DRGs and converted to cDNA for qPCR analysis of the mRNA. The NTC showed a small non-significant reduction in *Kcnq2* compared to the naïve cells, whereas all siRNAs elicited significant *Kcnq2* knockdown compared to naïve cells and NTCs **(Figure 5.2A)**. Treating cells with individual siRNAs revealed that siRNA1 was least effective, reducing *Kcnq2* expression by 50±2% (N=3). Both siRNA2 and siRNA3 were more effective than siRNA1, reducing *Kcnq2* expression by 75±7% (N=4 $P<0.01$) and 80±6% (N=4 $P<0.001$), respectively **(Figure 5.2A)**. Combining all the siRNA into a pool or siRNA2 and 3 into a pool did not significantly increase the efficacy compared to the siRNA2 and 3 individually, but the mean reduction in the pools was 85±3% (N=8) for all siRNAs and 88±1% (N=5) for siRNA2 and 3 together **(Figure 5.2A)**. Therefore, the pool was used for continuing experimentation due to the significant reduction in mRNA

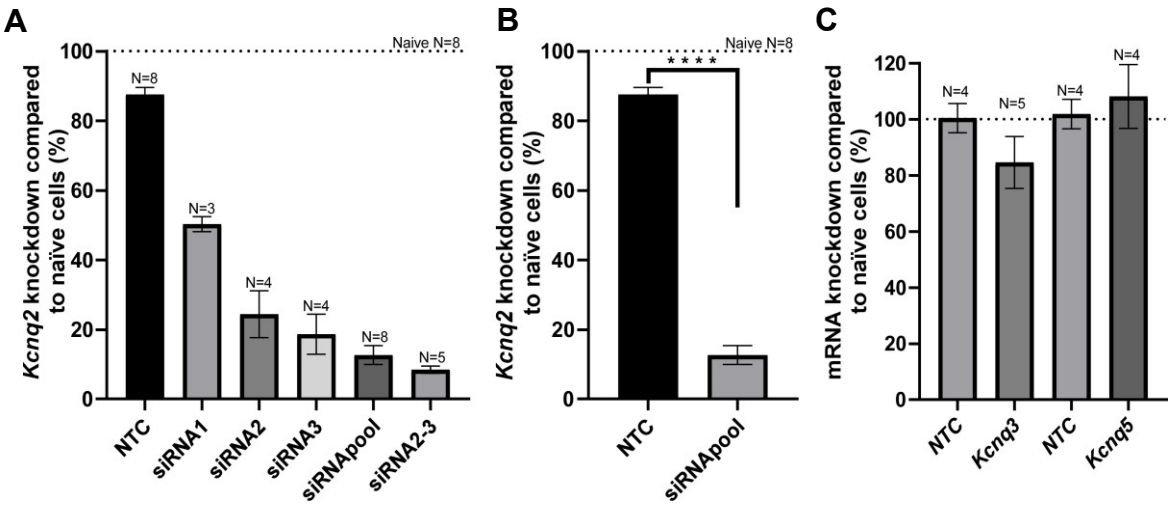

Figure 5.2 Effectiveness of transfected Kcnq2 siRNA in cultured rat sensory neurons and the impact of this on other Kcnq subunits. **(A)** *Kcnq2* mRNA knockdown with three *Kcnq2* siRNAs (siRNA1-3) and non-targeting control RNA (NTC) compared to *Kcnq2* expression in naïve untransfected sensory neurons normalised to *Hprt1*. **(B)** Effectiveness of *Kcnq2* siRNA induced knockdown used in voltage and current clamp experiments compared to NTC. **(C)** Gene expression of *Kcnq3* and *Kcnq5* after siRNA knockdown. Data presented is Mean ±S.E.M, statistical evaluation on ΔCt with independent measures or repeated measures One-Way ANOVA with Tukey's post hoc as appropriate ****P<0.0001. Number of animals indicated on figures.

expression (85±3%, N=8 P<0.0001) and low variability, making the pool reliable for continued use in patch clamp experimentation **(Figure 5.2B)**.

Previously, we identified that K_V7.2, K_V7.3 and K_V7.5 were well expressed (Chapter 3) and functionally important (see chapter 4) in DRG neurons. Although K_V7.2 and K_V7.5 were not reported to form heteromers, there is evidence when heterologously expressing all three subunits that K_V7.2, K_V7.3 and K_V7.5 can combine to form tri-subunit heteromers (Zhang *et al.*, 2016a). Also, in chapter 3.2.3, it has been proposed that in long term *Kcnq2* knockouts there may be a compensatory increase in K_V7.5 expression. This was considered by assessing any potential changes in other *Kcnq* subunits in the same cells. In this acute knockdown experiment, *Kcnq3* and *Kcnq5* expression was largely unaffected by *Kcnq2* siRNA knockdown **(Figure 5.2C)**. *Kcnq3* expression was found at 85±10% (N=5) of the naïve cells level and *Kcnq5* expression was on average 110±11% (N=4), neither of which was significantly different to naïve nor control cells (N=4) **(Figure 3.2C)**. The information obtained from measuring mRNA expression suggested that the siRNA was effective in knocking down *Kcnq2* and this had no indirect (off-target) or compensatory impact on other highly expressed *Kcnq* subunits.

5.2.2 Changes in K_V7 (M) Current after *Kcnq2* siRNA Knockdown

As an obvious next step, I measured the functional effects of *Kcnq2* knockdown in DRG neurons. M current was assessed in cultured sensory DRG using voltage clamp electrophysiology. The same protocols used in chapter 4 were utilized again in order to evaluate changes in M current amplitude and density; we also utilised the test of differential sensitivity to retigabine and ICA-27243, as a measure of specific contribution of K_V7.2-containing subunits to the macroscopic M current. Again, capsaicin was used at the end of each recording to characterise cells as TRPV1 positive or TRPV1 negative. siRNA knockdown of *Kcnq2* induced marked reduction of M current, specifically in TRPV1-positive neurons. In TRPV1 positive neurons a significant reduction in current density from 5.6±1.1 pA/pF (NTC n=14) to 2.2±0.5 pA/pF (siRNA n=18 P<0.05) and in normalised current from 1.10±0.15 pA/pA_n (NTC n=14) to 0.43±0.07 pA/pA_n (siRNA n=18 P<0.05) was observed **(Figure 5.3A/C)**. This suggests a reduction in functional K_V7 channels within TRPV1 positive neurons after *Kcnq2* knockdown. In TRPV1 negative neurons, current density (NTC 4.1±0.9 pA/pF n=11; siRNA 2.4±0.3 pA/pF n=14) and normalised current (NTC 1.1±0.3 I/I_0 n=11;

siRNA 0.62±0.1 I/I_0 n=14). were reduced but this was not significant **(Figure 5.3B/D)**. This is likely owing to higher heterogeneity of *Kcnq* expression in this subpopulation of DRG neurons with some cells having $K_V7.2$ controlled M current and some cells being controlled by other K_v7 subunits.

The above data provides information on the effect of *Kcnq2* siRNA knockdown on TRPV1 positive or negative neurons compared to controls. In order to understand whether the role of $K_v7.2$ differs between these cells we had to directly compare TRPV1 positive to TRPV1 negative cells. In doing so, we found that without applying any compounds, cells treated with the NTC had similar current densities and normalised currents regardless of their TRPV1 positive or negative classification. NTC current normalised to naïve cells was 1.10±0.15 pA/pA_n (n=14) and 1.10±0.35 pA/pA_n (n=11) in TRPV1 positive and negative neurons, respectively **(Figure 5.3E)**. TRPV1 negative neurons did have a lower average (not normalised) current density of 4.1±0.9 pA/pF (n=11) compared to 5.57±1.16 pA/pF (n=14) in TRPV1 positive neurons **(Figure 5.3F)**.

On the other hand, cells transfected with *Kcnq2* siRNA were affected differently depending on whether they responded to capsaicin or not. Both groups of cells showed a reduction in current and in current density compared to the NTC group. In TRPV1 positive neurons the 62% reduction in normalised current (1.1±0.2 pA/pA_n n=14 to 0.43±0.07 pA/pA_n n=18 P<0.01) **(Figure 5.3E)** and 3.36 pA/pF reduction in current density (5.57±1.16 pA/pF n=14 to 2.2±0.5 pA/pF n=18; P<0.01) was significantly different **(Figure 5.3F)**. TRPV1 negative neurons had a 40% reduction in normalised current (1.1±0.1 pA/pA_n n=11 to 0.62±0.12 pA/pA_n n=14) **(Figure 5.3E)** and the 1.7 pA/pF reduction in current density compared to NTC (4.1±0.9 pA/pF n=11 to 2.4±0.3 pA/pF n=14) **(Figure 5.3F)** were not statistically significant. The further 22% (1.5-fold) reduction in current in TRPV1 positive neurons compared to TRPV1 negative neurons proved to be significant ($TRPV1^+$ 0.43±0.07 pA/pA_n n=18; $TRPV1^-$ 0.62±0.12 pA/pA_n n=14; P<0.05) **(Figure 5.3E)**. Suggesting that $K_v7.2$ has a greater contribution to the K_v7 current in TRPV1 positive neurons than in TRPV1 negative neurons, which is agreement with the data presented in the previous chapter.

The M current kinetics and time-course of the effects induced by retigabine ICA-2743 and XE-991 were largely similar **(Figure 5.3G/H inset)** in the naïve neurons, negative

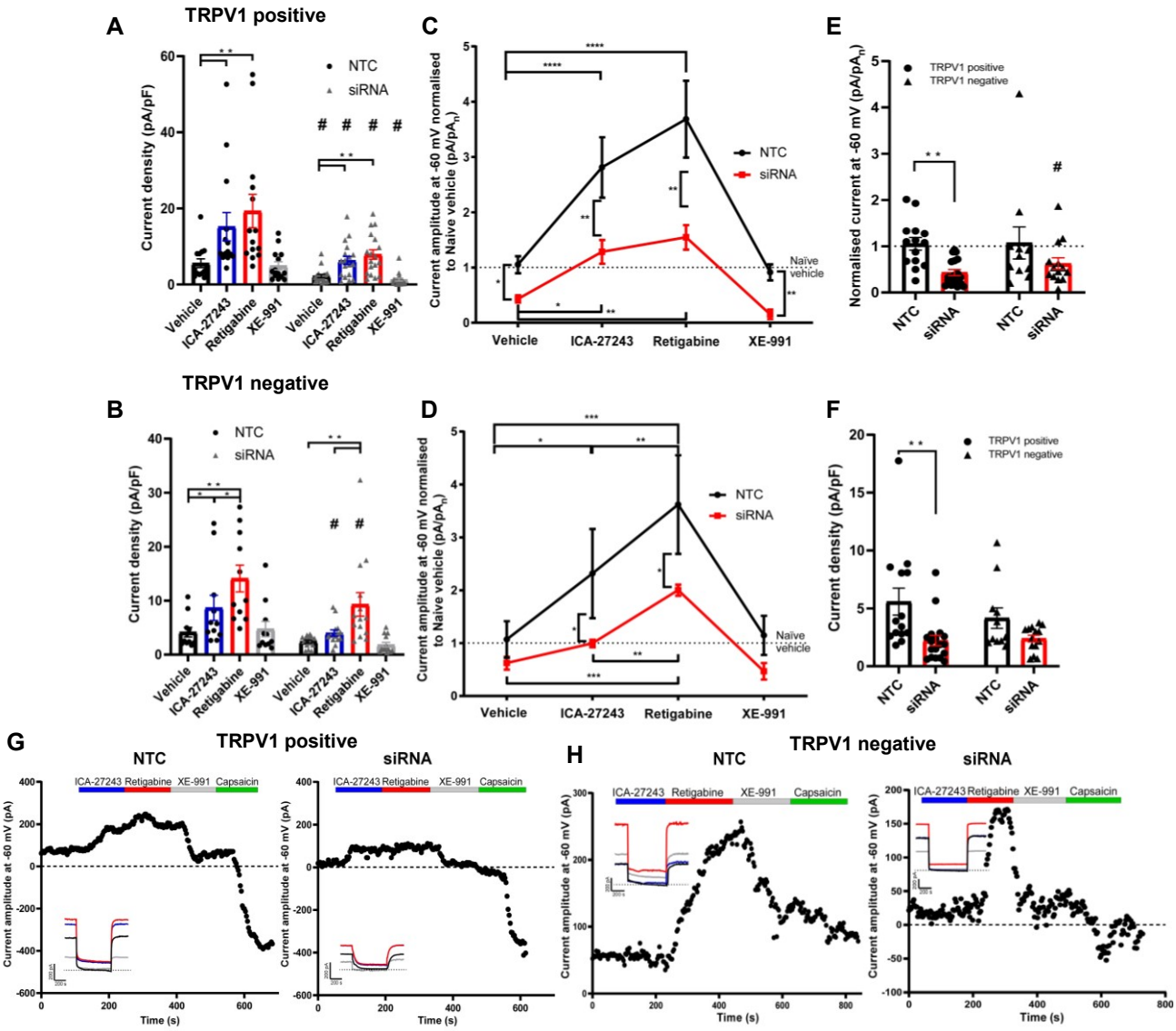

Figure 5.3 siRNA knockdown of Kcnq2 drastically reduces the M current in TRPV1 positive sensory neurons. **(A-B)** Current density of NTC and siRNA treated cells and the change in response to 2 μM ICA-27243, 10 μM retigabine and 10 μM XE-991 at -60 mV in **(A)** TRPV1 positive and **(B)** TRPV1 negative neurons calculated by dividing current by capacitance (pA/pF). **(C-D)** Current at -60 mV in NTC and siRNA treated cells normalised to the vehicle treated naïve cells (pA/pA$_n$) (dotted line) in **(C)** TRPV1 positive and **(D)** TRPV1 negative neurons. **(E-F)** Comparison of TRPV1 positive and TRPV1 negative baseline current both **(E)** normalised to naïve baseline (pA/pA$_n$) and **(F)** current density (pA/pF). **(G-H)** Representative examples of time-courses in TRPV1 positive and TRPV1 negative neurons treated with non-targeting control RNA (NTC) or *Kcnq2* siRNA at -60 mV. Insets are M current traces from the same examples. Data presented is Mean ±S.E.M statistical evaluation with Mixed Two-Way ANOVA with Sidak's post hoc between all compounds and across Naïve, NTC and siRNA groups (only NTC and siRNA shown for clarity). Paired: *P<0.05 **P<0.01 ***P<0.001 ****P<0.0001. Unpaired: #P<0.05. Independent Measures One-Way ANOVA with Tukey's post hoc *P<0.05. TRPV1 positive: Naïve n=20, NTC n=14 and siRNA n=18. TRPV1 negative: Naïve n=17, NTC n=11 and siRNA n=14. Animals (N=8).

controls and siRNA groups **(Figure 5.3G/H)**. This was important as it showed that knocking down *Kcnq2* was not drastically changing the properties of the residual current **(Figure 5.3G/H inset)**, also, it demonstrated that the pharmacological compounds were producing similar effects in all experimental conditions **(Figure 5.3G/H)**. In fact, analysis of the currents from each condition confirmed that, despite the reduction in total M current amplitude, the fold change in current amplitude (as compared to the baseline) after the application of either ICA-27243 or retigabine was comparable in the NTC and siRNA group **(Figure 5.4A&B)**. We found a similar pattern in terms of drug response to the pharmacological profiling of cells as that presented in chapter 4. A strong effect of ICA-27243 in increasing the outward current compared to baseline in TRPV1 positive cells in the NTC group (2.94±0.4 I/I_0; n=14 P<0.0001) and in the siRNA group (3.0±0.3 I/I_0; n=18 P<0.05) **(Figure 5.4A)**, but a much smaller increase in TRPV1 negative cells in both the NTC group (2.16±0.41 I/I_0; n=11 P<0.05) and siRNA group (1.9±0.3 I/I_0; n=14 P=0.7) **(Figure 5.4B)**.

In TRPV1 positive neurons, ICA-27243 and retigabine evoked currents were both reduced to a similar extent after *Kcnq2* siRNA. ICA-27243 current reduced from (2.94±0.4 pA/pA_n n=14) in NTC to (1.3±0.2 pA/pA_n n=18) in siRNA, retigabine from (3.7±0.7 pA/pA_n n=14) in NTC to (1.5±0.2 pA/pA_n n=18) in siRNA, the difference between ICA-27243 and retigabine was not significant in either condition. The similar reduction after the downregulation of *Kcnq2* suggests that in these neurons $K_V7.2$ was responsible for the effect of both compounds **(Figure 5.3C)**. In TRPV1 negative neurons, ICA-27243 induced current reduced from 2.3±0.8 pA/pA_n (n=11) in NTC to 0.996±0.070 pA/pA_n (n=14 P<0.05) in siRNA group and retigabine from 3.6±0.9 pA/pA_n (n=11) to 2.0±0.1 pA/pA_n (n=14 P<0.05) **(Figure 5.3D)**.

Although, the difference in current density between TRPV1 positive and TRPV1 negative neurons in the siRNA group was not significantly different **(Figure 5.3F)**, this may be due to a lower current density to begin with in TRPV1 negative neurons (4.1 pA/pF n=14) compared to (5.6 pA/pF n=18) TRPV1 positive neurons **(Figure 5.3F)**. Compensating for differences in current density between TRPV1 positive and TRPV1 negative cells by normalising the current density to naïve cells (at vehicle application), revealed that the current density was 33% lower in TRPV1 positive neurons than TRPV1 negative neurons after *Kcnq2* knockdown (0.33 $pA/pF/pA/pF_n$ P<0.05)

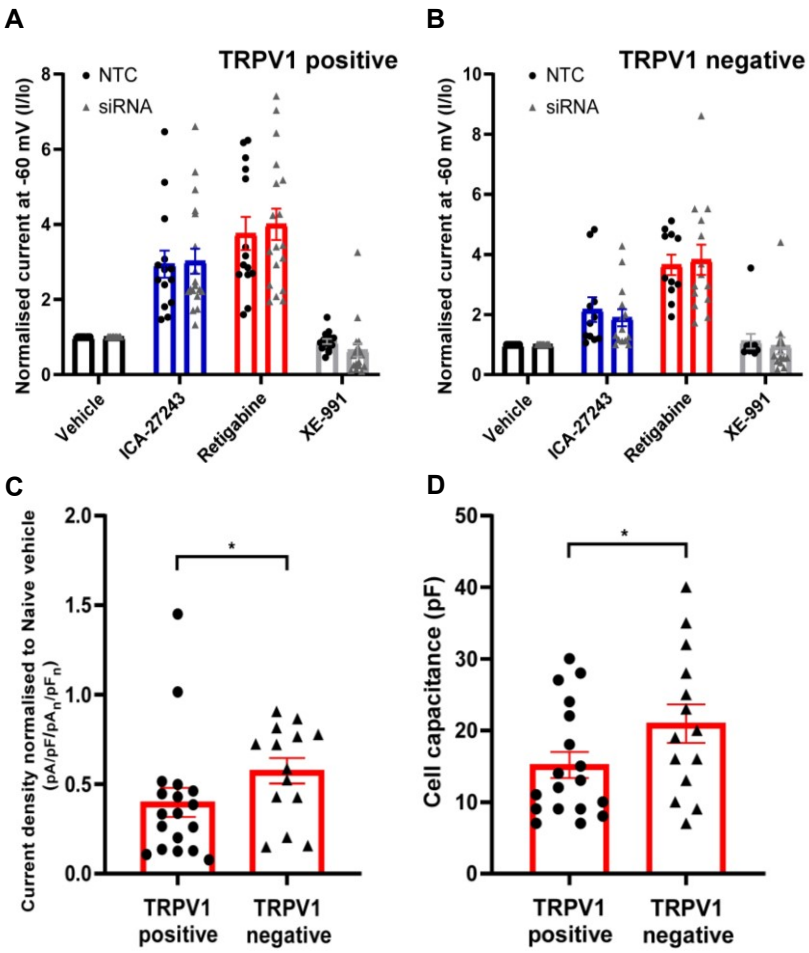

Figure 5.4 siRNA knockdown of Kcnq2 resulted in a lower M current density in TRPV1 positive sensory neurons but enhancement of the remaining current was unchanged. **(A)** TRPV1 positive and **(B)** TRPV1 negative neurons normalised to vehicle for the same cell (I/I_0) for NTC and siRNA treated cells and the change in response to 2 μM ICA-27243, 10 μM retigabine and 10 μM XE-991 at -60 mV. **(C)** Current density in siRNA treated cells normalised to the naïve vehicle current density ($pA/pF/pA_n/pF_n$) in TRPV1 positive and TRPV1 negative neurons. **(D)** Cell capacitance (pF) in TRPV1 positive and TRPV1 negative neurons as an indicator of cell size. Data presented is Mean ±S.E.M statistical evaluation with Mixed Two-Way ANOVA with Sidak's post hoc between all compounds and across Naïve, NTC and siRNA groups (only NTC and siRNA shown for clarity). (C-D) Independent Measures One-Way ANOVA with Tukey's post hoc *P<0.05. TRPV1 positive: Naïve n=20, NTC n=14 and siRNA n=18. TRPV1 negative: Naïve n=17, NTC n=11 and siRNA n=14. Animals (N=8).

(0.39±0.08 pA/pF/pA/pF$_n$ n=18; compared to 0.58±0.07 pA/pF/pA/pF$_n$ n=14; p<0.05) **(Figure 5.4C)**.

We interpret these results as evidence that with *Kcnq2* transcript level reduced (but not completely eliminated), the residual M current in TRPV1-positive neurons is still conducted by the K_v7.2-containing channels, while in the TRPV1-negative neurons M current is carried by a more variable complement of subunits. These results further suggest that the efficacy of the compounds does not change after siRNA knockdown.

Perhaps predictably, as in the pharmacological profiling experiments, the TRPV1 positive siRNA treated cells were smaller in size than the TRPV1 negative neurons on average. Mean TRPV1 positive neuron capacitance was 15±2 pF (n=18) compared to 21±3 pF (n=14) in TRPV1 negative neurons. This difference was statistically significant (P<0.05), and the data plot shows a population of larger cells in TRPV1 negative neurons that was not present in TRPV1 positive neurons **(Figure 5.4D)**. Again, this provides further correlative evidence between the data shown in both the current and previous chapters.

5.2.3 The Impact of *Kcnq2* on Sensory Neuron Excitability

So far, we have demonstrated that K_v7 current in TRPV1 positive neurons is largely controlled by K_v7.2 therefore, we decided to examine the contribution of K_v7.2 specifically on sensory neuron excitability.

To this end, we recorded action potential firing in neurons exposed to *Kcnq2* siRNA, NTC or naïve cells, again separating cells by their response to 1 μM capsaicin at the end of the recording as done above. I analysed many action potential parameters (Table 5.1), however not all of these have been represented graphically. Most action potential parameters were unchanged after siRNA knockdown; thus, amplitude, duration and width of the action potentials were not significantly different between any of the conditions **(Figure 5.5A-C)**. This is to be expected as due to their biophysical properties, K_v7.2 channels are not likely to be involved in the upstroke or repolarisation of the individual action potential like other voltage-dependent potassium channels. Similarly, the afterhyperpolarisation amplitude and duration was largely unaffected **(Figure 5.5E/F)**. Interestingly, in TRPV1 positive neurons, *Kcnq2* knockdown did result in a trend towards a reduction in the duration of afterhyperpolarisation, though not to statistical significance (P=0.09)

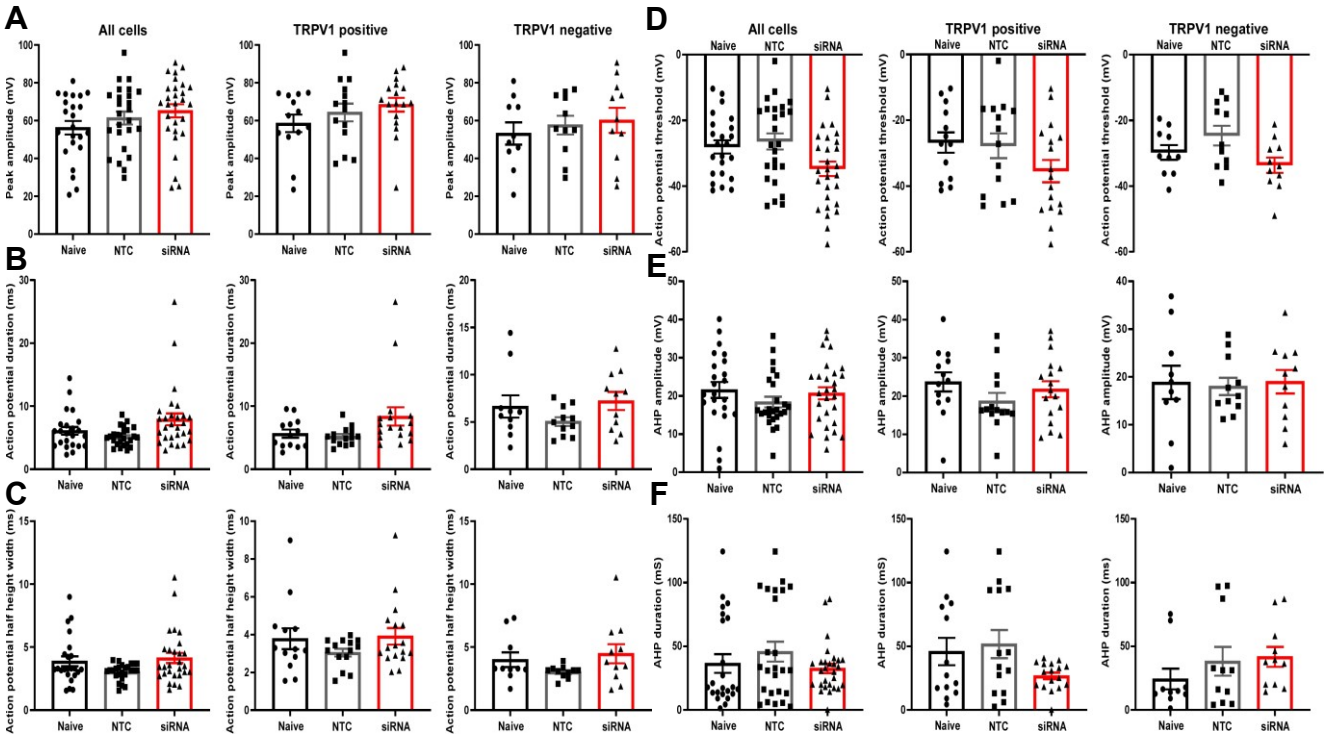

Figure 5.5 Kcnq2 knockdown has no effect on action potential or after-hyperpolarisation. **(A-D)** Action potential parameters across all cells and separated into TRPV1 positive and TRPV1 negative neurons **(A)** Action potential amplitude, **(B)** Action potential duration, **(C)** Action potential width at half of the action potential height, **(D)** Action potential threshold. **(E-F)** After-hyperpolarisation parameters across all cells and separated into TRPV1 positive and TRPV1 negative neurons. **(E)** After-hyperpolarisation amplitude, **(F)** After-hyperpolarisation duration. Data presented is Mean ±S.E.M, statistical evaluation with independent measures One-Way ANOVA with Tukey's post hoc (*P<0.05). All cells: Naïve n=24, NTC n=26, siRNA n=30. TRPV1 positive: Naïve n=14, NTC n=15, siRNA n=17. TRPV1 negative: Naïve n=10, NTC n=11, siRNA n=13.

(Figure 5.5F). This may be likely as K_v7 channels are not major drivers of afterhyperpolarisation but may prolong the duration somewhat due to the slow deactivation of the channels (Lima and Marrion, 2007, Church *et al.*, 2019, Gu *et al.*, 2005). Due to the fact that these channels are active during the generator potential, one may expect the threshold of action potential firing to be affected. Yet the small decrease in threshold was not significantly different, probably due to the slow activation of K_v7 channels being unable to compensate for the rapid influx of sodium **(Figure 5.5D)**.

Analysing the relationship between excitability parameters confirmed a correlation between M current and rheobase in the NTC (R^2 = 0.6; n= 26) and *Kcnq2* siRNA group (R^2 = 0.65; n= 30) **(Figure 5.6A)**. However, there was a shift towards origin in the plot points of the siRNA group (red) compared to the NTC group, suggesting a reduction in both parameters. Further analysis of the relationship between M current and measures of neuronal excitability from current clamp recordings of 54 sensory neurons revealed a strong correlation (R^2 = 0.60) between the level of M current and the current injection required to elicit an action potential (rheobase) **(Figure 5.7A)**. Similar correlation was not seen between either M current and resting membrane potential or rheobase and resting membrane potential **(Figure 5.7B/C)**. A similar strong correlation was seen when combining results from all cells (Control, NTC and siRNA) from both current clamp experiments (*Kcnq2* and *Kcnq5* siRNA experiments) (R^2 = 0.50) from 178 cells **(Figure 5.7D)**. These findings suggest a possible relationship between K_v7 channels and rheobase.

In the following section I will report a detailed analysis of the effect of *Kcnq2* knockdown on the excitability parameters, firstly of the general population of DRG neurons and then in neurons separated by whether they are TRPV1 positive or TRPV1 negative and analyse these populations separately.

As previously mentioned, the biophysical properties of K_v7 channels suggest they would inhibit the chance of repeated action potential firing after the first depolarisation due to the length of time the channel is open. Indeed, we found this to be the case in some cells as the average firing frequency in response to 50 pA 1000 ms pulses, increased significantly from 1.3±0.1 Hz (naïve cells) and 1.2±0.1 Hz (NTC) to 4±1 Hz in the siRNA group **(Figure 5.6B)**.

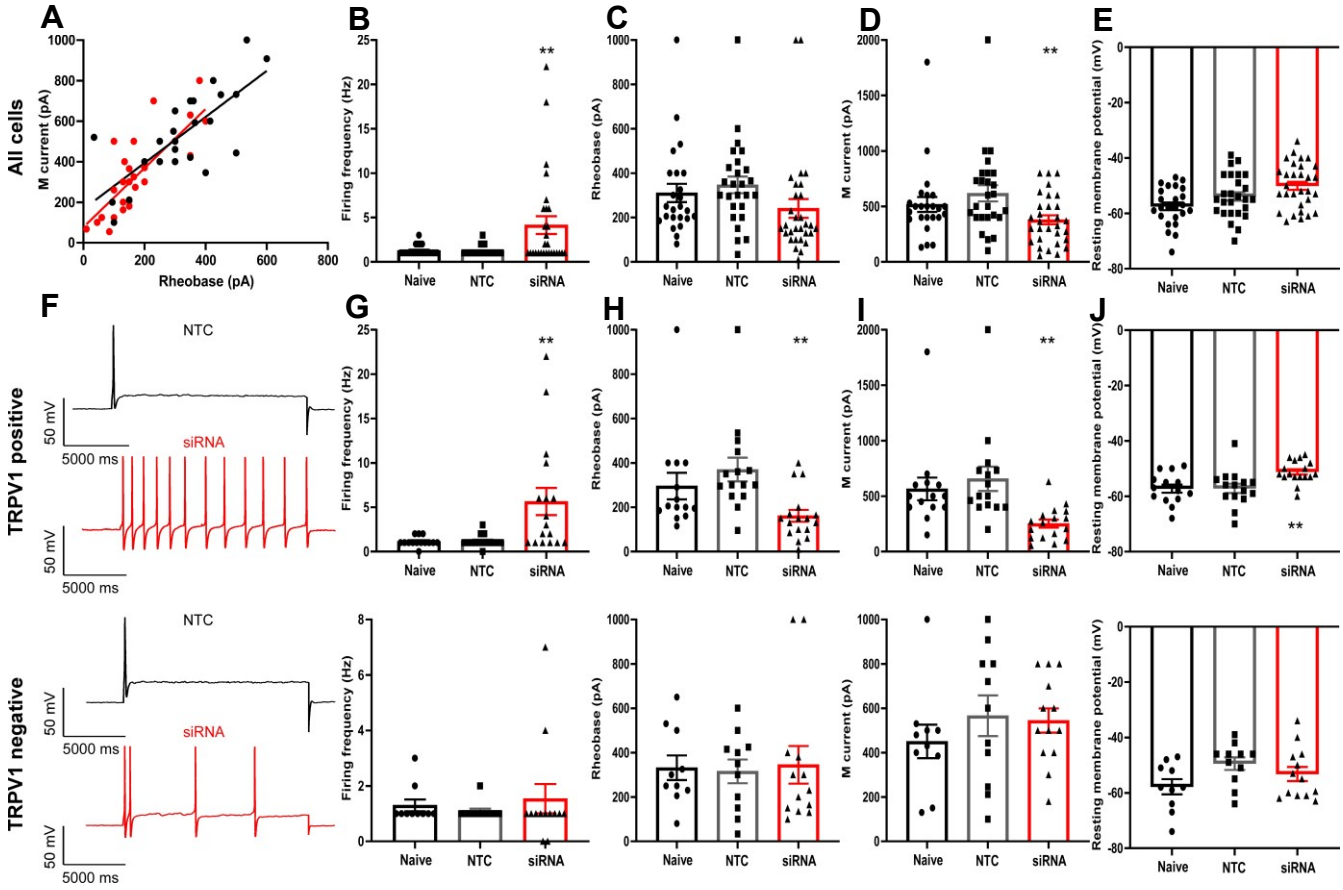

Figure 5.6 Kcnq2 siRNA knockdown increases excitability in TRPV1 positive sensory neurons. **(A)** Correlation between M current (pA) and Rheobase (pA) in non-targeting control RNA (NTC) (black) or *Kcnq2* siRNA treated cells (red) (n=53). Analysis of all Naïve cells (n=24), NTC (n=26) and siRNA (n=30) treated cells in **(B)** Firing frequency (Hz) **(C)** Rheobase (pA) **(D)** M current (pA) **(E)** Resting membrane potential (mV). **(F)** Representative examples of action potential firing in **(Top)** TRPV1 positive and **(Bottom)** TRPV1 negative neurons. Analysis of **(Top)** TRPV1 positive Naïve cells (n=14), NTC (n=15) and siRNA (n=17) treated cells and **(Bottom)** TRPV1 negative Naïve cells (n=10), NTC (n=11) and siRNA (n=13) treated cells in **(G)** Firing frequency (Hz) **(H)** Rheobase (pA) **(I)** M current (pA) **(J)** Resting membrane potential (mV). Data presented is Mean ±S.E.M statistical evaluation with Independent measures One-Way ANOVA with Tukey's post hoc *P<0.05 **P<0.01. Animals (N=8).

Analysis of the change in K_v7 current and rheobase in *Kcnq2* knockdown conditions revealed that rheobase was slightly reduced from 347±38 pA in the NTC group (n=26) to 241±42 pA in the siRNA group (n=30) (naïve 311±41 pA); but was not significantly reduced **(Figure 5.6C)**. K_v7 current was significantly reduced on average from 618±73 pA in the NTC group (n=26) to 379±41 pA in the siRNA group (n=30 P<0.01) (naïve 518±67 pA; n=24 P<0.01) **(Figure 5.6D)**. Resting membrane potential was slightly more depolarised in the siRNA condition -50±2 mV (n=30) compared to -54±2 mV in the NTC group (n=26) (naïve -57±1 mV; n=24) but this was not significant **(Figure 5.6E)**. This is in line with the lack of correlation between resting membrane potential and K_v7 current or rheobase **(Figure 5.7C)**. Thus, in the general population, the main effect of *Kcnq2* knockdown was reduced M current and increased firing frequency.

The firing frequency of TRPV1 positive neurons increased significantly from 1.14±0.14 Hz in naïve cells (n=14) and 1.20±0.17 Hz in NTC (n=15) to 5.6±1.5 Hz after *Kcnq2* knockdown (n=17 P<0.01) **(Figure 5.6F/G Top)**. The rheobase in TRPV1 positive neurons was reduced significantly from 300±60 pA in naïve cells (n=14) or 370±54 pA in NTC cells (n=15) to 161.5±27.0 pA in cells treated with siRNA (n=17 P<0.01) **(Figure 5.6H Top)**. This reduction in rheobase was accompanied by a significant reduction in M current, with an average current of 252±36 pA in the siRNA group (n=17) compared to 566±102 pA (n=14) or 656±109 pA (n=15) in naïve and NTC treated cells, respectively (P<0.01) **(Figure 5.6I Top)**. A small but significant depolarisation was seen in RMP in TRPV1 positive neurons from -57±1.5 mV (n=14) in naïve and -57±1.7 mV (n=15) in NTC to -51±0.9 mV (n=17 P<0.01) **(Figure 5.6J Top)**.

Despite the reduction in rheobase in TRPV1 positive neurons, a large number of cells did not increase firing. This suggests that the mechanism for controlling firing frequency is more complicated than just a change in K_v7 current or rheobase but that K_v7 current does have some influence on firing frequency and sets excitability in TRPV1 positive neurons.

Some TRPV1 negative neurons did show an increase in firing frequency but overall was largely unchanged; 1.5±0.5 Hz in the siRNA group (n=13) compared to 1.1±0.1 Hz and 1.3±0.2 in NTC (n=11) and naïve groups (n=10), respectively **(Figure 5.6F/G Bottom)**. TRPV1 negative cells did not display any change in rheobase (naïve

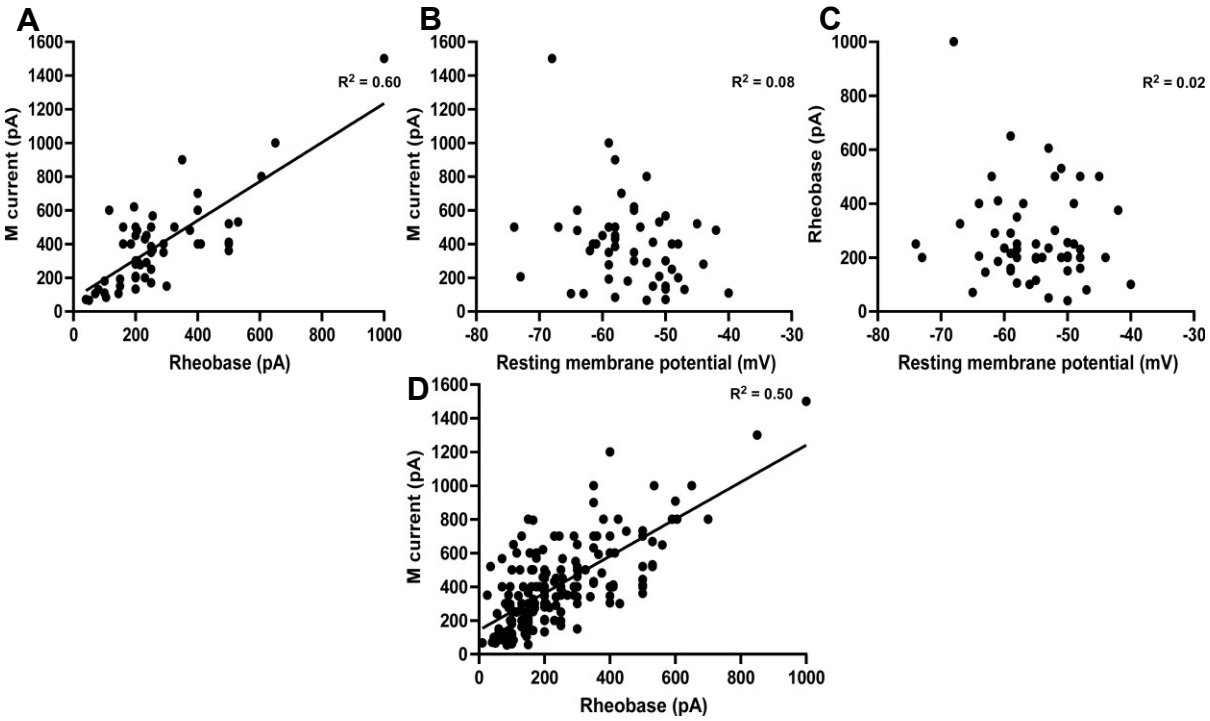

Figure 5.7 M current amplitude correlates with Rheobase but not resting membrane potential in rat sensory neurons. **(A)** M current plotted against Rheobase (n=54) or **(B)** resting membrane potential (n=54) from the same cell in non-RNAi treated sensory neurons. **(C)** Rheobase plotted against resting membrane potential of the same cell (n=54). **(D)** Accumulation of all cells recorded from including control, NTC and siRNA conditions for *Kcnq2* and *Kcnq5* knockdown experiments (n=178).

332±55, n=10; NTC 316±53, n=11; siRNA 345±85, n=13) **(Figure 5.6H Bottom)** or M current (naïve 451±76, n=10; NTC 566±92, n=11; siRNA 545±55, n=13) **(Figure 5.6I Bottom)**. Resting membrane potential was also unchanged in TRPV1 negative neurons (siRNA -54±3, n=13; NTC -50±2, n=11; naïve -57±3, n=10) **(Figure 5.6J)**. Recordings from these neurons suggest that excitability of TRPV1 negative neurons is less reliant on $K_v7.2$.

These findings, together with the correlation between the rheobase and M current amplitude suggest that K_v7 channels, particularly $K_v7.2$, possess a strong degree of control over sensory neuron excitability by increasing the level of stimulation required to excite the cell and acting as a brake on repeated action potential firing due to the long channel conductance time. This control is particularly evident in TRPV1 positive neurons.

We can assume that a combination of the reduction in current required to elicit action potential firing and the lack of prolonged potassium current after depolarisation caused by knockdown of *Kcnq2* was the cause of increased firing rate and reduced rheobase in TRPV1 positive neurons. In addition, further evidence for K_v7 channels having some influence in setting resting membrane potential is also presented here, as suggested previously with pharmacological modulation of K_v7 channels, along with a number of other ion channels (Du *et al.*, 2014).

5.2.4 Adapting siRNA for *in vivo* Use

As the above experiments were conducted by transfecting siRNA into cultured sensory neurons, we sought to find a different method to deliver siRNA to the DRG *in vivo*. There are two aspects to this process which we must assess; (1) getting the siRNA to the DRG *in vivo* and (2) getting the siRNA into the cells. Transfection has been used as a method for transiently delivering siRNA previously (Tompkins *et al.*, 2004), however, biological or chemical transfection, such as viral delivery or transfection reagents such as lipofectamine permeate all types of cells so would need to be delivered directly to the DRG. Therefore, we decided that “self-delivering” cholesterol-conjugated siRNA would be a safe and effective option if delivered intrathecally, as done by Hogea and colleagues (Hogea *et al.*, 2021). Cholesterol-conjugated siRNA are self-delivering because the cholesterol is able to embed into the lipid bilayer, where the siRNA can be cleaved and enter freely into the cytosol (Soutschek *et al.*, 2004, Rossi, 2004).

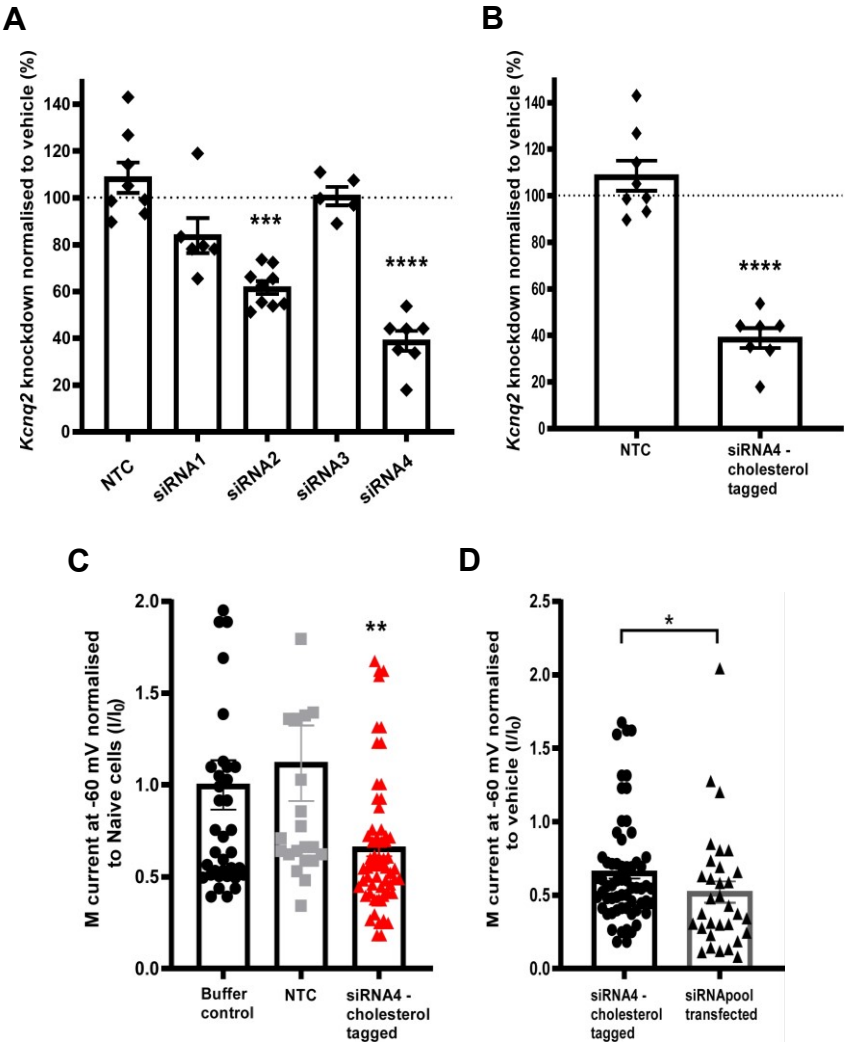

Figure 5.8 Kcnq2 knockdown with cholesterol-tagged siRNA is similarly effective to transfected siRNA in cultured rat sensory neurons. **(A)** *Kcnq2* mRNA knockdown with four cholesterol-tagged *Kcnq2* siRNAs (siRNA1-4) and non-targeting control RNA (NTC) compared to *Kcnq2* expression in naïve buffer control sensory neurons normalised to *Hprt1*. Number of animals indicated on figures. **(B)** Effectiveness of cholesterol-tagged *Kcnq2* siRNA induced knockdown used in voltage experiments compared to NTC. **(C)** Outward current of buffer control (n=37), NTC (n=22) and siRNA (n=62) at -60 mV normalised to average outward current in buffer control/vehicle neurons (I/I_0). **(D)** M current normalised to control (I/I_0) in cholesterol-tagged *Kcnq2* siRNA (n=62) verses transfected *Kcnq2* siRNA (n=32). Data presented is Mean ±S.E.M, statistical evaluation on ΔCt with independent measures One-Way ANOVA with Dunnett post hoc (***P<0.001, ****P<0.0001) (A-B), Kruskal-Wallis with Dunn's post hoc (**P<0.01) (C) or Mann-Whitney (*P<0.05) (D).

Before *in vivo* application, we confirmed the efficacy of self-delivering siRNA knockdown in cultured DRG sensory neurons. Four cholesterol-conjugated siRNAs targeting different sequences of *Kcnq2* mRNA were tested against a cholesterol-conjugated non-targeting control (NTC) and the suspension buffer for the RNAi's. There was no difference in mRNA expression of *Kcnq2* between the buffer and NTC conditions (109±3%), or siRNA3 (101±4%). siRNA1 sequence only reduced mRNA by 16% (84±7%) in these conditions, siRNA2 knocked down mRNA by around 40% (61.5±3.0%) but the best knockdown observed was 61% with siRNA4 (39±4%) **(Figure 5.8A/B)**. Thus, *Kcnq2* siRNA4 was used for functional testing of cholesterol-conjugated siRNA.

As demonstrated in section 5.2.2, M current was reduced overall in cultured DRG neurons when *Kcnq2* is knocked down with siRNA. To confirm the effects of this cholesterol-conjugated siRNA, we patched cultured DRG neurons and recorded M current using the aforementioned inverted step protocol (-20 mV - -60 mV - -20 mV) but did not apply pharmacological compounds. siRNA4 knocked down cells had a significant reduction in outward potassium current at -60 mV as compared to cells treated with buffer or NTC, which did not significantly differ **(Figure 5.8C)**. Normalising M current to the average current of the buffer ($I/I0_{av}$) showed a 35% reduction in M current in the siRNA4 treated cells (siRNA4 0.65±0.045 $I/I0_{av}$). The NTC did not show the same reduction (NTC 1.12±0.20 compared to buffer 1.0±0.1 $I/I0_{av}$) **(Figure 5.8C)**. This suggests that the mRNA knockdown is translating into a functional effect.

Next, we assessed the comparability of the functional effect of the self-delivering siRNA to the transfected siRNA. Indeed, the reduction in M current was comparable; though cells transfected with siRNA (pooled oligos) had a further reduction in current by 13% compared to the cholesterol-conjugated siRNA (transfected siRNA 0.52±0.07 $I/I0_{av}$ n=32; compared to cholesterol siRNA 0.65±0.05 $I/I0_{av}$ n=62; $P<0.05$) **(Figure 5.8D).** Despite somewhat lower knockdown efficiency of the cholesterol-conjugated single siRNA as compared to transfected siRNA pool, we still achieve robust knockdown efficiency with the former knockdown method.

Taken together, this data suggests we can achieve a suitable level of mRNA knockdown with self-delivering cholesterol-conjugated siRNA, comparable in

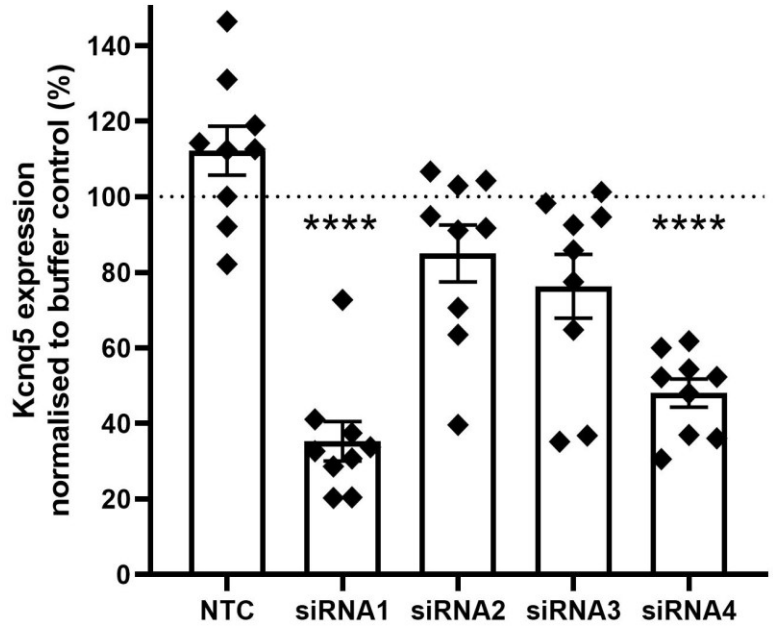

Figure 5.9 Effectiveness of cholesterol conjugated Kcnq5 siRNA in cultured rat sensory neurons. *Kcnq5* mRNA knockdown with four *Kcnq5* siRNAs (siRNA1-4) and non-targeting control RNA (NTC) compared to *Kcnq5* expression in buffer treated sensory neurons normalised to *Hprt1*. Data presented is Mean ±S.E.M, statistical evaluation on ΔCt with independent measures or repeated measures One-Way ANOVA with Tukey's post hoc as appropriate ****P<0.0001. N=9

knockdown and functional effectiveness to transfected siRNA. Therefore, we can take advantage of the siRNAs self-delivering nature in designing the *in vivo* knockdown experiments.

5.2.5 *Kcnq5* siRNA Knockdown Effect on Neuronal Excitability

Much of the pharmacological and expression manipulation work has been focussed on $K_V7.2$ based on previous work, expression profiling and pharmacological tools. However, as documented in chapter 3, we observed detectable expression of $K_V7.5$ and this corroborates similar observations by other studies (Passmore *et al.*, 2003, King and Scherer, 2012, Djouhri *et al.*, 2020). Moreover, pharmacological profiling suggested a significant contribution of ICA-insensitive $K_V7.2$ subunit to M current in TRPV1 negative DRG neurons. Therefore, in lieu of established $K_V7.5$ selective enhancers, we also used cholesterol-conjugated siRNA to knockdown *Kcnq5* in cultured DRG neurons and analyse the functional effects.

Again, four *Kcnq5* siRNA sequences were tested for mRNA knockdown efficiency against the NTC and buffer treated cells using qPCR. There was no significant effect of the NTC as compared to the buffer treated cells (112±7% of buffer control N=9) suggesting any change in *Kcnq5* expression is a direct effect of the siRNA. siRNA1 most consistently and efficiently knocked down *Kcnq5* by 60-80%, with a mean knockdown of 65% (35±6% of buffer control N=9 $P<0.0001$) compared to lesser effects of the other siRNAs (siRNA2 85.0±8.5%, N=9; siRNA3 76.0±9.6%, N=9 of buffer control). siRNA4 also significantly knocked down *Kcnq5* (siRNA4 48±4% of buffer control, N=9 $P<0.0001$) but to a lesser extent than siRNA1 ($P<0.05$). Therefore, siRNA1 was used for analysis of the functional effect of *Kcnq5* knockdown **(Figure 5.9)**.

To assess the functional effect of *Kcnq5* knockdown, we recorded M current and action potentials in DRG neurons, followed by application of 1 µM capsaicin to determine TRPV1 positive or negative neurons. All methods and protocols were identical to the current clamp analysis of *Kcnq2* knockdown (see above).

As previously, analysis is presented first of the effect of *Kcnq5* knockdown on the general population of DRG neurons and then TRPV1 positive and TRPV1 negative neurons separately.

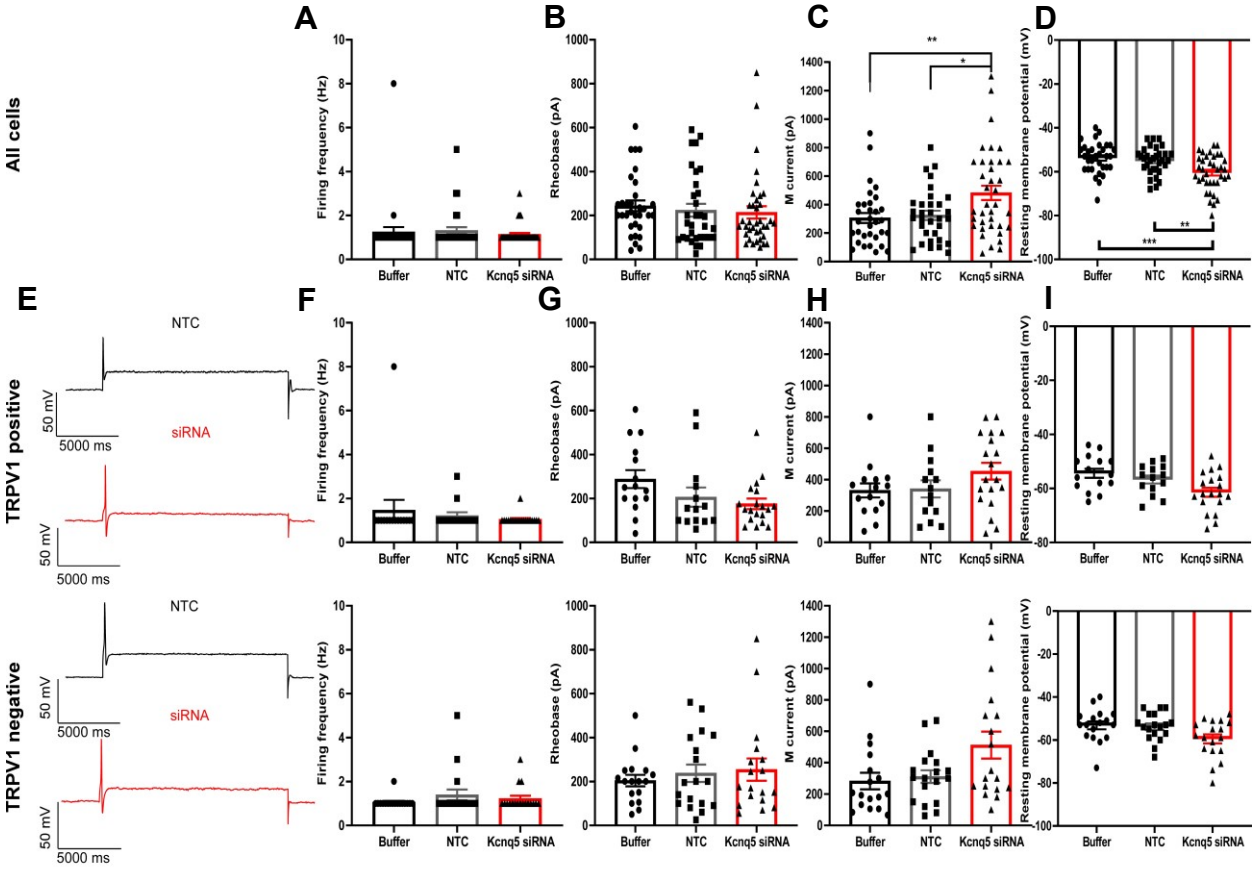

Figure 5.10 Kcnq5 siRNA knockdown does not impact excitability in rat sensory neurons. **(A-D)** Analysis of *Kcnq5* knockdown impact across all cells **(A)** Firing frequency, **(B)** Rheobase, **(C)** M current amplitude and **(D)** Resting membrane potential. **(E-I)** Analysis of cells separated into TRPV1 positive and negative cells. **(E)** Representative action potential traces from TRPV1 positive and negative cells. **(F)** Firing frequency, **(G)** Rheobase, **(H)** M current amplitude and **(I)** Resting membrane potential. Data presented is Mean ±S.E.M statistical evaluation with Independent measures One-Way ANOVA with Tukey's post hoc *P<0.05 **P<0.01. Animals (N=8). All cells: Buffer n=32, NTC n=32, siRNA n=37. TRPV1 positive: Buffer n=15, NTC n=14, siRNA n=19. TRPV1 negative: Buffer n=17, NTC n=18, siRNA n=18.

In the general population of DRG neurons, after knockdown of *Kcnq5*, firing frequency was not affected (buffer 1.25±0.22 Hz, n=32; NTC 1.31±0.15 Hz, n=32; siRNA 1.14±0.07 Hz, n=37) **(Figure 5.10A)**, neither was rheobase (buffer 243.4±24.5 pA, n=32; NTC 224±29 pA, n=32; siRNA 214±28 pA, n=37) **(Figure 5.10B)**. In contrast to *Kcnq2* knockdown, M current amplitude was significantly increased after *Kcnq5* knockdown compared to NTC and buffer control (buffer 305±35 pA n=32; NTC 325±33 pA, n=32; siRNA 482±50 pA, n=37; P<0.) and RMP showed a small but significant negative shift after knockdown (buffer -54±1.2 mV, n=32; NTC -55±1.1 mV, n=32; siRNA -60.5±1.3 mV, n=37; buffer-siRNA P<0.05, NTC-siRNA P<0.01) **(Figure 5.10C/D)**.

In TRPV1 positive neurons, firing frequency (buffer 1.47±0.47 Hz, n=15; NTC 1.21±0.15 Hz, n=14; siRNA Hz 1.05±0.05 n=19) **(Figure 5.10E/F Top)**, rheobase (buffer 288±41 pA n=15; NTC 206±44 pA n=14; siRNA 176±24 pA n=19) **(Figure 5.10G Top)**, M current (buffer 331±45 pA, n=15; NTC 341±55 pA, n=14; siRNA 454±54, n=19) **(Figure 5.10H Top)** and RMP (buffer -54.4±1.7 mV, n=15; NTC -56.7±1.5 mV, n=14; siRNA -61.4±1.7 n=19) **(Figure 5.10I Top)** were not significantly changed by *Kcnq5* knockdown.

Kcnq5 knockdown had no effect in TRPV1 negative neurons on firing frequency (buffer 1.06±0.06 Hz, n=17; NTC 1.4±0.2 Hz, n=18; siRNA 1.22±0.13 Hz, n=18) **(Figure 5.10E/F Bottom)**, rheobase (buffer 204±26 pA, n=17 ; NTC 238±40 pA n=18; siRNA 254±51 pA, n=18) **(Figure 5.10G Bottom)**, M current (buffer 283±53 pA n=17 ; NTC 312±40 pA, n=18; siRNA 512±86 pA, n=18) **(Figure 5.10H Bottom)** and RMP (buffer -53.1±1.9 mV, n=17 ; NTC -53.8±1.5 mV, n=18; siRNA -59.5±2.1 mV, n=18) **(Figure 5.10I Bottom)** were not significantly changed by *Kcnq5* knockdown.

This data suggests $K_v7.5$ does not contribute significantly to excitability or to tonic M current but may have a potential inhibitory effect on M current in some TRPV1 positive and negative neurons.

Assessing the same additional action potential parameters as with *Kcnq2* knockdown, where we observed no significant changes, *Kcnq5* knockdown provided some interesting results.

Analysing all cells showed no change in action potential duration, half height width or threshold (data presented in Table 5.2), however, action potential peak amplitude did

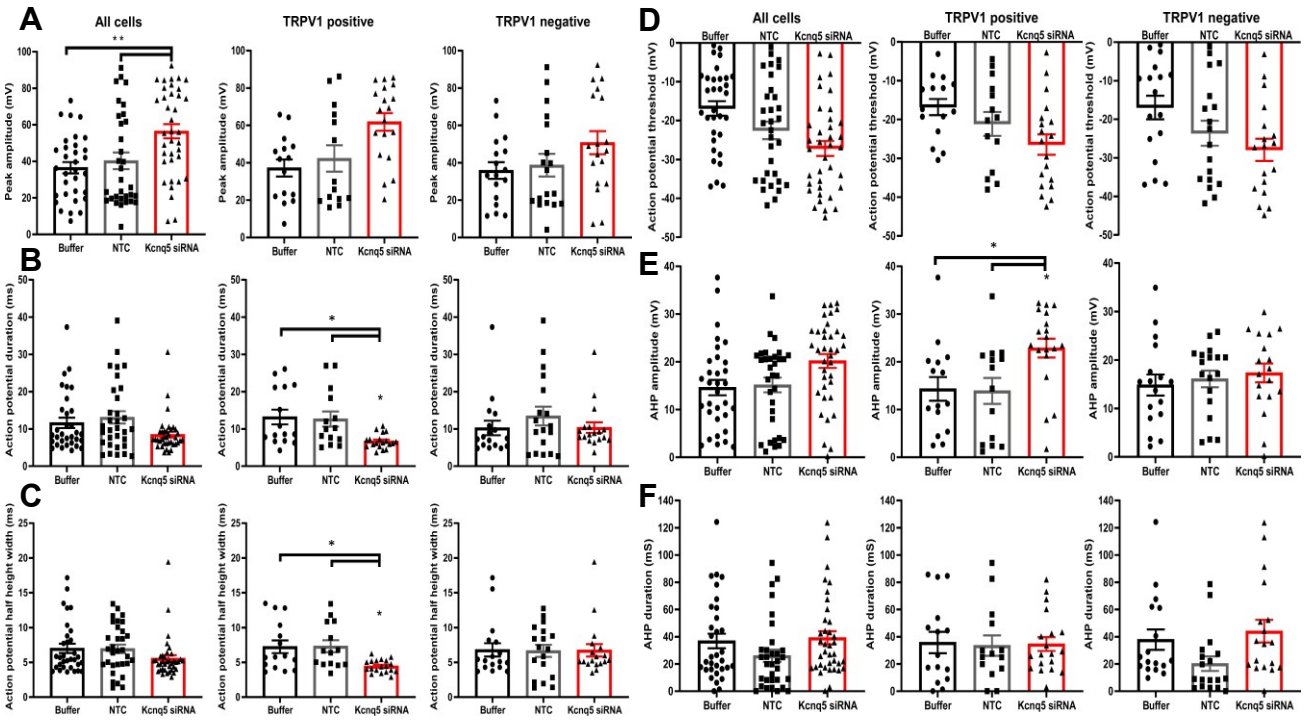

Figure 5.11 Kcnq5 knockdown impact on action potential or after-hyperpolarisation parameters. **(A-D)** Action potential parameters across all cells and separated into TRPV1 positive and TRPV1 negative neurons **(A)** Action potential amplitude, **(B)** Action potential duration, **(C)** Action potential width at half of the action potential height, **(D)** Action potential threshold. **(E-F)** After-hyperpolarisation parameters across all cells and separated into TRPV1 positive and TRPV1 negative neurons. **(E)** After-hyperpolarisation amplitude, **(F)** After-hyperpolarisation duration. Data presented is Mean ±S.E.M, statistical evaluation with independent measures One-Way ANOVA with Tukey's post hoc (*P<0.05). All cells: Buffer n=32, NTC n=32, siRNA n=37. TRPV1 positive: Buffer n=15, NTC n=14, siRNA n=19. TRPV1 negative: Buffer n=17, NTC n=18, siRNA n=18.

increase significantly by 16-19 mV after knockdown (siRNA 56±4 mV, n=37; NTC 40±5 mV, n=32; buffer 37±3 mV, n=32; P<0.01) **(Figure 5.11A-D)**, with this increase likely owing to the hyperpolarised RMP. After-hyperpolarisation amplitude and duration were unchanged (Table 5.2) **(Figure 5.11E/F)**.

In TRPV1 positive neurons, the small increase in action potential amplitude was not statistically significant (siRNA 61.9±4.7 mV, n=19; NTC 42.3±7.1 mV, n=14; buffer 37.2±4.6 mV, n=15;) **(Figure 5.11A)**, though a small but significant decrease in action potential duration was observed (siRNA 7.0±0.5 ms n=19; NTC 12±2 ms n=14; buffer 13±2 ms n=15; P<0.05) **(Figure 5.11B)**. A significant decrease was also seen in half height action potential width of TRPV1 positive neurons (siRNA 4.0±0.2 ms, n=19; NTC 7.0±0.9 ms, n=14; Buffer 7.0±0.9 ms n=15; P<0.05) **(Figure 5.11C).** Action potential threshold was also unaffected in TRPV1 positive neurons (Table 5.2) **(Figure 5.11D)** but after-hyperpolarisation amplitude was significantly higher (siRNA 22±2 mV, n=19; NTC 14±3 mV, n=14; buffer 14±3 mV, n=15; P<0.05) **(Figure 5.11E)**. After-hyperpolarisation duration was not changed (Table 5.2) **(Figure 5.11F)**. The significant effects could perhaps be due to the hyperpolarisation of the membrane at rest, explored in the discussion.

Kcnq5 knockdown in TRPV1 negative neurons did not affect action potential amplitude (buffer 35.9±4.5 mV, n=17; NTC 38.7±6.2 mV, n=18; 50.7±6.0 mV, n=18) **(Figure 5.11A)**, action potential duration (buffer 10.3±2.0 ms, n=17; NTC 13.4±2.6 ms, n=18; 10.3±1.5 ms, n=18) **(Figure 5.11B)** or half height width (buffer 6.8±1.0 ms, n=17; NTC 6.7±0.9 ms, n=18; 6.7±0.9 ms, n=18) **(Figure 5.11C)**. Similarly, action potential threshold (buffer -17.0±3.0 mV, n=17; NTC -23.6±3.3 mV, n=18; -27.9±2.9 mV, n=18) **(Figure 5.11D)**, after-hyperpolarisation amplitude (buffer 14.8±2.2 mV, n=17; NTC 16.1±1.6 mV, n=18; 17.3±2.0 mV, n=18) **(Figure 5.11E)** and after-hyperpolarisation duration (buffer 37.9±7.6 ms, n=17; NTC 20.2±5.4 ms, n=18; 44.1±8.6 ms, n=18) **(Figure 5.11F)** were unchanged.

Overall, these results suggest *Kcnq5* does not contribute significantly to M current or excitability in most neurons with some possible ‘dominant-negative’ effect in some neurons.

5.3 Discussion

In this chapter, we demonstrated that siRNA knockdown of *Kcnq2* was sufficient to significantly reduce the M current, particularly in TRPV1 positive neurons. This reduction in turn increased neuronal excitability, again particularly in TRPV1 positive neurons. Thus, *Kcnq2* knockdown decreased rheobase, increased firing frequency and induced small but significant depolarisation of RMP; all of these parameters are indicative of increasing neuronal excitability (Zhu *et al.*, 2012, Zhang and Dougherty, 2014, Du *et al.*, 2014). Knockdown of *Kcnq5* had a differing yet somewhat surprising effect. Firing frequency and rheobase were unchanged after *Kcnq5* siRNA knockdown whereas M current was slightly increased overall, and resting membrane potential became slightly hyperpolarized. After *Kcnq5* knockdown, both action potential and after-hyperpolarization amplitude were increased, while action potential duration was reduced in certain conditions, which is likely due to the negative shift in resting membrane potential hence releasing more voltage-dependent sodium channels from their inactivation.

It is well understood that K_v7 channels are important in acting as a brake on neuronal excitability, this is achieved because the slow activation and deactivation, together with relatively negative activation threshold, which means the channels are open for a long period after depolarisation. Thus, in some neurons K_v7 channels may only act as a brake after an initial significant depolarisation or action potential. This could be the case in neurons with more polarised resting membrane potentials. However, peripheral sensory neurons have a resting membrane potential of around -60 mV as reported here and in previous studies (Du *et al.*, 2014), meaning a portion of K_v7 channels will be conducting potassium at these voltages. Therefore, at rest, M current is active and potentially impacting neuronal excitability constantly in peripheral sensory neurons, not only controlling subsequent excitability after depolarisation, but may not be the case for all neurons.

The increase in M current after *Kcnq5* knockdown was unexpected but it is tempting to speculate that the reason is the shift in ratio of $K_v7.2/7.3$ and $K_v7.3/7.5$ heteromers, towards an increase in $K_v7.2/7.3$ channels in cells expressing all three subunits. As $K_v7.2/7.3$ heteromers produce higher potassium currents than $K_v7.3/7.5$ (Schroeder *et al.*, 2000a, Lerche *et al.*, 2000a, Soldovieri *et al.*, 2011b, Roeloffs *et al.*, 2008), such a shift would result in an increase in M current in such cells. This opens up some

interesting possibilities, including that the presence of $K_v7.5$ in cells also expressing $K_v7.2$ and $K_v7.3$ results in a lower M current amplitude in that cell than if $K_v7.5$ was not expressed, suggesting that cells can control the M current amplitude and pharmacological properties by regulating $K_v7.5$ expression.

On the other hand, the data presented here suggest that $K_v7.2$ is a significant contributor to the M current in sensory neurons, particularly in the TRPV1 positive neurons, where it seems to be the predominant active subunit in terms of K_v7 channels. Comparing the current to control cells or analysing current density both show a reduction in the tonic M current and the overall responses to ICA-27243 and retigabine. TRPV1 positive neurons showed a similar reduction in the potentiating effect of both ICA-27243 and retigabine, suggesting reduced $K_v7.2$ reduced response to ICA-27243 and retigabine similarly. Whereas TRPV1 negative neurons retained more of a response to retigabine despite a strong reduction in ICA-27243 response, suggesting reducing $K_v7.2$ expression had less impact on the retigabine than ICA-27243. This supports the notion that $K_v7.2$ is the major subunit responsible for M current in TRPV1 positive neurons as responses to ICA-27243 and retigabine reduced together and tonic M current was strongly reduced. Whereas, in TRPV1 negative neurons there was a residual retigabine response despite reduced ICA-27243 responses, perhaps hinting at the expression of another subunit in these cells that is retigabine sensitive but not ICA-27243 sensitive. Based on expression, this is likely $K_v7.5$ and fits with the idea that $K_v7.5$ contributes to potentiation of M current, at least with pharmacological tools, but perhaps endogenous potentiation also, despite the subunit having little to no control over tonic neuronal excitability.

Furthermore, there is less of a reduction in tonic M current in TRPV1 negative neurons, as compared to the TRPV1 positive ones after *Kcnq2* knockdown, which may be due to the expression of $K_v7.5$, though we see excitability when knocking down *Kcnq5*. It is possible that when *Kcnq2* is expressed, *Kcnq5* has little contribution to the overall M current or even the effect of whole-cell M current being lower, but upon *Kcnq2* knockdown, $K_v7.5$ is able to compensate to a certain degree, hence mitigating the loss of *Kcnq2*. The reason it is possible that $K_v7.5$ could compensate for loss of $K_v7.2$ without an increase in *Kcnq5* at the genetic level, is because of the presence of $K_v7.3$. Thus, if $K_v7.2$, $K_v7.3$ and $K_v7.5$ are all present and $K_v7.2$ expression is reduced, $K_v7.3$ can also form heteromers with $K_v7.5$ to maintain a degree of M current that would not

be possible if only K_v7.2 and K_v7.3 were expressed. Therefore, the possible compensation is likely more a result of these subunits to heteromize and not due to an effect of the siRNA knockdown on mRNA expression of other subunits or increased receptor trafficking. This change in the ratio of K_v7.2/7.3 to K_v7.3/7.5 heteromers would explain the more variable responses of TRPV1 negative neurons to ICA-27243 and retigabine if that population consists of some neurons that express various combinations of the expressed subunits (K_v7.2; K_v7.2 and K_v7.3; K_v7.2, K_v7.3 and K_v7.5; K_v7.3 and K_v7.5; or K_v7.5; plus some that may be K_v7.4 or K_v7.4 and K_v7.5). It is also consistent with K_v7.2 and K_v7.5 co-expressing in 20% of sensory neurons (Section 3.2.4).

Previous attempts to study the effect of reducing K_v7.2 expression on pain response *in vivo* have either been in knockout conditions or neuropathic conditions. Knockout mice have been shown to increase action potential frequency in response to a 500 ms 0.4-3.6 nA electrical impulse (King *et al.*, 2014), also demonstrated here and suggested some change in after-hyperpolarisation (King *et al.*, 2014), something we did not see with *Kcnq2* knockdown. In behavioural pain tests, these knockouts report a moderate increase in neuronal excitability and decreased thermal and mechanical pain threshold (King *et al.*, 2014) (Eli Lilly & Co-confidential), similar to the present study. Compensation by *Kcnq5* or from other ion channels involved in setting neuronal excitability is very plausible. King and colleagues demonstrated that K_v7.5 was still present in *Kcnq2* knockout mice but did not analyse the expression level at mRNA or protein level in their conditional but not neural crest specific knockout (King *et al.*, 2014). In section 3.2.4, we demonstrated that the protein expression of K_v7.5 increases in sensory neuron specific but not inducible *Kcnq2* knockout mice.

In previous reports where pan K_v7 potentiators and blockers such as retigabine and XE-991 are applied to sensory neurons, researchers have observed increases in firing frequency and depolarisation of resting membrane potential with XE-991 and the opposite with retigabine (Du *et al.*, 2014, Liu *et al.*, 2010). Knockdown of *Kcnq2*, demonstrated the same increase in firing frequency and depolarisation of the membrane as seen when inhibiting all K_v7 channels with XE-991, particularly in TRPV1 positive neurons. This suggests that the effects of XE-991 and retigabine on neuronal excitability in TRPV1 positive neurons is largely a result of K_v7.2 expression. This is further supported by the lack of effect of *Kcnq5* knockdown on firing frequency

and an apparent hyperpolarisation of RMP. This is in line with the notion that *Kcnq2* has a role in keeping the RMP hyperpolarised and *Kcnq5* is exerting some dominant-negative effect on some cells, with its removal resetting the RMP to a more negative voltage.

In addition to the suggestion that the increased firing frequency and depolarisation of RMP by pan-K_v7 blockers is predominantly due to $K_v7.2$ inhibition (over other K_v7 subunits). This is the first direct evidence showing that M current is important for the level of stimulus required to elicit an action potential (rheobase) in sensory neurons, though the link between K_v7 and rheobase was previously alluded to when modelling sensory neuron excitability (Du *et al.*, 2014). We also demonstrate that there is a correlation between the tonic M current in sensory neurons and the rheobase.

In conclusion, *Kcnq2* is the predominant functionally active subunit controlling M current in TRPV1 positive sensory neurons and in some TRPV1 negative neurons. M current can control neuronal excitability through aiding in setting the resting membrane potential and the level of stimulus required to reach threshold potential. In sensory neurons, *Kcnq2* makes it more difficult for a train of action potentials to fire and more difficult for a stimulus to elicit an action potential, through increasing the outward potassium current, counteracting the inward sodium current and also by hyperpolarising the resting membrane potential somewhat. *Kcnq5* does not seem to have a strong impact on the tonic M current or on the excitability, though it may exert a dominant-negative on M current, depolarising resting membrane potential in some cells. The significance of this data is that there is the potential to target peripheral $K_v7.2$ specifically, to increase activation or expression and reduce excitability of the neurons. Though, *in vivo* data is required to identify whether changing $K_v7.2$ expression in sensory neurons, changes pain response; this question will be addressed experimentally in the next chapter.

Table 5.1: Action potential parameters analysed for *Kcnq2* siRNA knockdown

Action potential parameter	Treatment	All cells (mean ± sem)	TRPV1 positive (mean ± sem)	TRPV1 negative (mean ± sem)
Peak amplitude	Buffer	56.2±3.6 mV	58.5±4.6 mV	53.2±5.9 mV
	NTC	61.4±3.4 mV	64.3±4.7 mV	57.6±4.9 mV
	siRNA	65.2±3.4 mV	68.4±3.7 mV	60.2±6.6 mV
AP duration	Buffer	6.1±0.6 ms	5.6±0.6 ms	6.6±1.2 ms
	NTC	5.1±0.3 ms	5.2±0.4 ms	5.0±0.5 ms
	siRNA	7.9±0.9 ms	8.4±1.4 ms	7.2±0.9 ms
AP half height width	Buffer	3.9±0.4 ms	3.8±0.6 ms	4.0±0.6 ms
	NTC	3.0±0.1 ms	3.0±0.2 ms	3.0±0.1 ms
	siRNA	4.1±0.4 ms	3.9±0.4 ms	4.5±0.8 ms
AP height	Buffer	77.8±4.9 mV	82.2±6.1 mV	72.0±8.0 mV
	NTC	79.8±2.7 mV	83.0±3.4 mV	75.7±4.3 mV
	siRNA	85.1±4.1 mV	89.0±4.4 mV	79.2±8.0 mV
Depolarisation time	Buffer	2.4±0.3 ms	2.1±0.3 ms	2.7±0.5 ms
	NTC	2.0±0.2 ms	2.0±0.2 ms	2.0±0.3 ms
	siRNA	2.9±0.2 ms	2.9±0.3 ms	2.8±0.5 ms
Repolarisation time	Buffer	3.7±0.4 ms	3.1±0.2 ms	3.9±0.7 ms
	NTC	3.1±0.2 ms	3.2±0.2 ms	3.1±0.3 ms
	siRNA	5.0±0.9 ms	5.5±1.4 ms	4.4±0.6 ms
AP threshold	Buffer	-28.1±2.0 mV	-26.8±3.1 mV	-29.7±2.2 mV
	NTC	-26.4±2.5 mV	-27.8±3.8 mV	-24.6±3.0 mV
	siRNA	-34.7±2.2 mV	-35.5±3.8 mV	-33.6±2.3 mV
AHP peak	Buffer	21.6±2.1 mV	23.7±2.5 mV	18.8±3.5 mV
	NTC	18.4±1.4 mV	18.7±2.1 mV	18.0±1.8 mV
	siRNA	19.9±1.9 mV	20.5±2.8 mV	19.0±2.5 mV
AHP duration	Buffer	36.4±7.3 ms	45.8±10.8 ms	24.2±8.2 ms
	NTC	45.7±7.8 ms	51.7±11.0 ms	38.2±11.2 ms
	siRNA	32.6±3.6 ms	26.7±2.6 ms	41.7±7.7 ms
Interspike interval	Buffer	386.8±78.3 ms	506.9±151.5 ms	266.6±81.8 ms
	NTC	432.2±70.3 ms	422.3±114.9 ms	461.8±0.1 ms
	siRNA	38.7±2.3 ms	40.1±3.1 ms	31.4±1.1 ms
Frequency	Buffer	1.3±0.1 Hz	1.1±0.1 Hz	1.3±0.2 Hz
	NTC	1.2±0.1 Hz	1.2±0.2 Hz	1.1±0.1 Hz
	siRNA	4.1±1.0 Hz	5.6±1.5 Hz	1.5±0.6 Hz
RMP	Buffer	-57.5±1.4 mV	-57.3±1.5 mV	-57.8±2.7 mV
	NTC	-54.0±1.6 mV	-59.1±2.4 mV	-49.5±2.3 mV
	siRNA	-50.1±1.5 mV	-47.6±1.6 mV	-53.2±2.8 mV
Rheobase	Buffer	310.6±41.2 pA	295.4±59.9 pA	332.0±55.1 pA
	NTC	347.0±37.9 pA	370.0±53.5 pA	315.7±53.3 pA
	siRNA	241.2±42.4 pA	161.5±26.6 pA	345.4±84.8 pA
M current	Buffer	517.7±67.2 pA	565.7±102.1 pA	450.5±75.6 pA
	NTC	618.2±73.3 pA	656.3±109.3 pA	566.1±91.9 pA
	siRNA	379.0±40.8 pA	252.3±36.1 pA	544.6±54.7 pA

Table 5.2: Action potential parameters analysed for *Kcnq5* siRNA knockdown

Action potential parameter	Treatment	All cells (mean ± sem)	TRPV1 positive (mean ± sem)	TRPV1 negative (mean ± sem)
Peak amplitude	Buffer	36.5±3.1 mV	37.2±4.6 mV	35.9±4.5 mV
	NTC	40.3±4.6 mV	42.3±7.1 mV	38.7±6.2 mV
	siRNA	56.4±3.9 mV	61.9±4.7 mV	50.7±6.0 mV
AP duration	Buffer	11.6±1.4 ms	13.2±2.0 ms	10.3±2.0 ms
	NTC	13.1±1.7 ms	12.7±2.0 ms	13.4±2.6 ms
	siRNA	8.4±0.8 ms	6.7±0.4 ms	10.3±1.5 ms
AP half height width	Buffer	3.8±0.7 ms	7.2±0.9 ms	6.8±1.0 ms
	NTC	6.9±0.6 ms	7.3±0.9 ms	6.7±0.9 ms
	siRNA	5.6±0.5 ms	4.4±0.2 ms	6.7±0.9 ms
AP height	Buffer	49.4±4.4 mV	48.1±6.8 mV	50.7±6.0 mV
	NTC	51.1±6.2 mV	54.5±9.6 mV	48.4±8.2 mV
	siRNA	78.8±5.3 mV	87.9±6.6 mV	69.2±7.8 mV
Depolarisation time	Buffer	4.2±0.4 ms	4.3±0.5 ms	4.1±0.6 ms
	NTC	3.6±0.3 ms	3.7±0.5 ms	3.5±0.5 ms
	siRNA	3.0±0.3 ms	2.3±0.2 ms	3.7±0.5 ms
Repolarisation time	Buffer	7.7±1.4 ms	10.1±2.7 ms	4.4±0.6 ms
	NTC	8.0±1.3 ms	6.3±1.4 ms	7.0±2.2 ms
	siRNA	5.5±0.6 ms	4.4±0.3 ms	6.6±1.1 ms
AP threshold	Buffer	-17.1±1.8 mV	-16.8±2.1 mV	-17.0±3.0 mV
	NTC	-22.5±2.3 mV	-21.1±3.1 mV	-23.6±3.3 mV
	siRNA	-27.2±1.9 mV	-26.5±2.6 mV	-27.9±2.9 mV
AHP peak	Buffer	14.6±1.6 mV	14.3±2.5 mV	14.8±2.2 mV
	NTC	15.1±1.5 mV	13.9±2.7 mV	16.1±1.6 mV
	siRNA	20.2±1.5 mV	22.9±2.0 mV	17.3±2.0 mV
AHP duration	Buffer	36.9±5.4 ms	35.8±7.9 ms	37.9±7.6 ms
	NTC	26.0±4.6 ms	33.5±7.5 ms	20.2±5.4 ms
	siRNA	39.2±4.9 ms	34.6±5.0 ms	44.1±8.6 ms
Frequency	Buffer	1.25±0.2 Hz	1.5±0.5 Hz	1.1±0.1 Hz
	NTC	1.3±0.2 Hz	1.2±0.2 Hz	1.4±0.3 Hz
	siRNA	1.1±0.1 Hz	1.1±0.1 Hz	1.2±0.1 Hz
RMP	Buffer	-53.8±1.3 mV	-54.4±1.7 mV	-53.2±1.9 mV
	NTC	-55.1±1.0 mV	-56.7±1.5 mV	-53.8±1.4 mV
	siRNA	-60.5±1.3 mV	-61.4±1.7 mV	-59.5±2.2 mV
Rheobase	Buffer	243.4±24.9 pA	288.0±41.1 pA	204.1±26.8 pA
	NTC	223.9±29.6 pA	206.1±43.8 pA	237.8±41.0 pA
	siRNA	213.8±28.2 pA	175.5±23.6 pA	254.2±51.8 pA
M current	Buffer	305.4±35.2 pA	331.3±44.8 pA	282.6±54.4 pA
	NTC	324.6±32.9 pA	341.4±54.7 pA	311.5±41.2 pA
	siRNA	482.1±50.1 pA	453.7±53.8 pA	511.9±87.5 pA

Chapter 6: Assessing the Effect of *Kcnq* Gene Knockdown on Nociceptive Transmission and Pain Behaviour *in vivo*

6.1 Introduction

The perception of pain is a complicated and multi-system sensation where even in species like rats, the heterogeneity in response to pain is particularly variable. Therefore, understanding the contributions of certain aspects of the molecular paradigm to the overall pain-sensation process requires analysis of the behavioural response, not just *in vitro* identification of a change in sensory neuronal excitability. Thus far, we have demonstrated that siRNA knockdown of *Kcnq2* and, to a lesser extent, *Kcnq5* leads to a change in both the level of M current and excitability in sensory neurons. The *in vitro* approach also demonstrated that cholesterol-conjugated siRNA was effective in entering the cell and knocking down the desired gene. Therefore, there was the potential to treat animals *in vivo* with self-delivering siRNA which would allow us to analyse the effects of acute knockdown of *Kcnq* subunits in the DRG. This is particularly important as it is difficult to localise the effect of pharmacological tools to specific tissues aside from topical application to the skin. In addition, this provides an opportunity to analyse the impact of gene knockdown in species other than mice and allows for compared comparison of animals before and after knockdown.

To this end, we injected cholesterol-conjugated siRNA into the intrathecal space of adult rats (**Figure 6.1A**). The intrathecal space is the cerebrospinal fluid-filled space surrounding the spinal cord, also known as the subarachnoid space, as it is located between the arachnoid mater and the pia mater surrounding the spinal cord (Elsharkawy *et al.*, 2017). This injection differs from an epidural, due to it being delivered deeper in the spinal column characterised by a lack of resistance against the needle when beginning the injection in humans and rodents (**Figure 6.1A**). The DRG and dorsal root containing the sensory nerve fibres are exposed to the intrathecal space, meaning this method of injection delivery may provide local access to these structures, without effecting the peripheral tissues or entering the blood (**Figure 6.1B**). Furthermore, tagging the siRNA with cholesterol allows the entry of siRNA into the DRG by embedding in the lipid membrane; the spinal cord could also take up the

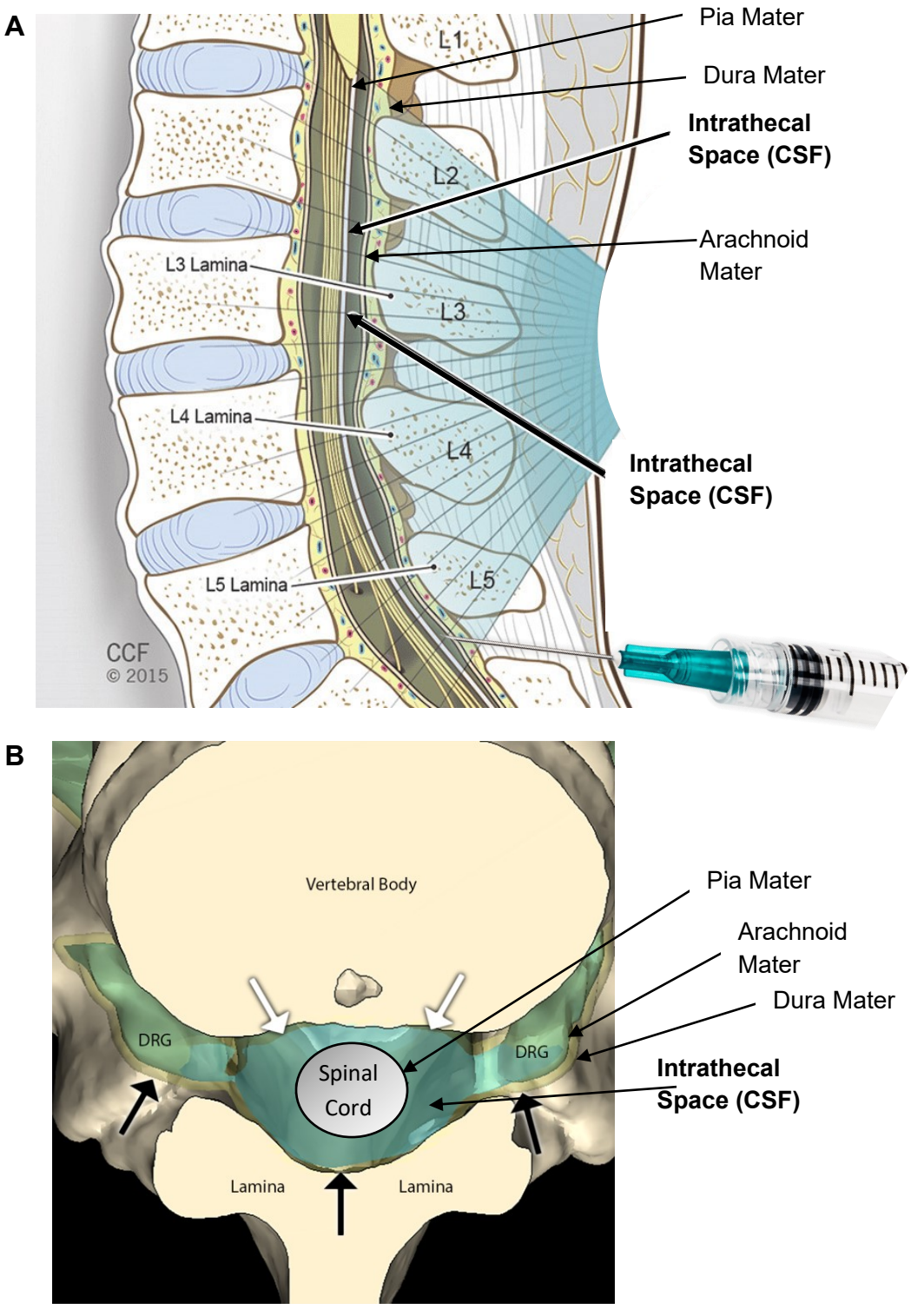

Figure 6.1 Organisation of the spinal column. **(A)** Diagram of the structures and spaces in the spinal column and the position of the needle (adapted from (Elsharkawy *et al.*, 2017)); copyright Cleveland Clinic art photography department CCF 2015). **(B)** Location of the spinal cord and Dorsal Root Ganglia (DRG) In the cerebrospinal fluid (CSF) filled intrathecal space. (Adapted from (Cramer, 2021)).

siRNA but the pia mater presents an additional barrier and siRNA entering the dorsal root is unlikely to 'jump' synapses and enter this tissue.

Using the most effective siRNAs identified in Chapter 5, we injected the siRNA intrathecally to investigate the effect of knocking down *Kcnq2* or *Kcnq5* in the DRG on the rodent's behavioural response to painful stimuli.

6.2 Results

6.2.1 Knockdown Efficiency of Cholesterol-Tagged *Kcnq2* siRNA *in vivo*

Adult Wistar rats were injected in the intrathecal space between L5 and L6 with *Kcnq2* siRNA, non-targeting siRNA control or RNase free PBS as the vehicle for four consecutive days for a total injection concentration of 400 µg of RNA. Two additional days of recovery were allowed for optimum knockdown of both gene and protein expression. Behavioural tests were conducted on day 7 with animals sacrificed and dissected on the same day (capsaicin test) or on day 8 (Pain threshold tests). The primary researcher was blinded throughout the process (Injections, behaviour and qPCR). Dissected lumbar DRGs (L4-S1), lumbar spinal cord (LSC) and brain (cortex and hippocampus) were assessed for knockdown of *Kcnq2* mRNA and *Kcnq5* mRNA to check for any potential compensatory upregulation of other *Kcnq* genes. *Kcnq2* mRNA was reduced by 50% compared to the NTC and vehicle in the lumbar DRGs after intrathecal injection (Vehicle 104±9%; NTC 98±6.5%; *Kcnq2* siRNA 49±3.6%; N=13 $P<0.001$). *Kcnq2* mRNA was not significantly reduced in the spinal cord or brain (LSC: Vehicle 101±4%; NTC 104±9%; *Kcnq2* siRNA 86±3.7%; N=13) (Brain: Vehicle 102±6%; NTC 102±4.4%; *Kcnq2* siRNA 103±4.4%; N=13) **(Figure 6.2A)**. *Kcnq5* expression was unchanged in any condition in DRGs, LSC or brain (DRG: Vehicle 104±8%; NTC 108±10%; *Kcnq2* siRNA 97±8%; N=13), (LSC: Vehicle 101±3.6%; NTC 112±11%; *Kcnq2* siRNA 101±4%; N=13), (Brain: Vehicle 102±6%; NTC 101±5%; *Kcnq2* siRNA 104.5±6%; N=13) **(Figure 6.2B)**. The expression of *Kcnq2* in DRG was significantly reduced after siRNA knockdown compared to in the central nervous system, suggesting that intrathecal injection of the siRNA had a preferential effect on peripheral sensory ganglia compared to the central nervous system in rats **(Figure 6.2C)**.

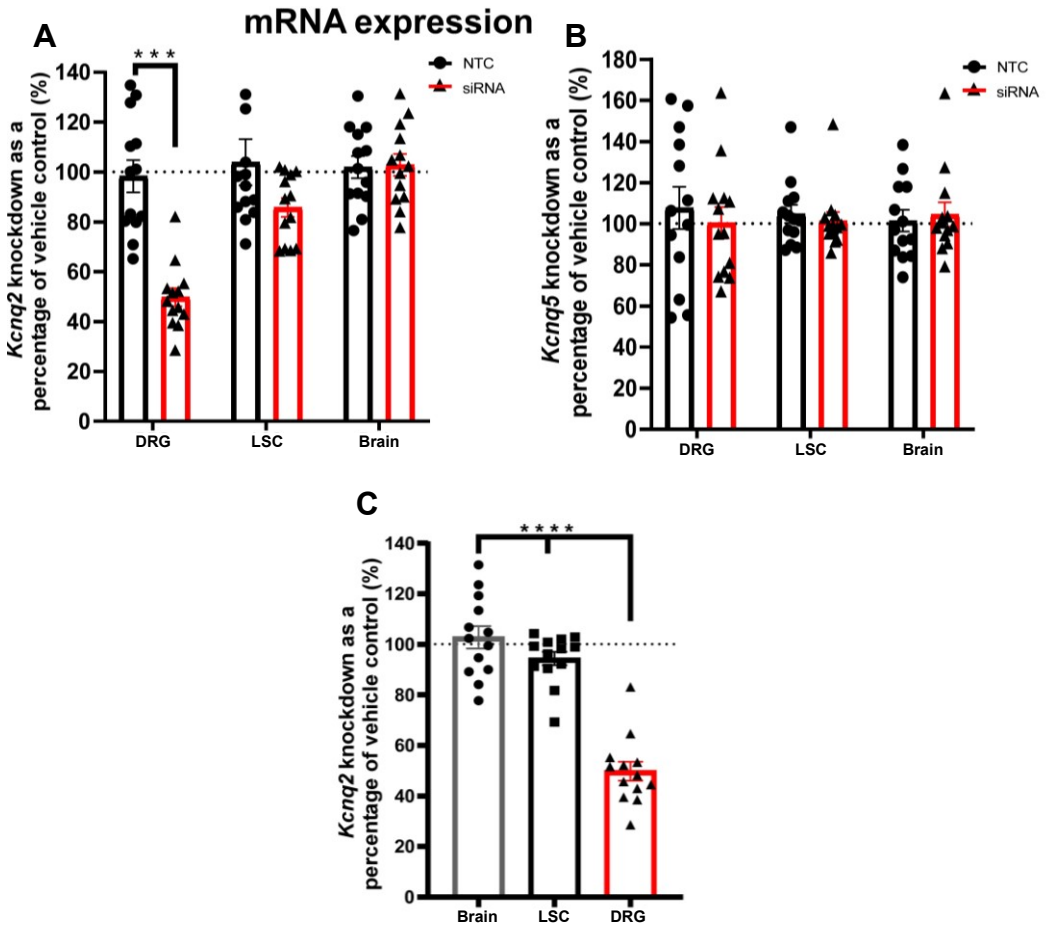

Figure 6.2 Intrathecal injection of Kcnq2 siRNA reduces sensory Kcnq2 expression. **(A-C)** Analysis of mRNA expression of *Kcnq2* and *Kcnq5* normalised to housekeeper *Hprt1* in lumbar dorsal root ganglion (DRG), lumbar spinal cord (LSC) and the hippocampus and cortex (Brain) post behavioural experimentation. **(A)** *Kcnq2* and **(B)** *Kcnq5* expression in DRGs, LSC and brain samples from the vehicle (N=13), NTC (N=13) and siRNA (N=13) groups post behavioural experimentation. **(C)** Paired comparison of *Kcnq2* knockdown in DRGs, LSC and Brain. Data from qPCR is as compared to the vehicle control results. Data presented is Mean ±S.E.M, statistical evaluation with independent measures or repeated measures One-Way ANOVA with Tukey's post hoc *P<0.05 **P<0.01 ***P<0.001 ****P<0.0001.

This data confirms that *Kcnq2* mRNA was significantly reduced in the siRNA treated animals at the time of behavioural experimentation.

6.2.2 Impact of Intrathecal Knockdown of *Kcnq2* on Sensitivity to Noxious Stimuli and Acute Nocifensive Behaviour.

Animals were assessed for their sensitivity to thermal and mechanical stimuli before and after *Kcnq2* knockdown or assessed for their response to acute painful stimuli (hindpaw injection of capsaicin) to analyse the impact of *Kcnq2* knockdown on normal noxious sensitivity and on acute pain response.

Rats administered with *Kcnq2* siRNA showed a significant reduction in thermal pain threshold (Hargreaves method) by around 30% after siRNA injections; thermal sensitivity was unchanged in NTC and vehicle treated animals (siRNA 73±1.8%; NTC 105±3.4%; Vehicle 107±5%; N=7 P<0.0001) **(Figure 6.3A)**. Changes in thermal sensitivity for the left and right hind paws were also similar suggesting that the knockdown was bilateral **(Figure 6.3B)**.

Mechanical sensitivity (assessed using the von Frey method) was also increased by around 30% compared to before siRNA knockdown (siRNA 72±2.8%; NTC 92±4.6% P<0.05; Vehicle 96±6%; N=7 P<0.01) **(Figure 6.3C)**. As with the thermal pain experiments, results from the left and right paw were similar, suggesting a similar, bilateral knockdown **(Figure 6.3D)**. In sum, this data suggests that peripheral knockdown of *Kcnq2* in the DRG is sufficient to increase thermal and mechanical pain sensitivity and also that intrathecal knockdown is bilateral.

We also analysed the role of $K_V7.2$ in controlling the extent of acute pain response by delivering 300 µM capsaicin into the intraplantar region of the hindpaw and measuring the nocifensive (pain related behaviours i.e. licking, flinching, tending to the affected area) responses to pain during a 5-minute period. The total time the animals spent tending to the injected paw increased by 35 seconds in siRNA injected animals compared to NTC and 25 seconds compared to vehicle (siRNA 79±7.8 s; NTC 44±5.7 s; vehicle 53±4 s; N=6 P<0.01) **(Figure 6.3E)**. The number of licking bouts was also significantly higher in the siRNA treated group (12±1 bouts N=6) compared to NTC (7.3±0.8 bouts N=6 P<0.01) or vehicle (7.3±0.9 bouts N=6 P<0.05) **(Figure 6.3F)**. The time it took for the animals to first lick the paw did not change significantly under any condition (siRNA 9±2.2 s; NTC 8±1.6 s; vehicle 6.5±2.5 s N=6) **(Figure 6.3G)**. We also

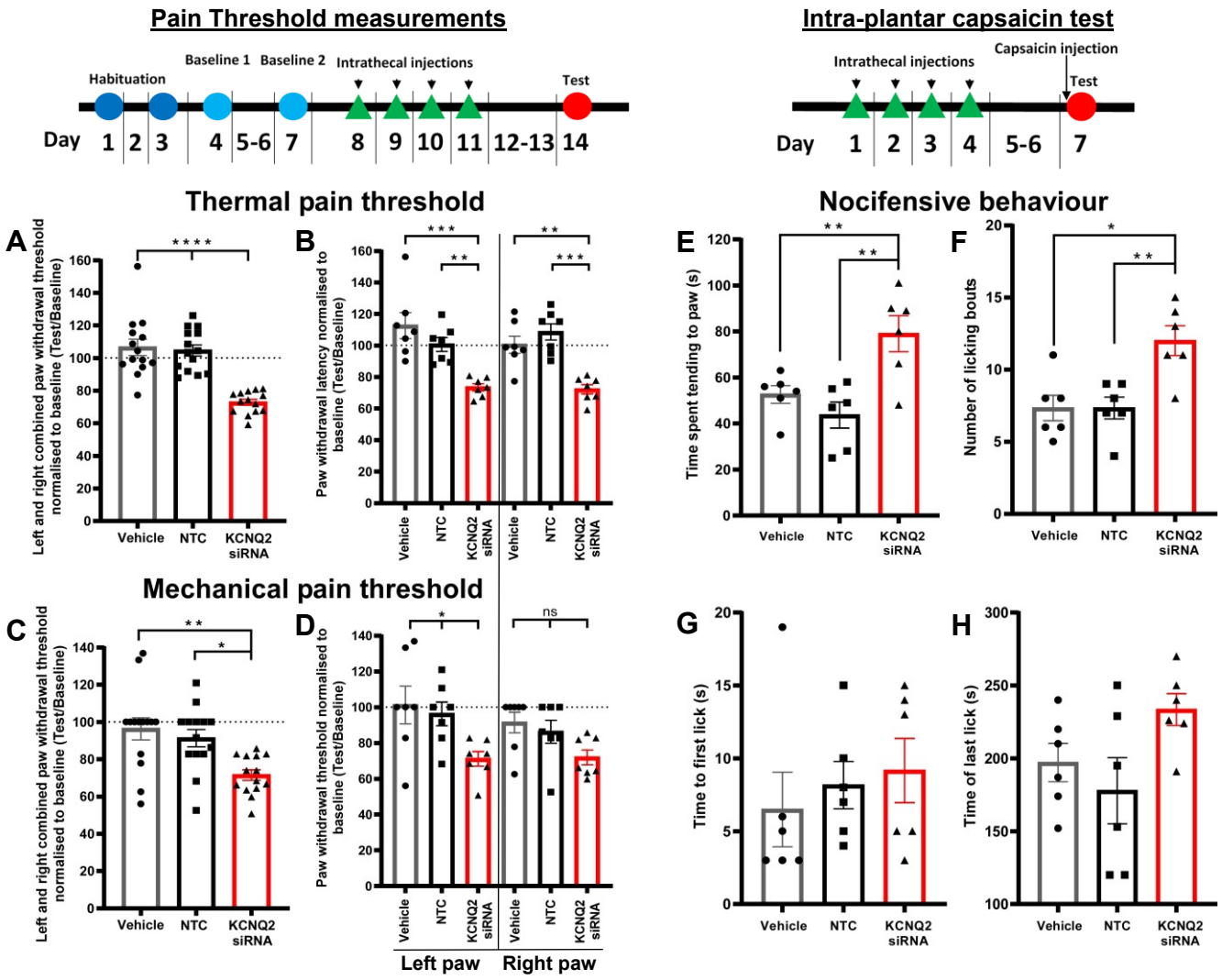

Figure 6.3 Intrathecal injection of Kcnq2 siRNA reduces pain threshold and increases animals' response to painful stimuli. **(A-D)** Changes in **(A-B)** thermal sensitivity **(C-D)** mechanical sensitivity after 4 consecutive 100 µg intrathecal injections of vehicle (N=7), non-targeting control RNA (NTC) (N=7) or *kcnq2* siRNA (N=7). **(A-B)** Thermal pain threshold after intrathecal injections normalised to baseline pain threshold before injections with left and right paw **(A)** combined or **(B)** separated. **(C-D)** Mechanical pain threshold after intrathecal injections normalised to baseline pain threshold before injections with left and right paw **(C)** combined or **(D)** separated. **(E-H)** Effect of vehicle (N=6), NTC (N=6) and siRNA (N=6) on acute 300 µM capsaicin induced pain through measuring nocifensive behaviour in a 5-minute period. Nocifensive behaviour was measured through **(E)** time spent tending to paw in seconds, **(F)** number of licking bouts, **(G)** time to first lick in seconds and **(H)** time the animals stopped tending to the paw in seconds. Data presented is Mean ±S.E.M, statistical evaluation with an independent measures One-Way ANOVA with Tukey's post hoc. Significances are indicated where the siRNA condition differed compared to vehicle or NTC. Vehicle and NTC were also compared but were not significantly different *P<0.05 **P<0.01 ***P<0.001 ****P<0.0001.

measured the time at which the animals stopped further licking of the paw again, which was somewhat increased in the siRNA treated animals, but the stopping time was variable across all conditions and not significantly different (siRNA 233.5±11 s; NTC 178±23 s; Vehicle 197±13 s; N=6) **(Figure 6.3H)**.

Overall, *Kcnq2* knockdown reduced pain threshold and increased nocifensive behavioural responses, suggesting that $K_V7.2$ is involved in the setting of pain threshold and in controlling the extent of painful response to an acute nociceptive stimulation.

6.2.3 Knockdown Efficiency of Cholesterol-Tagged *Kcnq5* siRNA *in vivo*

As with *Kcnq2*, the mRNA expression of *Kcnq5* was assessed in DRG, LSC and brain after behavioural testing, either the same day (nocifensive behaviour) or next day (pain threshold testing). In DRG, *Kcnq5* expression was reduced by 53% (47±2.4% of vehicle; N=14 P<0.0001) when normalised to the vehicle condition and unchanged in the NTC (94±9.4% of vehicle; N=14). *Kcnq5* expression was unchanged in the LSC (siRNA 93±4.4%; NTC 94±9%; N=14) and the brain (siRNA 98±3%; NTC 101±4.4% N=14) **(Figure 6.4A)**. Thus, intrathecal siRNA knockdown reduced *Kcnq5* expression significantly and specifically in the DRG, compared to LSC and the brain (N=14 P<0.0001) **(Figure 6.4B)**.

6.2.4 Impact of Intrathecal *Kcnq5* knockdown on Sensitivity to Nociceptive Stimulation and Acute Nocifensive Behaviour

Performing identical experiments as with *Kcnq2* knockdown, we analysed the impact of *Kcnq5* knockdown on sensitivity to noxious thermal and mechanical stimuli and on acute pain response. Neither thermal nor mechanical pain threshold was affected by the reduction in *Kcnq5* expression. Withdrawal latencies to thermal stimulation were similar before and after intrathecal injection in all conditions (siRNA 102±2.7%; NTC 101±4%; vehicle 96±3.8%; N=7) **(Figure 6.5A)**; there was no difference between left and right paws **(Figure 6.5B)**. Mechanical thresholds were also left unchanged (siRNA 104±7.3%; NTC 102±6.3%; vehicle 113±7%; N=7), with similar left and right paw withdrawal thresholds **(Figure 6.5C/D)**. This suggests $K_V7.5$ does not have a strong role in setting thermal or mechanical pain threshold.

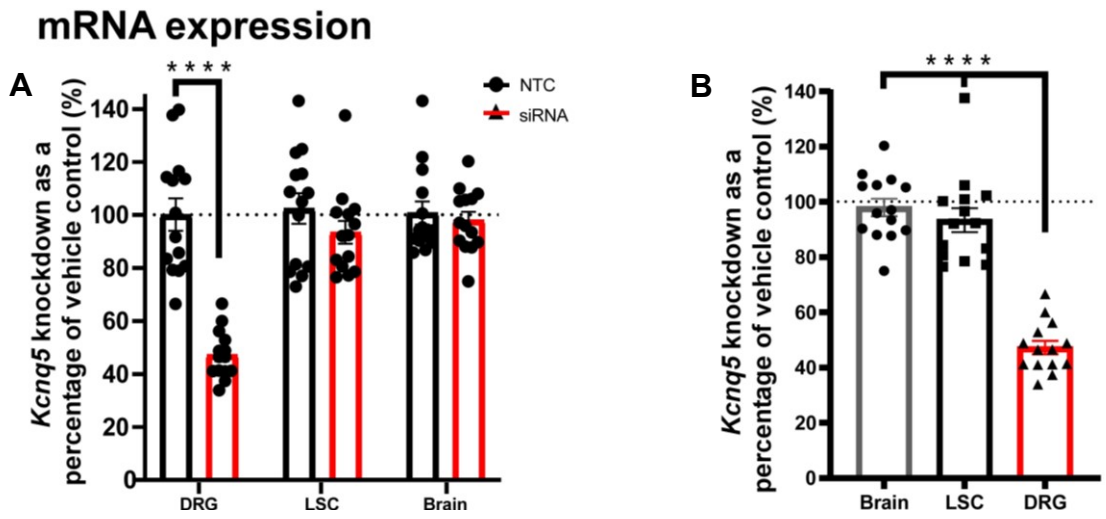

Figure 6.4 Intrathecal injection of Kcnq5 siRNA reduces sensory Kcnq5 expression. **(A)** Analysis of mRNA expression of *Kcnq5* normalised to housekeeper *Hprt1* in lumbar dorsal root ganglion (DRG), lumbar spinal cord (LSC) and the hippocampus and cortex (Brain) post behavioural experimentation in vehicle (N=14), NTC (N=14) and *Kcnq5* siRNA (N=14) treated animals. **(B)** Paired comparison of *Kcnq5* knockdown in DRGs, LSC and Brain. Data from qPCR is as compared to the vehicle control results. Data presented is Mean ±S.E.M, statistical evaluation with independent measures or repeated measures One-Way ANOVA with Tukey's post hoc *P<0.05 **P<0.01 ***P<0.001 ****P<0.0001.

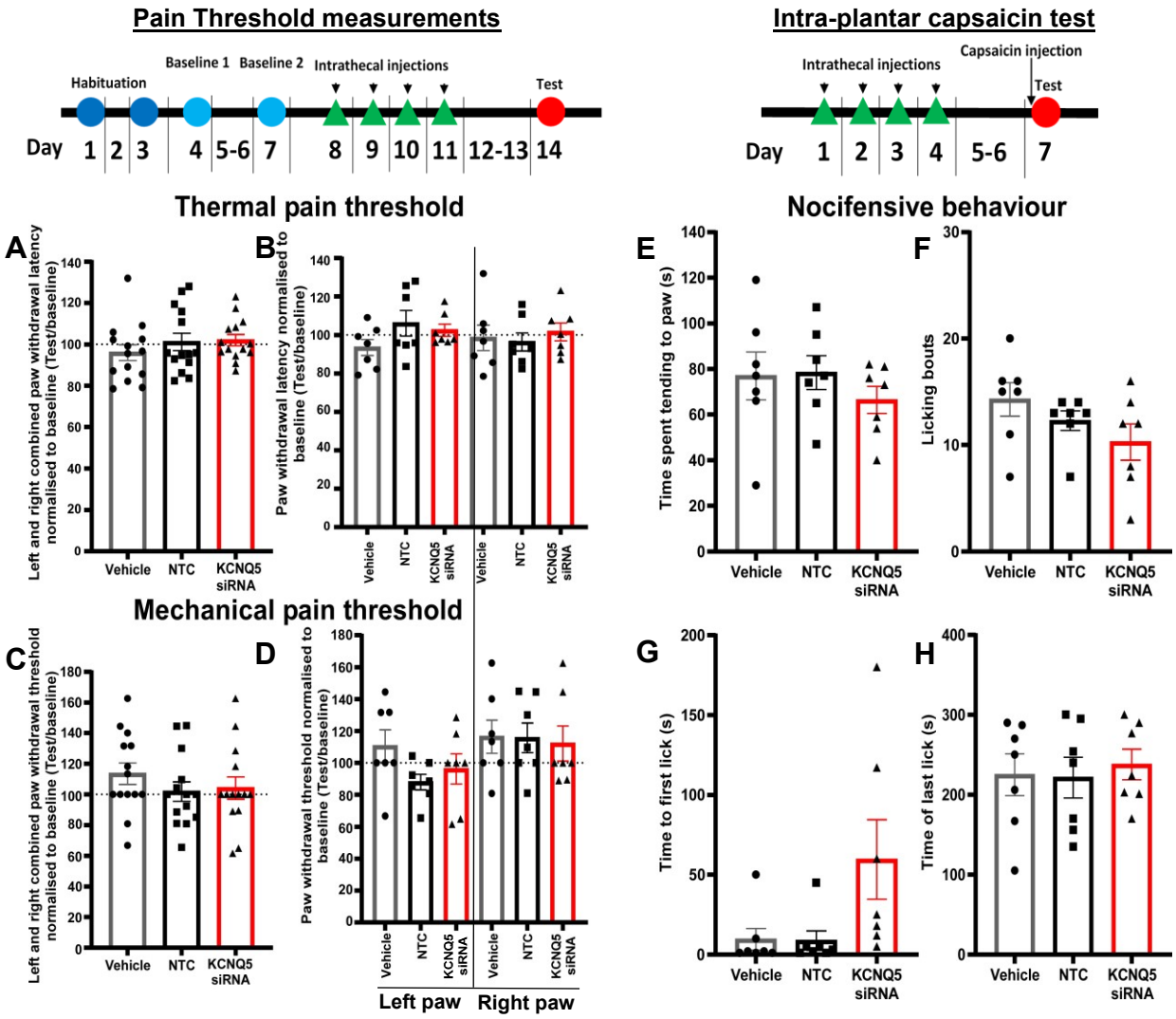

Figure 6.5 Intrathecal injection of Kcnq5 siRNA does not impact pain threshold or animals' response to painful stimuli. **(A-D)** Changes in **(A-B)** thermal sensitivity **(C-D)** mechanical sensitivity after 4 consecutive 100 µg intrathecal injections of vehicle (N=7), non-targeting control RNA (NTC) (N=7) or *Kcnq5* siRNA (N=7). **(A-B)** Thermal pain threshold after intrathecal injections normalised to baseline pain threshold before injections with left and right paw **(A)** combined or **(B)** separated. **(C-D)** Mechanical pain threshold after intrathecal injections normalised to baseline pain threshold before injections with left and right paw **(C)** combined or **(D)** separated. **(E-H)** Effect of vehicle (N=7), NTC (N=7) and siRNA (N=7) on acute 300 µM capsaicin induced hyperalgesia through measuring nocifensive behaviour in a 5-minute period. Nocifensive behaviour was measured through **(E)** time spent tending to paw in seconds, **(F)** number of licking bouts, **(G)** time to first lick in seconds and **(H)** time the animals stopped tending to the paw in seconds. Data presented is Mean ±S.E.M, statistical evaluation with a independent measures One-Way ANOVA with Tukey's post hoc. Significances are indicated where the siRNA condition differed compared to vehicle or NTC. Vehicle and NTC were also compared but were not significantly different *P<0.05.

When injected with 300 μM capsaicin, time spent tending to the paw was reduced by 12 seconds (siRNA 66±6 s; NTC 78±7.4 s; vehicle 77±10 s; N=7); this reduction was not significant. There was also a tendency towards reduction in the number of licking bouts (siRNA 10.3±1.7 bouts; NTC 12.3±0.9 bouts; vehicle 14.3±1.6 bouts; N=7) and a tendency towards an increase in time to first lick (siRNA 60±25 s; NTC 8.9±6.0 s; vehicle 9.6±7.0 s; N=7) **(Figure 6.5A-C)**. The time the animals stopped licking was unchanged (siRNA 238±19 s; NTC 221±26 s; vehicle 225±26 s; N=7) **(Figure 6.5D)**. Neither of these changes were significant, but these apparent trends do entertain the possibility that there was a small analgesic effect of knocking down *Kcnq5*. This is in accordance with the mild 'dominant-negative' effect of *Kcnq5* suggested from electrophysiological recordings from dissociated neurons (Chapter 5).

Discussion

Here we demonstrate that knocking down *Kcnq2* in the DRG reduces thermal and mechanical pain threshold and increases response to noxious stimulation, whereas *Kcnq5* knockdown did not have the same effects. These data suggest that $K_v7.2$ is important in controlling pain thresholds under normal conditions and preventing additional hyperexcitability when responding to painful stimuli. The lack of effect of *Kcnq5* knockdown further support our earlier conclusions that $K_v7.2$ is the primary K_v7 subunit in pain-sensing DRG neurons, with $K_v7.5$ perhaps exhibiting some sort of dominant-negative effect. The *in vivo* data are consistent with our *in vitro* data, demonstrating that *Kcnq2* knockdown reduced tonic M current and increased hyperexcitability, whereas *Kcnq5* knockdown increased tonic M current in some cells but did not affect excitability (Chapter 5). The change in pain thresholds following *Kcnq2* knockdown is consistent with the phenotype of the sensory neuron-specific *Kcnq2* knockout mice (King *et al.*, 2014).

It is clear from the pharmacology, *in vitro* and *in vivo* knockdown of $K_v7.2$ that this subunit is predominant K_v7 subunit in controlling neuronal excitability and the analgesic effect of K_v7 channel potentiators in nociceptors. However, the role of $K_v7.5$ is more nuanced; there seems to be little role for $K_v7.5$ in tonic neuronal control and perhaps some dominant-negative effect in some cells. Yet, when potentiated with K_v7 current enhancers, $K_v7.5$ does contribute to their analgesic effect (in the neurons where it is expressed). Therefore, the role of $K_v7.5$ is less clear-cut. There is also the possibility that *Kcnq5* knockdown was not sufficient to produce significant reduction in

K_v7.5 protein level. This was not the case with K_v7.2 however; knocking down *Kcnq2* (to a similar level, as compared to *Kcnq5* knockdown) was sufficient to see a clear functional effect on both DRG neuron M current and excitability and, importantly on the behavioural pain responses *in vivo*.

Apparent increase in M current and hyperpolarisation if RMP after *Kcnq5* knockdown seen in the previous chapter may be behind a tendency towards lesser pain responses observed in *in vivo* experiments (albeit these were not significant). It is tempting to theorise that under inflammatory or prolonged pain conditions, increasing *Kcnq5* expression could reduce the overall M current through by co-expressing with K_v7.3 subunits that would otherwise co-assemble with K_v7.2, thus reducing the overall current in the neuron. Opposingly, a decrease in K_v7.5 could have increased M current, allowing more K_v7.2/7.3 heteromers to form to combat hyperexcitability. Indeed, there is some evidence from a diabetic neuropathy model of pain that K_v7.5 expression decreases and K_v7.2 expression increases in diabetic neuropathy (Djouhri *et al.*, 2020). Combining the expression change with our functional data, it suggests that the change in expression could be a compensatory mechanism, reducing the effect of K_v7.5, resulting in an increase in M current, rather than leading to hyperexcitability, as the authors suggest (Djouhri *et al.*, 2020). However, to truly understand the role of *Kcnq5*, a sensory neuron (perhaps sub-population) specific, conditional knockout, would be required.

The acute nature of the siRNA knockdown did not result in any compensation from other K_v7 subunits, something that was demonstrated after *Kcnq2* knockout mice used in the present study (chapter 3) and has occurred previously during chronic knockout of *Kcnq2* (Robbins *et al.*, 2013). Moreover, the delivery of this particular cholesterol-conjugated siRNA to the intrathecal space showed a strong preference for the peripheral sensory ganglia over the central nervous system, resulting in a peripheral neuron-specific acute knockdown of *Kcnq* subunits. Although, the analysis was done on the spinal cord in the lumbar region, not specific cell types, thus it is possible that despite little effect on the cells in the spinal cord overall, some populations may have been affected. Neurons of the dorsal horn, ventral horn motor neurons and ventro-medial interneurons express K_v7.2. Therefore, analysis of these groups of neurons in isolation may have revealed a knockdown in one population over the other populations present in the spinal cord. Thus, we show no change in K_v7.2 or K_v7.5 overall in the

spinal cord after intrathecal injection of cholesterol-tagged siRNA but there is the possibility for that different populations of neurons may have been affected differently. The approach could be refined by taking sections of spinal cord in the region and using RNA scope of fluorescence in situ hybridisation to assess individual neurons in the spinal cord. The limitation of this is that fluorescence intensity is not easily quantifiable, particularly between samples in this way, whereas qPCR is a much more sensitive method to detect changes in mRNA expression levels, so what is gained in cell population specificity has the compromise of a lesser ability to measure mRNA expression than qPCR. It would also be a different experimental approach to how DRG and brain samples were analysed so would not be directly comparable.

Nonetheless, whether intrathecal delivery of cholesterol-tagged siRNA affects the spinal cord or not is important to understand and indeed other compounds delivered intrathecally do exert their effects on the spinal cord (Verneuil *et al.*, 2020). Currently, there is no consensus on why some compounds enter the spinal cord and others preferentially target the peripheral structures, likely the chemical structure plays an important part in whether the compound enters the spinal cord. A cholesterol-tagged siRNA is not able to pass through the pia mater or other structures but is able to enter the fibres passing through the intrathecal space. In this case, the fibres are part of neurons with cell bodies in the DRG, whereas, although they enter the spinal cord, the fibres terminate at second-order neurons, so the siRNA would have to exit the nerve terminal in the spinal cord to enter other neurons before having the cholesterol cleaved from the siRNA. Degradation of the compound may also be a factor, siRNA is quickly degraded outside of the cell, there has been an effort to increase this time in systemically delivered siRNAs, whereas drug compounds have much longer half-lives than double stranded mRNAs. Site of injection, speed and volume injected may also be important, as needle placement may be closer to (perhaps touching) the cord, or just in the space; a slow injection of low volume likely spreads more evenly, less like a jet being forced from the needle. However, motoneurons also leave the spinal cord in the intrathecal space through the ventral root, so an intrathecal injection could have implications for locomotion. Indeed, intrathecal delivery of retigabine and the K_V7.2/7.3 selective compound ICA-069673 increased the speed of locomotion, which was suggested to be through K_V7.2 (Verneuil *et al.*, 2020). Yet, this effect was shown to be due to the inhibition of interneuron firing in the spinal cord disinhibiting the

motoneurons, suggesting this was a central effect in the spinal cord and did not affect the ventral root (Verneuil *et al.*, 2020). This is further supported because locomotion speed was increased not decreased, the effect of a K_v7 potentiator on motoneurons would likely be to inhibit excitability, thus reduce speed of locomotion. Animals on the present study were observed multiple times a day as well as being observed during behavioural experimentation and no obvious changes in locomotion were observed throughout the intrathecal knockdown studies. However, there is the potential for changes in locomotion to occur and locomotion was not assessed through rigorous testing in the present study. As there were no obvious changes when under general observation, it is unlikely changes in locomotion would have impacted the behavioural tests used here but testing for changes in locomotion would be important to assess when targeting K_v7 channels for therapies.

Taken together, the peripheral knockdown of $K_v7.2$ and the local administration of $K_v7.2/7.3$ a specific potentiator having strong opposing effects on hyperalgesia, suggesting that $K_v7.2$ in the peripheral sensory neurons is very important in controlling nociception and pain. This conclusion has been supported by the previous experiments where K_v7 potentiators were shown to still exert a strong analgesic effect, in spite of blocking the central K_v7 channels with Intracerebroventricular (ICV) injected XE-991 (Hayashi *et al.*, 2014). These findings are important as they suggest targeting of $K_v7.2$ (or Kv7.2/3) channels in the periphery may be an effective approach to analgesia, without impacting K_v7 channels expressed in the central nervous system or other subunits expressed in peripheral tissues (e.g. $K_v7.5$, which has strong expression in the vasculature).

In addition, we provide further evidence for the delivery of therapeutic substances to the intrathecal space as a means of bypassing the peripheral tissues, breakdown by the liver and avoiding the blood. In this particular case, *Kcnq* siRNA delivery would not be appropriate as a therapy, however, delivering K_v7 channel potentiators with reduced blood-brain barrier permeability, thus a reduced CNS effect, may be possible. Or perhaps using siRNA to knockdown proteins responsible for downregulation of K_v7 channels in chronic pain conditions, such as REST (Rose *et al.*, 2011, Zhang *et al.*, 2019). Future studies could attempt to understand whether knockdown of REST halts *Kcnq* downregulation and stops the development of neuropathic pain.

Chapter 7: Discussion

Since the discovery of the M current in 1982, much has been learned about the structure and function of K_v7 channels and their importance in cellular excitability. With regards to the somatosensory system, the importance of K_v7/M current for excitability of sensory neurons is recognised, yet, until now the expression and functional role of each K_v7 subunit in the sensory system has not been fully explored. Increasingly, the analgesic effects of widely clinically used compounds are being attributed to increasing K_v7 current in sensory neurons. Particularly COX inhibitors such as the paracetamol metabolite NAPQI, diclofenac and celecoxib have been shown to potentiate K_v7 channel current at concentrations within the clinically administered dose of these compounds (Ray *et al.*, 2019, Peretz *et al.*, 2005, Brueggemann *et al.*, 2011, Du *et al.*, 2011). Suggesting that some of the analgesic effect of these compounds is a result of increased K_v7 current. Similarly, GABA, an endogenous chemical known to have an analgesic effect (Manville *et al.*, 2018), also potentiates K_v7 current and even some endocannabinoids also potentiate $K_v7.2/7.3$ and $K_v7.4$ channels directly, despite being endogenous ligands for cannabinoid receptors (Larsson *et al.*, 2020). This suggests that some of the analgesic benefits of cannabis could be mediated through K_v7 channels also. Indeed, other natural substances are now known to modulate K_v7 channels as part of their effect. *Mallotus oppositifolius,* a herb used in traditional medicine to treat seizures, contains mallotoxin and isovaleric acid, that when combined potentiate K_v7 current (Manville and Abbott, 2018) and Ssm spooky toxin present in centipede venom is a potent inhibitor of K_v7 channels (Luo *et al.*, 2018). As the importance of K_v7 channels as therapeutic targets increases, further understanding of the subunit expression in sensory neurons and the functional role for individual subunits in nociception has become essential if an effective, safe and specific therapy is to be developed. The present work has provided answers for a number of these considerations, as well as presenting new avenues of research for future work.

This current study has demonstrated that $K_v7.2$, $K_v7.3$ and $K_v7.5$ are the most widely expressed subunits in sensory neurons with $K_v7.2$ being the predominant subunit controlling activity of nociceptors, with $K_v7.5$ contributing an unexpected inhibitory effect on K_v7 current. This work is the first to attempt a full characterisation of the expression, function and impact of all five K_v7 subunits with regards to pain. The

rationale for eventual focus on $K_v7.2$ and $K_v7.5$ was due to the limited expression of $K_v7.1$ and $K_v7.4$ in sensory neurons and the understanding that heterologous expression of $K_v7.3$ homomers produces negligible current flow (Zhang *et al.*, 2003).

It cannot be guaranteed that because exogenous expression of $K_v7.3$ homomers does not produce current in heterologous expression systems, the same will be the case in native cells. However, the lack of current in $K_v7.3$ homomers has been demonstrated to be an inability of $K_v7.3$ subunits to form stable oligomers due to the reduced number of electrostatic contacts in the D helix of $K_v7.3$ homomers compared to $K_v7.1$, $K_v7.2$, $K_v7.4$ and $K_v7.5$ (Howard *et al.*, 2007). As well as a large phenylalanine and negatively charged residues that interrupted the electrostatic interactions occurring between $K_v7.3$ subunits but allow additional interactions with other subunits due to their positively charged residues in the same position (Howard *et al.*, 2007, Nakajo and Kubo, 2008). Thus, we may assume that the lack of current recorded from $K_v7.3$ homomers is the result of an innate instability in homotetramer formation, which is likely to also be the case in native cells. With this information, the understanding of the role of $K_v7.2$ and $K_v7.5$ as the main expressed, active subunits, took priority over $K_v7.3$.

7.1 K_v7 Expression of K_v7 subunits in Sensory Neurons is Not Uniform

The data on K_v7 expression presented in the current study provides significant further clarity on previous findings. We confirm that in rat DRGs, $K_v7.1$ is not expressed at detectable levels, consistent with the initial discovery of *Kcnq* gene expression in DRGs (Passmore *et al.*, 2003). We also identified $K_v7.4$ in a small population of NF200 positive neurons. These neurons were likely to be the low-threshold mechanoreceptors with Meissner's corpuscles at their terminal, based on $K_v7.4$ previously being identified in the cell bodies and Meissner's corpuscles at the terminals of afferent fibres (Heidenreich *et al.*, 2012). *Kcnq4* knockout mice presented with enhanced recognition of low frequency vibration suggesting *Kcnq4* plays a role in low threshold mechanical stimuli detection (Heidenreich *et al.*, 2012).

Much of the K_v7 expression in DRG was comprised of $K_v7.2$, $K_v7.3$ and $K_v7.5$ and was limited to the sensory neurons rather than glial cells. This is in accordance with other studies that have also detected the presence of $K_v7.2$, $K_v7.3$ and $K_v7.5$ antigens using immuno-fluorescence (Passmore *et al.*, 2003, King and Scherer, 2012). However, it

must be noted that mRNA transcripts for *Kcnq3* and particularly *Kcnq5* are low (by transcript count compared to other subunits) and in the case of *Kcnq5*, even lower than *Kcnq4* (Zheng *et al.*, 2019). Previously, K_v7.2 and K_v7.5 have been identified in small and large neurons (Passmore *et al.*, 2003, Rose *et al.*, 2011, King and Scherer, 2012), with Rose and colleagues suggesting small diameter neurons express mainly K_v7.2 and King and Scherer proposing it to be K_v7.5. Understandably, a mix of K_v7.2 and K_v7.5 in small-diameter neurons has also been suggested (Passmore *et al.*, 2003). However, the current study is the first to separate myelinated from unmyelinated neurons with NF200 and peripherin markers being used to achieve this. Much of the previous evidence relied on cell body size for identification, however the issue with this is that the largest unmyelinated and smallest myelinated neurons may overlap significantly. Using our method, we demonstrate that a large portion of peripherin positive unmyelinated neurons expressed K_v7.2, with fewer expressing K_v7.5. On the other hand, myelinated NF200 positive neurons expressed both K_v7.2 and K_v7.5 with bias towards K_v7.5. K_v7.3 was expressed in around half of both myelinated and unmyelinated neurons. In addition, here, for the first time, the extent of co-expression of K_v7.2 and K_v7.3 or K_v7.2 and K_v7.5 was thoroughly analysed in both rats and mice; 50% of K_v7.2 was expressed with K_v7.3 and only 18% with K_v7.5. Interestingly, this suggests there may be neurons that express K_v7.2 alone without K_v7.3.

Our comprehensive study of all the subunits helps to piece together reports from other groups that focus on one or a few subunits only. Indeed K_v7.2 has been identified in small neurons (Rose *et al.*, 2011) and myelinated neurons, particularly in the fibres where it is localised to the nodes of Ranvier (Schwarz *et al.*, 2006), thus must be myelinated. K_v7.3 was expressed but not localised to the nodes and K_v7.5 was not analysed (Schwarz *et al.*, 2006). Less is known about K_v7 expression in unmyelinated axons. In the nodose ganglia which provide somatic sensation from the taste buds and visceral sensory information from the lungs, transcripts from single cells were analysed by PCR. *Kcnq5* transcripts were not well expressed in TRPV1 negative C-fibres and only expressed in very few TRPV1 positive C-fibres overall whereas *Kcnq2* was expressed in most TRPV1 positive and negative C-fibres. Specifically isolating visceral lung innervating neurons, *Kcnq2* was expressed in more TRPV1 negative than positive C-fibres and *Kcnq5* was expressed in some TRPV1-positive fibres (Sun *et al.*, 2019).

After neuropathic injury, through direct cutting of the nerve or inducing bone cancer, *Kcnq2* (Rose *et al.*, 2011, Zheng *et al.*, 2013) and *Kcnq3* (Zheng *et al.*, 2013) were downregulated but *Kcnq5* was not studied. Taken with the data presented here, I suggest that all K_v7 subunits expressed should also be considered when studying M current to provide a well-rounded picture.

This is the first full characterization of the protein expression of all five subunits in the same conditions, by explicitly verified antibodies, using markers of myelinated and unmyelinated neurons and quantification of said expression. Despite these attempts by us, no one single subunit emerged as the sole subunit producing the M current in sensory neurons by expression alone, however $K_v7.2$ is the most likely candidate, which may or may not be expressed with $K_v7.3$. Moreover, another important point raised in this study is the possibility of an important role for $K_v7.5$ in sensory neurons.

Differential expression of K_v7 subunits in various types of neuron, is not a phenomenon that only occurs in the DRG. The present study demonstrates differential expression between $K_v7.2$, 7.3 and 7.5, with $K_v7.4$ expressed in a small subset of neurons and no expression of $K_v7.1$ in DRGs. Other studies have demonstrated other tissues that specifically express only a subset of K_v7 subunits. In the signal transducing cells (IHC and OHCs) and sensory innervating neurons of the inner ear, $K_v7.4$ is the most highly expressed and functionally important, $K_v7.4$ is also important in the central areas involved in hearing (Beisel *et al.*, 2000) but with more of a role for $K_v7.5$ in the auditory nuclei (Tzingounis *et al.*, 2010). Similarly, $K_v7.4$ is most functionally important in the VTA dopaminergic neurons of the mesolimbic pathway, possibly in some combination with $K_v7.3$ (Friedman *et al.*, 2016). However, the nucleus innervated by the VTA in the mesolimbic pathway, the nucleus accumbens, consists of neurons that functionally express $K_v7.2/7.3$ channels (Kim *et al.*, 2019, McGuier *et al.*, 2016). $K_v7.2/7.3$ channels are also expressed in the dopaminergic neurons of the substantia nigra, part of the nigrostriatal pathway (Cooper *et al.*, 2001). In the hippocampus $K_v7.2/7.3$ channels are the predominantly expressed channels whereas in smooth muscle, $K_v7.4$ and $K_v7.5$ channels are the most expressed. This leads to the question as to why different subunits are expressed in different tissues, or even different neurons within the same tissue. The answer to this is not known but there are a number of factors to consider, these include modulation, kinetics and protein-protein interactions.

The modulation of individual subunits may be one factor influencing why a particular subunit is expressed. On the most essential level, each subunit has a different affinity for the critical co-factor PIP2, so this would influence the channels' ability to open depending on the availability of PIP2 and its affinity. $K_v7.3$ has a high affinity for PIP2 compared to the other subunits, with $K_v7.5$ having the lowest affinity, therefore, the presence of $K_v7.3$ in a cell with other subunits likely improves the probability of opening when PIP2 is not abundantly available. In neurons, PIP2 can be depleted significantly due to the number of processes relying on $G_{q/11}$ protein pathways, perhaps partially explaining the presence of $K_v7.3$ in many neuronal K_v7 channels. Contrastingly, $K_v7.3$ is not expressed in smooth muscle cells, suggesting that PIP2 deficits are less common or less important in this context, thus, $K_v7.4/7.5$ channels are sufficient for this cell type. PIP2 synthesis is around 20-times slower than PIP2 hydrolysis in smooth muscle but it could be such that there is enough of a balance in smooth muscle that $K_v7.3$ is not required (Harraz *et al.*, 2020). The major subunit composition of K_v7 channels in smooth muscle is $K_v7.4$ and $K_v7.5$, subunits that do form heteromers. The heteromerization of these two channels is critical to the function of K_v7 channels in smooth muscle because opening of K_v7 channels in response to β adrenal stimulation is important for the vasodilatory effect in vascular smooth muscle. However, $K_v7.4$ homomers are insensitive to adrenalin mediated PKA release, yet $K_v7.5$ homomeric current is potentiated by adrenalin (Mani *et al.*, 2016). This would suggest that only $K_v7.5$ needs to be expressed for K_v7 channels to function in smooth muscle, yet disruption of $K_v7.4$ expression results in vascular hypertension (Jepps *et al.*, 2011, Fosmo and Skraastad, 2017) and $K_v7.5$ homomeric currents are very low compared the $K_v7.4/7.5$ heteromer, so it is possible that $K_v7.4$ presence is required for a functional level of current and $K_v7.5$ presence is required for sensitivity to vasodilators and vasoconstrictors.

The macroscopic current produced by various subunits may also be a factor in why cells express different subunits. Neurons that must be less excitable or even silent for their function, will benefit from higher macroscopic K_v7 currents, whereas neurons that are more excitable may require a lower current. The current evoked by $K_v7.2/7.3$ heteromers is higher than $K_v7.3/7.5$ heteromers or $K_v7.2$ homomers, it is also the most common pairing of K_v7 subunits in neurons. This could be because the higher current is necessary for preventing hyperexcitability. The presence of $K_v7.5$ in the same cell

would result in a lower overall current output than if only K_v7.2/7.3 heteromers were expressed because a portion of K_v7.3 would be forming heteromers with K_v7.5 and these channels have a lower current output than K_v7.2/7.3 channels. This phenomenon is alluded to in the present study, with the increase in M current upon K_v7.5 knockdown and may explain why some neurons express all three subunits but others do not, and it is dependent on the level of current required for the neurons to correctly function. Indeed, K_v7.5 is unable to naturally compensate for K_v7.2 loss-of-function resulting in epilepsy (Greene *et al.*, 2018) but it would be informative to induce K_v7.5 expression in cells with K_v7.2 mutation/knockout to observe whether hyperexcitability/epilepsy can be protected against or reversed.

The kinetics of K_v7.2/7.3 heteromers are such that the activation and deactivation times of macroscopic current is faster than current evoked by other forms of the channel. The faster activation kinetics means reaching maximal current output at a given voltage faster, but the fast deactivation suggests current is flowing for less time. The faster change in kinetics could mean faster changes in current flow, K_v7 channels more adaptable in the cells that express the heteromer. K_v7.4/7.5 heteromers are seemingly responsible for providing the level of current required in smooth muscle cells also, suggesting that heteromers are generally required to provide enough of a brake on cellular excitability. However, in the case of K_v7.4 in other tissues such as the ear, it is expressed alone, although K_v7.4 homomers produce the highest current amplitude of all the homomers when exogenously expressed. There is also evidence that K_v7.4 homomers are able to cluster together, increasing current amplitude and shifting voltage dependence to more hyperpolarised potentials (Perez-Flores *et al.*, 2020). Therefore, this phenomenon may remove the requirement for heteromer formation in cells where this clustering occurs. Thus, it seems that in most cases the higher current amplitude and faster activation kinetics of heteromers compared to homomers are necessary for controlling neuronal excitability, but in the case of K_v7.4/7.5 heteromers in smooth muscle, K_v7.4 is sufficient in terms of current produced to control excitability, but K_v7.5 is necessary in the channels for conveying sensitivity to specific modulatory proteins (PKA and PKC). In this sense, the reason is likely more complicated than cells express K_v7 heteromers because higher current amplitudes are necessary for setting cellular excitability.

This relates to the findings presented here because the expression pattern of $K_v7.2$, $K_v7.3$ and $K_v7.5$ indicates that there are neurons expressing $K_v7.2/7.3$ heteromers, $K_v7.3/7.5$ heteromers, as well as $K_v7.2$ or $K_v7.5$ homomers. The possibility that there are populations of neurons that express $K_v7.2/7.3$ and $K_v7.3/7.5$ heteromers or even $K_v7.2/7.3/7.5$ heteromers, also exists. Based on the information above, neurons expressing $K_v7.2$ or $K_v7.5$ homomers either are dormant channels awaiting $K_v7.3$ expression to be functional or homomers are in fact sufficient to set excitability in these neurons. The latter is somewhat more likely with $K_v7.2$ homomers as these channels produce larger macroscopic currents than $K_v7.5$ homomers, and there is increasing evidence that $K_v7.5$ channels are not functional as homomers. It is still unclear why sensory neurons express different combinations of subunits. It may be dependent upon the amplitude of current required in each neuron. There has been no clear identification of populations neurons that have higher or lower M current amplitudes (Du *et al.*, 2014, Du *et al.*, 2018) but the present study has demonstrated a correlation between M current and the current required to elicit an action potential (rheobase) in sensory neurons. Or it may be that the variation in homomer and heteromer formation in sensory neurons determines how the neuron modulates K_v7 channel activity, this implicates the type of stimulus or GPCRs (or other proteins) also. In addition, new research suggests that GABA is able to increase M current depending on which subunit is expressed (Manville *et al.*, 2018). Thus, neurons expressing $K_v7.2/7.3$ channels would be sensitive to increased K^+ efflux through $K_v7.2/7.3$ channels in the presence of GABA, whereas neurons expressing $K_v7.2$ alone would be insensitive to this GABA mediated K^+ efflux. At this time, both of these possibilities are plausible and there may be other reasons, but the fact it has evolved in this way suggests an evolutionary advantage to this differential expression of K_v7 subunits.

To truly understand the relevance of different cells expressing different subunits beyond differences in modulation, an approach is required whereby the subunits expressed in a given cell or tissue are silenced and replaced with another subunit to assess the functional impact of this, both at the cellular level and *in vivo*. Currently this would likely need to be done through development of a knockout animal specific to a given cell type that then has a knock-in of another subunit that can be activated afterwards. This would be possible if inserted through different inducible promotors

where the first induction is to knock-out the first gene and the second induction begins the expression of the knocked-in gene.

7.2 K_v7.2 is the Predominant Functional Subunit in TRPV1 Positive Neurons

Another of our aims was to study the functional effect of potentiating or downregulating K_v7.2 in sensory neurons. It was observed that in capsaicin responsive (TRPV1 positive) neurons, K_v7 current was strongly potentiated by ICA-27243, similarly to retigabine and after *Kcnq2* siRNA knockdown, K_v7 current was strongly reduced. Combining these approaches suggests that K_v7.2 is the major subunit underlying K_v7 current in TRPV1 positive sensory neurons, possibly as homomers or K_v7.2/7.3 heteromers.

In TRPV1 negative neurons, some of those with lower capacitances (presumably smaller neurons) also responded to ICA-27243, fewer larger neurons responded to ICA-27243 but did respond to retigabine. K_v7.2 knockdown had much lesser effect on K_v7 current amplitude in this neuronal population. Taken together, these pharmacological and siRNA results suggest that K_v7.2 plays much more modest role in TRPV1 negative neurons, although it is expressed in some of those. Combined, the above data are consistent with *Kcnq2* transcript expression in the somatosensory neurons of the nodose ganglia, although this may not be the case in neurons innervating the visceral organs (Sun *et al.*, 2019). Furthermore, our data suggest that K_v7.5 or K_v7.5/7.3 (or K_v7.4 in a minor subpopulation) are functionally expressed and responsive to retigabine in TRPV1 negative neurons, where ICA-27243 was less effective than retigabine. This is supported by previous reports that, of the small neurons expressing K_v7.5, the majority are non-peptidergic, IB4-positive (King and Scherer, 2012, Djouhri *et al.*, 2020) and only a minority of IB4-positive neurons express TRPV1 (Woodbury *et al.*, 2004) with the number of *Kcnq5* transcripts being the highest in Aβ low threshold mechanoreceptors (Zheng *et al.*, 2019). However, in nodose neurons *Kcnq5* transcripts were not detected in most TRPV1 negative neurons (Sun *et al.*, 2019).

We present the first direct evidence for K_v7.2 specifically playing an important role in the excitability of TRPV1 positive neurons specifically. The influence of K_v7 channels in setting neuronal excitability has been demonstrated in experiments where increased

excitability and depolarised resting membrane potentials in sensory neurons was achieved by application of XE-991 and retigabine application resulted in decreased excitability and hyperpolarised resting membrane potential (Passmore *et al.*, 2012, Du *et al.*, 2014). However, the non-selective nature of these compounds does not infer the subunits responsible directly. In my work, by downregulating *Kcnq2* and *Kcnq5,* it was possible to analyse the contribution of each of these channels to sensory neuron excitability. It was observed that there was an increase in firing frequency, depolarised resting membrane potential and reduced rheobase after *Kcnq2* downregulation in TRPV1 positive neurons, which was not seen in *Kcnq5* knockdown. Thus, demonstrating for the first time that $K_v7.2$ is responsible for the changes in excitability seen with regards to modulating K_v7 channels, in TRPV1 positive neurons at least. The situation in TRPV1 negative neurons is seemingly more complicated and we were unable to pinpoint a major subunit responsible for K_v7 current in these neurons, likely due to the inherent heterogeneity of this population as it would include a large portion of IB4 positive nociceptors and low threshold mechanoreceptors. Separating this group into further subpopulations for study may reveal more about the K_v7 subunit composition in those populations.

7.3 Extent of Pain Response can be Modulated by $K_v7.2$

The previous section describes that $K_v7.2$ containing K_v7 channels are fit to control sensory neuron excitability and that ICA-27243 can potentiate K_v7 current produced by $K_v7.2$-containing channels only. Therefore, it was reasoned that the analgesic effect of such a compound could be compared to retigabine to ascertain the contribution of $K_v7.2$ to K_v7-mediated analgesia. ICA-27243 has been shown to not evoke current from $K_v7.3$, $K_v7.5$ or $K_v7.3/7.5$ channels at even very high concentrations but did potentiate $K_v7.4$ at more than 10 times the concentration of maximally activating $K_v7.2/7.3$ (Wickenden *et al.*, 2008, Padilla *et al.*, 2009). As $K_v7.4$ was only expressed in a subset of mechanosensitive neurons (present study, (Heidenreich *et al.*, 2012), its contribution to any analgesic effect of ICA-27243 was unlikely so the effect of ICA-27243 could be largely attributed to its action on $K_v7.2$-containing channels ($K_v7.2$ or $K_v7.2/7.3$). The present work demonstrated a strong analgesic effect of ICA-27243, similar to retigabine against both capsaicin-induced acute pain and CFA-induced inflammatory pain, whether delivered systemically or locally. As retigabine has a comparable analgesic efficacy to tramadol for acute and neuropathic pain it can be

reasoned that ICA-27243 would also be similarly effective to retigabine and tramadol but without the associated side effects of retigabine and opioid analgesics. However, ICA-27243 treatment resulted in liver toxicity as a result of its chemistry rather than its effect on K_v7 channels and is BBB penetrable. Our data suggests that a peripheral only, $K_v7.2/7.3$ channel potentiator would be an effective analgesic, so there is scope to improve further on the currently available compounds. Although, the effect of local treatment with a K_v7 channel potentiator has not been compared to compounds such as tramadol.

ICA-27243 and siRNA knockdown of *Kcnq2* had opposing effects on capsaicin-induced acute pain, with siRNA knockdown resulting in increased nocifensive behaviour whereas ICA-27243 had an analgesic effect. This indicates that $K_v7.2$ is important in preventing hyperexcitability of nociceptors and potentiation of $K_v7.2$ (or $K_v7.2/7.3$) reduces the intensity of acute pain response, whether applied systemically or locally. An additional analgesic effect of retigabine only occurred during systemic application of the compounds; during local injection the effects of both compounds was not significantly different to each other. This may have clinical relevance as it may be due to retigabine having a further analgesic effect via central pain pathways or sedation; indeed, some animals were excluded from the study for showing clear signs of sedation. Upon unblinding, these were found to be in the retigabine-treated group which was not the case in local injection to rat hindpaws. Thus, the above results identify peripheral Kv7.2 as an analgesic target with reduced side effects. When knocking down *Kcnq2*, the time tending to the paw and number of licking bouts were increased compared to controls, but the time point at which the animal started and stopped tending the paw were unaffected by the downregulation of $K_v7.2$. This is consistent with slow activation of K_v7 channels reducing the likelihood or length of action potential trains; increasing the length of trains would have the effect of increasing the intensity of the pain. Therefore, knocking down *Kcnq2* caused an increased firing frequency, elevated the response to pain but did not have an effect on the detection of pain.

Measuring the thermal and mechanical withdrawal thresholds of the uninjured paw contralateral to the CFA-injected paw is something that has not been done previously (Hayashi *et al.*, 2014) but may provide information on the impact of K_v7 compounds on an uninjured site. Therefore, we also analysed the impact of CFA injection and drug

administration on the uninjured paw. Systemic injection of ICA-27243 and retigabine, increased thermal pain threshold compared to the pre-CFA thresholds in the contralateral paw, indicating that K_v7 current, in part, mediates thermal pain threshold. This was supported by knockdown of *Kcnq2* reducing rheobase and depolarising resting membrane potential and by the depolarising of membrane potential by XE-991 and hyperpolarising by retigabine demonstrated previously (Du *et al.*, 2014). The reduction of thermal and mechanical pain threshold after *Kcnq2* knockdown further supports the suggestion that K_v7 current aids in the setting pain threshold, likely through the effect of K_v7 current on rheobase and RMP.

An important question to be answered has been the contribution of central and peripheral K_v7 channels to the analgesic effect of K_v7 channel potentiators such as retigabine and flupirtine. One such study separated these components by ICV injection of XE-991 to block the central K_v7 channels and upon systemic administration of retigabine. Sedation and motor impairments were significantly reduced when co-treated with retigabine and XE-991 compared to retigabine alone. Importantly, systemic retigabine analgesia was not affected by central XE-991 administration, suggesting K_v7 current in peripheral sensory neurons to contribute heavily to the analgesic effect of retigabine (Hayashi *et al.*, 2014). It is not possible to be sure of the extent to which XE-991 blocked K_v7 channels in the CNS in the previous study, especially with the differing affinities of the various subunits to XE-991, therefore retigabine crossing the BBB may still have been providing some central effect, albeit at a reduced capacity. In leu of a potential BBB impenetrable enhancer, the present study has unravelled the identity of the much speculated, peripheral-dominant K_v7 subunit contributor towards analgesia; we provide direct evidence that peripheral $K_v7.2$ is the dominant contributor to the analgesic effect of K_v7 channel potentiators. Local injection of retigabine and ICA-27243 were sufficient to produce an analgesic effect when capsaicin was injected into the same paw, but not when injected into the opposite (contralateral) paw, suggesting the effect was indeed local and not due to entry into systemic circulation. Intrathecal injection of *Kcnq* siRNA was remarkably selective for the peripheral neurons of the DRG over that of the spinal cord when knocking down *Kcnq2* and *Kcnq5* in independent experiments. This meant that any change in nociception after siRNA knockdown could be deemed due to the downregulation of $K_v7.2$ or $K_v7.5$ in peripheral sensory neurons, which was seen as

an increased response to pain. Indeed, the increased response to pain and reduced thermal and mechanical pain threshold after *Kcnq2* siRNA can be attributed to downregulation of peripheral K_v7.2. Taken together, our pharmacological and genetic knockdown data, together with previous studies on peripheral analgesic action of retigabine (Hayashi *et al.*, 2014, Liu *et al.*, 2010) provide strong evidence that peripheral K_v7 potentiation contributes the majority of analgesic effect of K_v7 channel potentiators and that peripheral K_v7.2 specifically contributes to the excitability of nociceptors.

However, there are some considerations to account for when creating potential therapies. This work demonstrates that animals became more resilient to acute physiological pain, as pain thresholds were reduced when *Kcnq2* was knocked down. With this being the case, this creates the potential for K_v7.2 targeting analgesics to also make patients more resistant to pain. This effect could be of benefit or detriment depending on situation and how resilient patients may be. It may be of benefit to people who play contact sports or do other things where a short-term mild increase in pain resilience may be of benefit. In contrast, pain is important for preventing longer term tissue damage, so increasing pain threshold closer to where tissue damage can occur could result in harm. This may be controlled by the dose administered and in the present study, neither mechanical nor thermal pain thresholds were increased to levels close to where tissue damage occurred in the CFA-injured paw or the non-injured paw after ICA-27243 or retigabine treatment, but it was increased past baseline in the uninjured paw of some animals, so is important to account for. Additionally, K_v7.2/7.3 channel potentiators can cause mitochondrial membrane depolarisation and led to apoptosis of hippocampal neurons as a result of intracellular K^+ depletion (Zhou *et al.*, 2011). The meaning of this research is currently not clear, as potentiation of K_v7 current is generally neuroprotective (Li *et al.*, 2004a, Gamper *et al.*, 2006, Roza and Lopez-Garcia, 2008, Roza *et al.*, 2011, Cisneros *et al.*, 2015), yet this research demonstrates the opposite. Concentrations of K_v7 potentiator used in the study were significantly higher than the effective doses of the compounds in neurons and in the clinic, suggesting that apoptosis is more of a concern only at high concentrations of flupirtine and NEM (Zhou *et al.*, 2011). Therefore, selecting an appropriate dose may be required for K_v7 based analgesics, as well as further research into understanding the apoptotic effect of K_v7 potentiators and what level of current increase is required

to result in these detrimental effects. The effect of long-term treatment with potential compounds on neuron apoptosis would also aid in assessing the safety and potential for side effects of any potential compounds.

Similarly, expression of K_v7 channels in the motor and autonomic nervous system also makes it important to monitor possible increases in locomotion (Verneuil *et al.*, 2020) and possible impacts on learning and memory and sedation. A number of these effects can be mediated with BBB-impermeable compounds. Much of the impact of K_v7 channels on motor function have been located in the brain or in the spinal cord and learning and memory and sleep processes are also centrally located, so impermeable compounds should not greatly impact these processes. Although, $K_v7.2$ expression has been demonstrated in the cell bodies of motor neurons within the spinal cord (Verneuil *et al.*, 2020) and could therefore be expressed in the axons, evidence for expression in the peripheral fibres is lacking but should still be considered. In addition, ganglionic sympathetic neurons also express K_v7 channels in the peripheral nervous system, thus the peripheral autonomic nervous system could be impacted by even a peripherally active $K_v7.2$ potentiating compound. However, a BBB-impermeable compound with the correct chemistry may also not affect the peripheral fibres because these fibres are protected by the blood-nerve barrier (BNB) (Tothonglor *et al.*, 2022) so would also be less exposed to a peripheral non-BBB or BNB penetrable compound. Whereas DRGs are highly vascularised (Godel *et al.*, 2016) so the compound could be active in the cell bodies of peripheral sensory neurons by accessing the DRG and the terminals through the skin but have little effect on peripheral nerves due to the BNB and no effect on motor neuron cell bodies as they are protect by the BBB. Other approaches would be to deliver compounds to the DRG more directly, either through intrathecal injection, as done in the present study, or direct injection into the DRG. This would remove most of the off-tissue effects of K_v7 potentiators but delivering substances directly to DRGs is difficult and a specialist surgery so is reserved for treatment-resistant chronic pain patients and not a viable solution for the majority of people that experience pain. Intrathecal injections do not require surgery but are still difficult, requiring ultrasound imaging, specialist training and can be painful to administer (Chekole *et al.*, 2022) and the chemistry of administered substance, as well as the volume, concentration, position of needle and possibly other factors can influence whether intrathecal injections have a site of effect in the DRG, spinal cord,

ventral root or various combinations of these sites, this may also be variable among patients and person administering injection. Both routes of administration would not be justified in most instances for repeated administration and installing a canula may also not be desirable for most people (Chekole *et al.*, 2022). However, a more viable approach in these instances would be the use of osmotic pumps that can be installed and release drug over a long period of time (Shimizu *et al.*, 2018) or to administer long-acting interfering RNAs, as done in the present study but with much longer acting types of interfering RNA such as shRNA. This approach would reduce expression genetically but not interfere with DNA and should be reversible. In the case of K_v7 channels, the approach would be to disinhibit its expression through knocking down an upstream target, candidates and further detail is discussed in section 7.6. Local application of compounds is also a viable treatment option, in the case of the compounds tested in this study, local application of the compounds stayed local for the duration of the experiment, because the contralateral paw was unaffected by local injection. However, longer term application was not assessed, so over the course of hours, local application may begin to distribute more systemically. This could be balanced by local concentrations being of a level that once dispersed systemically are not effective. In instances like this, the chemistry of a compound can provide some information on the distribution after local administration, but only robust and reasoned experimentation will confirm whether any of these treatment options are viable.

7.4 The Potential for a Novel Role of $K_v7.5$ Reducing K_v7 Current

While expression of $K_v7.5$ has been demonstrated in DRGs (Passmore *et al.*, 2003, King and Scherer, 2012, Djouhri *et al.*, 2020), a functional effect for this channel has not yet been identified or assessed to our knowledge. It was theorised here, based on our results with ICA-27243, that in some TRPV1 negative neurons, $K_v7.5$ would take the role of $K_v7.2$, acting as the active subunit for the K_v7 channels in those cells. One would assume that $K_v7.5$ knockdown would result in some reduction in K_v7 current and cause hyperexcitability in some cells. In fact, a 65-70% reduction in *Kcnq5* did not result in any such effect, leaving firing frequency and rheobase unchanged. Though curiously, taking all neurons into account, overall M current was increased after knockdown and resting membrane potential was significantly more hyperpolarised. In addition, action potential amplitude and after-hyperpolarisation amplitude were

increased, likely as a result of the hyperpolarisation of the membrane. It could be theorised that as K_v7.2/7.3 heteromers produce a higher current amplitude than K_v7.5/7.3 channels (Wickenden *et al.*, 2008, Padilla *et al.*, 2009), any cells that expresses all three subunits would express both heteromers as well as homomers. Therefore, reducing the level of K_v7.5 would shift the ratio of expression towards K_v7.2/7.3 channels, increasing overall M current in these neurons. If confirmed, this would suggest that K_v7.5 exerts an inhibitory effect on M current in some cells. Neither thermal or mechanical pain threshold were affected by 50-60% knockdown of *Kcnq5* and there was little effect on capsaicin-induced acute pain. However, it is worth taking note that there was a small reduction in nocifensive behaviour in the *Kcnq5* knockdown group, both time spent tending to the paw and licking bouts. This difference was not significant so should be taken with caution but is consistent with K_v7.5 providing an inhibitory effect on M current only in a population of cells. Thus, the hypothesis that the K_v7.5 subunit inhibits M current is indeed plausible however, the incomplete knockdown achieved in our hands may have masked other functional roles of K_v7.5 subunits and the *in vivo* effect of *Kcnq5* downregulation. Moreover, only nociception was analysed so other sensations may have also been impacted that are out of the scope of this study. Further work on the role of K_v7.5 is required to fully understand and appreciate the activity of K_v7.5 in different populations of sensory neurons. This could be achieved by employing a sensory neuron specific knockout animal and a plethora of behavioural tests.

7.5 K_v7.3 as a Modulatory Subunit

After identifying K_v7.2, K_v7.3 and K_v7.5 as the most abundantly expressed K_v7 subunits within the DRG, the priority was in understanding the functional role of the 'active' subunits, K_v7.2 and K_v7.5, as K_v7.3 alone produces negligible current (Zhang *et al.*, 2003). In doing so, it has emerged that K_v7.3 may be important in controlling level of K_v7 current and therefore neuronal excitability. This is a reasonable assumption because the co-assembly of K_v7.3 with either K_v7.2 or K_v7.5 may be an important determinant in the level of K_v7 current produced; this is in addition to the understanding that heteromers containing K_v7.3 have a higher current amplitude than the homomeric counterparts (Zhang *et al.*, 2003). Thus, it is important to now assess the impact K_v7.3 subunits have in sensory neurons as with K_v7.2 and K_v7.5, discussed in the following section.

7.6 Future Perspectives

Despite this work expanding the current understanding of the K_v7 subunits expressed in DRGs and the contribution of $K_v7.2$ and $K_v7.5$ to peripheral pain signalling, further interrogation is required for complete clarity. Further experiments could involve, in the first incidence, investigating the contribution of $K_v7.3$ and may be done through siRNA knockdown in a similar manner to the way $K_v7.2$ and $K_v7.5$ were assessed. This should provide a more detailed understanding of the role of $K_v7.3$ in sensory neurons and explore the possibility of $K_v7.3$ providing a modulatory role to K_v7 current. Another question remains as to what the expression pattern of K_v7 channels is in human DRGs, as there is an overlap between subunits in rodents and some differences in protein expression between rodent and human tissue has been documented (Rostock *et al.*, 2018), while humans are the ultimate target for pain relief. In terms of expression profiling in human DRG, NF200, rather than being restricted to myelinated neurons as in mice, labelled all neurons in human DRGs. Furthermore, the proportion of neurons expressing TRPV1 was also increased in human DRG by 20% as compared to mice DRGs (Rostock *et al.*, 2018). This demonstrates the importance of using human samples to be able to correlate the findings in animals to such samples. Indeed, as the different expression profiles of NF200 and peripherin in rodents were used in the present study to differentiate sensory neuron type. In human tissue, this approach would not have successfully differentiated between neuron types, thus other markers would be required instead. There are candidates such as CGRP, MRGPRD and Piezo2 that may differentiate neuron types in human neurons (Nguyen *et al.*, 2021), however any targets require full bioinformatic analysis of their neuronal expression and assessment of antibody utility.

The work covered in this report concerns acute and inflammatory pain, however there is also the evidenced link between neuropathic pain, changes to K_v7 channel expression and increased REST. It stands to reason that this link should be further studied to assess the extent of the interplay between REST and K_v7 during neuropathic pain and the therapeutic avenues that may be open either through K_v7 or REST targeting. Beginning with targeting REST expression or the repressor components and assessing whether this prevents downregulation of K_v7 channels shown in some types of neuropathic pain (Rose *et al.*, 2011, Zheng *et al.*, 2013). Identifying if other forms of neuropathic pain, such as common chronic pain conditions

like diabetic neuropathy are also linked to changes in REST and *Kcnq* expression would also be of significance if a therapeutic target is to be found.

Further evidence for the role of peripheral $K_v7.2$ and $K_v7.3$ could be considered by viral overexpression of each in the DRG. The potential role of $K_v7.5$ may also be studied further based on our evidence that it provides an inhibitory effect to K_v7 current, knockout of *Kcnq5* in sensory neurons will provide the basis for further research into the role.

7.7 Concluding Remarks

In summary, $K_v7.2$ containing, $K_v7.2$ or $K_v7.2/7.3$ mediated current controls sensory neuron excitability, particularly in TRPV1 positive neurons. Peripheral activation of $K_v7.2$ is sufficient to provide analgesia for acute and inflammatory pain, while $K_v7.2$ downregulation is sufficient to reduce pain thresholds and increase behavioural pain responses. $K_v7.5$ is expressed in sensory neurons, but the functional effect of such expression is not clear, though there is possibly an inhibitory effect on K_v7 current.

References

Abbott, G. W. 2016. Novel Exon 1 Protein-Coding Regions N-Terminally Extend Human Kcne3 and Kcne4. *FASEB journal : official publication of the Federation of American Societies for Experimental Biology,* 30**,** 2959-2969.

Abdo, H., Calvo-Enrique, L., Lopez, J. M., Song, J., Zhang, M.-D., Usoskin, D., Manira, A. E., Adameyko, I., Hjerling-Leffler, J. & Ernfors, P. 2019. Specialized Cutaneous Schwann Cells Initiate Pain Sensation. *Science,* 365**,** 695-699.

Abdullah, L. H., Evans, J. R., Wang, T. T., Ford, A. A., Makhov, A. M., Nguyen, K., Coakley, R. D., Griffith, J. D., Davis, C. W., Ballard, S. T. & Kesimer, M. 2017. Defective Postsecretory Maturation of Muc5b Mucin in Cystic Fibrosis Airways. *JCI Insight,* 2.

Abe, H., Kamai, T., Hayashi, K., Anzai, N., Shirataki, H., Mizuno, T., Yamaguchi, Y., Masuda, A., Yuki, H., Betsunoh, H., Yashi, M., Fukabori, Y. & Yoshida, K. 2014. The Rho-Kinase Inhibitor Ha-1077 Suppresses Proliferation/Migration and Induces Apoptosis of Urothelial Cancer Cells. *BMC Cancer,* 14**,** 412.

Adams, P. R., Brown, D. A. & Constanti, A. 1982. M-Currents and Other Potassium Currents in Bullfrog Sympathetic Neurones. *The Journal of physiology,* 330**,** 537-572.

Ahuja, V., Mitra, S., Kazal, S. & Huria, A. 2015. Comparison of Analgesic Efficacy of Flupirtine Maleate and Ibuprofen in Gynaecological Ambulatory Surgeries: A Randomized Controlled Trial. *Indian journal of anaesthesia,* 59**,** 411-415.

Al-Hasani, R. & Bruchas, M. R. 2011. Molecular Mechanisms of Opioid Receptor-Dependent Signaling and Behavior. *Anesthesiology,* 115**,** 1363-1381.

Alaimo, A., Gómez-Posada, J. C., Aivar, P., Etxeberría, A., Rodriguez-Alfaro, J. A., Areso, P. & Villarroel, A. 2009. Calmodulin Activation Limits the Rate of Kcnq2

K+ Channel Exit from the Endoplasmic Reticulum. *The Journal of biological chemistry,* 284**,** 20668-20675.
Allouche, S., Noble, F. & Marie, N. 2014. Opioid Receptor Desensitization: Mechanisms and Its Link to Tolerance. *Frontiers in Pharmacology,* 5.
Amato, G., Roeloffs, R., Rigdon, G. C., Antonio, B., Mersch, T., Mcnaughton-Smith, G., Wickenden, A. D., Fritch, P. & Suto, M. J. 2011. N-Pyridyl and Pyrimidine Benzamides as Kcnq2/Q3 Potassium Channel Openers for the Treatment of Epilepsy. *ACS Medicinal Chemistry Letters,* 2**,** 481-484.
Anderson, U. A., Carson, C., Johnston, L., Joshi, S., Gurney, A. M. & Mccloskey, K. D. 2013. Functional Expression of Kcnq (Kv7) Channels in Guinea Pig Bladder Smooth Muscle and Their Contribution to Spontaneous Activity. *Br J Pharmacol,* 169**,** 1290-304.
Antzelevitch, C. & Burashnikov, A. 2011. Overview of Basic Mechanisms of Cardiac Arrhythmia. *Cardiac Electrophysiology Clinics,* 3**,** 23-45.
Armstrong , C. M. 1971. Interaction of Tetraethylammonium Ion Derivatives with the Potassium Channels of Giant Axons. *Journal of General Physiology,* 58**,** 413-437.
Armstrong , C. M. & Hille , B. 1972. The Inner Quaternary Ammonium Ion Receptor in Potassium Channels of the Node of Ranvier. *Journal of General Physiology,* 59**,** 388-400.
Baculis, B. C., Zhang, J. & Chung, H. J. 2020. The Role of K(V)7 Channels in Neural Plasticity and Behavior. *Frontiers in physiology,* 11**,** 568667-568667.
Bähring, R. 2018. Kv Channel-Interacting Proteins as Neuronal and Non-Neuronal Calcium Sensors. *Channels (Austin, Tex.),* 12**,** 187-200.
Bal, M., Zhang, J., Zaika, O., Hernandez, C. C. & Shapiro, M. S. 2008. Homomeric and Heteromeric Assembly of Kcnq (Kv7) K+ Channels Assayed by Total Internal Reflection Fluorescence/Fluorescence Resonance Energy Transfer and Patch Clamp Analysis. *The Journal of biological chemistry,* 283**,** 30668-30676.
Barrese, V., Stott, J. B., Figueiredo, H. B., Aubdool, A. A., Hobbs, A. J., Jepps, T. A., Mcneish, A. J. & Greenwood, I. A. 2018. Angiotensin Ii Promotes Kv7.4 Channels Degradation through Reduced Interaction with Hsp90 (Heat Shock Protein 90). *Hypertension,* 71**,** 1091-1100.
Bartos, D. C., Giudicessi, J. R., Tester, D. J., Ackerman, M. J., Ohno, S., Horie, M., Gollob, M. H., Burgess, D. E. & Delisle, B. P. 2014. A Kcnq1 Mutation Contributes to the Concealed Type 1 Long Qt Phenotype by Limiting the Kv7.1 Channel Conformational Changes Associated with Protein Kinase a Phosphorylation. *Heart Rhythm,* 11**,** 459-468.
Beals, C. R., Clipstone, N. A., Ho, S. N. & Crabtree, G. R. 1997. Nuclear Localization of Nf-Atc by a Calcineurin-Dependent, Cyclosporin-Sensitive Intramolecular Interaction. *Genes Dev,* 11**,** 824-34.
Beisel, K. W., Nelson, N. C., Delimont, D. C. & Fritzsch, B. 2000. Longitudinal Gradients of Kcnq4 Expression in Spiral Ganglion and Cochlear Hair Cells Correlate with Progressive Hearing Loss in Dfna211. *Molecular Brain Research,* 82**,** 137-149.
Bellocq, C., Van Ginneken, A. C., Bezzina, C. R., Alders, M., Escande, D., Mannens, M. M., Baró, I. & Wilde, A. A. 2004. Mutation in the Kcnq1 Gene Leading to the Short Qt-Interval Syndrome. *Circulation,* 109**,** 2394-7.
Bendahhou, S., Marionneau, C., Haurogne, K., Larroque, M. M., Derand, R., Szuts, V., Escande, D., Demolombe, S. & Barhanin, J. 2005. In Vitro Molecular

Interactions and Distribution of Kcne Family with Kcnq1 in the Human Heart. *Cardiovasc Res,* 67**,** 529-38.
Bennett, G. J. 2001. Animal Models of Pain. *Methods in pain research,* 4**,** 67-91.
Bentzen, B. H., Schmitt, N., Calloe, K., Dalby Brown, W., Grunnet, M. & Olesen, S.-P. 2006. The Acrylamide (S)-1 Differentially Affects Kv7 (Kcnq) Potassium Channels. *Neuropharmacology,* 51**,** 1068-1077.
Bezanilla , F. & Armstrong , C. M. 1972. Negative Conductance Caused by Entry of Sodium and Cesium Ions into the Potassium Channels of Squid Axons. *Journal of General Physiology,* 60**,** 588-608.
Bientinesi, R., Mancuso, C., Martire, M., Bassi, P. F., Sacco, E. & Currò, D. 2017. K(V)7 Channels in the Human Detrusor: Channel Modulator Effects and Gene and Protein Expression. *Naunyn Schmiedebergs Arch Pharmacol,* 390**,** 127-137.
Biervert, C., Schroeder, B. C., Kubisch, C., Berkovic, S. F., Propping, P., Jentsch, T. J. & Steinlein, O. K. 1998. A Potassium Channel Mutation in Neonatal Human Epilepsy. *Science,* 279**,** 403-6.
Blackburn-Munro, G. & Jensen, B. S. 2003. The Anticonvulsant Retigabine Attenuates Nociceptive Behaviours in Rat Models of Persistent and Neuropathic Pain. *Eur J Pharmacol,* 460**,** 109-16.
Bleich, M. & Warth, R. 2000. The Very Small-Conductance K+ Channel Kvlqt1 and Epithelial Function. *Pflügers Archiv,* 440**,** 202-206.
Bock, C., Surur, A. S., Beirow, K., Kindermann, M. K., Schulig, L., Bodtke, A., Bednarski, P. J. & Link, A. 2019. Sulfide Analogues of Flupirtine and Retigabine with Nanomolar Kv7.2/Kv7.3 Channel Opening Activity. *ChemMedChem,* 14**,** 952-964.
Bosch, R. F., Gaspo, R., Busch, A. E., Lang, H. J., Li, G.-R. & Nattel, S. 1998. Effects of the Chromanol 293b, a Selective Blocker of the Slow, Component of the Delayed Rectifier K+ Current, on Repolarization in Human and Guinea Pig Ventricular Myocytes. *Cardiovascular Research,* 38**,** 441-450.
Brown, D. A., Abogadie, F. C., Allen, T. G. J., Buckley, N. J., Caulfield, M. P., Delmas, P., Haley, J. E., Lamas, J. A. & Selyanko, A. A. 1997. Muscarinic Mechanisms in Nerve Cells. *Life Sciences,* 60**,** 1137-1144.
Brown, D. A. & Adams, P. R. 1980. Muscarinic Suppression of a Novel Voltage-Sensitive K+ Current in a Vertebrate Neurone. *Nature,* 283**,** 673-676.
Brueggemann, L. I., Haick, J. M., Cribbs, L. L. & Byron, K. L. 2014a. Differential Activation of Vascular Smooth Muscle Kv7.4, Kv7.5, and Kv7.4/7.5 Channels by Ml213 and Ica-069673. *Molecular pharmacology,* 86**,** 330-341.
Brueggemann, L. I., Haick, J. M., Neuburg, S., Tate, S., Randhawa, D., Cribbs, L. L. & Byron, K. L. 2014b. Kcnq (Kv7) Potassium Channel Activators as Bronchodilators: Combination with a B2-Adrenergic Agonist Enhances Relaxation of Rat Airways. *American Journal of Physiology-Lung Cellular and Molecular Physiology,* 306**,** L476-L486.
Brueggemann, L. I., Kakad, P. P., Love, R. B., Solway, J., Dowell, M. L., Cribbs, L. L. & Byron, K. L. 2012. Kv7 Potassium Channels in Airway Smooth Muscle Cells: Signal Transduction Intermediates and Pharmacological Targets for Bronchodilator Therapy. *American journal of physiology. Lung cellular and molecular physiology,* 302**,** L120-L132.
Brueggemann, L. I., Mackie, A. R., Cribbs, L. L., Freda, J., Tripathi, A., Majetschak, M. & Byron, K. L. 2014c. Differential Protein Kinase C-Dependent Modulation

of Kv7.4 and Kv7.5 Subunits of Vascular Kv7 Channels. *The Journal of biological chemistry,* 289**,** 2099-2111.

Brueggemann, L. I., Mackie, A. R., Mani, B. K., Cribbs, L. L. & Byron, K. L. 2009. Differential Effects of Selective Cyclooxygenase-2 Inhibitors on Vascular Smooth Muscle Ion Channels May Account for Differences in Cardiovascular Risk Profiles. *Molecular pharmacology,* 76**,** 1053-1061.

Brueggemann, L. I., Mackie, A. R., Martin, J. L., Cribbs, L. L. & Byron, K. L. 2011. Diclofenac Distinguishes among Homomeric and Heteromeric Potassium Channels Composed of Kcnq4 and Kcnq5 Subunits. *Molecular pharmacology,* 79**,** 10-23.

Brueggemann, L. I., Moran, C. J., Barakat, J. A., Yeh, J. Z., Cribbs, L. L. & Byron, K. L. 2007. Vasopressin Stimulates Action Potential Firing by Protein Kinase C-Dependent Inhibition of Kcnq5 in A7r5 Rat Aortic Smooth Muscle Cells. *American journal of physiology. Heart and circulatory physiology,* 292**,** H1352-H1363.

Brummelkamp, T. R., Bernards, R. & Agami, R. 2002. A System for Stable Expression of Short Interfering Rnas in Mammalian Cells. *Science,* 296**,** 550-553.

Burgess, D. E., Bartos, D. C., Reloj, A. R., Campbell, K. S., Johnson, J. N., Tester, D. J., Ackerman, M. J., Fressart, V., Denjoy, I., Guicheney, P., Moss, A. J., Ohno, S., Horie, M. & Delisle, B. P. 2012. High-Risk Long Qt Syndrome Mutations in the Kv7.1 (Kcnq1) Pore Disrupt the Molecular Basis for Rapid K+ Permeation. *Biochemistry,* 51**,** 9076-9085.

Busch, A. E., Busch, G. L., Ford, E., Suessbrich, H., Lang, H. J., Greger, R., Kunzelmann, K., Attali, B. & Stühmer, W. 1997. The Role of the Isk Protein in the Specific Pharmacological Properties of the Iks Channel Complex. *British journal of pharmacology,* 122**,** 187-189.

Busch, A. E., Suessbrich, H., Waldegger, S., Sailer, E., Greger, R., Lang, H. J., Lang, F., Gibson, K. J. & Maylie, J. G. 1996. Inhibition of Iks in Guinea Pig Cardiac Myocytes and Guinea Pig Isk Channels by the Chromanol 293b. *Pflügers Archiv - European Journal of Physiology,* 432**,** 1094-1096.

Bushra, R. & Aslam, N. 2010. An Overview of Clinical Pharmacology of Ibuprofen. *Oman medical journal,* 25**,** 155-1661.

Caminos, E., Garcia-Pino, E., Martinez-Galan, J. R. & Juiz, J. M. 2007. The Potassium Channel Kcnq5/Kv7.5 Is Localized in Synaptic Endings of Auditory Brainstem Nuclei of the Rat. *J Comp Neurol,* 505**,** 363-78.

Carignano, C., Barila, E. P., Rías, E. I., Dionisio, L., Aztiria, E. & Spitzmaul, G. 2019. Inner Hair Cell and Neuron Degeneration Contribute to Hearing Loss in a Dfna2-Like Mouse Model. *Neuroscience,* 410**,** 202-216.

Cavaliere, S., Malik, B. R. & Hodge, J. J. L. 2013. Kcnq Channels Regulate Age-Related Memory Impairment. *PLOS ONE,* 8**,** e62445.

Chadha, P. S., Jepps, T. A., Carr, G., Stott, J. B., Zhu, H.-L., Cole, W. C. & Greenwood, I. A. 2014. Contribution of Kv7.4/Kv7.5 Heteromers to Intrinsic and Calcitonin Gene-Related Peptide Induced Cerebral Reactivity. *Arteriosclerosis, Thrombosis, and Vascular Biology,* 34**,** 887-893.

Chadha, P. S., Zunke, F., Zhu, H.-L., Davis, A. J., Jepps, T. A., Olesen, S. P., Cole, W. C., Moffatt, J. D. & Greenwood, I. A. 2012. Reduced Kcnq4-Encoded Voltage-Dependent Potassium Channel Activity Underlies Impaired B2-Adrenoceptor Mediated Relaxation of Renal Arteries in Hypertension. *Hypertension,* 59**,** 877-884.

Chaplan, S. R., Bach, F. W., Pogrel, J. W., Chung, J. M. & Yaksh, T. L. 1994. Quantitative Assessment of Tactile Allodynia in the Rat Paw. *Journal of Neuroscience Methods,* 53**,** 55-63.

Charlier, C., Singh, N. A., Ryan, S. G., Lewis, T. B., Reus, B. E., Leach, R. J. & Leppert, M. 1998. A Pore Mutation in a Novel Kqt-Like Potassium Channel Gene in an Idiopathic Epilepsy Family. *Nature Genetics,* 18**,** 53-55.

Chekole, A. T., Kassa, A. A., Yadeta, S. A. & Aytolign, H. A. 2022. Comparison of Sequential Versus Pre Mixed Administration of Intrathecal Fentanyl with Hyperbaric Bupivacaine for Patients Undergoing Elective Caesarean Section at Zewditu Memorial Referral Hospital: A Prospective Cohort Study. *Ann Med Surg (Lond),* 74**,** 103313.

Chen, L., Kurokawa, J. & Kass, R. S. 2005. Phosphorylation of the a-Kinase-Anchoring Protein Yotiao Contributes to Protein Kinase a Regulation of a Heart Potassium Channel *. *Journal of Biological Chemistry,* 280**,** 31347-31352.

Chen, Y.-H., Xu, S.-J., Bendahhou, S. D., Wang, X.-L., Wang, Y., Xu, W.-Y., Jin, H.-W., Sun, H., Su, X.-Y., Zhuang, Q.-N., Yang, Y.-Q., Li, Y.-B., Liu, Y., Xu, H.-J., Li, X.-F., Ma, N., Mou, C.-P., Chen, Z., Barhanin, J. & Huang, W. 2003. Kcnq1 Gain-of-Function Mutation in Familial Atrial Fibrillation. *Science,* 299**,** 251-254.

Church, T. W., Brown, J. T. & Marrion, N. V. 2019. B3-Adrenergic Receptor-Dependent Modulation of the Medium Afterhyperpolarization in Rat Hippocampal Ca1 Pyramidal Neurons. *Journal of Neurophysiology,* 121**,** 773-784.

Cisneros, E., Roza, C., Jackson, N. & López-García, J. A. 2015. A New Regulatory Mechanism for Kv7.2 Protein During Neuropathy: Enhanced Transport from the Soma to Axonal Terminals of Injured Sensory Neurons. *Front Cell Neurosci,* 9**,** 470.

Clark, S., Antell, A. & Kaufman, K. 2015. New Antiepileptic Medication Linked to Blue Discoloration of the Skin and Eyes. *Therapeutic advances in drug safety,* 6**,** 15-19.

Constanti, A. & Brown, D. A. 1981. M-Currents in Voltage-Clamped Mammalian Sympathetic Neurones. *Neuroscience Letters,* 24**,** 289-294.

Cooper, E. C. 2011. Made for "Anchorin": Kv7.2/7.3 (Kcnq2/Kcnq3) Channels and the Modulation of Neuronal Excitability in Vertebrate Axons. *Seminars in cell & developmental biology,* 22**,** 185-192.

Cooper, E. C., Aldape, K. D., Abosch, A., Barbaro, N. M., Berger, M. S., Peacock, W. S., Jan, Y. N. & Jan, L. Y. 2000. Colocalization and Coassembly of Two Human Brain M-Type Potassium Channel Subunits That Are Mutated in Epilepsy. *Proceedings of the National Academy of Sciences of the United States of America,* 97**,** 4914-4919.

Cooper, E. C., Harrington, E., Jan, Y. N. & Jan, L. Y. 2001. M Channel Kcnq2 Subunits Are Localized to Key Sites for Control of Neuronal Network Oscillations and Synchronization in Mouse Brain. *The Journal of neuroscience : the official journal of the Society for Neuroscience,* 21**,** 9529-9540.

Coucke, P. J., Van Hauwe, P., Kelley, P. M., Kunst, H., Schatteman, I., Van Velzen, D., Meyers, J., Ensink, R. J., Verstreken, M., Declau, F., Marres, H., Kastury, K., Bhasin, S., Mcguirt, W. T., Smith, R. J. H., Cremers, C. W. R. J., Van De Heyning, P., Willems, P. J., Smith, S. D. & Van Camp, G. 1999. Mutations in the Kcnq4 Gene Are Responsible for Autosomal Dominant Deafness in Four Dfna2 Families. *Human Molecular Genetics,* 8**,** 1321-1328.

Coutinho, A. E. & Chapman, K. E. 2011. The Anti-Inflammatory and Immunosuppressive Effects of Glucocorticoids, Recent Developments and Mechanistic Insights. *Molecular and cellular endocrinology,* 335**,** 2-13.
Cramer, J. 2021. Radmodules Lumbar Puncture.
Crump, S. & Abbott, G. 2014. Arrhythmogenic Kcne Gene Variants: Current Knowledge and Future Challenges. *Frontiers in Genetics,* 5.
Cruzblanca, H., Koh, D. S. & Hille, B. 1998. Bradykinin Inhibits M Current Via Phospholipase C and Ca2+ Release from Ip3-Sensitive Ca2+ Stores in Rat Sympathetic Neurons. *Proceedings of the National Academy of Sciences of the United States of America,* 95**,** 7151-7156.
D'mello, R. & Dickenson, A. H. 2008. Spinal Cord Mechanisms of Pain. *British Journal of Anaesthesia,* 101**,** 8-16.
Dahimène, S., Alcoléa, S., Naud, P., Jourdon, P., Escande, D., Brasseur, R., Thomas, A., Baró, I. & Mérot, J. 2006. The N-Terminal Juxtamembranous Domain of Kcnq1 Is Critical for Channel Surface Expression. *Circulation Research,* 99**,** 1076-1083.
Davies, P. J., Thomas, E. A. & Bornstein, J. C. 2006. Different Types of Potassium Channels Underlie the Long Afterhyperpolarization in Guinea-Pig Sympathetic and Enteric Neurons. *Auton Neurosci,* 124**,** 26-30.
De Souza, C. P., Dos Santos, M. G. G., Hamani, C. & Fonoff, E. T. 2018. Spinal Cord Stimulation for Gait Dysfunction in Parkinson's Disease: Essential Questions to Discuss. *Movement Disorders,* 33**,** 1828-1829.
Dedek, K., Kunath, B., Kananura, C., Reuner, U., Jentsch, T. J. & Steinlein, O. K. 2001. Myokymia and Neonatal Epilepsy Caused by a Mutation in the Voltage Sensor of the Kcnq2 K+ Channel. *Proceedings of the National Academy of Sciences of the United States of America,* 98**,** 12272-12277.
Dedek, K. & Waldegger, S. 2001. Colocalization of Kcnq1/Kcne Channel Subunits in the Mouse Gastrointestinal Tract. *Pflügers Archiv,* 442**,** 896-902.
Degenhardt, L. & Hall, W. D. 2008. The Adverse Effects of Cannabinoids: Implications for Use of Medical Marijuana. *Canadian Medical Association Journal,* 178**,** 1685.
Delmas, P. & Brown, D. A. 2002. Junctional Signaling Microdomains: Bridging the Gap between the Neuronal Cell Surface and Ca2+ Stores. *Neuron,* 36**,** 787-790.
Delmas, P. & Brown, D. A. 2005. Pathways Modulating Neural Kcnq/M (Kv7) Potassium Channels. *Nature Reviews Neuroscience,* 6**,** 850-862.
Demolombe, S., Franco, D., Boer, P. D., Kuperschmidt, S., Roden, D., Pereon, Y., Jarry, A., Moorman, A. F. M. & Escande, D. 2001. Differential Expression of Kvlqt1 and Its Regulator Isk in Mouse Epithelia. *American Journal of Physiology-Cell Physiology,* 280**,** C359-C372.
Desaix, P., Betts, G. J., Johnson, E., Johnson, J. E., Oksana, K., Kruse, D. H., Poe, B., Wise, J. A. & Young, K. A. 2013. Anatomy & Physiology (Openstax).
Devaux, J. J., Kleopa, K. A., Cooper, E. C. & Scherer, S. S. 2004. Kcnq2 Is a Nodal K+ Channel. *The Journal of neuroscience : the official journal of the Society for Neuroscience,* 24**,** 1236-1244.
Dickenson, A. H. & Sullivan, A. F. 1987. Evidence for a Role of the Nmda Receptor in the Frequency Dependent Potentiation of Deep Rat Dorsal Horn Nociceptive Neurones Following C Fibre Stimulation. *Neuropharmacology,* 26**,** 1235-8.
Ding, S., Ingleby, L., Ahern, C. A. & Horn, R. 2005. Investigating the Putative Glycine Hinge in Shaker Potassium Channel. *The Journal of general physiology,* 126**,** 213-226.

Dixon, W. J. 1980. Efficient Analysis of Experimental Observations. *Annual Review of Pharmacology and Toxicology,* 20**,** 441-462.
Djouhri, L., Malki, M. I., Zeidan, A., Nagi, K. & Smith, T. 2019. Activation of K(V)7 Channels with the Anticonvulsant Retigabine Alleviates Neuropathic Pain Behaviour in the Streptozotocin Rat Model of Diabetic Neuropathy. *J Drug Target,* 27**,** 1118-1126.
Djouhri, L., Zeidan, A. & Abd El-Aleem, S. A. 2020. Changes in Expression of Kv7.5 and Kv7.2 Channels in Dorsal Root Ganglion Neurons in the Streptozotocin Rat Model of Painful Diabetic Neuropathy. *Neuroscience Letters,* 736**,** 135277.
Doan, R. A. & Monk, K. R. 2019. Glia in the Skin Activate Pain Responses. *Science,* 365**,** 641-642.
Dost, R., Rostock, A. & Rundfeldt, C. 2004. The Anti-Hyperalgesic Activity of Retigabine Is Mediated by Kcnq Potassium Channel Activation. *Naunyn-Schmiedeberg's Archives of Pharmacology,* 369**,** 382-390.
Doyle, A., Mcgarry, M. P., Lee, N. A. & Lee, J. J. 2012. The Construction of Transgenic and Gene Knockout/Knockin Mouse Models of Human Disease. *Transgenic research,* 21**,** 327-349.
Doyle, D. A., Cabral, J. M., Pfuetzner, R. A., Kuo, A., Gulbis, J. M., Cohen, S. L., Chait, B. T. & Mackinnon, R. 1998. The Structure of the Potassium Channel: Molecular Basis of K+ Conduction and Selectivity. *Science,* 280**,** 69-77.
Dray, A. 1995. Inflammatory Mediators of Pain. *British Journal of Anaesthesia,* 75**,** 125-131.
Du, X., Gao, H., Jaffe, D., Zhang, H. & Gamper, N. 2018. M-Type K(+) Channels in Peripheral Nociceptive Pathways. *British journal of pharmacology,* 175**,** 2158-2172.
Du, X., Hao, H., Gigout, S., Huang, D., Yang, Y., Li, L., Wang, C., Sundt, D., Jaffe, D. B., Zhang, H. & Gamper, N. 2014. Control of Somatic Membrane Potential in Nociceptive Neurons and Its Implications for Peripheral Nociceptive Transmission. *PAIN,* 155**,** 2306-2322.
Du, X., Hao, H., Yang, Y., Huang, S., Wang, C., Gigout, S., Ramli, R., Li, X., Jaworska, E., Edwards, I., Deuchars, J., Yanagawa, Y., Qi, J., Guan, B., Jaffe, D. B., Zhang, H. & Gamper, N. 2017. Local Gabaergic Signaling within Sensory Ganglia Controls Peripheral Nociceptive Transmission. *The Journal of Clinical Investigation,* 127**,** 1741-1756.
Du, X. N., Zhang, X., Qi, J. L., An, H. L., Li, J. W., Wan, Y. M., Fu, Y., Gao, H. X., Gao, Z. B., Zhan, Y. & Zhang, H. L. 2011. Characteristics and Molecular Basis of Celecoxib Modulation on K(V)7 Potassium Channels. *British journal of pharmacology,* 164**,** 1722-1737.
Durell, S. R. & Guy, H. R. 2001. A Putative Prokaryote Voltage-Gated Ca(2+) Channel with Only One 6tm Motif Per Subunit. *Biochem Biophys Res Commun,* 281**,** 741-6.
Eisenman, G. 1962. Cation Selective Glass Electrodes and Their Mode of Operation. *Biophysical journal,* 2**,** 259-323.
El-Brolosy, M. A. & Stainier, D. Y. R. 2017. Genetic Compensation: A Phenomenon in Search of Mechanisms. *PLoS genetics,* 13**,** e1006780-e1006780.
Elsharkawy, H., Maheshwari, A., Babazade, R., Perlas, A., Zaky, S. & Mounir-Soliman, L. 2017. Real-Time Ultrasound-Guided Spinal Anesthesia in Patients with Predicted Difficult Anatomy. *Minerva Anestesiol,* 83**,** 465-473.

Emery, E. C. & Ernfors, P. 2020. Dorsal Root Ganglion Neuron Types and Their Functional Specialization. *The Oxford Handbook of the Neurobiology of Pain*, 129.

Etxeberria, A., Aivar, P., Rodriguez-Alfaro, J. A., Alaimo, A., Villace, P., Gomez-Posada, J. C., Areso, P. & Villarroel, A. 2008. Calmodulin Regulates the Trafficking of Kcnq2 Potassium Channels. *The FASEB Journal,* 22**,** 1135-1143.

Etxeberria, A., Santana-Castro, I., Regalado, M. P., Aivar, P. & Villarroel, A. 2004. Three Mechanisms Underlie Kcnq2/3 Heteromeric Potassium M-Channel Potentiation. *The Journal of neuroscience : the official journal of the Society for Neuroscience,* 24**,** 9146-9152.

Fehrenbacher, J. C., Vasko, M. R. & Duarte, D. B. 2012. Models of Inflammation: Carrageenan- or Complete Freund's Adjuvant (Cfa)-Induced Edema and Hypersensitivity in the Rat. *Current protocols in pharmacology,* Chapter 5**,** Unit5.4-Unit5.4.

Fontana, D. J., Inouye, G. T. & Johnson, R. M. 1994. Linopirdine (Dup 996) Improves Performance in Several Tests of Learning and Memory by Modulation of Cholinergic Neurotransmission. *Pharmacol Biochem Behav,* 49**,** 1075-82.

Fosmo, A. L. & Skraastad, Ø. B. 2017. The Kv7 Channel and Cardiovascular Risk Factors. *Frontiers in cardiovascular medicine,* 4**,** 75-75.

Friedman, A. K., Juarez, B., Ku, S. M., Zhang, H., Calizo, R. C., Walsh, J. J., Chaudhury, D., Zhang, S., Hawkins, A., Dietz, D. M., Murrough, J. W., Ribadeneira, M., Wong, E. H., Neve, R. L. & Han, M.-H. 2016. Kcnq Channel Openers Reverse Depressive Symptoms Via an Active Resilience Mechanism. *Nature Communications,* 7**,** 11671.

Fu, R., Mei, Q., Shiwalkar, N., Zuo, W., Zhang, H., Gregor, D., Patel, S. & Ye, J.-H. 2020. Anxiety During Alcohol Withdrawal Involves 5-Ht2c Receptors and M-Channels in the Lateral Habenula. *Neuropharmacology,* 163**,** 107863.

Gamper, N., Fillon, S., Huber, S. M., Feng, Y., Kobayashi, T., Cohen, P. & Lang, F. 2002. Igf-1 up-Regulates K+ Channels Via Pi3-Kinase, Pdk1 and Sgk1. *Pflugers Arch,* 443**,** 625-34.

Gamper, N., Li, Y. & Shapiro, M. S. 2005. Structural Requirements for Differential Sensitivity of Kcnq K+ Channels to Modulation by Ca2+/Calmodulin. *Molecular biology of the cell,* 16**,** 3538-3551.

Gamper, N. & Shapiro, Mark s. 2015. Kcnq Channels. *In:* Zheng, J. & Trudeau, M. C. (eds.) *Handbook of Ion Channels.* Boca Raton, FL: CRC Press.

Gamper, N., Stockand, J. D. & Shapiro, M. S. 2003a. Subunit-Specific Modulation of Kcnq Potassium Channels by Src Tyrosine Kinase. *The Journal of neuroscience : the official journal of the Society for Neuroscience,* 23**,** 84-95.

Gamper, N., Stockand, J. D. & Shapiro, M. S. 2003b. Subunit-Specific Modulation of Kcnq Potassium Channels by Src Tyrosine Kinase. *The Journal of Neuroscience,* 23**,** 84.

Gamper, N., Zaika, O., Li, Y., Martin, P., Hernandez, C. C., Perez, M. R., Wang, A. Y. C., Jaffe, D. B. & Shapiro, M. S. 2006. Oxidative Modification of M-Type K(+) Channels as a Mechanism of Cytoprotective Neuronal Silencing. *The EMBO journal,* 25**,** 4996-5004.

Gan, L. & Kaczmarek, L. K. 1998. When, Where, and How Much? Expression of the Kv3.1 Potassium Channel in High-Frequency Firing Neurons. *J Neurobiol,* 37**,** 69-79.

Gao, H., Boillat, A., Huang, D., Liang, C., Peers, C. & Gamper, N. 2017. Intracellular Zinc Activates Kcnq Channels by Reducing Their Dependence on

Phosphatidylinositol 4,5-Bisphosphate. *Proceedings of the National Academy of Sciences of the United States of America,* 114**,** E6410-E6419.
Gao, Y., Yechikov, S., Vázquez, A. E., Chen, D. & Nie, L. 2013. Impaired Surface Expression and Conductance of the Kcnq4 Channel Lead to Sensorineural Hearing Loss. *Journal of Cellular and Molecular Medicine,* 17**,** 889-900.
Gao, Z., Zhang, T., Wu, M., Xiong, Q., Sun, H., Zhang, Y., Zu, L., Wang, W. & Li, M. 2010. Isoform-Specific Prolongation of Kv7 (Kcnq) Potassium Channel Opening Mediated by New Molecular Determinants for Drug-Channel Interactions. *The Journal of biological chemistry,* 285**,** 28322-28332.
Gentet, L. J., Stuart, G. J. & Clements, J. D. 2000. Direct Measurement of Specific Membrane Capacitance in Neurons. *Biophysical Journal,* 79**,** 314-320.
Ghosh, S., Nunziato, D. A. & Pitt, G. S. 2006. Kcnq1 Assembly and Function Is Blocked by Long-Qt Syndrome Mutations That Disrupt Interaction with Calmodulin. *Circulation Research,* 98**,** 1048-1054.
Gilling, M., Rasmussen, H. B., Calloe, K., Sequeira, A. F., Baretto, M., Oliveira, G., Almeida, J., Lauritsen, M. B., Ullmann, R., Boonen, S. E., Brondum-Nielsen, K., Kalscheuer, V. M., Tümer, Z., Vicente, A. M., Schmitt, N. & Tommerup, N. 2013. Dysfunction of the Heteromeric Kv7.3/Kv7.5 Potassium Channel Is Associated with Autism Spectrum Disorders. *Front Genet,* 4**,** 54.
Godel, T., Pham, M., Heiland, S., Bendszus, M. & Bäumer, P. 2016. Human Dorsal-Root-Ganglion Perfusion Measured in-Vivo by Mri. *Neuroimage,* 141**,** 81-87.
Gold, M. S. & Traub, R. J. 2004. Cutaneous and Colonic Rat Drg Neurons Differ with Respect to Both Baseline and Pge2-Induced Changes in Passive and Active Electrophysiological Properties. *J Neurophysiol,* 91**,** 2524-31.
Goldman-Rakic, P. S. 1995. Cellular Basis of Working Memory. *Neuron,* 14**,** 477-85.
Goldman, A. M., Glasscock, E., Yoo, J., Chen, T. T., Klassen, T. L. & Noebels, J. L. 2009. Arrhythmia in Heart and Brain: Kcnq1 Mutations Link Epilepsy and Sudden Unexplained Death. *Science translational medicine,* 1**,** 2ra6-2ra6.
Goldman , D. E. 1965. Gate Control of Ion Flux in Axons. *Journal of General Physiology,* 48**,** 75-77.
Gould, H. J., 3rd, England, J. D., Liu, Z. P. & Levinson, S. R. 1998. Rapid Sodium Channel Augmentation in Response to Inflammation Induced by Complete Freund's Adjuvant. *Brain Res,* 802**,** 69-74.
Gould, H. J., Iii 2000. Complete Freund's Adjuvant-Induced Hyperalgesia: A Human Perception. *PAIN,* 85.
Grahammer, F., Wittekindt, O. H., Nitschke, R., Herling, A. W., Lang, H. J., Bleich, M., Schmitt–Gräff, A., Barhanin, J. & Warth, R. 2001. The Cardiac K+ Channel Kcnq1 Is Essential for Gastric Acid Secretion. *Gastroenterology,* 120**,** 1363-1371.
Greene, D. L., Kang, S. & Hoshi, N. 2017. Xe991 and Linopirdine Are State-Dependent Inhibitors for Kv7/Kcnq Channels That Favor Activated Single Subunits. *The Journal of pharmacology and experimental therapeutics,* 362**,** 177-185.
Greene, D. L., Kosenko, A. & Hoshi, N. 2018. Attenuating M-Current Suppression in Vivo by a Mutant Kcnq2 Gene Knock-in Reduces Seizure Burden and Prevents Status Epilepticus-Induced Neuronal Death and Epileptogenesis. *Epilepsia,* 59**,** 1908-1918.
Gu, N., Vervaeke, K., Hu, H. & Storm, J. F. 2005. Kv7/Kcnq/M and Hcn/H, but Not Kca2/Sk Channels, Contribute to the Somatic Medium after-Hyperpolarization and Excitability Control in Ca1 Hippocampal Pyramidal Cells. *The Journal of Physiology,* 566**,** 689-715.

Guerrero, A. P. 2007. Centipede Bites in Hawai'i: A Brief Case Report and Review of the Literature. *Hawaii Med J,* 66**,** 125-7.
Gunthorpe, M. J., Large, C. H. & Sankar, R. 2012. The Mechanism of Action of Retigabine (Ezogabine), a First-in-Class K+ Channel Opener for the Treatment of Epilepsy. *Epilepsia,* 53**,** 412-24.
Gurumurthy, C. B. & Lloyd, K. C. K. 2019. Generating Mouse Models for Biomedical Research: Technological Advances. *Disease Models & Mechanisms,* 12.
Hadley, J. K., Noda, M., Selyanko, A. A., Wood, I. C., Abogadie, F. C. & Brown, D. A. 2000. Differential Tetraethylammonium Sensitivity of Kcnq1-4 Potassium Channels. *British journal of pharmacology,* 129**,** 413-415.
Haick, J. M., Brueggemann, L. I., Cribbs, L. L., Denning, M. F., Schwartz, J. & Byron, K. L. 2017. Pkc-Dependent Regulation of Kv7.5 Channels by the Bronchoconstrictor Histamine in Human Airway Smooth Muscle Cells. *American Journal of Physiology-Lung Cellular and Molecular Physiology,* 312**,** L822-L834.
Hamada, K., Matsuura, H., Sanada, M., Toyoda, F., Omatsu-Kanbe, M., Kashiwagi, A. & Yasuda, H. 2003. Properties of the Na+/K+ Pump Current in Small Neurons from Adult Rat Dorsal Root Ganglia. *British journal of pharmacology,* 138**,** 1517-1527.
Hammami Bomholtz, S., Refaat, M., Buur Steffensen, A., David, J.-P., Espinosa, K., Nussbaum, R., Wojciak, J., Hjorth Bentzen, B., Scheinman, M. & Schmitt, N. 2020. Functional Phenotype Variations of Two Novel Kv7.1 Mutations Identified in Patients with Long Qt Syndrome. *Pacing and Clinical Electrophysiology,* 43**,** 210-216.
Hansen, H. H., Andreasen, J. T., Weikop, P., Mirza, N., Scheel-Krüger, J. & Mikkelsen, J. D. 2007. The Neuronal Kcnq Channel Opener Retigabine Inhibits Locomotor Activity and Reduces Forebrain Excitatory Responses to the Psychostimulants Cocaine, Methylphenidate and Phencyclidine. *Eur J Pharmacol,* 570**,** 77-88.
Hargreaves, K., Dubner, R., Brown, F., Flores, C. & Joris, J. 1988. A New and Sensitive Method for Measuring Thermal Nociception in Cutaneous Hyperalgesia. *PAIN,* 32**,** 77-88.
Harish, S., Bhuvana, K., Bengalorkar, G. M. & Kumar, T. 2012. Flupirtine: Clinical Pharmacology. *Journal of anaesthesiology, clinical pharmacology,* 28**,** 172-177.
Harraz, O. F., Hill-Eubanks, D. & Nelson, M. T. 2020. Pip₂: A Critical Regulator of Vascular Ion Channels Hiding in Plain Sight. *Proceedings of the National Academy of Sciences,* 117**,** 20378-20389.
Hawkey, C. J. 2001. Cox-1 and Cox-2 Inhibitors. *Best Pract Res Clin Gastroenterol,* 15**,** 801-20.
Hayashi, H., Iwata, M., Tsuchimori, N. & Matsumoto, T. 2014. Activation of Peripheral Kcnq Channels Attenuates Inflammatory Pain. *Molecular pain,* 10**,** 15-15.
Hedegaard, E. R., Nielsen, B. D., Kun, A., Hughes, A. D., Krøigaard, C., Mogensen, S., Matchkov, V. V., Fröbert, O. & Simonsen, U. 2014. Kv 7 Channels Are Involved in Hypoxia-Induced Vasodilatation of Porcine Coronary Arteries. *British journal of pharmacology,* 171**,** 69-82.
Heer, F. T., Posson, D. J., Wojtas-Niziurski, W., Nimigean, C. M. & Bernèche, S. 2017. Mechanism of Activation at the Selectivity Filter of the Kcsa K+ Channel. *eLife,* 6**,** e25844.
Heginbotham, L., Lu, Z., Abramson, T. & Mackinnon, R. 1994. Mutations in the K+ Channel Signature Sequence. *Biophysical journal,* 66**,** 1061-1067.

Heginbotham, L. & Mackinnon, R. 1992. The Aromatic Binding Site for Tetraethylammonium Ion on Potassium Channels. *Neuron,* 8**,** 483-91.
Heidenreich, M., Lechner, S. G., Vardanyan, V., Wetzel, C., Cremers, C. W., De Leenheer, E. M., Aránguez, G., Moreno-Pelayo, M. Á., Jentsch, T. J. & Lewin, G. R. 2012. Kcnq4 K+ Channels Tune Mechanoreceptors for Normal Touch Sensation in Mouse and Man. *Nature Neuroscience,* 15**,** 138-145.
Heitzmann, D., Grahammer, F., Von Hahn, T., Schmitt-Gräff, A., Romeo, E., Nitschke, R., Gerlach, U., Lang, H. J., Verrey, F., Barhanin, J. & Warth, R. 2004. Heteromeric Kcne2/Kcnq1 Potassium Channels in the Luminal Membrane of Gastric Parietal Cells. *The Journal of Physiology,* 561**,** 547-557.
Hille , B. 1973. Potassium Channels in Myelinated Nerve : Selective Permeability to Small Cations. *Journal of General Physiology,* 61**,** 669-686.
Hille, B. 1978. Ionic Channels in Excitable Membranes. Current Problems and Biophysical Approaches. *Biophysical journal,* 22**,** 283-294.
Hille , B. 2001. *Ion Channels of Excitable Membranes*, Sinauer Associates.
Hille, B., Armstrong, C. M. & Mackinnon, R. 1999. Ion Channels: From Idea to Reality. *Nature medicine,* 5**,** 1105-1109.
Hirano, K., Kuratani, K., Fujiyoshi, M., Tashiro, N., Hayashi, E. & Kinoshita, M. 2007. Kv7.2–7.5 Voltage-Gated Potassium Channel (Kcnq2–5) Opener, Retigabine, Reduces Capsaicin-Induced Visceral Pain in Mice. *Neuroscience Letters,* 413**,** 159-162.
Hodgkin, A. L. & Huxley, A. F. 1952. A Quantitative Description of Membrane Current and Its Application to Conduction and Excitation in Nerve. *The Journal of physiology,* 117**,** 500-544.
Hogea, A., Shah, S., Jones, F., Carver, C. M., Hao, H., Liang, C., Huang, D., Du, X. & Gamper, N. 2021. Junctophilin-4 Facilitates Inflammatory Signalling at Plasma Membrane-Endoplasmic Reticulum Junctions in Sensory Neurons. *The Journal of Physiology,* 599**,** 2103-2123.
Holmes, C. L., Landry, D. W. & Granton, J. T. 2003. Science Review: Vasopressin and the Cardiovascular System Part 1 – Receptor Physiology. *Critical Care,* 7**,** 427.
Holt, J. R. & Corey, D. P. 1999. Ion Channel Defects in Hereditary Hearing Loss. *Neuron,* 22**,** 217-219.
Holt, J. R., Stauffer, E. A., Abraham, D. & Géléoc, G. S. G. 2007. Dominant-Negative Inhibition of M-Like Potassium Conductances in Hair Cells of the Mouse Inner Ear. *The Journal of Neuroscience,* 27**,** 8940.
Horikawa, N., Suzuki, T., Uchiumi, T., Minamimura, T., Tsukada, K., Takeguchi, N. & Sakai, H. 2005. Cyclic Amp-Dependent Cl- Secretion Induced by Thromboxane A2 in Isolated Human Colon. *The Journal of physiology,* 562**,** 885-897.
Horowitz, L. F., Hirdes, W., Suh, B.-C., Hilgemann, D. W., Mackie, K. & Hille, B. 2005. Phospholipase C in Living Cells: Activation, Inhibition, Ca2+ Requirement, and Regulation of M Current. *The Journal of general physiology,* 126**,** 243-262.
Hoshi, N., Zhang, J.-S., Omaki, M., Takeuchi, T., Yokoyama, S., Wanaverbecq, N., Langeberg, L. K., Yoneda, Y., Scott, J. D., Brown, D. A. & Higashida, H. 2003. Akap150 Signaling Complex Promotes Suppression of the M-Current by Muscarinic Agonists. *Nature Neuroscience,* 6**,** 564-571.
Howard, R. J., Clark, K. A., Holton, J. M. & Minor, D. L., Jr. 2007. Structural Insight into Kcnq (Kv7) Channel Assembly and Channelopathy. *Neuron,* 53**,** 663-675.
Iannotti, F. A., Barrese, V., Formisano, L., Miceli, F. & Taglialatela, M. 2013. Specification of Skeletal Muscle Differentiation by Repressor Element-1

Silencing Transcription Factor (Rest)-Regulated Kv7.4 Potassium Channels. *Molecular biology of the cell,* 24**,** 274-284.

Iannotti, F. A., Panza, E., Barrese, V., Viggiano, D., Soldovieri, M. V. & Taglialatela, M. 2010. Expression, Localization, and Pharmacological Role of Kv7 Potassium Channels in Skeletal Muscle Proliferation, Differentiation, and Survival after Myotoxic Insults. *J Pharmacol Exp Ther,* 332**,** 811-20.

Israelachvili, J. N. 2011. 4 - Interactions Involving Polar Molecules. *In:* Israelachvili, J. N. (ed.) *Intermolecular and Surface Forces (Third Edition).* San Diego: Academic Press.

Jacobson, D. A. & Philipson, L. H. 2007. Action Potentials and Insulin Secretion: New Insights into the Role of Kv Channels. *Diabetes Obes Metab,* 9 Suppl 2**,** 89-98.

Jensen, H. S., Callø, K., Jespersen, T., Jensen, B. S. & Olesen, S.-P. 2005. The Kcnq5 Potassium Channel from Mouse: A Broadly Expressed M-Current Like Potassium Channel Modulated by Zinc, Ph, and Volume Changes. *Molecular Brain Research,* 139**,** 52-62.

Jepps, T. A., Chadha, P. S., Davis, A. J., Harhun, M. I., Cockerill, G. W., Olesen, S. P., Hansen, R. S. & Greenwood, I. A. 2011. Downregulation of Kv7.4 Channel Activity in Primary and Secondary Hypertension. *Circulation,* 124**,** 602-11.

Jepps, T. A., Greenwood, I. A., Moffatt, J. D., Sanders, K. M. & Ohya, S. 2009. Molecular and Functional Characterization of Kv7 K+ Channel in Murine Gastrointestinal Smooth Muscles. *American journal of physiology. Gastrointestinal and liver physiology,* 297**,** G107-G115.

Jia, Z., Bei, J., Rodat-Despoix, L., Liu, B., Jia, Q., Delmas, P. & Zhang, H. 2008. Ngf Inhibits M/Kcnq Currents and Selectively Alters Neuronal Excitability in Subsets of Sympathetic Neurons Depending on Their M/Kcnq Current Background. *The Journal of general physiology,* 131**,** 575-587.

Jiang, Y., Lee, A., Chen, J., Cadene, M., Chait, B. T. & Mackinnon, R. 2002. The Open Pore Conformation of Potassium Channels. *Nature,* 417**,** 523-526.

Jin, X., Shah, S., Liu, Y., Zhang, H., Lees, M., Fu, Z., Lippiat, J. D., Beech, D. J., Sivaprasadarao, A., Baldwin, S. A., Zhang, H. & Gamper, N. 2013. Activation of the Cl- Channel Ano1 by Localized Calcium Signals in Nociceptive Sensory Neurons Requires Coupling with the Ip3 Receptor. *Science signaling,* 6**,** ra73-ra73.

Jones, F., Gamper, N. & Gao, H. 2021. Kv7 Channels and Excitability Disorders. Berlin, Heidelberg: Springer Berlin Heidelberg.

Kaczmarek, L. K. & Blumenthal, E. M. 1997. Properties and Regulation of the Mink Potassium Channel Protein. *Physiological Reviews,* 77**,** 627-641.

Kamb, A., Iverson, L. E. & Tanouye, M. A. 1987. Molecular Characterization of Shaker, a Drosophila Gene That Encodes a Potassium Channel. *Cell,* 50**,** 405-13.

Kanda, H. & Gu, J. G. 2017. Effects of Cold Temperatures on the Excitability Of rat Trigeminal Ganglion Neurons That Are Not For cold Sensing. *Journal of Neurochemistry,* 141**,** 532-543.

Kang, C., Tian, C., Sönnichsen, F. D., Smith, J. A., Meiler, J., George, A. L., Jr., Vanoye, C. G., Kim, H. J. & Sanders, C. R. 2008. Structure of Kcne1 and Implications for How It Modulates the Kcnq1 Potassium Channel. *Biochemistry,* 47**,** 7999-8006.

Kang, P. W., Westerlund, A. M., Shi, J., White, K. M., Dou, A. K., Cui, A. H., Silva, J. R., Delemotte, L. & Cui, J. 2020. Calmodulin Acts as a State-Dependent Switch to Control a Cardiac Potassium Channel Opening. *Science advances,* 6**,** eabd6798.

Kang, S., Li, J., Zuo, W., Fu, R., Gregor, D., Krnjevic, K., Bekker, A. & Ye, J.-H. 2017. Ethanol Withdrawal Drives Anxiety-Related Behaviors by Reducing M-Type Potassium Channel Activity in the Lateral Habenula. *Neuropsychopharmacology,* 42**,** 1813-1824.

Kendall, D. A. & Yudowski, G. A. 2017. Cannabinoid Receptors in the Central Nervous System: Their Signaling and Roles in Disease. *Frontiers in Cellular Neuroscience,* 10.

Kerr, R. C., Maxwell, D. J. & Todd, A. J. 1998. Glur1 and Glur2/3 Subunits of the Ampa-Type Glutamate Receptor Are Associated with Particular Types of Neurone in Laminae I-Iii of the Spinal Dorsal Horn of the Rat. *Eur J Neurosci,* 10**,** 324-33.

Kharkovets, T., Dedek, K., Maier, H., Schweizer, M., Khimich, D., Nouvian, R., Vardanyan, V., Leuwer, R., Moser, T. & Jentsch, T. J. 2006. Mice with Altered Kcnq4 K+ Channels Implicate Sensory Outer Hair Cells in Human Progressive Deafness. *The EMBO Journal,* 25**,** 642-652.

Kharkovets, T., Hardelin, J.-P., Safieddine, S., Schweizer, M., El-Amraoui, A., Petit, C. & Jentsch, T. J. 2000. Kcnq4, a K+ Channel Mutated in a Form of Dominant Deafness, Is Expressed in the Inner Ear and the Central Auditory Pathway. *Proceedings of the National Academy of Sciences,* 97**,** 4333.

Kim, D. M. & Nimigean, C. M. 2016. Voltage-Gated Potassium Channels: A Structural Examination of Selectivity and Gating. *Cold Spring Harbor perspectives in biology,* 8**,** a029231.

Kim, E. C., Patel, J., Zhang, J., Soh, H., Rhodes, J. S., Tzingounis, A. V. & Chung, H. J. 2020. Heterozygous Loss of Epilepsy Gene Kcnq2 Alters Social, Repetitive and Exploratory Behaviors. *Genes Brain Behav,* 19**,** e12599.

Kim, K. W., Kim, K., Lee, H. & Suh, B. C. 2019. Ethanol Elevates Excitability of Superior Cervical Ganglion Neurons by Inhibiting Kv7 Channels in a Cell Type-Specific and Pi(4,5)P(2)-Dependent Manner. *Int J Mol Sci,* 20.

King, B. F. & Szurszewski, J. H. 1988. Effects of Potassium Channel-Blocking Agents on Neurons in the Inferior Mesenteric Ganglion in Guinea-Pig. *Journal of the Autonomic Nervous System,* 23**,** 241-252.

King, C. H., Lancaster, E., Salomon, D., Peles, E. & Scherer, S. S. 2014. Kv7.2 Regulates the Function of Peripheral Sensory Neurons. *The Journal of comparative neurology,* 522**,** 3262-3280.

King, C. H. & Scherer, S. S. 2012. Kv7.5 Is the Primary Kv7 Subunit Expressed in C-Fibers. *The Journal of comparative neurology,* 520**,** 1940-1950.

Klinger, F., Geier, P., Dorostkar, M. M., Chandaka, G. K., Yousuf, A., Salzer, I., Kubista, H. & Boehm, S. 2012. Concomitant Facilitation of Gabaa Receptors and Kv7 Channels by the Non-Opioid Analgesic Flupirtine. *British journal of pharmacology,* 166**,** 1631-1642.

Klinger, F., Gould, G., Boehm, S. & Shapiro, M. S. 2011. Distribution of M-Channel Subunits Kcnq2 and Kcnq3 in Rat Hippocampus. *NeuroImage,* 58**,** 761-769.

Knapp, C. M., O'malley, M., Datta, S. & Ciraulo, D. A. 2014. The Kv7 Potassium Channel Activator Retigabine Decreases Alcohol Consumption in Rats. *Am J Drug Alcohol Abuse,* 40**,** 244-50.

Korsgaard, M. P., Hartz, B. P., Brown, W. D., Ahring, P. K., Strøbaek, D. & Mirza, N. R. 2005. Anxiolytic Effects of Maxipost (Bms-204352) and Retigabine Via Activation of Neuronal Kv7 Channels. *J Pharmacol Exp Ther,* 314**,** 282-92.

Kosenko, A. & Hoshi, N. 2013. A Change in Configuration of the Calmodulin-Kcnq Channel Complex Underlies Ca2+-Dependent Modulation of Kcnq Channel Activity. *PLOS ONE,* 8**,** e82290.

Kosenko, A., Moftakhar, S., Wood, M. A. & Hoshi, N. 2020. In Vivo Attenuation of M-Current Suppression Impairs Consolidation of Object Recognition Memory. *The Journal of Neuroscience,* 40**,** 5847.

Koyama, S., Brodie, M. S. & Appel, S. B. 2007. Ethanol Inhibition of M-Current and Ethanol-Induced Direct Excitation of Ventral Tegmental Area Dopamine Neurons. *J Neurophysiol,* 97**,** 1977-85.

Krishnan, V., Han, M.-H., Graham, D. L., Berton, O., Renthal, W., Russo, S. J., Laplant, Q., Graham, A., Lutter, M., Lagace, D. C., Ghose, S., Reister, R., Tannous, P., Green, T. A., Neve, R. L., Chakravarty, S., Kumar, A., Eisch, A. J., Self, D. W., Lee, F. S., Tamminga, C. A., Cooper, D. C., Gershenfeld, H. K. & Nestler, E. J. 2007. Molecular Adaptations Underlying Susceptibility and Resistance to Social Defeat in Brain Reward Regions. *Cell,* 131**,** 391-404.

Kubisch, C., Schroeder, B. C., Friedrich, T., Lütjohann, B., El-Amraoui, A., Marlin, S., Petit, C. & Jentsch, T. J. 1999. Kcnq4, a Novel Potassium Channel Expressed in Sensory Outer Hair Cells, Is Mutated in Dominant Deafness. *Cell,* 96**,** 437-446.

Laing, T., Siddiqui, A. & Sood, M. 2015. The Management of Neuropathic Pain from Neuromas in the Upper Limb: Surgical Techniques and Future Directions. *Plastic and Aesthetic Research,* 2**,** 165-170.

Lang, H. 2016. Loss, Degeneration, and Preservation of the Spiral Ganglion Neurons and Their Processes. *In:* Dabdoub, A., Fritzsch, B., Popper, A. N. & Fay, R. R. (eds.) *The Primary Auditory Neurons of the Mammalian Cochlea.* New York, NY: Springer New York.

Lange, W., Geißendörfer, J., Schenzer, A., Grötzinger, J., Seebohm, G., Friedrich, T. & Schwake, M. 2009. Refinement of the Binding Site and Mode of Action of the Anticonvulsant Retigabine on Kcnq K≪Sup≫+≪/Sup≫ Channels. *Molecular Pharmacology,* 75**,** 272.

Larsson, H. P., Baker, O. S., Dhillon, D. S. & Isacoff, E. Y. 1996. Transmembrane Movement of the Shaker K+ Channel S4. *Neuron,* 16**,** 387-397.

Larsson, J. E., Karlsson, U., Wu, X. & Liin, S. I. 2020. Combining Endocannabinoids with Retigabine for Enhanced M-Channel Effect and Improved Kv7 Subtype Selectivity. *The Journal of general physiology,* 152**,** e202012576.

Läuger, P. 1976. Diffusion-Limited Ion Flow through Pores. *Biochimica et Biophysica Acta (BBA) - Biomembranes,* 455**,** 493-509.

Lawson K, Singh A, Kantsedikas I, Jenner Ca & Dk, A. 2021. Flupirtine as a Potential Treatment for Fibromyalgia. *J Explor Res Pharmacol***,** 53-63.

Lee, J., Kang, M., Kim, S. & Chang, I. 2020. Structural and Molecular Insight into the Ph-Induced Low-Permeability of the Voltage-Gated Potassium Channel Kv1.2 through Dewetting of the Water Cavity. *PLOS Computational Biology,* 16**,** e1007405.

Lehman, A., Thouta, S., Mancini, G. M. S., Naidu, S., Van Slegtenhorst, M., Mcwalter, K., Person, R., Mwenifumbo, J., Salvarinova, R., Guella, I., Mckenzie, M. B., Datta, A., Connolly, M. B., Kalkhoran, S. M., Poburko, D., Friedman, J. M., Farrer, M. J., Demos, M., Desai, S. & Claydon, T. 2017. Loss-of-Function and Gain-of-Function Mutations in Kcnq5 Cause Intellectual Disability or Epileptic Encephalopathy. *Am J Hum Genet,* 101**,** 65-74.

Leitner, M. G., Feuer, A., Ebers, O., Schreiber, D. N., Halaszovich, C. R. & Oliver, D. 2012. Restoration of Ion Channel Function in Deafness-Causing Kcnq4 Mutants by Synthetic Channel Openers. *British Journal of Pharmacology,* 165**,** 2244-2259.

Lerche, C., Bruhova, I., Lerche, H., Steinmeyer, K., Wei, A. D., Strutz-Seebohm, N., Lang, F., Busch, A. E., Zhorov, B. S. & Seebohm, G. 2007. Chromanol 293b Binding in Kcnq1 (Kv7.1) Channels Involves Electrostatic Interactions with a Potassium Ion in the Selectivity Filter. *Molecular Pharmacology,* 71**,** 1503.

Lerche, C., Scherer, C. R., Seebohm, G., Derst, C., Wei, A. D., Busch, A. E. & Steinmeyer, K. 2000a. Molecular Cloning and Functional Expression of Kcnq5, a Potassium Channel Subunit That May Contribute to Neuronal M-Current Diversity *. *Journal of Biological Chemistry,* 275**,** 22395-22400.

Lerche, C., Seebohm, G., Wagner, C. I., Scherer, C. R., Dehmelt, L., Abitbol, I., Gerlach, U., Brendel, J., Attali, B. & Busch, A. E. 2000b. Molecular Impact of Mink on the Enantiospecific Block of Iks by Chromanols. *British Journal of Pharmacology,* 131**,** 1503-1506.

Levinsohn, E. A. & Hill, K. P. 2020. Clinical Uses of Cannabis and Cannabinoids in the United States. *Journal of the Neurological Sciences,* 411**,** 116717.

Lezmy, J., Lipinsky, M., Khrapunsky, Y., Patrich, E., Shalom, L., Peretz, A., Fleidervish, I. A. & Attali, B. 2017. M-Current Inhibition Rapidly Induces a Unique Ck2-Dependent Plasticity of the Axon Initial Segment. *Proceedings of the National Academy of Sciences,* 114**,** E10234.

Li, C.-L., Li, K.-C., Wu, D., Chen, Y., Luo, H., Zhao, J.-R., Wang, S.-S., Sun, M.-M., Lu, Y.-J., Zhong, Y.-Q., Hu, X.-Y., Hou, R., Zhou, B.-B., Bao, L., Xiao, H.-S. & Zhang, X. 2016. Somatosensory Neuron Types Identified by High-Coverage Single-Cell Rna-Sequencing and Functional Heterogeneity. *Cell Research,* 26**,** 83-102.

Li, C., Huang, P., Lu, Q., Zhou, M., Guo, L. & Xu, X. 2014. Kcnq/Kv7 Channel Activator Flupirtine Protects against Acute Stress-Induced Impairments of Spatial Memory Retrieval and Hippocampal Ltp in Rats. *Neuroscience,* 280**,** 19-30.

Li, J., Maghera, J., Lamothe, S. M., Marco, E. J. & Kurata, H. T. 2020. Heteromeric Assembly of Truncated Neuronal Kv7 Channels: Implications for Neurologic Disease and Pharmacotherapy. *Molecular Pharmacology,* 98**,** 192.

Li, L., Sun, H., Ding, J., Niu, C., Su, M., Zhang, L., Li, Y., Wang, C., Gamper, N., Du, X. & Zhang, H. 2017. Selective Targeting of M-Type Potassium K(V) 7.4 Channels Demonstrates Their Key Role in the Regulation of Dopaminergic Neuronal Excitability and Depression-Like Behaviour. *British journal of pharmacology,* 174**,** 4277-4294.

Li, T., Wu, K., Yue, Z., Wang, Y., Zhang, F. & Shen, H. 2021a. Structural Basis for the Modulation of Human Kcnq4 by Small-Molecule Drugs. *Molecular Cell,* 81**,** 25-37.e4.

Li, X., Zhang, Q., Guo, P., Fu, J., Mei, L., Lv, D., Wang, J., Lai, D., Ye, S., Yang, H. & Guo, J. 2021b. Molecular Basis for Ligand Activation of the Human Kcnq2 Channel. *Cell Research,* 31**,** 52-61.

Li, Y., Gamper, N., Hilgemann, D. W. & Shapiro, M. S. 2005. Regulation of Kv7 (Kcnq) K+ Channel Open Probability by Phosphatidylinositol 4,5-Bisphosphate. *The Journal of neuroscience : the official journal of the Society for Neuroscience,* 25**,** 9825-9835.

Li, Y., Gamper, N. & Shapiro, M. S. 2004a. Single-Channel Analysis of Kcnq K+ Channels Reveals the Mechanism of Augmentation by a Cysteine-Modifying

Reagent. *The Journal of neuroscience : the official journal of the Society for Neuroscience,* 24**,** 5079-5090.
Li, Y., Langlais, P., Gamper, N., Liu, F. & Shapiro, M. S. 2004b. Dual Phosphorylations Underlie Modulation of Unitary Kcnq K+ Channels by Src Tyrosine Kinase *Journal of Biological Chemistry,* 279**,** 45399-45407.
Lima, P. A. & Marrion, N. V. 2007. Mechanisms Underlying Activation of the Slow Ahp in Rat Hippocampal Neurons. *Brain Research,* 1150**,** 74-82.
Ling, J., Erol, F. & Gu, J. G. 2018. Role of Kcnq2 Channels in Orofacial Cold Sensitivity: Kcnq2 Upregulation in Trigeminal Ganglion Neurons after Infraorbital Nerve Chronic Constrictive Injury. *Neuroscience Letters,* 664**,** 84-90.
Ling, J., Erol, F., Viatchenko-Karpinski, V., Kanda, H. & Gu, J. G. 2017. Orofacial Neuropathic Pain Induced by Oxaliplatin:Downregulation of Kcnq2 Channels in V2 Trigeminal Ganglion Neurons and Treatment by the Kcnq2 Channel Potentiator Retigabine. *Molecular Pain,* 13**,** 1744806917724715.
Linley, J. E., Ooi, L., Pettinger, L., Kirton, H., Boyle, J. P., Peers, C. & Gamper, N. 2012. Reactive Oxygen Species Are Second Messengers of Neurokinin Signaling in Peripheral Sensory Neurons. *Proceedings of the National Academy of Sciences,* 109**,** E1578.
Linley, J. E., Rose, K., Patil, M., Robertson, B., Akopian, A. N. & Gamper, N. 2008. Inhibition of M Current in Sensory Neurons by Exogenous Proteases: A Signaling Pathway Mediating Inflammatory Nociception. *The Journal of Neuroscience,* 28**,** 11240.
Liu, B., Linley, J. E., Du, X., Zhang, X., Ooi, L., Zhang, H. & Gamper, N. 2010. The Acute Nociceptive Signals Induced by Bradykinin in Rat Sensory Neurons Are Mediated by Inhibition of M-Type K+ Channels and Activation of Ca2+-Activated Cl– Channels. *The Journal of Clinical Investigation,* 120**,** 1240-1252.
Ljungstrom, T., Grunnet, M., Jensen, B. S. & Olesen, S. P. 2003. Functional Coupling between Heterologously Expressed Dopamine D(2) Receptors and Kcnq Channels. *Pflugers Arch,* 446**,** 684-94.
Lo Iacono, L., Catale, C., Martini, A., Valzania, A., Viscomi, M. T., Chiurchiù, V., Guatteo, E., Bussone, S., Perrone, F., Di Sabato, P., Aricò, E., D'argenio, A., Troisi, A., Mercuri, N. B., Maccarrone, M., Puglisi-Allegra, S., Casella, P. & Carola, V. 2018. From Traumatic Childhood to Cocaine Abuse: The Critical Function of the Immune System. *Biological Psychiatry,* 84**,** 905-916.
Lohrmann, E., Burhoff, I., Nitschke, R. B., Lang, H. J., Mania, D., Englert, H. C., Hropot, M., Warth, R., Rohm, W., Bleich, M. & Greger, R. 1995. A New Class of Inhibitors of Camp-Mediated Cl− Secretion in Rabbit Colon, Acting by the Reduction of Camp-Activated K+ Conductance. *Pflügers Archiv,* 429**,** 517-530.
Long, S. B., Tao, X., Campbell, E. B. & Mackinnon, R. 2007. Atomic Structure of a Voltage-Dependent K+ Channel in a Lipid Membrane-Like Environment. *Nature,* 450**,** 376-382.
Loonen, A. J. M., Schellekens, A. F. A. & Ivanova, S. A. 2016. Circuits Regulating Pleasure and Happiness: A Focus on Addiction, Beyond the Ventral Striatum. *In:* Ruby, W. M. M. a. C. L. (ed.) *Advances in Drug Addiction Research and Clinical Applications*

Loussouarn, G., Baró, I. & Escande, D. 2006. Kcnq1 K+ Channel—Mediated Cardiac Channelopathies. *In:* Stockand, J. D. & Shapiro, M. S. (eds.) *Ion Channels: Methods and Protocols.* Totowa, NJ: Humana Press.

Lowry, C. A., Hale, M. W., Evans, A. K., Heerkens, J., Staub, D. R., Gasser, P. J. & Shekhar, A. 2008. Serotonergic Systems, Anxiety, and Affective Disorder. *Annals of the New York Academy of Sciences,* 1148**,** 86-94.

Lübke, M., Schreiber, J. A., Le Quoc, T., Körber, F., Müller, J., Sivanathan, S., Matschke, V., Schubert, J., Strutz-Seebohm, N., Seebohm, G. & Scherkenbeck, J. 2020. Rottlerin: Structure Modifications and Kcnq1/Kcne1 Ion Channel Activity. *ChemMedChem,* 15**,** 1078-1088.

Luo, L., Li, B., Wang, S., Wu, F., Wang, X., Liang, P., Ombati, R., Chen, J., Lu, X., Cui, J., Lu, Q., Zhang, L., Zhou, M., Tian, C., Yang, S. & Lai, R. 2018. Centipedes Subdue Giant Prey by Blocking Kcnq Channels. *Proceedings of the National Academy of Sciences,* 115**,** 1646.

Lv, P., Wei, D. & Yamoah, E. N. 2010. Kv7-Type Channel Currents in Spiral Ganglion Neurons: Involvement in Sensorineural Hearing Loss. *Journal of Biological Chemistry,* 285**,** 34699-34707.

Macdonald, P. E., Ha, X. F., Wang, J., Smukler, S. R., Sun, A. M., Gaisano, H. Y., Salapatek, A. M., Backx, P. H. & Wheeler, M. B. 2001. Members of the Kv1 and Kv2 Voltage-Dependent K(+) Channel Families Regulate Insulin Secretion. *Mol Endocrinol,* 15**,** 1423-35.

Macdonald, P. E. & Wheeler, M. B. 2003. Voltage-Dependent K(+) Channels in Pancreatic Beta Cells: Role, Regulation and Potential as Therapeutic Targets. *Diabetologia,* 46**,** 1046-62.

Mackie, A. R., Brueggemann, L. I., Henderson, K. K., Shiels, A. J., Cribbs, L. L., Scrogin, K. E. & Byron, K. L. 2008. Vascular Kcnq Potassium Channels as Novel Targets for the Control of Mesenteric Artery Constriction by Vasopressin, Based on Studies in Single Cells, Pressurized Arteries, and in Vivo Measurements of Mesenteric Vascular Resistance. *The Journal of pharmacology and experimental therapeutics,* 325**,** 475-483.

Malinow, R., Madison, D. V. & Tsien, R. W. 1988. Persistent Protein Kinase Activity Underlying Long-Term Potentiation. *Nature,* 335**,** 820-824.

Malinow, R., Schulman, H. & Tsien, R. W. 1989. Inhibition of Postsynaptic Pkc or Camkii Blocks Induction but Not Expression of Ltp. *Science,* 245**,** 862-866.

Maljevic, S., Lerche, C., Seebohm, G., Alekov, A. K., Busch, A. E. & Lerche, H. 2003. Rapid Report. *The Journal of Physiology,* 548**,** 353-360.

Mall, M., Wissner, A., Schreiber, R., Kuehr, J., Seydewitz, H. H., Brandis, M., Greger, R. & Kunzelmann, K. 2000. Role of Kvlqt1 in Cyclic Adenosine Monophosphate–Mediated Cl− Secretion in Human Airway Epithelia. *American Journal of Respiratory Cell and Molecular Biology,* 23**,** 283-289.

Mani, B. K., O'dowd, J., Kumar, L., Brueggemann, L. I., Ross, M. & Byron, K. L. 2013. Vascular Kcnq (Kv7) Potassium Channels as Common Signaling Intermediates and Therapeutic Targets in Cerebral Vasospasm. *J Cardiovasc Pharmacol,* 61**,** 51-62.

Mani, B. K., Robakowski, C., Brueggemann, L. I., Cribbs, L. L., Tripathi, A., Majetschak, M. & Byron, K. L. 2016. Kv7.5 Potassium Channel Subunits Are the Primary Targets for Pka-Dependent Enhancement of Vascular Smooth Muscle Kv7 Currents. *Molecular pharmacology,* 89**,** 323-334.

Manville, R. W. & Abbott, G. W. 2018. Ancient and Modern Anticonvulsants Act Synergistically in a Kcnq Potassium Channel Binding Pocket. *Nature Communications,* 9**,** 3845.

Manville, R. W., Papanikolaou, M. & Abbott, G. W. 2018. Direct Neurotransmitter Activation of Voltage-Gated Potassium Channels. *Nature Communications,* 9**,** 1847.

Marcotti, W. & Kros, C. J. 1999. Developmental Expression of the Potassium Current Ik,N Contributes to Maturation of Mouse Outer Hair Cells. *The Journal of Physiology,* 520**,** 653-660.

Marrion, N. V. 1996. Calcineurin Regulates M Channel Modal Gating in Sympathetic Neurons. *Neuron,* 16**,** 163-173.

Marrion, N. V., Zucker, R. S., Marsh, S. J. & Adams, P. R. 1991. Modulation of M-Current by Intracellular Ca2+. *Neuron,* 6**,** 533-545.

Marx, S. O., Kurokawa, J., Reiken, S., Motoike, H., D'armiento, J., Marks, A. R. & Kass, R. S. 2002. Requirement of a Macromolecular Signaling Complex for B2 Adrenergic Receptor Modulation of the Kcnq1-Kcne1 Potassium Channel. *Science,* 295**,** 496-499.

Mcbride, J. L., Boudreau, R. L., Harper, S. Q., Staber, P. D., Monteys, A. M., Martins, I., Gilmore, B. L., Burstein, H., Peluso, R. W., Polisky, B., Carter, B. J. & Davidson, B. L. 2008. Artificial Mirnas Mitigate Shrna-Mediated Toxicity in the Brain: Implications for the Therapeutic Development of Rnai. *Proceedings of the National Academy of Sciences,* 105**,** 5868.

Mccallum, L. A., Greenwood, I. A. & Tribe, R. M. 2009. Expression and Function of K(V)7 Channels in Murine Myometrium Throughout Oestrous Cycle. *Pflugers Arch,* 457**,** 1111-20.

Mcgill, M. R. & Jaeschke, H. 2013. Metabolism and Disposition of Acetaminophen: Recent Advances in Relation to Hepatotoxicity and Diagnosis. *Pharmaceutical research,* 30**,** 2174-2187.

Mcguier, N. S., Griffin, W. C., 3rd, Gass, J. T., Padula, A. E., Chesler, E. J. & Mulholland, P. J. 2016. Kv7 Channels in the Nucleus Accumbens Are Altered by Chronic Drinking and Are Targets for Reducing Alcohol Consumption. *Addict Biol,* 21**,** 1097-1112.

Mcmahon, S., Koltzenburg, M., Tracey, I. & Turk, D. C. 2013. *Wall & Melzack's Textbook of Pain E-Book*, Elsevier Health Sciences.

Mehregan, H., Mohseni, M., Akbari, M., Jalalvand, K., Arzhangi, S., Nikzat, N., Kahrizi, K. & Najmabadi, H. 2019. Novel Mutations in Kcnq4, Lhfpl5 and Coch Genes in Iranian Families with Hearing Impairment. *Arch Iran Med,* 22**,** 189-197.

Mencía, Á., González-Nieto, D., Modamio-Høybjør, S., Etxeberría, A., Aránguez, G., Salvador, N., Del Castillo, I., Villarroel, Á., Moreno, F., Barrio, L. & Moreno-Pelayo, M. Á. 2008. A Novel Kcnq4 Pore-Region Mutation (P.G296s) Causes Deafness by Impairing Cell-Surface Channel Expression. *Human Genetics,* 123**,** 41-53.

Mercer, E. a. J., Abbott, G. W., Brazier, S. P., Ramesh, B., Haris, P. I. & Srai, S. K. S. 1997. Synthetic Putative Transmembrane Region of Minimal Potassium Channel Protein (Mink) Adopts an A-Helical Conformation in Phospholipid Membranes. *Biochemical Journal,* 325**,** 475-479.

Miceli, F., Soldovieri, M. V., Ambrosino, P., Barrese, V., Migliore, M., Cilio, M. R. & Taglialatela, M. 2013. Genotype-Phenotype Correlations in Neonatal Epilepsies Caused by Mutations in the Voltage Sensor of K(V)7.2 Potassium Channel Subunits. *Proc Natl Acad Sci U S A,* 110**,** 4386-91.

Michaelis , L. 1925. Contribution to the Theory of Permeability of Membranes for Electrolytes. *Journal of General Physiology,* 8**,** 33-59.
Mondejar-Parreño, G., Perez-Vizcaino, F. & Cogolludo, A. 2020. Kv7 Channels in Lung Diseases. *Frontiers in Physiology,* 11.
Moreno, C., Oliveras, A., Bartolucci, C., Muñoz, C., De La Cruz, A., Peraza, D. A., Gimeno, J. R., Martín-Martínez, M., Severi, S., Felipe, A., Lambiase, P. D., Gonzalez, T. & Valenzuela, C. 2017. D242n, a Kv7.1 Lqts Mutation Uncovers a Key Residue for Iks Voltage Dependence. *Journal of Molecular and Cellular Cardiology,* 110**,** 61-69.
Moreno, C., Oliveras, A., De La Cruz, A., Bartolucci, C., Muñoz, C., Salar, E., Gimeno, J. R., Severi, S., Comes, N., Felipe, A., González, T., Lambiase, P. & Valenzuela, C. 2015. A New Kcnq1 Mutation at the S5 Segment That Impairs Its Association with Kcne1 Is Responsible for Short Qt Syndrome. *Cardiovascular Research,* 107**,** 613-623.
Moshirfar, M., Parker, L., Birdsong, O. C., Ronquillo, Y. C., Hofstedt, D., Shah, T. J., Gomez, A. T. & Hoopes, P. C. S. 2018. Use of Rho Kinase Inhibitors in Ophthalmology: A Review of the Literature. *Med Hypothesis Discov Innov Ophthalmol,* 7**,** 101-111.
Moss, A. J., Shimizu, W., Wilde, A. a. M., Towbin, J. A., Zareba, W., Robinson, J. L., Qi, M., Vincent, G. M., Ackerman, M. J., Kaufman, E. S., Hofman, N., Seth, R., Kamakura, S., Miyamoto, Y., Goldenberg, I., Andrews, M. L. & Mcnitt, S. 2007. Clinical Aspects of Type-1 Long-Qt Syndrome by Location, Coding Type, and Biophysical Function of Mutations Involving the Kcnq1 Gene. *Circulation,* 115**,** 2481-2489.
Mucha, M., Ooi, L., Linley, J. E., Mordaka, P., Dalle, C., Robertson, B., Gamper, N. & Wood, I. C. 2010. Transcriptional Control of Kcnq Channel Genes and the Regulation of Neuronal Excitability. *The Journal of neuroscience : the official journal of the Society for Neuroscience,* 30**,** 13235-13245.
Munro, G., Erichsen, H. K. & Mirza, N. R. 2007. Pharmacological Comparison of Anticonvulsant Drugs in Animal Models of Persistent Pain and Anxiety. *Neuropharmacology,* 53**,** 609-18.
Murnion, B. P. 2018. Neuropathic Pain: Current Definition and Review of Drug Treatment. *Australian prescriber,* 41**,** 60-63.
Nakajo, K. & Kubo, Y. 2008. Second Coiled-Coil Domain of Kcnq Channel Controls Current Expression and Subfamily Specific Heteromultimerization by Salt Bridge Networks. *The Journal of Physiology,* 586**,** 2827-2840.
Neyroud, N., Tesson, F., Denjoy, I., Leibovici, M., Donger, C., Barhanin, J., Fauré, S., Gary, F., Coumel, P., Petit, C., Schwartz, K. & Guicheney, P. 1997. A Novel Mutation in the Potassium Channel Gene Kvlqt1 Causes the Jervell and Lange-Nielsen Cardioauditory Syndrome. *Nature Genetics,* 15**,** 186-189.
Ng, F. L., Davis, A. J., Jepps, T. A., Harhun, M. I., Yeung, S. Y., Wan, A., Reddy, M., Melville, D., Nardi, A., Khong, T. K. & Greenwood, I. A. 2011. Expression and Function of the K+ Channel Kcnq Genes in Human Arteries. *British Journal of Pharmacology,* 162**,** 42-53.
Nguyen, M. Q., Von Buchholtz, L. J., Reker, A. N., Ryba, N. J. P. & Davidson, S. 2021. Single-Nucleus Transcriptomic Analysis of Human Dorsal Root Ganglion Neurons. *eLife,* 10**,** e71752.
Nicolas, M.-T., Demêmes, D., Martin, A., Kupershmidt, S. & Barhanin, J. 2001. Kcnq1/Kcne1 Potassium Channels in Mammalian Vestibular Dark Cells. *Hearing Research,* 153**,** 132-145.

Nishio, T., Koike, S., Okano, H. & Hisa, Y. 2016. Sensory Receptors and Nerve Endings. *In:* Hisa, Y. (ed.) *Neuroanatomy and Neurophysiology of the Larynx.* Tokyo: Springer Japan.

Noda, M., Ikeda, T., Suzuki, H., Takeshima, H., Takahashi, T., Kuno, M. & Numa, S. 1986. Expression of Functional Sodium Channels from Cloned Cdna. *Nature,* 322**,** 826-828.

Nouvian, R., Ruel, J., Wang, J., Guitton, M. J., Pujol, R. & Puel, J.-L. 2003. Degeneration of Sensory Outer Hair Cells Following Pharmacological Blockade of Cochlear Kcnq Channels in the Adult Guinea Pig. *European Journal of Neuroscience,* 17**,** 2553-2562.

O'neill, J., Brock, C., Olesen, A. E., Andresen, T., Nilsson, M. & Dickenson, A. H. 2012. Unravelling the Mystery of Capsaicin: A Tool to Understand and Treat Pain. *Pharmacological reviews,* 64**,** 939-971.

Ohya, S., Asakura, K., Muraki, K., Watanabe, M. & Imaizumi, Y. 2002. Molecular and Functional Characterization of Erg, Kcnq, and Kcne Subtypes in Rat Stomach Smooth Muscle. *Am J Physiol Gastrointest Liver Physiol,* 282**,** G277-87.

Ohya, S., Sergeant, G. P., Greenwood, I. A. & Horowitz, B. 2003. Molecular Variants of Kcnq Channels Expressed in Murine Portal Vein Myocytes. *Circulation Research,* 92**,** 1016-1023.

Okada, M., Zhu, G., Hirose, S., Ito, K. I., Murakami, T., Wakui, M. & Kaneko, S. 2003. Age-Dependent Modulation of Hippocampal Excitability by Kcnq-Channels. *Epilepsy Res,* 53**,** 81-94.

Oliver, D., Knipper, M., Derst, C. & Fakler, B. 2003. Resting Potential and Submembrane Calcium Concentration of Inner Hair Cells in the Isolated Mouse Cochlea Are Set by Kcnq-Type Potassium Channels. *The Journal of Neuroscience,* 23**,** 2141.

Otto, J. F., Kimball, M. M. & Wilcox, K. S. 2002. Effects of the Anticonvulsant Retigabine on Cultured Cortical Neurons: Changes in Electroresponsive Properties and Synaptic Transmission. *Mol Pharmacol,* 61**,** 921-7.

Padilla, K., Wickenden, A. D., Gerlach, A. C. & Mccormack, K. 2009. The Kcnq2/3 Selective Channel Opener Ica-27243 Binds to a Novel Voltage-Sensor Domain Site. *Neuroscience Letters,* 465**,** 138-142.

Pan, Z., Kao, T., Horvath, Z., Lemos, J., Sul, J.-Y., Cranstoun, S. D., Bennett, V., Scherer, S. S. & Cooper, E. C. 2006. A Common Ankyrin-G-Based Mechanism Retains Kcnq and Nav Channels at Electrically Active Domains of the Axon. *The Journal of neuroscience : the official journal of the Society for Neuroscience,* 26**,** 2599-2613.

Papazian, D. M., Schwarz, T. L., Tempel, B. L., Jan, Y. N. & Jan, L. Y. 1987. Cloning of Genomic and Complementary DNA from <I>Shaker</I>, a Putative Potassium Channel Gene from <I>Drosophila</I>. *Science,* 237**,** 749-753.

Paricio-Montesinos, R., Schwaller, F., Udhayachandran, A., Rau, F., Walcher, J., Evangelista, R., Vriens, J., Voets, T., Poulet, J. F. A. & Lewin, G. R. 2020. The Sensory Coding of Warm Perception. *Neuron,* 106**,** 830-841.e3.

Parker, R. & Sheth, U. 2007. P Bodies and the Control of Mrna Translation and Degradation. *Molecular Cell,* 25**,** 635-646.

Parrilla-Carrero, J., Buchta, W. C., Goswamee, P., Culver, O., Mckendrick, G., Harlan, B., Moutal, A., Penrod, R., Lauer, A., Ramakrishnan, V., Khanna, R., Kalivas, P. & Riegel, A. C. 2018. Restoration of Kv7 Channel-Mediated Inhibition Reduces Cued-Reinstatement of Cocaine Seeking. *J Neurosci,* 38**,** 4212-4229.

Passmore, G., Reilly, J., Thakur, M., Keasberry, V., Marsh, S., Dickenson, A. & Brown, D. 2012. Functional Significance of M-Type Potassium Channels in Nociceptive Cutaneous Sensory Endings. *Frontiers in Molecular Neuroscience,* 5.

Passmore, G. M., Selyanko, A. A., Mistry, M., Al-Qatari, M., Marsh, S. J., Matthews, E. A., Dickenson, A. H., Brown, T. A., Burbidge, S. A., Main, M. & Brown, D. A. 2003. Kcnq/M Currents in Sensory Neurons: Significance for Pain Therapy. *The Journal of Neuroscience,* 23**,** 7227.

Peiris, M., Hockley, J. R., Reed, D. E., Smith, E. S. J., Bulmer, D. C. & Blackshaw, L. A. 2017. Peripheral Kv7 Channels Regulate Visceral Sensory Function in Mouse and Human Colon. *Molecular Pain,* 13**,** 1744806917709371.

Penfield, W. & Boldrey, E. 1937. Somatic Motor and Sensory Representation in the Cerebral Cortex of Man as Studied by Electrical Stimulation. *Brain,* 60**,** 389-443.

Peretz, A., Degani, N., Nachman, R., Uziyel, Y., Gibor, G., Shabat, D. & Attali, B. 2005. Meclofenamic Acid and Diclofenac, Novel Templates of Kcnq2/Q3 Potassium Channel Openers, Depress Cortical Neuron Activity and Exhibit Anticonvulsant Properties. *Molecular Pharmacology,* 67**,** 1053.

Peretz, A., Pell, L., Gofman, Y., Haitin, Y., Shamgar, L., Patrich, E., Kornilov, P., Gourgy-Hacohen, O., Ben-Tal, N. & Attali, B. 2010. Targeting the Voltage Sensor of Kv7.2 Voltage-Gated K+ Channels with a New Gating-Modifier. *Proceedings of the National Academy of Sciences of the United States of America,* 107**,** 15637-15642.

Peretz, A., Sheinin, A., Yue, C., Degani-Katzav, N., Gibor, G., Nachman, R., Gopin, A., Tam, E., Shabat, D., Yaari, Y. & Attali, B. 2007. Pre- and Postsynaptic Activation of M-Channels by a Novel Opener Dampens Neuronal Firing and Transmitter Release. *Journal of Neurophysiology,* 97**,** 283-295.

Perez-Flores, M. C., Lee, J. H., Park, S., Zhang, X.-D., Sihn, C.-R., Ledford, H. A., Wang, W., Kim, H. J., Timofeyev, V., Yarov-Yarovoy, V., Chiamvimonvat, N., Rabbitt, R. D. & Yamoah, E. N. 2020. Cooperativity of Kv7.4 Channels Confers Ultrafast Electromechanical Sensitivity and Emergent Properties in Cochlear Outer Hair Cells. *Science Advances,* 6**,** eaba1104.

Peroz, D., Dahiméne, S., Baró, I., Loussouarn, G. & Mérot, J. 2009. Lqt1-Associated Mutations Increase Kcnq1 Proteasomal Degradation Independently of Derlin-1 *. *Journal of Biological Chemistry,* 284**,** 5250-5256.

Perry, M. J., Lawson, S. N. & Robertson, J. 1991. Neurofilament Immunoreactivity in Populations of Rat Primary Afferent Neurons: A Quantitative Study of Phosphorylated and Non-Phosphorylated Subunits. *J Neurocytol,* 20**,** 746-58.

Peters, H. C., Hu, H., Pongs, O., Storm, J. F. & Isbrandt, D. 2005. Conditional Transgenic Suppression of M Channels in Mouse Brain Reveals Functions in Neuronal Excitability, Resonance and Behavior. *Nature Neuroscience,* 8**,** 51-60.

Polgár, E., Watanabe, M., Hartmann, B., Grant, S. G. & Todd, A. J. 2008. Expression of Ampa Receptor Subunits at Synapses in Laminae I-Iii of the Rodent Spinal Dorsal Horn. *Mol Pain,* 4**,** 5.

Potet, F., Scott, J. D., Mohammad-Panah, R., Escande, D. & Baró, I. 2001. Akap Proteins Anchor Camp-Dependent Protein Kinase to Kvlqt1/Isk Channel Complex. *American Journal of Physiology-Heart and Circulatory Physiology,* 280**,** H2038-H2045.

Prole , D. L., Lima , P. A. & Marrion , N. V. 2003. Mechanisms Underlying Modulation of Neuronal Kcnq2/Kcnq3 Potassium Channels by Extracellular Protons. *Journal of General Physiology,* 122**,** 775-793.

Prole, D. L. & Marrion, N. V. 2004. Ionic Permeation and Conduction Properties of Neuronal Kcnq2/Kcnq3 Potassium Channels. *Biophysical journal,* 86**,** 1454-1469.

Proulx, C. D., Hikosaka, O. & Malinow, R. 2014. Reward Processing by the Lateral Habenula in Normal and Depressive Behaviors. *Nature Neuroscience,* 17**,** 1146-1152.

Provence, A., Angoli, D. & Petkov, G. V. 2018. K(V)7 Channel Pharmacological Activation by the Novel Activator Ml213: Role for Heteromeric K(V)7.4/K(V)7.5 Channels in Guinea Pig Detrusor Smooth Muscle Function. *J Pharmacol Exp Ther,* 364**,** 131-144.

Provence, A., Malysz, J. & Petkov, G. V. 2015a. The Novel Kv7.2/Kv7.3 Channel Opener Ica-069673 Reveals Subtype-Specific Functional Roles in Guinea Pig Detrusor Smooth Muscle Excitability and Contractility. *J Pharmacol Exp Ther,* 354**,** 290-301.

Provence, A., Malysz, J. & Petkov, G. V. 2015b. The Novel Kv7.2/Kv7.3 Channel Opener Ica-069673 Reveals Subtype-Specific Functional Roles in Guinea Pig Detrusor Smooth Muscle Excitability and Contractility. *The Journal of pharmacology and experimental therapeutics,* 354**,** 290-301.

Pusch, M. 1998. Increase of the Single-Channel Conductance of Kvlqt1 Potassium Channels Induced by the Association with Mink. *Pflügers Archiv,* 437**,** 172-174.

Ramamoorthy, S. & Cidlowski, J. A. 2016. Corticosteroids: Mechanisms of Action in Health and Disease. *Rheumatic diseases clinics of North America,* 42**,** 15-vii.

Ray, S., Salzer, I., Kronschläger, M. T. & Boehm, S. 2019. The Paracetamol Metabolite N-Acetylp-Benzoquinone Imine Reduces Excitability in First- and Second-Order Neurons of the Pain Pathway through Actions on Kv7 Channels. *Pain,* 160**,** 954-964.

Regev, N., Degani-Katzav, N., Korngreen, A., Etzioni, A., Siloni, S., Alaimo, A., Chikvashvili, D., Villarroel, A., Attali, B. & Lotan, I. 2009. Selective Interaction of Syntaxin 1a with Kcnq2: Possible Implications for Specific Modulation of Presynaptic Activity. *PloS one,* 4**,** e6586-e6586.

Restier, L., Cheng, L. & Sanguinetti, M. C. 2008. Mechanisms by Which Atrial Fibrillation-Associated Mutations in the S1 Domain of Kcnq1 Slow Deactivation of Iks Channels. *The Journal of Physiology,* 586**,** 4179-4191.

Rivera-Arconada, I. & Lopez-Garcia, J. A. 2006. Retigabine-Induced Population Primary Afferent Hyperpolarisation in Vitro. *Neuropharmacology,* 51**,** 756-763.

Rizzuto, R. & Pozzan, T. 2006. Microdomains of Intracellular Ca2+: Molecular Determinants and Functional Consequences. *Physiological Reviews,* 86**,** 369-408.

Robbins, J., Passmore, G. M., Abogadie, F. C., Reilly, J. M. & Brown, D. A. 2013. Effects of Kcnq2 Gene Truncation on M-Type Kv7 Potassium Currents. *PLoS One,* 8**,** e71809.

Roeloffs, R., Wickenden, A. D., Crean, C., Werness, S., Mcnaughton-Smith, G., Stables, J., Mcnamara, J. O., Ghodadra, N. & Rigdon, G. C. 2008. In Vivo Profile of Ica-27243 N-(6-Chloro-Pyridin-3-Yl)-3,4-Difluoro-Benzamide], a Potent and Selective Kcnq2/Q3 (Kv7.2/Kv7.3) Activator in Rodent Anticonvulsant Models. *Journal of Pharmacology and Experimental Therapeutics,* 326**,** 818.

Romano, A., Guéant-Rodriguez, R.-M., Viola, M., Gaeta, F., Caruso, C. & Guéant, J.-L. 2005. Cross-Reactivity among Drugs: Clinical Problems. *Toxicology,* 209**,** 169-179.

Rose, K., Ooi, L., Dalle, C., Robertson, B., Wood, I. C. & Gamper, N. 2011. Transcriptional Repression of the M Channel Subunit Kv7.2 in Chronic Nerve Injury. *Pain,* 152**,** 742-754.

Rossi, J. J. 2004. A Cholesterol Connection in Rnai. *Nature,* 432**,** 155-156.

Rostock, C., Schrenk-Siemens, K., Pohle, J. & Siemens, J. 2018. Human Vs. Mouse Nociceptors – Similarities and Differences. *Neuroscience,* 387**,** 13-27.

Rouillard, A. D., Gundersen, G. W., Fernandez, N. F., Wang, Z., Monteiro, C. D., Mcdermott, M. G. & Ma'ayan, A. 2016. The Harmonizome: A Collection of Processed Datasets Gathered to Serve and Mine Knowledge About Genes and Proteins. *Database,* 2016.

Roura-Ferrer, M., Etxebarria, A., Solé, L., Oliveras, A., Comes, N., Villarroel, A. & Felipe, A. 2009. Functional Implications of Kcne Subunit Expression for the Kv7.5 (Kcnq5) Channel. *Cell Physiol Biochem,* 24**,** 325-34.

Roza, C., Castillejo, S. & Lopez-García, J. A. 2011. Accumulation of Kv7.2 Channels in Putative Ectopic Transduction Zones of Mice Nerve-End Neuromas. *Molecular pain,* 7**,** 58-58.

Roza, C. & Lopez-Garcia, J. A. 2008. Retigabine, the Specific Kcnq Channel Opener, Blocks Ectopic Discharges in Axotomized Sensory Fibres. *PAIN,* 138**,** 537-545.

Russell, F. A., King, R., Smillie, S. J., Kodji, X. & Brain, S. D. 2014. Calcitonin Gene-Related Peptide: Physiology and Pathophysiology. *Physiol Rev,* 94**,** 1099-142.

Ryan, A. & Dallos, P. 1975. Effect of Absence of Cochlear Outer Hair Cells on Behavioural Auditory Threshold. *Nature,* 253**,** 44-46.

Rygh, L. J., Suzuki, R., Rahman, W., Wong, Y., Vonsy, J. L., Sandhu, H., Webber, M., Hunt, S. & Dickenson, A. H. 2006. Local and Descending Circuits Regulate Long-Term Potentiation and Zif268 Expression in Spinal Neurons. *European Journal of Neuroscience,* 24**,** 761-772.

Salzer, I., Ray, S. & Boehm, S. 2020. Cysteine-Modification of Kv7 Channels as Analgesic Mechanism of Action of Acetaminophen. *Biophysical Journal,* 118**,** 115a.

Sanguinetti, M. C., Curran, M. E., Zou, A., Shen, J., Specter, P. S., Atkinson, D. L. & Keating, M. T. 1996. Coassembly of Kvlqt1 and Mink (Isk) Proteins to Form Cardiac Iks Potassium Channel. *Nature,* 384**,** 80-83.

Sanguinetti, M. C. & Jurkiewicz, N. K. 1990. Two Components of Cardiac Delayed Rectifier K+ Current. Differential Sensitivity to Block by Class Iii Antiarrhythmic Agents. *J Gen Physiol,* 96**,** 195-215.

Schenzer, A., Friedrich, T., Pusch, M., Saftig, P., Jentsch, T. J., Grötzinger, J. & Schwake, M. 2005a. Molecular Determinants of Kcnq (Kv7) K+ Channel Sensitivity to the Anticonvulsant Retigabine. *The Journal of neuroscience : the official journal of the Society for Neuroscience,* 25**,** 5051-5060.

Schenzer, A., Friedrich, T., Pusch, M., Saftig, P., Jentsch, T. J., Grötzinger, J. & Schwake, M. 2005b. Molecular Determinants of Kcnq (Kv7) K+ Channel Sensitivity to the Anticonvulsant Retigabine. *J Neurosci,* 25**,** 5051-60.

Schmitt, N., Schwarz, M., Peretz, A., Abitbol, I., Attali, B. & Pongs, O. 2000. A Recessive C-Terminal Jervell and Lange-Nielsen Mutation of the Kcnq1 Channel Impairs Subunit Assembly. *The EMBO Journal,* 19**,** 332-340.

Schroeder, B. C., Hechenberger, M., Weinreich, F., Kubisch, C. & Jentsch, T. J. 2000a. Kcnq5, a Novel Potassium Channel Broadly Expressed in Brain,

Mediates M-Type Currents *. *Journal of Biological Chemistry,* 275**,** 24089-24095.
Schroeder, B. C., Kubisch, C., Stein, V. & Jentsch, T. J. 1998. Moderate Loss of Function of Cyclic-Amp-Modulated Kcnq2/Kcnq3 K+ Channels Causes Epilepsy. *Nature,* 396**,** 687-690.
Schroeder, B. C., Waldegger, S., Fehr, S., Bleich, M., Warth, R., Greger, R. & Jentsch, T. J. 2000b. A Constitutively Open Potassium Channel Formed by Kcnq1 and Kcne3. *Nature,* 403**,** 196-199.
Schulze-Bahr, E., Wang, Q., Wedekind, H., Haverkamp, W., Chen, Q., Sun, Y., Ruble, C., Hördt, M., Towbin, J. A., Borggrefe, M., Assmann, G., Qu, X., Somberg, J. C., Breithardt, G., Oberti, C. & Funke, H. 1997. Kcne1 Mutations Cause Jervell and Lange-Nielsen Syndrome. *Nature Genetics,* 17**,** 267-268.
Schwake, M., Jentsch, T. J. & Friedrich, T. 2003. A Carboxy-Terminal Domain Determines the Subunit Specificity of Kcnq K+ Channel Assembly. *EMBO reports,* 4**,** 76-81.
Schwarz, J. R., Glassmeier, G., Cooper, E. C., Kao, T.-C., Nodera, H., Tabuena, D., Kaji, R. & Bostock, H. 2006. Kcnq Channels Mediate Iks, a Slow K+ Current Regulating Excitability in the Rat Node of Ranvier. *The Journal of Physiology,* 573**,** 17-34.
Seebohm, G., Scherer, C. R., Busch, A. E. & Lerche, C. 2001. Identification of Specific Pore Residues Mediating Kcnq1 Inactivation: A Novel Mechanism for Long Qt Syndrome *. *Journal of Biological Chemistry,* 276**,** 13600-13605.
Seebohm, G., Strutz-Seebohm, N., Birkin, R., Dell, G., Bucci, C., Spinosa, M. R., Baltaev, R., Mack, A. F., Korniychuk, G., Choudhury, A., Marks, D., Pagano, R. E., Attali, B., Pfeufer, A., Kass, R. S., Sanguinetti, M. C., Tavare, J. M. & Lang, F. 2007. Regulation of Endocytic Recycling of Kcnq1/Kcne1 Potassium Channels. *Circulation Research,* 100**,** 686-692.
Seebohm, G., Strutz-Seebohm, N., Ureche, O. N., Henrion, U., Baltaev, R., Mack, A. F., Korniychuk, G., Steinke, K., Tapken, D., Pfeufer, A., Kääb, S., Bucci, C., Attali, B., Merot, J., Tavare, J. M., Hoppe, U. C., Sanguinetti, M. C. & Lang, F. 2008. Long Qt Syndrome Associated Mutations in Kcnq1 and Kcne1 Subunits Disrupt Normal Endosomal Recycling of Iks Channels. *Circulation Research,* 103**,** 1451-1457.
Seefeld, M. A., Lin, H., Holenz, J., Downie, D., Donovan, B., Fu, T., Pasikanti, K., Zhen, W., Cato, M., Chaudhary, K. W., Brady, P., Bakshi, T., Morrow, D., Rajagopal, S., Samanta, S. K., Madhyastha, N., Kuppusamy, B. M., Dougherty, R. W., Bhamidipati, R., Mohd, Z., Higgins, G. A., Chapman, M., Rouget, C., Lluel, P. & Matsuoka, Y. 2018. Novel Kv7 Ion Channel Openers for the Treatment of Epilepsy and Implications for Detrusor Tissue Contraction. *Bioorganic & Medicinal Chemistry Letters,* 28**,** 3793-3797.
Seltzer, Z. E., Dubner, R. & Shir, Y. 1990. A Novel Behavioral Model of Neuropathic Pain Disorders Produced in Rats by Partial Sciatic Nerve Injury. *PAIN,* 43.
Selyanko, A. A. & Brown, D. A. 1996. Intracellular Calcium Directly Inhibits Potassium M Channels in Excised Membrane Patches from Rat Sympathetic Neurons. *Neuron,* 16**,** 151-162.
Selyanko, A. A., Hadley, J. K. & Brown, D. A. 2001. Properties of Single M-Type Kcnq2/Kcnq3 Potassium Channels Expressed in Mammalian Cells. *The Journal of physiology,* 534**,** 15-24.
Selyanko, A. A., Hadley, J. K., Wood, I. C., Abogadie, F. C., Jentsch, T. J. & Brown, D. A. 2000. Inhibition of Kcnq1-4 Potassium Channels Expressed in

Mammalian Cells Via M1 Muscarinic Acetylcholine Receptors. *The Journal of Physiology,* 522**,** 349-355.
Selyanko, A. A., Stansfeld, C. E. & Brown, D. A. 1992. Closure of Potassium M-Channels by Muscarinic Acetylcholine-Receptor Stimulants Requires a Diffusible Messenger. *Proceedings of the Royal Society of London. Series B: Biological Sciences,* 250**,** 119-125.
Shalaby, F. Y., Levesque, P. C., Yang, W.-P., Little, W. A., Conder, M. L., Jenkins-West, T. & Blanar, M. A. 1997. Dominant-Negative Kvlqt1 Mutations Underlie the Lqt1 Form of Long Qt Syndrome. *Circulation,* 96**,** 1733-1736.
Shamgar, L., Ma, L., Schmitt, N., Haitin, Y., Peretz, A., Wiener, R., Hirsch, J., Pongs, O. & Attali, B. 2006. Calmodulin Is Essential for Cardiac Iks Channel Gating and Assembly. *Circulation Research,* 98**,** 1055-1063.
Shapiro, M. S., Roche, J. P., Kaftan, E. J., Cruzblanca, H., Mackie, K. & Hille, B. 2000. Reconstitution of Muscarinic Modulation of the Kcnq2/Kcnq3 K(+) Channels That Underlie the Neuronal M Current. *The Journal of neuroscience : the official journal of the Society for Neuroscience,* 20**,** 1710-1721.
Shimizu, N., Wada, N., Shimizu, T., Suzuki, T., Takaoka, E. I., Kanai, A. J., De Groat, W. C., Hirayama, A., Hashimoto, M., Uemura, H. & Yoshimura, N. 2018. Effects of Nerve Growth Factor Neutralization on Trp Channel Expression in Laser-Captured Bladder Afferent Neurons in Mice with Spinal Cord Injury. *Neurosci Lett,* 683**,** 100-103.
Siegel, A. & Sapru, H. N. 2011. *Essential Neuroscience,* Philadelphia, Wolters Kluwer Health/Lippincott Williams & Wilkins.
Singh, N. A., Charlier, C., Stauffer, D., Dupont, B. R., Leach, R. J., Melis, R., Ronen, G. M., Bjerre, I., Quattlebaum, T., Murphy, J. V., Mcharg, M. L., Gagnon, D., Rosales, T. O., Peiffer, A., Anderson, V. E. & Leppert, M. 1998. A Novel Potassium Channel Gene, Kcnq2, Is Mutated in an Inherited Epilepsy of Newborns. *Nature Genetics,* 18**,** 25-29.
Singh, N. A., Otto, J. F., Jill Dahle, E., Pappas, C., Leslie, J. D., Vilaythong, A., Noebels, J. L., Steve White, H., Wilcox, K. S. & Leppert, M. F. 2008. Mouse Models of Human Kcnq2 and Kcnq3 Mutations for Benign Familial Neonatal Convulsions Show Seizures and Neuronal Plasticity without Synaptic Reorganization. *The Journal of Physiology,* 586**,** 3405-3423.
Singh, N. A., Westenskow, P., Charlier, C., Pappas, C., Leslie, J., Dillon, J., Anderson, V. E., Sanguinetti, M. C. & Leppert, M. F. 2003. Kcnq2 and Kcnq3 Potassium Channel Genes in Benign Familial Neonatal Convulsions: Expansion of the Functional and Mutation Spectrum. *Brain,* 126**,** 2726-37.
Sleigh, J. N., Dawes, J. M., West, S. J., Wei, N., Spaulding, E. L., Gómez-Martín, A., Zhang, Q., Burgess, R. W., Cader, M. Z., Talbot, K., Yang, X.-L., Bennett, D. L. & Schiavo, G. 2017. Trk Receptor Signaling and Sensory Neuron Fate Are Perturbed in Human Neuropathy Caused by ≪Em≫Gars≪/Em≫ Mutations. *Proceedings of the National Academy of Sciences,* 114**,** E3324.
Slomko, A. M., Naseer, Z., Ali, S. S., Wongvravit, J. P. & Friedman, L. K. 2014. Retigabine Calms Seizure-Induced Behavior Following Status Epilepticus. *Epilepsy & Behavior,* 37**,** 123-132.
Smalley, J. L., Kontou, G., Choi, C., Ren, Q., Albrecht, D., Abiraman, K., Santos, M. a. R., Bope, C. E., Deeb, T. Z., Davies, P. A., Brandon, N. J. & Moss, S. J. 2020. Isolation and Characterization of Multi-Protein Complexes Enriched in the K-Cl Co-Transporter 2 from Brain Plasma Membranes. *Frontiers in Molecular Neuroscience,* 13.

Smolders, K., Lombaert, N., Valkenborg, D., Baggerman, G. & Arckens, L. 2015. An Effective Plasma Membrane Proteomics Approach for Small Tissue Samples. *Scientific Reports,* 5**,** 10917.

Søgaard, R., Ljungstrøm, T., Pedersen, K. A., Olesen, S.-P. & Jensen, B. S. 2001a. Kcnq4 Channels Expressed in Mammalian Cells: Functional Characteristics and Pharmacology. *American Journal of Physiology-Cell Physiology,* 280**,** C859-C866.

Søgaard, R., Ljungstrøm, T., Pedersen, K. A., Olesen, S. P. & Jensen, B. S. 2001b. Kcnq4 Channels Expressed in Mammalian Cells: Functional Characteristics and Pharmacology. *Am J Physiol Cell Physiol,* 280**,** C859-66.

Soldovieri, M. V., Miceli, F. & Taglialatela, M. 2011a. Driving with No Brakes: Molecular Pathophysiology of Kv7 Potassium Channels. *Physiology,* 26**,** 365-376.

Soldovieri, M. V., Miceli, F. & Taglialatela, M. 2011b. Driving with No Brakes: Molecular Pathophysiology of Kv7 Potassium Channels. *Physiology (Bethesda),* 26**,** 365-76.

Soutschek, J., Akinc, A., Bramlage, B., Charisse, K., Constien, R., Donoghue, M., Elbashir, S., Geick, A., Hadwiger, P., Harborth, J., John, M., Kesavan, V., Lavine, G., Pandey, R. K., Racie, T., Rajeev, K. G., Röhl, I., Toudjarska, I., Wang, G., Wuschko, S., Bumcrot, D., Koteliansky, V., Limmer, S., Manoharan, M. & Vornlocher, H.-P. 2004. Therapeutic Silencing of an Endogenous Gene by Systemic Administration of Modified Sirnas. *Nature,* 432**,** 173-178.

Stevens, J. C., Marks, L. E. & Simonson, D. C. 1974. Regional Sensitivity and Spatial Summation in the Warmth Sense. *Physiology & Behavior,* 13**,** 825-836.

Stott, J. B., Barrese, V., Jepps, T. A., Leighton, E. V. & Greenwood, I. A. 2015. Contribution of Kv7 Channels to Natriuretic Peptide Mediated Vasodilation in Normal and Hypertensive Rats. *Hypertension,* 65**,** 676-82.

Stott, J. B., Jepps, T. A. & Greenwood, I. A. 2014. Kv7 Potassium Channels: A New Therapeutic Target in Smooth Muscle Disorders. *Drug Discovery Today,* 19**,** 413-424.

Su, C. C., Yang, J. J., Shieh, J. C., Su, M. C. & Li, S. Y. 2007. Identification of Novel Mutations in the Kcnq4 Gene of Patients with Nonsyndromic Deafness from Taiwan. *Audiol Neurootol,* 12**,** 20-6.

Su, M., Li, L., Wang, J., Sun, H., Zhang, L., Zhao, C., Xie, Y., Gamper, N., Du, X. & Zhang, H. 2019. Kv7.4 Channel Contribute to Projection-Specific Auto-Inhibition of Dopamine Neurons in the Ventral Tegmental Area. *Frontiers in cellular neuroscience,* 13**,** 557-557.

Suh, B.-C. & Hille, B. 2002. Recovery from Muscarinic Modulation of M Current Channels Requires Phosphatidylinositol 4,5-Bisphosphate Synthesis. *Neuron,* 35**,** 507-520.

Suh, B.-C., Horowitz, L. F., Hirdes, W., Mackie, K. & Hille, B. 2004. Regulation of Kcnq2/Kcnq3 Current by G Protein Cycling: The Kinetics of Receptor-Mediated Signaling by Gq. *The Journal of general physiology,* 123**,** 663-683.

Sun, H., Lin, A.-H., Ru, F., Patil, M. J., Meeker, S., Lee, L.-Y. & Undem, B. J. 2019. Kcnq/M-Channels Regulate Mouse Vagal Bronchopulmonary C-Fiber Excitability and Cough Sensitivity. *JCI insight,* 4**,** e124467.

Sun, J. & Mackinnon, R. 2017. Cryo-Em Structure of a Kcnq1/Cam Complex Reveals Insights into Congenital Long Qt Syndrome. *Cell,* 169**,** 1042-1050.e9.

Sun, J. & Mackinnon, R. 2020. Structural Basis of Human Kcnq1 Modulation and Gating. *Cell,* 180**,** 340-347.e9.

Svalø, J., Bille, M., Parameswaran Theepakaran, N., Sheykhzade, M., Nordling, J. & Bouchelouche, P. 2013. Bladder Contractility Is Modulated by Kv7 Channels in Pig Detrusor. *European Journal of Pharmacology,* 715**,** 312-320.

Svalø, J., Hansen, H. H., Rønn, L. C., Sheykhzade, M., Munro, G. & Rode, F. 2012. Kv 7 Positive Modulators Reduce Detrusor Overactivity and Increase Bladder Capacity in Rats. *Basic Clin Pharmacol Toxicol,* 110**,** 145-53.

Svalø, J., Sheykhzade, M., Nordling, J., Matras, C. & Bouchelouche, P. 2015. Functional and Molecular Evidence for Kv7 Channel Subtypes in Human Detrusor from Patients with and without Bladder Outflow Obstruction. *PLOS ONE,* 10**,** e0117350.

Takimoto, K. & Ren, X. 2002. Kchips (Kv Channel-Interacting Proteins)--a Few Surprises and Another. *The Journal of physiology,* 545**,** 3-3.

Takumi, T., Ohkubo, H. & Nakanishi, S. 1988. Cloning of a Membrane Protein That Induces a Slow Voltage-Gated Potassium Current. *Science,* 242**,** 1042-1045.

Talebizadeh, Z., Kelley, P. M., Askew, J. W., Beisel, K. W. & Smith, S. D. 1999. Novel Mutation in the Kcnq4 Gene in a Large Kindred with Dominant Progressive Hearing Loss. *Human Mutation,* 14**,** 493-501.

Tan, P.-H., Yang, L.-C. & Ji, R.-R. 2009. Therapeutic Potential of Rna Interference in Pain Medicine. *The open pain journal,* 2**,** 57-63.

Tanabe, T., Takeshima, H., Mikami, A., Flockerzi, V., Takahashi, H., Kangawa, K., Kojima, M., Matsuo, H., Hirose, T. & Numa, S. 1987. Primary Structure of the Receptor for Calcium Channel Blockers from Skeletal Muscle. *Nature,* 328**,** 313-8.

Tandrup, T. 2004. Unbiased Estimates of Number and Size of Rat Dorsal Root Ganglion Cells in Studies of Structure and Cell Survival. *Journal of Neurocytology,* 33**,** 173-192.

Tatulian, L. & Brown, D. A. 2003. Effect of the Kcnq Potassium Channel Opener Retigabine on Single Kcnq2/3 Channels Expressed in Cho Cells. *The Journal of physiology,* 549**,** 57-63.

Tatulian, L., Delmas, P., Abogadie, F. C. & Brown, D. A. 2001a. Activation of Expressed Kcnq Potassium Currents and Native Neuronal M-Type Potassium Currents by the Anti-Convulsant Drug Retigabine. *The Journal of neuroscience : the official journal of the Society for Neuroscience,* 21**,** 5535-5545.

Tatulian, L., Delmas, P., Abogadie, F. C. & Brown, D. A. 2001b. Activation of Expressed Kcnq Potassium Currents and Native Neuronal M-Type Potassium Currents by the Anti-Convulsant Drug Retigabine. *The Journal of Neuroscience,* 21**,** 5535.

Terenghi, G. 1999. Peripheral Nerve Regeneration and Neurotrophic Factors. *Journal of anatomy,* 194 (Pt 1)**,** 1-14.

Testai, L., Barrese, V., Soldovieri, M. V., Ambrosino, P., Martelli, A., Vinciguerra, I., Miceli, F., Greenwood, I. A., Curtis, M. J., Breschi, M. C., Sisalli, M. J., Scorziello, A., Canduela, M. J., Grandes, P., Calderone, V. & Taglialatela, M. 2015. Expression and Function of Kv7.4 Channels in Rat Cardiac Mitochondria: Possible Targets for Cardioprotection. *Cardiovascular Research,* 110**,** 40-50.

Thorneloe, K. S. & Nelson, M. T. 2003. Properties and Molecular Basis of the Mouse Urinary Bladder Voltage-Gated K+ Current. *J Physiol,* 549**,** 65-74.

Tian, C., Vanoye, C. G., Kang, C., Welch, R. C., Kim, H. J., George, A. L., Jr. & Sanders, C. R. 2007. Preparation, Functional Characterization, and Nmr Studies of Human Kcne1, a Voltage-Gated Potassium Channel Accessory

Subunit Associated with Deafness and Long Qt Syndrome. *Biochemistry,* 46**,** 11459-11472.
Tinel, N., Diochot, S., Borsotto, M., Lazdunski, M. & Barhanin, J. 2000a. Kcne2 Confers Background Current Characteristics to the Cardiac Kcnq1 Potassium Channel. *Embo j,* 19**,** 6326-30.
Tinel, N., Diochot, S., Lauritzen, I., Barhanin, J., Lazdunski, M. & Borsotto, M. 2000b. M-Type Kcnq2–Kcnq3 Potassium Channels Are Modulated by the Kcne2 Subunit. *FEBS Letters,* 480**,** 137-141.
Tinel, N., Lauritzen, I., Chouabe, C., Lazdunski, M. & Borsotto, M. 1998. The Kcnq2 Potassium Channel: Splice Variants, Functional and Developmental Expression. Brain Localization and Comparison with Kcnq3. *FEBS Lett,* 438**,** 171-6.
Tomić, M., Micov, A., Pecikoza, U. & Stepanović-Petrović, R. 2017. Chapter 1 - Clinical Uses of Nonsteroidal Anti-Inflammatory Drugs (Nsaids) and Potential Benefits of Nsaids Modified-Release Preparations. *In:* Čalija, B. (ed.) *Microsized and Nanosized Carriers for Nonsteroidal Anti-Inflammatory Drugs.* Boston: Academic Press.
Tompkins, S. M., Lo, C.-Y., Tumpey, T. M. & Epstein, S. L. 2004. Protection against Lethal Influenza Virus Challenge by Rna Interference in Vivo. *Proceedings of the National Academy of Sciences of the United States of America,* 101**,** 8682.
Tothonglor, A., Kobutree, P., Roumwong, A., Jindatip, D. & Agthong, S. 2022. Cisplatin-Induced Alterations in the Blood-Nerve Barrier: Effects of Combination of Vitamin B1, B6 and B12. *Folia Morphol (Warsz)*.
Tristani-Firouzi, M. & Sanguinetti, M. C. 1998. Voltage-Dependent Inactivation of the Human K+ Channel Kvlqt1 Is Eliminated by Association with Minimal K+ Channel (Mink) Subunits. *The Journal of physiology,* 510 (Pt 1)**,** 37-45.
Tsai, Y.-M., Jones, F., Mullen, P., Porter, K. E., Steele, D., Peers, C. & Gamper, N. 2020. Vascular Kv7 Channels Control Intracellular Ca2+ Dynamics in Smooth Muscle. *Cell Calcium,* 92**,** 102283.
Tykocki, N. R., Heppner, T. J., Dalsgaard, T., Bonev, A. D. & Nelson, M. T. 2019. The K(V) 7 Channel Activator Retigabine Suppresses Mouse Urinary Bladder Afferent Nerve Activity without Affecting Detrusor Smooth Muscle K(+) Channel Currents. *J Physiol,* 597**,** 935-950.
Tzingounis, A. V., Heidenreich, M., Kharkovets, T., Spitzmaul, G., Jensen, H. S., Nicoll, R. A. & Jentsch, T. J. 2010. The Kcnq5 Potassium Channel Mediates a Component of the Afterhyperpolarization Current in Mouse Hippocampus. *Proceedings of the National Academy of Sciences,* 107**,** 10232.
Tzour, A., Leibovich, H., Barkai, O., Biala, Y., Lev, S., Yaari, Y. & Binshtok, A. M. 2017. K(V) 7/M Channels as Targets for Lipopolysaccharide-Induced Inflammatory Neuronal Hyperexcitability. *J Physiol,* 595**,** 713-738.
Uchida, H., Ma, L. & Ueda, H. 2010. Epigenetic Gene Silencing Underlies C-Fiber Dysfunctions in Neuropathic Pain. *The Journal of neuroscience : the official journal of the Society for Neuroscience,* 30**,** 4806-4814.
Uhlén, M., Fagerberg, L., Hallström, B. M., Lindskog, C., Oksvold, P., Mardinoglu, A., Sivertsson, Å., Kampf, C., Sjöstedt, E., Asplund, A., Olsson, I., Edlund, K., Lundberg, E., Navani, S., Szigyarto, C. A., Odeberg, J., Djureinovic, D., Takanen, J. O., Hober, S., Alm, T., Edqvist, P. H., Berling, H., Tegel, H., Mulder, J., Rockberg, J., Nilsson, P., Schwenk, J. M., Hamsten, M., Von Feilitzen, K., Forsberg, M., Persson, L., Johansson, F., Zwahlen, M., Von Heijne, G., Nielsen,

J. & Pontén, F. 2015. Proteomics. Tissue-Based Map of the Human Proteome. *Science,* 347**,** 1260419.
Usoskin, D., Furlan, A., Islam, S., Abdo, H., Lönnerberg, P., Lou, D., Hjerling-Leffler, J., Haeggström, J., Kharchenko, O., Kharchenko, P. V., Linnarsson, S. & Ernfors, P. 2015. Unbiased Classification of Sensory Neuron Types by Large-Scale Single-Cell Rna Sequencing. *Nature Neuroscience,* 18**,** 145-153.
Vallon, V., Grahammer, F., Richter, K., Bleich, M., Lang, F., Barhanin, J., Völkl, H. & Warth, R. 2001. Role of Kcne1-Dependent K≪Sup≫+≪/Sup≫ Fluxes in Mouse Proximal Tubule. *Journal of the American Society of Nephrology,* 12**,** 2003.
Van Camp, G., Coucke, P. J., Akita, J., Fransen, E., Abe, S., De Leenheer, E. M. R., Huygen, P. L. M., Cremers, C. W. R. J. & Usami, S.-I. 2002. A Mutational Hot Spot in the Kcnq4 Gene Responsible for Autosomal Dominant Hearing Impairment. *Human Mutation,* 20**,** 15-19.
Van Hauwe, P., Coucke, P. J., Ensink, R. J., Huygen, P., Cremers, C. W. R. J. & Van Camp, G. 2000. Mutations in the Kcnq4 K+ Channel Gene, Responsible for Autosomal Dominant Hearing Loss, Cluster in the Channel Pore Region. *American Journal of Medical Genetics,* 93**,** 184-187.
Van Rijn, C. M. & Willems-Van Bree, E. 2003. Synergy between Retigabine and Gaba in Modulating the Convulsant Site of the Gabaa Receptor Complex. *European Journal of Pharmacology,* 464**,** 95-100.
Verneuil, J., Brocard, C., Trouplin, V., Villard, L., Peyronnet-Roux, J. & Brocard, F. 2020. The M-Current Works in Tandem with the Persistent Sodium Current to Set the Speed of Locomotion. *PLOS Biology,* 18**,** e3000738.
Vetter, I., Hein, A., Sattler, S., Hessler, S., Touska, F., Bressan, E., Parra, A., Hager, U., Leffler, A., Boukalova, S., Nissen, M., Lewis, R. J., Belmonte, C., Alzheimer, C., Huth, T., Vlachova, V., Reeh, P. W. & Zimmermann, K. 2013. Amplified Cold Transduction in Native Nociceptors by M-Channel Inhibition. *The Journal of Neuroscience,* 33**,** 16627.
Vohra, J. 2007. The Long Qt Syndrome. *Heart, Lung and Circulation,* 16**,** S5-S12.
Walsh, K. B. & Kass, R. S. 1988. Regulation of a Heart Potassium Channel by Protein Kinase a and C. *Science,* 242**,** 67-69.
Wang, H.-S., Brown, B. S., Mckinnon, D. & Cohen, I. S. 2000. Molecular Basis for Differential Sensitivity of Kcnq and Lks Channels to the Cognitive Enhancer Xe991. *Molecular Pharmacology,* 57**,** 1218.
Wang, H. S. & Mckinnon, D. 1995. Potassium Currents in Rat Prevertebral and Paravertebral Sympathetic Neurones: Control of Firing Properties. *The Journal of physiology,* 485 (Pt 2)**,** 319-335.
Wang, H. S., Pan, Z., Shi, W., Brown, B. S., Wymore, R. S., Cohen, I. S., Dixon, J. E. & Mckinnon, D. 1998. Kcnq2 and Kcnq3 Potassium Channel Subunits: Molecular Correlates of the M-Channel. *Science,* 282**,** 1890-3.
Wang, L., Qiao, G. H., Hu, H. N., Gao, Z. B. & Nan, F. J. 2019. Discovery of Novel Retigabine Derivatives as Potent Kcnq4 and Kcnq5 Channel Agonists with Improved Specificity. *ACS Med Chem Lett,* 10**,** 27-33.
Wang, M., Gamo, N. J., Yang, Y., Jin, L. E., Wang, X. J., Laubach, M., Mazer, J. A., Lee, D. & Arnsten, A. F. 2011. Neuronal Basis of Age-Related Working Memory Decline. *Nature,* 476**,** 210-3.
Wang, Q., Curran, M. E., Splawski, I., Burn, T. C., Millholland, J. M., Vanraay, T. J., Shen, J., Timothy, K. W., Vincent, G. M., De Jager, T., Schwartz, P. J., Towbin, J. A., Moss, A. J., Atkinson, D. L., Landes, G. M., Connors, T. D. & Keating, M.

T. 1996. Positional Cloning of a Novel Potassium Channel Gene: Kvlqt1 Mutations Cause Cardiac Arrhythmias. *Nature Genetics,* 12**,** 17-23.
Warth, R., Riedemann, N., Bleich, M., Van Driessche, W., Busch, A. E. & Greger, R. 1996. The Camp-Regulated and 293b-Inhibited K+ Conductance of Rat Colonic Crypt Base Cells. *Pflügers Archiv,* 432**,** 81-88.
Watanabe, H., Nagata, E., Kosakai, A., Nakamura, M., Yokoyama, M., Tanaka, K. & Sasai, H. 2000. Disruption of the Epilepsy Kcnq2 Gene Results in Neural Hyperexcitability. *Journal of Neurochemistry,* 75**,** 28-33.
Webb, T. I., Kshatri, A. S., Large, R. J., Akande, A. M., Roy, S., Sergeant, G. P., Mchale, N. G., Thornbury, K. D. & Hollywood, M. A. 2015. Molecular Mechanisms Underlying the Effect of the Novel Bk Channel Opener Goslo: Involvement of the S4/S5 Linker and the S6 Segment. *Proceedings of the National Academy of Sciences,* 112**,** 2064.
Weckhuysen, S., Ivanovic, V., Hendrickx, R., Van Coster, R., Hjalgrim, H., Møller, R. S., Grønborg, S., Schoonjans, A.-S., Ceulemans, B., Heavin, S. B., Eltze, C., Horvath, R., Casara, G., Pisano, T., Giordano, L., Rostasy, K., Haberlandt, E., Albrecht, B., Bevot, A., Benkel, I., Syrbe, S., Sheidley, B., Guerrini, R., Poduri, A., Lemke, J. R., Mandelstam, S., Scheffer, I., Angriman, M., Striano, P., Marini, C., Suls, A., De Jonghe, P. & On Behalf of The, K. S. G. 2013. Extending the Kcnq2 Encephalopathy Spectrum. *Neurology,* 81**,** 1697.
Wen, H. & Levitan, I. B. 2002. Calmodulin Is an Auxiliary Subunit of Kcnq2/3 Potassium Channels. *The Journal of neuroscience : the official journal of the Society for Neuroscience,* 22**,** 7991-8001.
Werry, D., Eldstrom, J., Wang, Z. & Fedida, D. 2013. Single-Channel Basis for the Slow Activation of the Repolarizing Cardiac Potassium Current, I(Ks). *Proceedings of the National Academy of Sciences of the United States of America,* 110**,** E996-1005.
Wickenden, A. D., Krajewski, J. L., London, B., Wagoner, P. K., Wilson, W. A., Clark, S., Roeloffs, R., Mcnaughton-Smith, G. & Rigdon, G. C. 2008. N-(6-Chloro-Pyridin-3-Yl)-3,4-Difluoro-Benzamide (Ica-27243): A Novel, Selective Kcnq2/Q3 Potassium Channel Activator. *Molecular Pharmacology,* 73**,** 977.
Wickenden, A. D., Zou, A., Wagoner, P. K. & Jegla, T. 2001. Characterization of Kcnq5/Q3 Potassium Channels Expressed in Mammalian Cells. *Br J Pharmacol,* 132**,** 381-4.
Woodbury, C. J., Zwick, M., Wang, S., Lawson, J. J., Caterina, M. J., Koltzenburg, M., Albers, K. M., Koerber, H. R. & Davis, B. M. 2004. Nociceptors Lacking Trpv1 and Trpv2 Have Normal Heat Responses. *The Journal of Neuroscience,* 24**,** 6410.
Wu, Y.-J., Conway, C. M., Sun, L.-Q., Machet, F., Chen, J., Chen, P., He, H., Bourin, C., Calandra, V., Polino, J. L., Davis, C. D., Heman, K., Gribkoff, V. K., Boissard, C. G., Knox, R. J., Thompson, M. W., Fitzpatrick, W., Weaver, D., Harden, D. G., Natale, J., Dworetzky, S. I. & Starrett, J. E. 2013. Discovery of (S,E)-3-(2-Fluorophenyl)-N-(1-(3-(Pyridin-3-Yloxy)Phenyl)Ethyl)-Acrylamide as a Potent and Efficacious Kcnq2 (Kv7.2) Opener for the Treatment of Neuropathic Pain. *Bioorganic & Medicinal Chemistry Letters,* 23**,** 6188-6191.
Xia, X., Zhang, Q., Jia, Y., Shu, Y., Yang, J., Yang, H. & Yan, Z. 2020. Molecular Basis and Restoration of Function Deficiencies of Kv7.4 Variants Associated with Inherited Hearing Loss. *Hearing Research,* 388**,** 107884.
Xu, Q. & Minor Jr., D. L. 2009. Crystal Structure of a Trimeric Form of the Kv7.1 (Kcnq1) a-Domain Tail Coiled-Coil Reveals Structural Plasticity and Context

Dependent Changes in a Putative Coiled-Coil Trimerization Motif. *Protein Science,* 18**,** 2100-2114.

Xu, T., Nie, L., Zhang, Y., Mo, J., Feng, W., Wei, D., Petrov, E., Calisto, L. E., Kachar, B., Beisel, K. W., Vazquez, A. E. & Yamoah, E. N. 2007. Roles of Alternative Splicing in the Functional Properties of Inner Ear-Specific Kcnq4 Channels. *Journal of Biological Chemistry,* 282**,** 23899-23909.

Xu, W., Wu, Y., Bi, Y., Tan, L., Gan, Y. & Wang, K. 2010. Activation of Voltage-Gated Kcnq/Kv7 Channels by Anticonvulsant Retigabine Attenuates Mechanical Allodynia of Inflammatory Temporomandibular Joint in Rats. *Molecular pain,* 6**,** 49-49.

Yadav, G., Choupoo, S., Das, S. K., Das, S. K., Behera, S. S., Khuba, S., Mishra, L. D. & Singh, D. K. 2014. Evaluating the Role of Flupirtine for Postcraniotomy Pain and Compare It with Diclofenac Sodium: A Prospective, Randomized, Double Blind, Placebo-Controlled Study. *Journal of Neurosurgical Anesthesiology,* 26.

Yadav, G., Jain, G. & Singh, M. 2017. Role of Flupirtine in Reducing Preoperative Anxiety of Patients Undergoing Craniotomy Procedure. *Saudi J Anaesth,* 11**,** 158-162.

Yang, W.-P., Levesque, P. C., Little, W. A., Conder, M. L., Ramakrishnan, P., Neubauer, M. G. & Blanar, M. A. 1998. Functional Expression of Two Kvlqt1-Related Potassium Channels Responsible for an Inherited Idiopathic Epilepsy *. *Journal of Biological Chemistry,* 273**,** 19419-19423.

Yang, W. P., Levesque, P. C., Little, W. A., Conder, M. L., Shalaby, F. Y. & Blanar, M. A. 1997. Kvlqt1, a Voltage-Gated Potassium Channel Responsible for Human Cardiac Arrhythmias. *Proceedings of the National Academy of Sciences of the United States of America,* 94**,** 4017-4021.

Young, M. B. & Thomas, S. A. 2014. M1-Muscarinic Receptors Promote Fear Memory Consolidation Via Phospholipase C and the M-Current. *J Neurosci,* 34**,** 1570-8.

Yu, S. P., Malley, D. M. & Adams, P. R. 1994. Regulation of M Current by Intracellular Calcium in Bullfrog Sympathetic Ganglion Neurons. *The Journal of Neuroscience,* 14**,** 3487.

Yue, C. & Yaari, Y. 2004. Kcnq/M Channels Control Spike Afterdepolarization and Burst Generation in Hippocampal Neurons. *J Neurosci,* 24**,** 4614-24.

Zaczek, R., Chorvat, R. J., Saye, J. A., Pierdomenico, M. E., Maciag, C. M., Logue, A. R., Fisher, B. N., Rominger, D. H. & Earl, R. A. 1998. Two New Potent Neurotransmitter Release Enhancers, 10,10-Bis(4-Pyridinylmethyl)-9(10h)-Anthracenone and 10,10-Bis(2-Fluoro-4-Pyridinylmethyl)-9(10h)-Anthracenone: Comparison to Linopirdine. *J Pharmacol Exp Ther,* 285**,** 724-30.

Zaika, O., Hernandez, C. C., Bal, M., Tolstykh, G. P. & Shapiro, M. S. 2008. Determinants within the Turret and Pore-Loop Domains of Kcnq3 Channels Governing Functional Activity. *Biophysical Journal,* 95**,** 5121-5137.

Zavaritskaya, O., Dudem, S., Ma, D., Rabab, K. E., Albrecht, S., Tsvetkov, D., Kassmann, M., Thornbury, K., Mladenov, M., Kammermeier, C., Sergeant, G., Mullins, N., Wouappi, O., Wurm, H., Kannt, A., Gollasch, M., Hollywood, M. A. & Schubert, R. 2020. Vasodilation of Rat Skeletal Muscle Arteries by the Novel Bk Channel Opener Goslo Is Mediated by the Simultaneous Activation of Bk and Kv7 Channels. *British Journal of Pharmacology,* 177**,** 1164-1186.

Zhang, D., Men, H., Zhang, L., Gao, X., Wang, J., Li, L., Zhu, Q., Zhang, H. & Jia, Z. 2020a. Inhibition of M/K(V)7 Currents Contributes to Chloroquine-Induced Itch in Mice. *Front Mol Neurosci,* 13**,** 105.

Zhang, D., Thimmapaya, R., Zhang, X. F., Anderson, D. J., Baranowski, J. L., Scanio, M., Perez-Medrano, A., Peddi, S., Wang, Z., Patel, J. R., Degoey, D. A., Gopalakrishnan, M., Honore, P., Yao, B. B. & Surowy, C. S. 2011a. Kcnq2/3 Openers Show Differential Selectivity and Site of Action across Multiple Kcnq Channels. *J Neurosci Methods,* 200**,** 54-62.

Zhang, F., Gigout, S., Liu, Y., Wang, Y., Hao, H., Buckley, N. J., Zhang, H., Wood, I. C. & Gamper, N. 2019. Repressor Element 1-Silencing Transcription Factor Drives the Development of Chronic Pain States. *Pain,* 160**,** 2398-2408.

Zhang, F., Liu, S., Jin, L., Tang, L., Zhao, X., Yang, T., Wang, Y., Huo, B., Liu, R. & Li, H. 2020b. Antinociceptive Efficacy of Retigabine and Flupirtine for Gout Arthritis Pain. *Pharmacology,* 105**,** 471-476.

Zhang, H., Craciun, L. C., Mirshahi, T., Rohács, T., Lopes, C. M. B., Jin, T. & Logothetis, D. E. 2003. Pip2 Activates Kcnq Channels, and Its Hydrolysis Underlies Receptor-Mediated Inhibition of M Currents. *Neuron,* 37**,** 963-975.

Zhang, H. & Dougherty, P. M. 2014. Enhanced Excitability of Primary Sensory Neurons and Altered Gene Expression of Neuronal Ion Channels in Dorsal Root Ganglion in Paclitaxel-Induced Peripheral Neuropathy. *Anesthesiology,* 120**,** 1463-1475.

Zhang, J., Bal, M., Bierbower, S., Zaika, O. & Shapiro, M. S. 2011b. Akap79/150 Signal Complexes in G-Protein Modulation of Neuronal Ion Channels. *The Journal of neuroscience : the official journal of the Society for Neuroscience,* 31**,** 7199-7211.

Zhang, J., Carver, Chase m., Choveau, Frank s. & Shapiro, Mark s. 2016a. Clustering and Functional Coupling of Diverse Ion Channels and Signaling Proteins Revealed by Super-Resolution Storm Microscopy in Neurons. *Neuron,* 92**,** 461-478.

Zhang, J., Chen, S.-R., Chen, H. & Pan, H.-L. 2018. Re1-Silencing Transcription Factor Controls the Acute-to-Chronic Neuropathic Pain Transition and Chrm2 Receptor Gene Expression in Primary Sensory Neurons. *The Journal of biological chemistry,* 293**,** 19078-19091.

Zhang, J. & Shapiro, M. S. 2012. Activity-Dependent Transcriptional Regulation of M-Type (Kv7) K(+) Channels by Akap79/150-Mediated Nfat Actions. *Neuron,* 76**,** 1133-1146.

Zhang, X., An, H., Li, J., Zhang, Y., Liu, Y., Jia, Z., Zhang, W., Chu, L. & Zhang, H. 2016b. Selective Activation of Vascular Kv7.4/Kv7.5 K+ Channels by Fasudil Contributes to Its Vasorelaxant Effect. *British Journal of Pharmacology,* 173**,** 3480-3491.

Zhao, C., Su, M., Wang, Y., Li, X., Zhang, Y., Du, X. & Zhang, H. 2017. Selective Modulation of K+ Channel Kv7.4 Significantly Affects the Excitability of Drn 5-Ht Neurons. *Frontiers in Cellular Neuroscience,* 11.

Zheng, J. & Trudeau, M. C. 2015. *Handbook of Ion Channels*, CRC Press.

Zheng, Q., Fang, D., Cai, J., Wan, Y., Han, J.-S. & Xing, G.-G. 2012. Enhanced Excitability of Small Dorsal Root Ganglion Neurons in Rats with Bone Cancer Pain. *Molecular pain,* 8**,** 24-24.

Zheng, Q., Fang, D., Liu, M., Cai, J., Wan, Y., Han, J.-S. & Xing, G.-G. 2013. Suppression of Kcnq/M (Kv7) Potassium Channels in Dorsal Root Ganglion

Neurons Contributes to the Development of Bone Cancer Pain in a Rat Model. *PAIN,* 154**,** 434-448.
Zheng, Y., Liu, P., Bai, L., Trimmer, J. S., Bean, B. P. & Ginty, D. D. 2019. Deep Sequencing of Somatosensory Neurons Reveals Molecular Determinants of Intrinsic Physiological Properties. *Neuron,* 103**,** 598-616.e7.
Zhou, X., Wei, J., Song, M., Francis, K. & Yu, S. P. 2011. Novel Role of Kcnq2/3 Channels in Regulating Neuronal Cell Viability. *Cell death and differentiation,* 18**,** 493-505.
Zhou, Y. & Mackinnon, R. 2003. The Occupancy of Ions in the K+ Selectivity Filter: Charge Balance and Coupling of Ion Binding to a Protein Conformational Change Underlie High Conduction Rates. *Journal of Molecular Biology,* 333**,** 965-975.
Zhu, Y. F., Wu, Q. & Henry, J. L. 2012. Changes in Functional Properties of a-Type but Not C-Type Sensory Neurons in Vivo in a Rat Model of Peripheral Neuropathy. *Journal of pain research,* 5**,** 175-192.